Doctoral thesis
Valencia, 2020

VNIVERSITAT DE VALÈNCIA

REBECA BURGOS PANADERO

DOCTORAL THESIS

2020

SEARCH FOR THERAPEUTIC TARGETS AT THE CONTACT POINTS OF THE TUMOR CELL WITH ITS EXTRACELLULAR MATRIX IN NEUROBLASTIC TUMORS

BÚSQUEDA DE DIANAS TERAPÉUTICAS EN LOS PUNTOS DE CONTACTO DE LA CÉLULA TUMORAL CON SU MATRIZ EXTRACELULAR EN TUMORES NEUROBLÁSTICOS

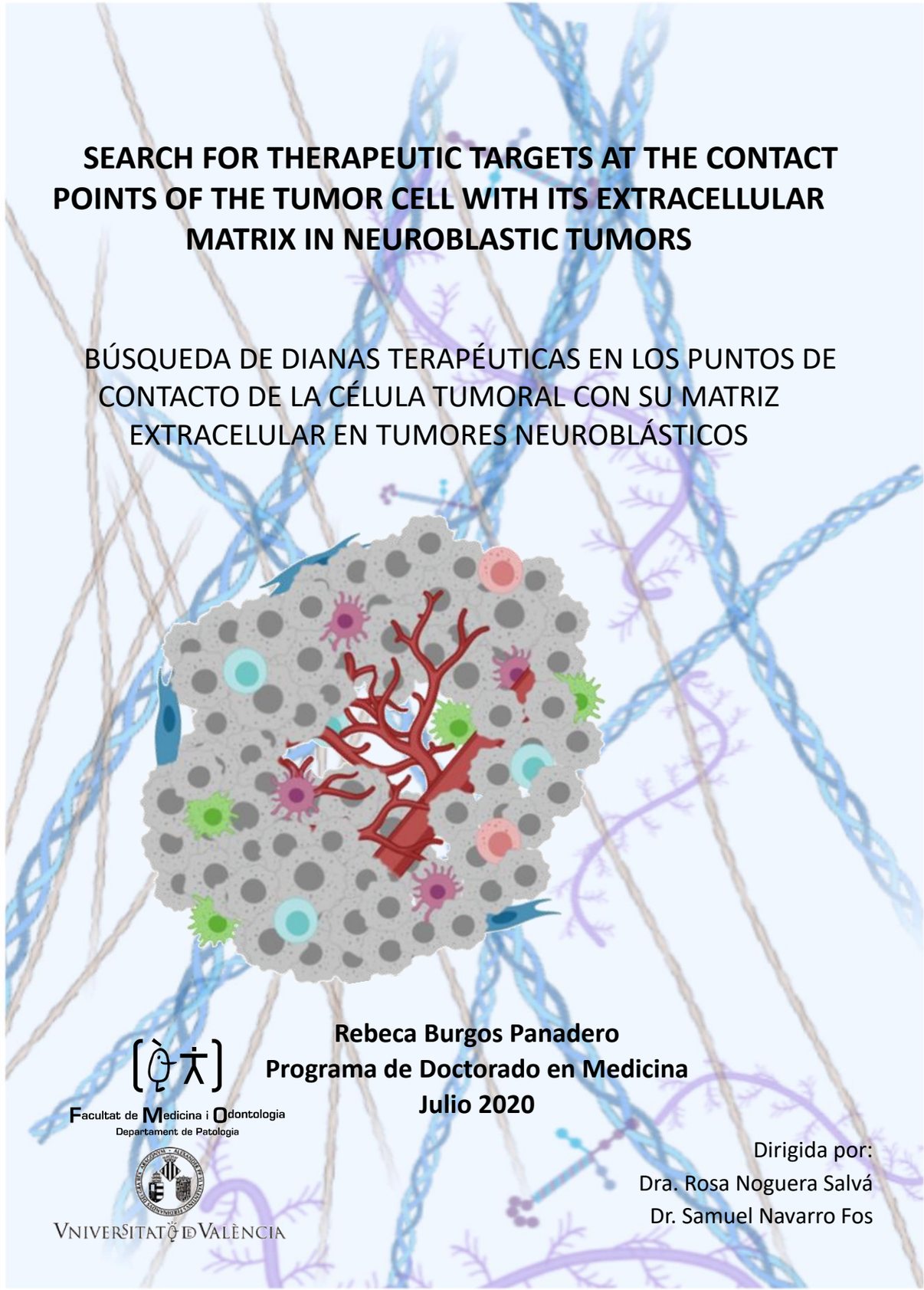

Facultat de Medicina i Odontologia
Departament de Patologia

VNIVERSITAT DE VALÈNCIA

Rebeca Burgos Panadero

Programa de Doctorado en Medicina
Julio 2020

Dirigida por:
Dra. Rosa Noguera Salvá
Dr. Samuel Navarro Fos

"No puedo enseñar nada a nadie. Solo puedo hacerles pensar"

Sócrates

SEARCH FOR THERAPEUTIC TARGETS AT THE CONTACT POINTS OF THE TUMOR CELL WITH ITS EXTRACELLULAR MATRIX IN NEUROBLASTIC TUMORS

BÚSQUEDA DE DIANAS TERAPÉUTICAS EN LOS PUNTOS DE CONTACTO DE LA CÉLULA TUMORAL CON SU MATRIZ EXTRACELULAR EN TUMORES NEUROBLÁSTICOS

Rebeca Burgos Panadero

Thesis directors: Dra. Rosa Noguera Salvá y Dr. Samuel Navarro Fos

Doctoral thesis

Programa de Doctorado: 3139 Medicina: Tumores sólidos pediátricos.

Departament de Patologia

Facultat de Medicina i Odontologia

Valencia, Julio 2020

Doña Rosa Noguera Salvá y Don Samuel Navarro Fos, doctores en Medicina y catedráticos de la Facultad de Medicina y Odontología de la Universitat de València,

CERTIFICAN:

Que Rebeca Burgos Panadero, graduada en Biología por la Universitat de València ha realizado, bajo nuestra dirección, el trabajo que lleva por título:

Búsqueda de dianas terapéuticas en los puntos de contacto de la célula tumoral con su matriz extracelular en tumores neuroblásticos

El cual consideramos satisfactorio y apto para ser presentado y defendido como Tesis Doctoral en el Departamento de Patología de la Universidad de Valencia.

Y para que así conste, expedimos este certificado en Valencia, a 03 de Julio de 2020.

Fdo.: Profª. Rosa Noguera Salvá
Profª. Catedrática de Histología

Fdo.: Prof. Samuel Navarro Fos
Prof. Catedrático de Anatomía Patológica

Agradecimientos:

Con estas líneas me gustaría agradecer a todas las personas que han ayudado a que la realización de esta tesis haya sido posible.

Quiero agradecer en primer lugar a todos los pacientes y sus familiares, al permitir la investigación con sus muestras.

A la Dra. Adela Cañete, Dra. Victoria Castel, y a Desireé Ramal, por proveer los datos clínicos de los pacientes que se han utilizado en este trabajo. Así como también, a la Sociedad Española de Hematología y Oncología Pediátrica que gracias a su labor posibilita la continuidad de los estudios clínicos.

Dar las gracias a todos los miembros del Servicio de Anatomía Patológica, del Hospital Clínico de Valencia, en especial a Elisa Alonso, Cristina Mongort, Alejo Sempere, Esther Álvarez y Laura Martínez por su implicación y sus consejos en el procesamiento de las muestras y otras técnicas del laboratorio.

Agradecer a todo el servicio de producción y experimentación animal de la Facultat de Farmacia, en especial destacar la implicación de Inma Noguera por su colaboración en este trabajo y por todo lo que me ha enseñado en este campo.

Gracias a Daniel Bexell, quien me acogió en su laboratorio durante dos estancias, darle las gracias por todo el aprendizaje y enriquecimiento personal. Agradecer también a los miembros de su equipo: Adriana Mañas, Kristina Altonen, Katarzyna Radke, Javanshir Esfandyari, Karin Hansson, Noémie Braekeveldt y Camilla Persson por todo su trabajo y por compartir conmigo su conocimiento. Muchas gracias por hacer que todo ese tiempo pasara tan rápido.

A mis compañeros Amparo López, Susana Martín, Ana Berbegall, Ezequiel Monferrer, Sabina Sanegre y Nuria Benavent, gracias por hacer más fácil el día a día y ser mis consejeros científicos. También dar las gracias a Esther Gamero, Federico Lucantoni y Aitor Carretero por haber formado parte en esta travesía. No quiero olvidarme de Irene Tadeo, Maite Blanquer y Victor Zuñiga, quienes me formaron y me guiaron en los primeros momentos del camino en el laboratorio. Muchísimas gracias a todos por vuestro trabajo y apoyo para que esta tesis viera la luz.

A mis compañeros del departamento y de pasillo, Bea, Gema, José, Teresa Sagrado, Marieta, Rubén, Lara, Manolo, Teresa San Miguel, Javier, Lissandra, Amara y Ana Clarí gracias por echarme una mano cuando la necesitaba y por todo lo que he aprendido con vosotros.

Agradezco a mis directores de tesis, el esfuerzo y dedicación que han invertido para que este trabajo saliera adelante. Gracias Samuel por tu sabiduría y paciencia. Gracias Rosa por tu incansable motivación e inagotable energía. Muchísimas gracias a ambos por la formación que me habéis proporcionado durante todo este tiempo, que me ha hecho crecer a nivel profesional y personal.

A mis amigos, gracias por escucharme y aconsejarme, pero principalmente gracias por estar ahí incluso sin pedíroslo.

A ti Jose, gracias por tu ayuda incondicional en mis momentos de desesperación, porque he aprendido que estar contigo es la fortaleza de mi vida, por todo lo que me das, muchas gracias.

A mi familia, en especial a mi hermana, y mis padres, por estar siempre y guiarme en el camino cuando tenía miedo de seguir mis sueños. Vosotros me habéis enseñado el valor del esfuerzo, gracias por haberme ayudado en todo lo que habéis podido y creer en mí.

Trabajo financiado por: FAECC (Cáncer Infantil (2015/006)), CIBERONC (CB16/12/00484), Instituto de salud Carlos III (FIS (PI17/01558)) y Asociación NEN/Nico contra el cáncer infantil.

INDEX

Figures index **1**

Tables index **3**

Summary **5**

Resumen **9**

Abbreviations **13**

Compendium of articles that support this thesis **15**

Article I: The tumour microenvironment as an integrated framework to understand cancer biology 17

Article II: Vitronectin as a molecular player of the tumor microenvironment in neuroblastoma 31

Article III: The topology of vitronectin: A complementary feature for neuroblastoma risk classification based on computer-aided detection 47

Papers as a co-author not included in this thesis **67**

CHAPTER 1. Introduction **69**

1.1 Neuroblastoma (NB) **71**

1.1.1. General aspects 71

1.1.2 Clinical, histological and genetic factors according to INRG classification system 72

1.1.3. Therapy and novel targets 76

1.2. Tumor microenvironment **78**

1.2.1. General aspects 78

1.2.2. Cellular components 79

1.2.3. Non-cellular components: extracellular matrix (ECM) and vitronectin (VN) 82

1.2.4. Use of this knowledge for treating patients 86

1. 3. Experimental models in cancer **90**

1.3.1. General aspects 90

1.3.2. *In vitro* models 90

1.3.3. *In vivo* models 93

1.4. Digital pathology in cancer **96**

1.4.1. General aspects 96

1.4.2. Computer-aided analysis in NB 97

CHAPTER 2. Hypothesis, aims and justification of article compendium **99**

2.1. Hypothesis **101**

2.2. Aims **101**

2.3. Justification of the thesis as publication compendium 102

CHAPTER 3. Results and Discussion 105

3.1 Human NB samples 108

3.1.1 The importance of an adequate biopsy in the era of personalized treatment..... 109

3.1.2. Expression studies of VN and its ligands highlight its relevance in NB biology 110

3.1.2.1 Morphometric measurements generate knowledge about tissue biotensegral responses 116

3.1.2.2 Topological measurements facilitate architectural tissue findings 119

3.1.3 ECM elements generate complex stress forces to cells 120

3.1.4. Studies to strengthen clinically relevant biomarkers or therapeutic targets 127

***3.2 In vitro* NB models 129**

3.2.1. Cell lines used 129

3.2.2. Expression of VN and its receptors by neuroblastic cells..... 130

3.3. *In vivo* NB models (orthotopic xenografts) 133

3.3.1. Excellent growth adaptation in deficient VN mice..... 133

3.3.2. Maintaining cell morphology of patient tumors 136

3.3.3. Hallmarks of microenvironmental components 138

3.3.4. VN cooperation in genomic instability 146

CHAPTER 4. Conclusions/Conclusiones 151

References 161

Appendix..... 181

Figures index

Figure 1. Representation of the interplay among the tumor microenvironment components.

Figure 2. Kaplan-Meier graphs showing the EFS (A, C) or OS (B, D) depending on genetic instability category.

Figure 3. VN expression pattern in neuroblastic tumors.

Figure 4. Structure of Vitronectin adapted from [127].

Figure 5. uPAR expression patterns in neuroblastic tumors using the antibody (ab218106,1:500 abcam).

Figure 6. PAI-1 expression patterns in neuroblastic tumors using the antibody (ab125687, 1:200, abcam).

Figure 7. Kaplan Meier curves showing the relation among the PAI-1 expression patterns in neuroblastic tumors and EFS.

Figure 8. α_vB_3 integrin expression patterns in neuroblastic tumors using (ab7166, 1:50, abcam).

Figure 9. Histopathological NB image of A) VN, B) $\alpha_v\beta_3$ integrin, C) CD68 marker for macrophages and D) CD45 marker to detect lymphoid cells

Figure 10. Immunohistochemical stained images for VN and their ligands belonged to the same NB biopsy.

Figure 11. Summary representation of the main associations between VN morphometric features and the INRG parameters.

Figure 12. Distribution of the amount of VN using IPP software depending on the INRG clinical and biological variables.

Figure 13. Distribution of the amount of VN, using DensitoQ. software depending on the INRG clinical and biological variables

Figure 14. Kaplan Meier curves of the categories from each variable that constitute models of morphological ECM patterns associated with the prognosis (EFS).

Figure 15. Kaplan Meier curves of the categories from each variable that constitute models of morphological ECM patterns associated with the prognosis (OS).

Figure 16. Graphs of the best predict variables associated to A) tumor genetic instability and B) risk stratification in NB patients.

Figure 17. Examples of VN and receptors expression in 2D NB models.

Figure 18. Bar diagramas of percentage (%) tumor growth rate in the MNA-derived xenografts.

Figure 19. Bar diagramas ofpercentage (%) tumor growth rate in the MNNA-derived xenografts.

Figure 20. Tumor growth curves.

Figure 21. Representative tumor masses (*) and HE stain images of MNA-derived xenografts.

Figure 22. Histological sections of different stains of TME elements in MNA-derived xenografts

Figure 23. Histological sections of different stains of TME elements in MNNA-derived xenografts.

Figure 24.uPAR expression in MNA and MNNA-derived xenografts according to their aggrupation in passages.

Figure 25. $\alpha_v\beta_3$ integrin expression in MNA and MNNA-derived xenografts according to their aggrupation in passages.

Figure 26. Reticulin fibers amount in MNA and MNNA-derived xenografts according to their aggrupation in passages.

Figure 27. Collagen type I fibers distribution in MNA and MNNA-derived xenografts according to their aggrupation in passages.

Figure 28. GAGs distribution in MNA and MNNA-derived xenografts according to their aggrupation in passages.

Figure 29. Lymph vessels distribution in MNA and MNNA-derived xenografts according to their aggrupation in passages.

Figure 30. New generation sequencing NB-mechanopanel.

Figure 31. Schematic representation of the chromosomal aberrations detected by aSNP in some of the samples derived from SK-N-BE (2) cell line

Figure 32. Schematic representation of the chromosomal aberrations detected by aSNP in some of the samples derived from SH-SY5Y cell line.

Tables index

Table 1. INRG pre-treatment classification system, established by consensus in 2009 [32].

Tables 2 and 3. Descriptor**s** of the clinical and genetic data regarding OS and EFS, respectively.

Table 4.p-values resulting of the Kaplan Meier test comparing INRG variables with EFS and OS.

Table 5. Results of the correlation between the morphometric data obtained after two algorithm customization in different softwares**.**

Table 6. Correlation between the subjective scoring and the morphometric data. The mean % of stained area is shown.

Table 7. Variables that compond models of morphometric patterns.

Table 8. Descriptive data for each analyzed element according to patient outcome.

Table 9. Cox regression of the morphometric categories of ECM elements.

Table 10. Cox Regression of the morphometric categories and INRG prognostic factors.

Table 11. Summary of NB cell lines.

Table 12. Summary of VN, uPAR, $\alpha_v\beta_3$ integrin, PAI-1 expression in NB cell lines.

Table 13. Description of data and p-valuues related to metasatasis and adjacent implant presence in MNA and MNNA-derived xenografts.

Table 14. Description of data and p-values related to % of neuroblastic cells in MNA and MNNA-derived xenografts.

Table 15. Description of data and p-values related to % of necrosis in MNA and MNNA-derived xenografts.

Table 16. Description of data and p-values related to % of hemorrhagic areas in MNA and MNNA-derivedxenografts.

Summary

Neuroblastoma is an embryonic tumor of the sympathetic nervous system which accounts for 15% of childhood cancer-related deaths. It is characterized by a wide spectrum of clinical behaviors derived from its great heterogeneity in clinical presentation and biological and genetic traits. Pre-treatment risk classification plays a central role in improving survival in these patients, however, yet the high-risk patient subgroup continues to have a particularly high mortality rate, highlighting a need to identify and validate new therapies, preclinical models and markers of therapeutic response. For this reason, it is crucial to keep in mind the concept that a tumor is a functional and interconnected tissue, where tumor cells proliferate uncontrollably in a dependent relationship with tumor macro and microenvironment, thus establishing a continuous and reciprocal dialogue through signaling, which is essential for survival and invasion. The biological complexity of neuroblastoma, clearly justifies the increasing use of quantitative studies to gain greater knowledge of biotensegrity, mechanotransduction, architecture, topology and interaction of its elements.

We hypothesize that tension signals transferred from the extracellular matrix to tumor cells influence growth, differentiation and migration of these cells, necessitating the use of different approaches to search for targets at the contact points between these elements. The arrangement of patterns derived from morphometric and topological analysis in human tumor samples, as well as those derived from *in vitro* and *in vivo* models, and their relationship with the impact of known clinical and biological prognostic factors, may improve survival in patients affected by neuroblastoma, especially those considered high risk.

The general aim of this research is to demonstrate that the vitronectin present in the neuroblastoma tumor microenvironment is a crucial connector within the elements of the extracellular matrix, modulating physical and chemical signaling between tumor cells and their surrounding elements to facilitate migration.

The specific objectives of the study in human neuroblastoma tumor samples are: a) morphometric and topological characterization of vitronectin expression through the design of various algorithms; b) correlating expression of vitronectin and its ligands with patient clinical features and other tumor biological characteristics with known prognostic value, to determine the histological patterns of vitronectin with different degrees of malignancy; and c) associating vitronectin expression and distribution with other tumor biotensegral elements such as reticular

fibers, type I collagen, glycosaminoglycans, blood/lymphatic vessels and immune cells, to establish a pattern of aggressive biotensegral extracellular matrix.

The specific objectives of neuroblastoma cell lines study are: a) identification and characterization of vitronectin and its binding ligands such as $\alpha_v\beta_3$ integrin, uPAR, and PAI-1; and b) establishing vitronectin and binding ligands patterns of neuroblastoma cell lines compared to human neuroblastoma samples.

The defined study aims of the *in vivo* neuroblastoma models are to: a) generate orthotopic tumor xenografts in vitronectin-deficient and immunodeficient mice using the initial inoculation of neuroblastoma cell lines and the subsequent implantation of their tumor fragments, to determine their clinical-biological homology with high-risk neuroblastoma patients; b) characterize various elements of the tumor microenvironment such as vitronectin and its ligands, reticular fibers, type I collagen fibers, glycosaminoglycans, blood and lymphatic vessels, to determine histological patterns in this model; and c) describe the genetic characteristics of the tumors obtained to uncover the impact of extracellular matrix properties on the genomic heterogeneity of neuroblastoma, particularly the contribution of vitronectin as an element of the tumor macroenvironment.

The present doctoral thesis is presented as a compendium of three publications and newly obtained related data providing insight into the mechanical interactions of neuroblastic cells and the extracellular elements that surround them, considering vitronectin adhesion glycoprotein as a key contact point to facilitate migration. The following articles make up this compendium:

I. The tumor microenvironment as an integrated framework to understand cancer biology. Burgos-Panadero R*, Lucantoni F*, Gamero-Sandemetrio E, Cruz-Merino L, Álvaro T, Noguera R Cancer Lett. 2019. 1; 461:112-122. 5-year impact factor: 6.232.

The purpose of this review is to emphasize the importance of identifying biomarkers that capture interactions occuring in the tumor microenvironment and that are related to the tumor aggressiveness, patient prognosis, and treatment response. A key highlight of the present work is the proposed classification of the tumor stroma into three grades, associated with clinical and therapeutic involvement, based primarily on data derived from neuroblastoma studies.

II. Vitronectin as a molecular player of the tumor microenvironment in neuroblastoma. Burgos-Panadero R, Noguera I, Cañete A, Navarro S, Noguera R BMC Cancer. 2019. 22;19(1):479. 5-year impact factor: 3.424

The objective of this study is to characterize vitronectin as an extracellular matrix target molecule, in a cohort of neuroblastic tumors chosen by genetic instability criteria. The initial study in *in vitro* and *in vivo* models of the vitronectin protein and its ligands associated with known clinical-biological prognostic factors has been expanded over a greater time period.

III. The topology of vitronectin: A complementary feature for neuroblastoma risk classification based on computer-aided detection.
Vicente-Munuera P*, Burgos-Panadero R*, Noguera I, Navarro S, Noguera R, Escudero LM. Int J Cancer. 2020 Jan 15; 146(2):553-565. 5-year impact factor: 6.210.

The goal of this research is to detect vitronectin distribution patterns in the tumor stroma that reflect neuroblastic cell behavior in a cohort of neuroblastoma tumors at the time of diagnosis chosen by criteria of genetic instability. Our discussion focuses on the comparative analysis between non-topological and topological characteristics and their association with aggressive tumor behavior.

After applying multidisciplinary approaches used in our studies, fundamentally image analysis techniques from patient tumor samples complemented by preclinical models, we conclude that it is both possible and useful to characterize the stromal and parenchymal architecture of tumors to advance understanding of new therapeutic targets, while also promoting collaboration strategies and suitable clinical trial proposals.

Resumen

El neuroblastoma es un tumor embrionario del sistema nervioso simpático que representa el 15% de las muertes relacionadas con cáncer en la infancia. Se caracteriza por un amplio espectro de comportamientos clínicos derivados de su gran heterogeneidad en la presentación clínica y en los rasgos biológicos y genéticos. La clasificación de riesgo pre-tratamiento desempeña un papel central en la mejora de la supervivencia en estos pacientes, sin embargo, el subgrupo de pacientes de alto riesgo continúa teniendo una tasa de mortalidad particularmente alta, destacando la necesidad de identificar y validar nuevas terapias, modelos preclínicos y marcadores de respuesta terapéutica. Por este motivo, es crucial tener en cuenta el concepto de que un tumor es un tejido funcional e interconectado, donde las células tumorales proliferan sin control en una relación dependiente del macro-microambiente tumoral, estableciendo así un diálogo continuo y recíproco a través de la transmisión de señales que es esencial para la supervivencia e invasión. La complejidad biológica del neuroblastoma justifica claramente el uso cada vez mayor de estudios cuantitativos para obtener un mayor conocimiento de la biotensegridad, mecanotransducción, arquitectura, topología e interacción de sus elementos.

Nuestra hipótesis es que las señales de tensión transferidas de la matriz extracelular a las células tumorales influyen en el crecimiento, diferenciación y migración de estas células, lo que exige el uso de diferentes enfoques para buscar dianas en los puntos de contacto entre estos elementos. La disposición de los patrones derivados del análisis morfométrico y topológico de muestras tumorales humanas, así como los derivados de modelos *in vitro* e *in vivo*, asociándolos con el impacto de factores pronósticos clínicos y biológicos conocidos, pueden mejorar la supervivencia en pacientes afectados por neuroblastoma, especialmente aquellos considerados de alto riesgo.

El objetivo general de esta investigación es demostrar que la vitronectina presente en el microambiente tumoral del neuroblastoma es un conector crucial dentro de los elementos de la matriz extracelular, modulando las señales físicas y químicas entre las células tumorales y sus elementos circundantes para facilitar la migración.

Los objetivos específicos de estudio en muestras de tumor de neuroblastoma humano son: a) caracterización morfométrica y topológica de la expresión de vitronectina a través del diseño de varios algoritmos; b) la correlación de la expresión de vitronectina y sus ligandos con las características clínicas de los pacientes y otras características biológicas del tumor con valor pronóstico conocido, para determinar los patrones histológicos de vitronectina con diferentes

grados de malignidad; y c) la asociación de la expresión y distribución de vitronectina con otros elementos biotensegrales tumorales tales como: fibras de reticulina, colágeno tipo I, glucosaminoglucanos, vasos sanguíneos/linfáticos y células inmunes, para establecer un patrón de matriz extracelular biotensegral agresivo.

Los objetivos específicos del estudio en líneas celulares de neuroblastoma son: a) identificación y caracterización de vitronectina y sus ligandos de unión tales como: integrina $\alpha_v\beta_3$, uPAR y PAI-1; y b) el establecimiento de los patrones de vitronectina y sus ligandos de unión en líneas celulares de neuroblastoma en comparación con muestras de neuroblastoma humano.

Los objetivos definidos de estudio en los modelos *in vivo* de neuroblastoma son: a) generar xenoinjertos de tumor ortotópico en ratones inmunodeficientes y con deficiencia de vitronectina, utilizando la inoculación inicial de líneas celulares de neuroblastoma y la implantación posterior de sus fragmentos tumorales, para determinar su homología clínico-biológica con pacientes con neuroblastoma de alto riesgo; b) la caracterización de varios elementos del microambiente tumoral, como la vitronectina y sus ligandos, fibras reticulares, fibras de colágeno tipo I, glucosaminoglucanos, vasos sanguíneos y linfáticos, para determinar los patrones histológicos en este modelo; y c) describir las características genéticas de los tumores obtenidos para conocer el impacto de las propiedades de la matriz extracelular en la heterogeneidad genómica del neuroblastoma, particularmente la contribución de la vitronectina como elemento del macroambiente tumoral.

La presente tesis doctoral se presenta como un compendio de tres publicaciones y datos relacionados, recientemente obtenidos, que proporcionan información sobre las interacciones mecánicas de las células neuroblásticas y los elementos extracelulares que las rodean, considerando la glucoproteína de adhesión, vitronectina, como un punto de contacto clave para facilitar la migración. Los artículos que constituyen el compendio son los siguientes:

I. The tumour microenvironment as an integrated framework to understand cancer biology. Burgos-Panadero R*, Lucantoni F*, Gamero-Sandemetrio E, Cruz-Merino L, Álvaro T, Noguera R Cancer Lett. 2019. 1; 461:112-122. Factor de impacto a 5 años: 6.232.

El objetivo de esta revisión es enfatizar la importancia de identificar biomarcadores que capturen las interacciones que ocurren en el microambiente tumoral y que estén relacionados con la agresividad del tumor, el pronóstico del paciente y la respuesta al tratamiento. El punto esencial en el presente trabajo, es la clasificación propuesta del estroma tumoral en tres grados,

asociada con la implicación clínica y terapéutica, basada fundamentalmente en datos derivados de los estudios en neuroblastoma.

II. Vitronectin as a molecular player of the tumor microenvironment in neuroblastoma. Burgos-Panadero R, Noguera I, Cañete A, Navarro S, Noguera R BMC Cancer. 2019. 22;19(1):479. Factor de impacto a 5 años: 3.424

El propósito de este estudio es caracterizar la vitronectina, como una molécula diana de la matriz extracelular, en una cohorte de tumores neuroblásticos elegidos por criterios de inestabilidad genética. El estudio inicial en modelos *in vitro* e *in vivo* de la proteína vitronectina y sus ligandos asociado con factores clínico-biológicos pronósticos conocidos, se ha ampliado durante un mayor período de tiempo.

III. The topology of vitronectin: A complementary feature for neuroblastoma risk classification based on computer-aided detection. Vicente-Munuera P*, Burgos-Panadero R*, Noguera I, Navarro S, Noguera R, Escudero LM. Int J Cancer. 2020 Jan 15; 146(2):553-565. Factor de impacto a 5 años: 6.210

El objetivo de esta investigación es detectar patrones de distribución de vitronectina en el estroma tumoral que reflejen el comportamiento de las células neuroblásticas en una cohorte de tumores de neuroblastoma en el momento del diagnóstico, elegido por criterios de inestabilidad genética. Nuestra discusión se centra en el análisis comparativo entre características no topológicas y topológicas, así como su asociación con el comportamiento tumoral agresivo.

Después de aplicar enfoques multidisciplinares utilizados en nuestros estudios, fundamentalmente técnicas de análisis de imagen en muestras tumorales de pacientes complementadas con modelos preclínicos, concluimos que es posible y útil caracterizar la arquitectura estromal y parenquimal de los tumores para avanzar en la comprensión de nuevas dianas terapéuticas, promoviendo a su vez estrategias de colaboración y propuestas de ensayos clínicos adecuadas.

Abbreviations

ALK: Anaplastic lymphoma kinase

CAFs: Cancer-associated fibroblasts

CAR: Chimeric antigen receptors

CDX: Cell-line-derived xenografts

COG: Children´s oncology group

D: Deletion

dNB: Differentiating neuroblastoma

DCs: Dendritic cells

ECM: Extracellular matrix

EFS: Event-free survival

EGF: Epidermal growth factor

EMT: Epithelial-mesenchymal transition

FAP: Fibroblast activation protein

FDA: Food and Drug Administration

FN: Fibronectin

GAGs: Glycosaminoglycans

GEMM: Genetically engineered mouse models

GN: Ganglioneuroma

GPs: Glycoproteins

HE: Hematoxylin-eosin

HR: High-risk

HetMNA: Heterogeneous MNA

iGNB: Intermixed ganglioneuroblastoma

IL: Interleukin

INPC: International Neuroblastoma Pathology Classification

INRG: International Neuroblastoma Risk Group

INRGSS: International Neuroblastoma Risk Group Staging System

LN: Laminin

LOX: Lysyl oxidase

M: metastatic stage

MS: special metastatic stage

MKI: Mitosis-Karyorrhexis Index

MNA: *MYCN* amplification

MNNA: *MYCN* non-amplified

MMPs: Metalloproteinases

nGNB: Nodular (ganglioneuroblastoma)

NB: Neuroblastoma

NCA: Numerical chromosome aberration

NK: Natural killer

OS: Overall survival

pdNB: Poorly differentiated neuroblastoma

PDGF-B: Platelet-derived growth factor

PDOs: Patient-derived organoids

PDX: Patient derived xenografts

PEG: Polyethylene glycol

PGs: Proteoglycans

PHOX2B: Paired-like homeobox 2B

RGD: Arginine-glycine-aspartic acid

SCA: Segmental chromosome aberration

SIOPEN: Society of Paediatric Oncology Europe Neuroblastoma

aSNP: Single nucleotide polymorphisms array

TAMs: Tumor-associated macrophages

TGF: Transforming growth factor

TILs: Tumor infiltrating lymphocytes

TMA: Tissue microarray

TME: Tumor microenvironment or niche

TN: Tenascin

Treg: T regulatory

TSP: Thrombospondin

uNB: Undifferentiated neuroblastoma

VEGF: Vascular endothelial growth factor

VM: Vascular mimicry

VN: Vitronectin

Compendium of articles that support this thesis

This thesis is based on three publications as a compendium in which the candidate is the first author or first co-author. Full text of the publications is shown below.

I. The tumour microenvironment as an integrated framework to understand cancer biology. **Burgos-Panadero R***, Lucantoni F*, Gamero-Sandemetrio E, Cruz-Merino L, Álvaro T, Noguera R Cancer Lett. 2019. 1; 461:112-122.

II. Vitronectin as a molecular player of the tumor microenvironment in neuroblastoma. **Burgos-Panadero R**, Noguera I, Cañete A, Navarro S, Noguera R BMC Cancer. 2019. 22;19(1):479.

III. The topology of vitronectin: A complementary feature for neuroblastoma risk classification based on computer-aided detection. Vicente-Munuera P*, **Burgos-Panadero R***, Noguera I, Navarro S, Noguera R, Escudero LM. Int J Cancer. 2020 Jan 15; 146(2):553-565.

The asterisk (*) indicates equal contribution.

Article I: The tumour microenvironment as an integrated framework to understand cancer biology

Burgos-Panadero R*, Lucantoni F*, Gamero-Sandemetrio E, Cruz-Merino L, Álvaro T, Noguera R.

*Equal colaboration

ARTICLE I

Cancer Lett. 2019. 1; 461:112-122. doi: 10.1016/j.canlet.2019.07.010.

ELSEVIER IRELAND LTD, ISSN: 1872-7980

Impact factor 2018: 6.508

5-year impact factor: 6.232

Cancer Letters 461 (2019) 112–122

Contents lists available at ScienceDirect

Cancer Letters

journal homepage: www.elsevier.com/locate/canlet

Mini-review

The tumour microenvironment as an integrated framework to understand ⊤ cancer biology ☆

Rebeca Burgos-Panadero[a,b,1], Federico Lucantoni[a,1], Esther Gamero-Sandemetrio[a,b], Luis de la Cruz-Merino[c], Tomás Álvaro[b,d,**], Rosa Noguera[a,b,*]

[a] Departament of Pathology, Medical School, University of Valencia - INCLIVA Biomedical Health Research Institute, Valencia, Spain
[b] CIBERONC, Madrid, Spain
[c] Departament of Oncology, Hospital Universitario Virgen Macarena, Sevilla, Spain
[d] Hospital Verge de la Cinta, Tortosa, Tarragona, Spain

ARTICLE INFO

Keywords:
Biophysics
Bioelectric
Metabolism
Cancer treatment
Extracellular matrix
Stromal classification

ABSTRACT

Cancer cells all share the feature of being immersed in a complex environment with altered cell-cell/cell-ex-tracellular element communication, physicochemical information, and tissue functions. The so-called tumour microenvironment (TME) is becoming recognised as a key factor in the genesis, progression and treatment of cancer lesions. Beyond genetic mutations, the existence of a malignant microenvironment forms the basis for a new perspective in cancer biology where connections at the system level are fundamental. From this standpoint, different aspects of tumour lesions such as morphology, aggressiveness, prognosis and treatment response can be considered under an integrated vision, giving rise to a new field of study and clinical management. Nowadays, somatic mutation theory is complemented with study of TME components such as the extracellular matrix, immune compartment, stromal cells, metabolism and biophysical forces. In this review we examine recent studies in this area and complement them with our own research data to propose a classification of stromal changes. Exploring these avenues and gaining insight into malignant phenotype remodelling, could reveal better ways to characterize this disease and its potential treatment.

1. Introduction

Cancer remains a major public health threat and one of the leading causes of death worldwide. Great effort has been invested into char-acterising and understanding this disease at a cellular, molecular and clinical level, and many achievements in the field have helped shape the therapies in use nowadays. However, most conventional che-motherapeutic drugs developed so far display only a narrow therapeutic window, due to their inability to distinguish cancerous from normal cells [89]. Developing new therapies against cancer often starts with use of non-physiological models of the disease such as cell mono-cultures, with no contribution from extracellular matrix (ECM) components. Unsurprisingly, this has meant that observations on cellular network functions do not translate readily into in vivo models. This reductionist approach hinders attempts to turn novel interventions to correct dysfunctional cellular behaviour into effective therapies that can be successfully translated to the clinic.

The majority of solid tumours have complex three-dimensional (3D) architecture, comprising different populations of abnormal cells divided into parenchymal and stromal compartments. The ECM that constitutes the stroma has a complex composition and is rich in growth factors and metabolites [20,33,100,140,144]. Communication between cancer cells and their surroundings contributes to changes and a high degree of heterogeneity at the phenotypic and genotypic level. Integrating the stromal components with the immune system, the non-cancerous niche and the consequent interplay of metabolic pathways sheds a different light on our understanding of cancer properties. This integrated view, termed the tumour microenvironment (TME), has modified our vision

Abbreviations: ECM, Extracellular matrix; TME, tumour microenvironment; PG, proteoglycans; GAG, glycosaminoglycans; GP, glycoproteins; TAM, tumour-asso-ciated macrophages; TANs, tumour-associated neutrophils; CAF, cancer associated fibroblast; CSC, cancer stem cells; OXPHOS, oxidative phosphorylation; EMT, epithelial-mesenchymal transition

* Corresponding author. Department of Pathology, Medical School, University of Valencia-INCLIVA, Valencia, Spain.
** Corresponding author. Hospital Verge de la Cinta, Tarragona, Spain.
E-mail addresses: talvaro.ebre.ics@gencat.cat (T. Álvaro), rnoguera@uv.es (R. Noguera).
[1] Authors contributed equally.

https://doi.org/10.1016/j.canlet.2019.07.010
Received 29 May 2019; Received in revised form 11 July 2019; Accepted 14 July 2019

of cancer towards a phenomenon that develops via cellular cooperation, moving away from a purely gene-centric framework [13].
The architectural role of ECM components is clear and central to tissue homeostasis [138]. In fact, scaffold architecture has been found to have a significant impact on cell growth [91]. Anomalous cell-mi-croenvironment interaction results in an aberrant cellular networks. The interaction between physical and chemical properties establishes a dynamic reciprocity between neoplastic cells, stromal cells, micro-vascularization, innervation, ECM scaffolding, bioelectric fields and soluble factors of tumour growth control [50]. In this review we highlight how different biological phenomena drive the development of the TME and consequently tumour malignancies. Providing an in-tegrated perspective of the different components of the TME might yield insights into cancer as a whole.

2. The TME niche

The ECM is composed of soluble factors and a network of biopo-lymer fibres of proteins, proteoglycans (PG), glycosaminoglycans (GAG) and glycoproteins (GP), that differ in composition and structure according to the organ and tissue [42]. The size and density of the fibre network determine mechanical properties, as well as morphology, porosity and size of the mesh. The spatial organisation of this network provides a mode of communication thanks to its elasticity, which de-pends on the intricate biophysical properties of its components, and provides movement and contraction to the matrix [118]. ECM rigidity, which depends on the presence of the molecular elements mentioned above with the consequent pore size, viscoelasticity, cross-linking, cellular density and interstitial pressure, influences the reprogramming of the tumour cell [101]. Additionally, electrical charges carried by protein elements such as collagen have a powerful impact on the function and diffusion of substances and stimuli transmission [83]. PGs, which are glycosylated proteins with covalently attached highly anionic GAG, contribute to tissue hydration and swelling pressure, and allow it to tolerate compression forces [86]. Fibrous proteins of the ECM in-clude collagen, elastin, fibronectin, vitronectin and laminin among other elements [42]. Collagen provides the principal structural com-ponent of the ECM and is the most abundant protein in the human body [70]. Elastin cooperates with collagen and confers elasticity to tissues

[84]. GPs have a similar fibril organisation to collagen and are bound to integrins, mediating cell processes such as cell adhesion [42]. Immersed in the ECM are the blood and lymphatic vessels and the stromal cells that synthesize the matrix and facilitate the immune response. Neoan-giogenesis in particular determines blood and lymphatic flow, oxygen and nutrient supply, interstitial pH and the bioelectrical and metabolic state of the tumour [131]. Intriguingly, the TME is also permeated by nerves, which have been shown to have an impact on cancer develop-ment [62].

The TME is infiltrated with a number of different cells that con-tribute to the progression of malignancy, enabling some cancer hall-marks [50]. Among the inflammatory cells of TME, tumour-associated macrophages (TAM) represent the most abundant population of in-filtrating cells and participate in both antitumor control (M1 pheno-type) and in malignant progression (M2 phenotype) [46], promoting vascularization, invasion, growth, cancer cell survival and im-munosuppression [149]. Indeed, it has recently been found that in-creased levels of $CD163^+$ TAM at the invasive front are indicative of poor prognosis and are responsible for releasing mesenchymal circu-lating tumour cells [143]. Throughout tumour progression, tumour-associated neutrophils (TANs) change from an antitumor function to a pro-tumorigenic phenotype, under the influence of the TME [49,105]. Conversely, T and B lymphocytes are also found within the TME and correlate with good prognosis [8]. Another cell type abundant in the stroma which has antitumor to pro-tumour switching properties is the fibroblast; cancer associated fibroblast (CAF) modifies the TME by se-creting ECM remodelling enzymes [3]. Finally, cancer stem cells (CSC) represent the source of heterogeneity in the tumour, the reason for resistance to chemotherapy and the origin of distant metastasis [27]. The inflammatory TME is a determinant of CSC and both are tightly linked [156].

2.1. Biophysical interactions in the TME

The mechanical properties and the bioelectric signals of the tumour stroma determine cellular, biological and clinical behaviour.

2.1.1. Stiffness of the ECM

One classic characteristic of tumours is stromal stiffness, which al-lows cancer detection through palpation or radiological examination and is associated with altered ECM profile in the TME [44]. Indeed, increased ECM protein deposition can be employed as a prognostic factor [58,78,135,136]. On a similar note, previous studies from our group highlighted that ECM composition and architecture can define an ultra-high-risk patient subgroup with 5-year survival rate < 15% in neuroblastoma [130]. Additionally, neuroblastoma patients with poor prognosis possess a reticular and poorly porous ECM [132]. Stiffness has been shown to increase from healthy to malignant tissues, together with fibrosis, and to be accompanied by chemo-resistance [111]. This increase in matrix stiffness reduces the elastic modulus and the 3D environment affects cell rheology [7]. Cancer cells have shown in-creased proliferation in a softer matrix that could be linked to the initial growth of a tumour lesion, before the development of tumour vascu-lature [26]. Likewise, during the invasion process, cancer cells showed increased intracellular viscosity, suggesting a mechanism that could facilitate cell motility in a dense matrix [147].

Increased tumour stiffness depends not only on the amount and organization of the fibrous elements and other components of the ECM but also on increased interstitial fluid pressure [122]. These elements, together with the stromal cellular infiltrate, determine phenotypic di-versity, gene expression and the therapeutic response of cancer cells [4,47]. Physical stimulus of the tissue has a significant effect on the chemical signals of the tumour cell, which is able to perceive the me-chanics of the substrate and transduce this information to the molecular signalling pathways [47]. The rigidity of the matrix profoundly influ-ences cellular morphology and behaviour and vice versa [66,121]. In-deed, it has been found that pancreatic stellate cell activation and durotactic response depends on the stiffness of the substrate [72]. Further investigation has linked the retinoic acid receptor to mechan-osensing response process [36].

Intracellular signalling in response to the mechanics of the TME mainly uses the integrin family and affects cancer gene expression, showing how tissue mechanics affect carcinogenesis [120]. In this context, it has been proposed that actin binds to integrin β3 by com-peting with talin protein; once this happens and mature adhesion has been established, forces are transmitted to the ECM thereby activating downstream signalling [112]. Partial inhibition of integrin results in a softer intracellular state [7] and revert tumour phenotype [108]. Me-chanosensing of the TME also depends on focal adhesion proteins whose signalling cascades promote changes in tumorigenicity [66]. The same pathways modulate compression forces, as cancer cells are often subjected to mechanical deformation during proliferation [131].

2.1.2. Bioelectric TME

Cells are able to generate and receive biological information in the form of bioelectric signals [34]. Cellular membranes provide an anchor for ion channels and protein pumps; through these avenues, cells can establish action potentials and depolarisation levels throughout the human body. Membrane potential develops a bioelectric field that en-ables cell-cell and cell-tissue communication. Tissues undergoing pro-liferation possess a positive charge when compared to quiescent cells [1]. Indeed, when negative charges are induced experimentally, cellular proliferation is inhibited [76]. Temporal variations in the membrane

potential exert a fundamental impact on cell cycle progression: cells become hyperpolarised before S phase and depolarise during mitosis, while G1 and G2 phases fluctuate between the two conditions [150]. The cyclic behaviour of the membrane potential during cell cycle can be linked to the dynamic properties of the cellular microenvironment [14]. Bioelectric gradients form an important part of the morphogenetic in-formation transmitted to structural tissue organisation to coordinate cell-cell interaction [28]. A quiescent non-transformed cell can modify its voltage threshold when switching to proliferative or malignant phenotype [1]. A negative membrane potential allows passive Ca^{2+} influx through specific ion channels, with an increase in actin poly-merisation, myosin contraction and adhesion decrease [88]. The re-pulsion of Ca^{2+} to the anodal side of the cell, mediated by the voltage-gated Na^{+} channel, causes asymmetry in Ca^{2+} concentration, resulting in actin polymerisation and myosin contraction [19].

Negative charges contract the cytoskeleton and deploy a tensional force with a determined directional and migratory vector. In this con-text, ions fluxes have been found to drive cell migration and metastasis initiation in several types of cancer [119]. Cancer cells are affected by several transcriptional changes that are activated by membrane po-tential depolarisation, such as motility regulation induced by serotonin, Ca^{2+} and inositol triphosphate fluxes through gap junctions [126]. Membrane depolarisation also triggers the process of metastasis which is mediated by the transcriptional and epigenetic dynamics induced by serotonin and butyrate fluxes coupled with electrical changes [79]. Moreover, forced hyperpolarization has been found to inhibit the for-mation of induced tumour structures, even in cells distant from the tumour site [35].

Ion channels, protein pumps and gap junctions are part of the on-cogene family [9] and are considered predictive biomarkers [106], supporting a more integrated vision of cancer development, where the TME, rather than the mutation of single specific genes, is fundamental in establishing carcinogenesis. Indeed, a recent study highlighted that biopotential levels are significantly different in cancerous tissue to paired non-malignant tissue; this characteristic was shown to be influ-enced by ECM stiffness, and high biopotential values correlated with advanced epithelial ovarian cancer stage [31]. Emerging theories view cancer as a coherent subsystem with the ability to control information exchange with the surrounding environment [125]. Thus, tumour le-sions gain independence by creating primitive morphogenetic fields such the one observed in the histopathological structure of a metastasis. Indeed, cancer cells can “prime” the environment at a distal site in order to set the foundation for metastasis establishment in the pre-metastatic niche [97]. Endogenous membrane potentials make up the bioelectric TME, an important element with the ability to increase or normalise malignancy [75]. In this scenario, the bioelectric code ap-plied to the reprogramming of cancer-TME interaction constitutes a malignant phenotype that can be used to develop new treatments to inhibit cancer membrane potential [74].

2.2. Role of metabolism in TME interaction

The physiological complexity of the TME and the 3D cellular or-ganization of a tumour also depends on existing metabolic differences. Varying oxygen, nutrient and waste diffusion gradients develop within the cancer tissue and contribute to its pathogenesis [24,73]. These gradients shape the TME and generate subcellular cancer populations with different gene expression patterns (Fig. 1) [29].

Altered metabolism is an emerging hallmark of cancer, proving es-sential to a diverse range of cellular properties in malignant lesions [51]. As a result of poor or aberrant vascularisation, cancers have limited access to oxygen and nutrients [104]. Thus, tumour cells can use a diverse range of nutrients to fuel proliferation, invasion and treatment resistance [139]. Furthermore, cancer metabolism has a high degree of plasticity, as malignant cells can switch from different sources to obtain the energy needed [87]. TME stiffness exacerbates the harsh

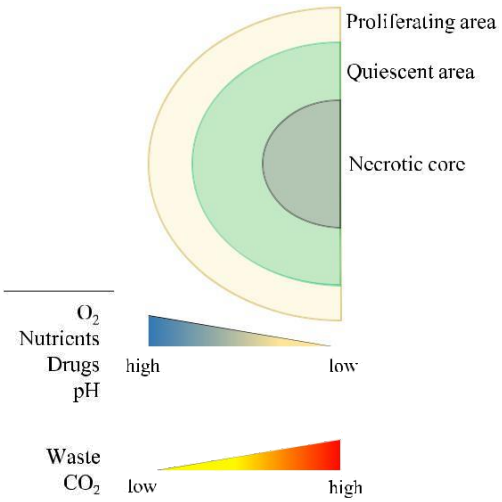

Fig. 1. Tumour architecture in relation to extracellular gradients. Most solid tumours are organized in 3D structures made up of a central core with a high prevalence of necrotic cells, a quiescent area with tumour cells in G0 phase, and an external area with cells undergoing proliferation. As a con-sequence of this multicellular environment and the presence of an external ECM, a set of gradients are established. Typically O2, nutrients, pH and drugs are mostly concentrated at the outer zones, while their concentration decreases as they diffuse inside the tumour mass. On the other hand, waste and CO2 are highly concentrated inside the tumour mass, while outer cells can easily diffuse them in the surrounding TME.

environment for these cells; the extensive fibrosis produced by the ac-cumulation of ECM proteins increases interstitial pressure and the content of macromolecules, which contributes towards sustaining cancer cells by recycling these cellular elements [41]. This is particu-larly evident in pancreatic cancer, where glucose and glutamine are comparatively low and amino acids are scavenged from extracellular proteins such as albumin [37,68]. A similar process occurs in breast cancer, where stromal cells deposit large amounts of ECM proteins, which sustain metabolism and metastasis initiation [59].

A higher glycolytic rate is a prominent feature of cancer, due to defective oxidative phosphorylation (OXPHOS) and limited oxygen availability: a phaenomenon called Warburg's effect [77]. While this is a widely accepted process, an emerging idea termed “reverse Warburg effect” has flourished. In this scenario, CAFs are metabolically impaired by H_20_2 produced by cancer cells, with the consequent switch to aerobic glycolysis and the synthesis of metabolites such as lactate, pyruvate, ketone bodies and fatty acids. These nutrients are employed by tumour cells through active OXPHOS [6,17,95,99,124,145]. Cancer cells internalise the lactate which in turn modify NAD+/NADH ratio and increase mitochondrial mass and activity, resulting in Krebs cycle deregulation and accumulation of oncometabolites [57]. There is a high degree of variability between different cancers in estimated levels of ATP production through glycolysis or OXPHOS [159]. The switch be-tween OXPHOS and glycolysis is a key process in immune cell activa-tion in the TME. Quiescent T cells use fatty acid oxidation and gluta-mine and move towards glycolysis when activated [5].

Fatty acids are also required for a rapid cell division process and are in high demand among cancer cells to support their survival [2]. It has been found that hypoxic and Ras-driven cancer cells scavenge fatty acid from the TME as they possess reduced fatty acid biogenesis [67]. Fur-thermore, adipocytes are abundant in the TME [93] and sustain cancer progression and metabolism [92,148,155]. Another example of com-munication between components of the stroma and cancer cells has been described in leukaemia, where adipose tissue stimulates lipolysis in malignancies and protects against chemotherapy [151].

An aberrant metabolism provides for a set of cancer hallmarks; for example, it can promote epithelial-mesenchymal transition (EMT),

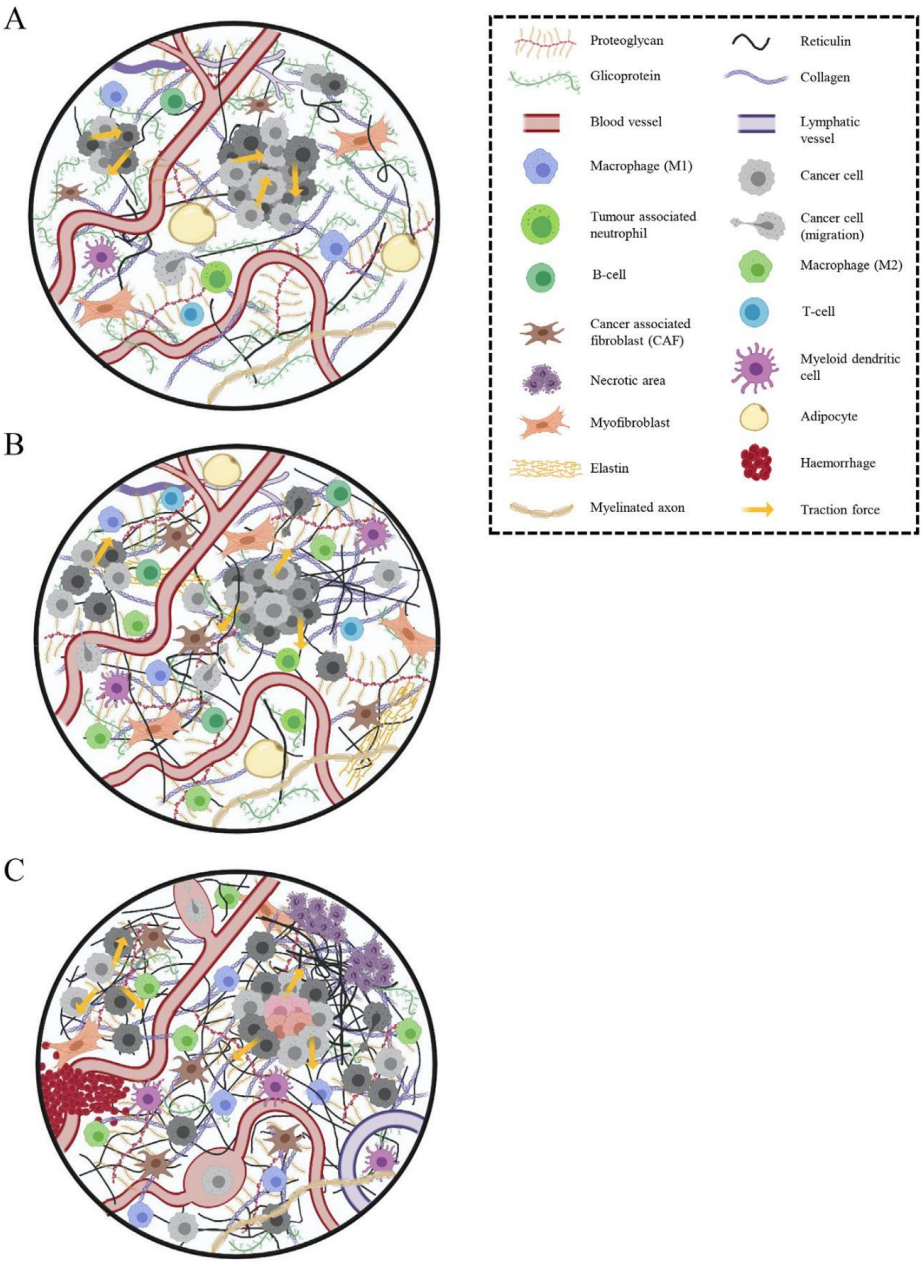

Fig. 2. Stromal alteration grades. Graphical representation of the three proposed levels of stromal alteration. (A) Grade I represents a lax and porous ECM with a low immune response and without modification in the tumoural vasculature system.
(B) In grade II the ECM increases in rigidity and distribution, allowing cancer migration and de-creasing diffusion of therapeutic agents. A moderate immune response is displayed, together with a vasculature system that permits cell migration. (C) Grade III is characterized by a significant increase in rigidity, and as a consequence, augmented cancer migration and heterogeneity with decreased diffu-sion of chemotherapy. A severe immune response is encountered, together with an increase in the vas-culature system which allows blood extravasation, haemorrhage and area of cellular necrosis.

which increases glycolysis through the key EMT regulator Snail [154]. Indeed, glycolysis has been identified as the main metabolic route uti-lised for cell motility [123] and its upregulation is important to main-tain cancer stemness and EMT phenotypes [158]. More importantly, the metabolites and waste gradient produced by cancer cells provide spatial information on vasculature position and modulate cell phenotypes within the TME [25].

3. Stromal alteration grades

Combining the available information with our own findings, the data presented shows how the tumour stroma is progressively trans-formed as the tumour phenotype advances. We propose classifying these changes into the three levels outlined in Fig. 2, according to the intensity of their alteration, clinical and therapeutic implications.

Slight changes in tumour stroma, grade I (Fig. 2A). Good prognosis, associated with early stages of various carcinomas and localized sar-comas. TME elements confer a minimal increase in stromal rigidity that does not stimulate tumour progression and allows diffusion of therapeutic agents. Morphologically, this corresponds to a lax and porous ECM, with few type I collagen fibres and poor reticular fibre cross-linking, high PG and low GP content, and absence of desmoplasia or perineural invasion [21,40,66,132]. Among the ECM elements it is possible to observe numerous CAF (without myofibroblasts), limited numbers of tumour stem cells and a mild inflammatory response, with a low proportion of macrophages. M2 macrophages are not identified, and there is a low to moderate number of T and NK lymphocytes [8]. A network of regular blood capillaries, open lymphatics and collecting vessels that show little or no change in the interstitial pressure of the ECM can be observed [21,128].

Moderate changes in tumour stroma, grade II (Fig. 2B). Uncertain prognosis associated with carcinomas and advanced regional sarcomas. TME elements generate stromal disruption that serves as a cleavage plane for tumour migration and lodges microscopic residual disease. Increased stiffness hinders the diffusion of therapeutic agents. There is incipient desmoplasia and a certain degree of tension due to the in-crease in the content of type I collagen fibres, cross-linking of reticular fibres, decrease in PG and increase in GP content [21,40,132]. CAFs are

found, with occasional myofibroblasts and limited tumour stem cells. There is a variable inflammatory response, characterized by infiltration of type M1 and M2 macrophages, T lymphocytes and natural killers (NK) cells. The vascular system is made up of regular blood capillaries together with tortuous sinusoids, and a moderate presence of small calibre lymphatic capillaries, frequently collapsed due to increased in-terstitial pressure in the ECM [21].

Severe changes in tumour stroma, grade III (Fig. 2C). Poor prognosis associated with various carcinomas, sarcomas, melanomas, lymphomas and neural tumours. Taken together, the TME elements confer an ap-pearance of high tumour heterogeneity, showing a remarkable increase in stromal rigidity, migratory capacity of tumour cells, poor response to treatment and very low diffusion of chemotherapeutic agents [132]. Perineural invasion and desmoplasia are frequently observed, asso-ciated with a rigid ECM due to the cross-linking and increased content of collagen I and reticular fibres, low PG and high GP content, with the presence of CAFs, myofibroblasts, tumour stem cells and a severe in-flammatory response characterized especially by infiltration of M1 and M2 macrophages [107]. The vascular system presents abundant sinu-soids, long and irregular vascular lakes, intermediate lymphatic capil-laries and small collecting vessels [130,133,134]. High interstitial pressure in the ECM leads to frequent blood extravasation areas, hae-morrhage and areas of necrosis.

4. Cancer progression depends on the TME and vice-versa

Previous research examined spatial growth and genetic evolution to model tumour progression, without considering the support provided from the surrounding environment [141]. While TME it is now con-sidered a key player in cancer evolution, there are several concerns that have not been resolved regarding the extent of its contribution.

The impact of the TME in modulating carcinogenesis, tumour de-velopment and progression has been documented by studying the effect of the physiological microenvironment on cancers. Based on this, a non-malignant phenotype could be restored if cancer cells receive adequate signals from a physiological environment rather than a malignant one. Metastatic breast cancer cells were found to behave like “normal” cells when transplanted into a mammary gland microenvironment without forming tumours and contributing to tissue development [22]. Another report highlighted that embryonic stem cell preconditioned micro-environment suppresses breast cancer tumorigenicity through the Stat3 pathway [52]. Exposure of cancer cells to Lefty, a Nodal-signalling in-hibitor secreted from the embryonic microenvironment, reduces their metastatic potential [103]. On a similar note, the embryonic chick microenvironment is able to reprogram the metastatic potential of melanoma cells following a neural fate [71]. Likewise, culturing pri-mary cells from lung tumour resections in in vitro TME-mimetic con-ditions made it possible to efficiently obtain and amplify tumour-as-sociated stromal progenitors which increased tumour malignancy [115].

Mutation and proliferation rates are not the only players in cancer progression: tumour development estimates are also influenced by the differential effect of selection processes on different cancer cell sub-populations. Under these circumstances, adaptive therapy modulated by chemotherapy minimises the competitive advantages between cancer cells to the extent that tumour size is not reduced but rather maintained. Notably, this approach increased therapy efficacy, as the fittest cancer cells are restrained and tumour proliferation is reduced [43]. It is plausible to suppose that the oncosuppressive functions of the embryonic microenvironment could be due to evolutionary competition between malignant and non-malignant cells [98].

The nutrients in the TME also have the ability to reprogram cancer cells into a more invasive phenotype. Cancer cells have nutrient-sensing mechanisms to track the surrounding environment and fine-tune the metabolism accordingly [94]. It has been found that extracellular pyr-uvate regulates collagen hydroxylation and promotes growth of breast cancer lung metastasis [39]. Stromal and cancer cells compete with each other to scavenge nutrients such as glucose from the TME. In-creased glucose consumption uptake by tumours outsources and re-stricts metabolism in T cells, allowing cancer to progress [32,54].

Importantly, both the TME and associated cancer change during therapy. Indeed, it has been reported that immune checkpoint in-hibitors alter the mutational landscape of the tumour and T-cell re-pertoire [110]. The immune TME can constrain cancer progression or not based on its composition, and different TMEs can co-exist, showing highly heterogeneous therapeutic responses [65]. A case-study high-lighted a high-grade serous ovarian cancer patient with several me-tastases who showed progression or regression depending on immune exclusion or infiltration, respectively [61]. Similarly, tumour stroma also evolves with cancer starting from an increase in vasculature and leading to the transformation of the stroma into the desmoplastic en-vironment [23]. A recent study analysing the human metastatic mi-croenvironment in ovarian cancer found matrisome genes and proteins to have prognostic significance. Extension of the disease was accom-panied by an increase in fibrinogen, fibronectin, PG and affiliated proteins, indicating that the ECM evolves during metastasis [96].

5. Current methods to study TME-tumour cell interactions

Cell monolayers have been employed for decades to study the cel-lular pathways involved in cancer progression and as a starting point of the drug discovery process. However, several other methods, as mul-ticellular tumour spheroids (MCTS), tumour explants, in vivo models, digital pathology and in silico models have been developed to better study the TME.

2D cell cultures are easy to set up and relatively cheap. Importantly and in relation with the ECM, 2D cultures can be used to analyse the mechanical properties at a single cell level. This model also allows to understand how down/upregulations of certain proteins/genes inter-vene in the TME. Nonetheless, there are a number of issues such as lack of three dimensionality and absence of ECM, even when employing co-cultures to increase the physiological cell heterogeneity found in the TME.

To overcome these limitations MCTS have been developed using mono or co-cultures. These add the dimensionality needed to develop the cellular and treatment gradients described previously. Spheroids co-cultures are fundamental to study the immune cells interaction with a solid tumour. However, this model is not as fast as standard mono-layers, in terms of usage and the researcher needs to carefully select the best protocol to fit a specific biological question [90]. Another dis-advantage would be the lack of a physiological ECM architecture. In this context, scaffolded MCTS have been developed in order to re-produce ECM contributions, but low reproducibility and cost are major disadvantages [30].

The tumor tissue explants are based on tumor tissue biopsies, which are placed in a collagen matrix or gelatin sponges after necrotic tissue clearance. Disadvantages include the reduced reproducibility of tumour heterogeneity and maintenance of the culture for more than three weeks [113]. An approach to overcome all the limitation mentioned above relies on organoids model from tissue explants: 3D tissues de-rived from patient-derived pluripotent stem cells, which mimic complex feature of the malignant cells, but poorly recapitulate TME character-istics. Further advances, known as "tumor on a chip", have been aimed at developing a more TME physiological environment with tumor perfusion and mechanical stimuli such as shear stress [137]. In this context, 3D cell cultures are placed in microfluidic devices connected to perfusion systems with the possibility to regulate both fluids (medium, nutrients and waste) and gasses (CO_2 and O_2).

An in vivo model that enables to study tumourigenesis in a natural immune microenvironment is the genetically engineered mouse model (GEMM). De novo tumors developed in GEMM share molecular and histopathological properties with the human counterpart and capture

intrinsic and extrinsic factors necessary for tumor initiations and me-tastasis [142]. Nonetheless, the validation and experimentation with GEMMs is costly, time-consuming and intricate.

An important model in the study of the TME is patient samples analysis with digital pathology. This rely on performing serial sections from a biopsy with the pertinent stains and consequent digital analysis. This technique is relatively easy to perform and can highlight an ap-proximate profile of the TME-cell interaction. With the correct staining it is possible to visualise the ECM components or the stromal cells for quantitative/qualitative analysis. The sectioning process of paraffin-embedded tissue can almost capture the full three dimensionality of the tumour architecture through overlapping the images derived of the digital analysis.

Finally, all the biological data coming from different methods in the era of "omics" techniques and personalized medicine, need to be properly integrated. In silico approaches using mathematical modelling and systems biology are increasingly being considered in the cancer biology field, because they capture the complexity of cellular systems as a whole. These rely on building biological networks using ordinary differential equations to analyse high throughput data, build predictive models and refine experimental hypothesis. Nonetheless, computa-tional models of all TME-cancer cell interactions needs to be carefully validated.

6. Targeting TME as an anti-cancer strategy

Given both the complexity of the TME, and its interaction with cancer and stromal cells, it is essential to identify targetable micro-environmental modules (Fig. 3 and Table 1 – reviewed in Refs. [11,113]) and, if present, any synergistic interaction with standard of care [65]. Several approaches have aimed at perturbing either the re-cruitment or function of stromal cells. As an example, modulation of the mesenchymal stromal cell compartment with tyrosine kinase inhibitors or immunosuppressive therapy could be a potential approach to limit the effect of the TME on cancer progression [102]. Blockage of mac-rophages by altering CSF1/CSF1R signalling can enhance the efficacy of conventional cytotoxic therapies [114]. CSF-1R inhibition acts

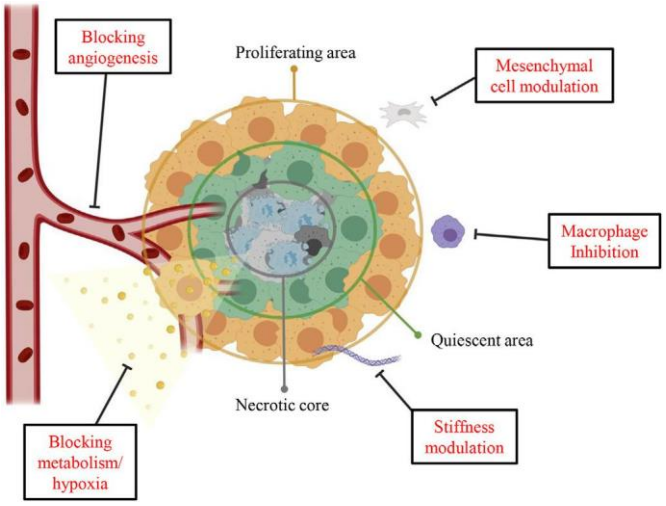

Fig. 3. Therapeutic modules of TME. The stratified cancer environment provides the basis for treatment resistance, as cells in the quiescent domain are more refractory to chemo- or immunotherapy. The extent of a drug's ability to penetrate the cancer 3D structure also affects treatment resistance. Among the therapies being developed nowadays, research has focused on blocking tumour angiogenesis, modulating stiffness to decrease cell migration and metastasis formation and inhibiting macrophage activity and other mesenchymal cells. Finally, several studies are concentrated on altering cellular metabolism to block cell proliferation, induce cell death and modulate interaction between cancer and immune cells.

Table 1
Major strategies used to target tumour microenvironment for cancer therapy[a].

TME element	Therapy strategies
Desmoplasia	
Activation TGF- β signaling pathway/	Angiotensin II receptor agonists
Increased secretion collagen I Increased expression of MMPs/collagen cross-linkers	Targeting MMPs
Presence of Cancer-Associated Fibroblasts	Targeting FAP-α and TGF-β
Hypoxia and acidosis	
Oxygen deficit Warburg effect	Tackle HIF-1 or its targets Inhibitor of proton exchangers/ transporters or carbonic anhydrase
Vascularization	
Proliferation endothelial cells and pericytes inhibitor	anti-VEGF/VEGFR and m-TOR
Altered immune system	
Active macrophages recruitment and differentiation	anti-CSF1/CSF1R Tyrosine kinase inhibitor
Chronic inflammation	anti-IL-1/IL-1R/IL-6
Pro-tumoural activity of immune system	GM-CSF, CTLA-4, PD-1 and PD-L1
Combined	
Immune check point PD-1 and angiogenesis	anti-PD-1 plus anti-VEGF/PD-L1 plus anti-VEGF

[a] Reviewed in Belli et al. and Roma-Rodrigues et al. CTLA-4: cytotoxic T-lymphocyte-associated protein 4; CSF1: colony-stimulating factor-1; CSF1R: CSF-1 receptor; FAP-α: fibroblast activation protein α; GM-CSF: Granulocyte-macrophage colony-stimulating factor; GTP: guanine nucleotides guanosine triphosphate; HIF-1: transcriptional factor hypoxia-induced factor-1; IL-1: in-terleukin-1; IL-1R: IL-1 receptor; IL-6: interleukin-6; MMPs: matrix metallo-proteinases; m-TOR: mammalian Target of Rapamycin; PD-1: programmed death 1 receptor; PD-L1: PD-1 ligand; TGF-β: transforming growth factor beta; VEGF: vascular endothelial growth factor; VEGFR: VEGF receptor.

synergistically with platinum-based chemotherapy, releasing an in-tratumoral type I interferon response [116]. Notably, iron metabolism, which is important for macrophage polarisation, has attracted interest in the development of new therapies [38]. Additionally, emerging elements are acquiring a key role in reprogramming the TME; vitamin D receptor has been found to have a role in metastatic cancer cells, stromal/immune compartment and the microbiota [60]. Several groups have focused on modulating angiogenesis as a tar-geted therapy against the TME. Modulation of VEGFR2 signalling can improve therapeutic efficacy [146]. Alteration of hypoxia-related sig-nalling might return aberrant vasculature to normal while decreasing tumour malignancy [82]. Promoting normal vasculature could also increase chemotherapy uptake in the hypoxic TME and avoid boosting the more aggressive cancer cell subpopulation [146,153]. Conversely, vasculature reduction by inhibiting tumour stiffness using β-amino-propionitrile decreased metastasis [18].

Modulating ECM stiffness and the prosurvival signals derived from the TME is another approach to improve the efficacy of conventional therapies. Treatment of melanoma-associated fibroblasts with BRAF inhibitor PLX4720 resulted in ECM deposition and resistance to treat-ment; thus, modulation of integrin β1 or FAK signalling in combination with BRAF inhibition induced cell death in melanoma [53]. Further-more, it has been shown that overexpression of laminin-411 correlates with poor outcome in glioblastoma multiforme and its inhibition in-creased in vivo survival [127]. In pancreatic cancer, depletion of βIG-H3, an ECM component, reduced tumour size and increased cancer cell clearance [45]. Inhibition of the GP vitronectin binding to its ligands (αvβ3 integrin, uPAR or PAI-1) has been tested as a potential ther-apeutic [55,81,109].

Several approaches have aimed at efficiently blocking aberrant metabolism and its interaction with the TME. Hypoxia, a potent barrier in radiotherapy, chemotherapy and immunotherapy, has been used to develop targeted drugs [48]. Several reports showed the efficacy of HIF-1α blockade on tumour progression [15,80,152]. Lactate production,

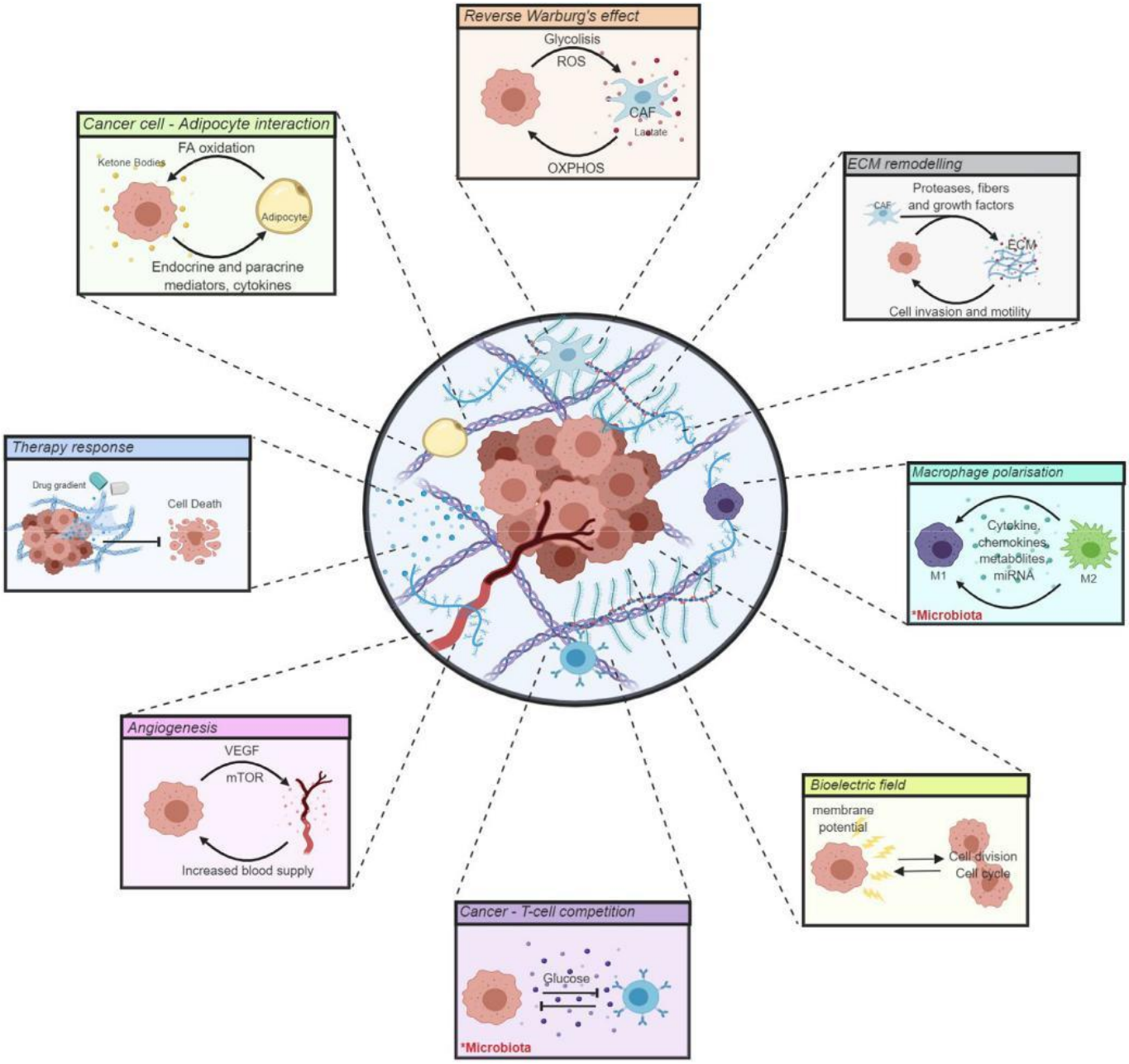

Fig. 4. TME as an integrated platform to understand cancer. Despite the classical view of cancer as a disease driven by mutation accumulation, emerging evidence highlights the role of the TME in tumorigenesis. In order to identify new biomarkers, improve drug development and better characterize this disease, cancer researchers need to keep in mind the integrated vision of a malignant lesion immersed in all the elements of the TME, the most important of which are showcased in this figure. A malignant metabolism contributes to carcinogenesis and cancer cell interaction with the immune system and mesenchymal cell compartments (with the help of the microbiota). Remodelling the ECM allows cancer migration and metastasis formation, and impedes chemotherapy diffusion. The bioelectric field gen-erated in the TME regulates cell division and cell cycle. Finally, new blood vessel formation facilitates nutrient diffusion and creates a hub for cancer cells to disseminate from the primary tumour site.

which correlates with tumour aggressiveness, increases in the TME as a consequence of the Warburg effect [117]. Indeed, inhibition of lactate uptake through MCT transporters has been found to reduce cancer growth, alone and in combination with current therapies [10,12,16,56,85]. The acidic TME has also been employed for specific targeting of cancer cells. In this context, a tumour acidic micro-environment targeted drug delivery system has been developed to carry doxorubicin to breast cancer [157]. Similar studies also focused on the production of pH/redox dual stimuli-responsive polymeric micelles for the intracellular delivery of doxorubicin [63,64].

7. Conclusions and perspectives

An optimal strategy to avoid therapeutic obstinacy and superfluous tests in cancer patients could be to develop new terminology to replace the word cancer in conditions showing low clinical aggressiveness. From a general point of view, carcinogenesis appears to be a differ-entiation phenomenon, which also includes proliferation and senes-cence alterations. The fact that cancer cells rewire their malignant phenotype to a normal one when grafted into a healthy micro-environment allows us to view carcinogenesis from a developmental change perspective (Fig. 4). This is in line with recent tissue

organization field theory, where cancer is viewed as a disease affecting the entire tissue rather than single cells [129].

Cells with similar proteomic and genomic profiles possess different physiological properties, and vice-versa. The biophysical forces that maintain the structural integrity of a tumour greatly influence cell ad-hesion, motility and proliferation. Changes in the bioelectric field can control tumorigenesis and cancer progression without major DNA da-mage. The metabolic interaction of cancer cells with the surrounding microenvironment shape not only the ECM architecture, but also the cellular/immune niche. The different TME elements promote angio-genesis and a set of changes that alter the tumour stroma. Moreover, therapeutic cytotoxic damage allows the tissue to remodel the en-vironment with different oncogenic changes such as growth factor ex-pression, cytokines and stromal disruption that ultimately generate new migratory signals for cancer cells [69].

In summary, integrating all these information levels could lead to tumour normalisation by remodelling to healthy tissue morphogenesis (including the stromal and cellular compartment) in a non-malignant bioelectric/biophysical field and metabolism. With an integrated per-spective, it is possible to view carcinogenesis as a reversible process which is not necessarily linked to mutation. In order to achieve this objective, it would be helpful to record the integrated TME information in a standardized and homogeneous manner. The framework proposed in this review could be useful in finding new biomarkers and treatments that could potentially benefit cancer patients.

Funding disclosure

This work was supported by grants from ISCIII (FIS) and FEDER (European Regional Development Fund) PI17/01558; CIBERONC (contract CB16/12/00484); Fundación Científica de la Asociación Española contra el Cáncer (FAECC2015/006); NEN Association (Nico contra el cancer infantil 2017 – PVR00157) and the Neuroblastoma Foundation (PVR00166). The funders had no involvement in the re-search process nor in the preparation and submission of the article.

Conflicts of interest

The authors declare no conflict of interest.

Acknowledgements

The authors would like to thank Kathryn for english correction.

References

[1] L. Abdul Kadir, M. Stacey, R. Barrett-Jolley, Emerging roles of the membrane potential: action beyond the action potential, Front. Physiol. 9 (2018) 1661.
[2] D. Ackerman, M.C. Simon, Hypoxia, lipids, and cancer: surviving the harsh tumor microenvironment, Trends Cell Biol. 24 (2014) 472–478.
[3] T. Alkasalias, L. Moyano-Galceran, M. Arsenian-Henriksson, K. Lehti, Fibroblasts in the tumor microenvironment: shield or spear? Int. J. Mol. Sci. 19 (2018) 1532.
[4] T. Alvaro, L. de la Cruz-Merino, F. Henao-Carrasco, J.L. Villar Rodriguez, D. Vicente Baz, M. Codes Manuel de Villena, M. Provencio, Tumor micro-environment and immune effects of antineoplastic therapy in lymphoproliferative syndromes, J. Biomed. Biotechnol. (2010) 2010.
[5] K.E. Allison, B.L. Coomber, B.W. Bridle, Metabolic reprogramming in the tumour microenvironment: a hallmark shared by cancer cells and T lymphocytes, Immunology 152 (2017) 175–184.
[6] A. Arcucci, M.R. Ruocco, G. Granato, A.M. Sacco, S. Montagnani, Cancer: an oxidative crosstalk between solid tumor cells and cancer associated fibroblasts, BioMed Res. Int. 2016 (2016) 4502846.
[7] E.L. Baker, R.T. Bonnecaze, M.H. Zaman, Extracellular matrix stiffness and ar-chitecture govern intracellular rheology in cancer, Biophys. J. 97 (2009) 1013–1021.
[8] F.R. Balkwill, M. Capasso, T. Hagemann, The tumor microenvironment at a glance, J. Cell Sci. 125 (2012) 5591–5596.
[9] A. Becchetti, Ion channels and transporters in cancer. 1. Ion channels and cell proliferation in cancer, Am. J. Physiol. Cell Physiol. 301 (2011) C255–C265.
[10] M. Beloueche-Babari, S. Wantuch, T. Casals Galobart, M. Koniordou, H.G. Parkes, V. Arunan, Y.L. Chung, T.R. Eykyn, P.D. Smith, M.O. Leach, MCT1 inhibitor AZD3965 increases mitochondrial metabolism, facilitating combination therapy and noninvasive magnetic resonance spectroscopy, Cancer Res. 77 (2017) 5913–5924.
[11] C. Belli, D. Trapani, G. Viale, P. D'Amico, B.A. Duso, P. Della Vigna, F. Orsi, G. Curigliano, Targeting the microenvironment in solid tumors, Cancer Treat Rev.65 (2018) 22–32.
[12] D. Benjamin, D. Robay, S.K. Hindupur, J. Pohlmann, M. Colombi, M.Y. El-Shemerly, S.M. Maira, C. Moroni, H.A. Lane, M.N. Hall, Dual inhibition of the lactate transporters MCT1 and MCT4 is synthetic lethal with metformin due to NAD+ depletion in cancer cells, Cell Rep. 25 (2018) 3047–3058 e3044.
[13] M. Bertolaso, A.M. Dieli, Cancer and intercellular cooperation, R. Soc. Open Sci. 4 (2017) 170470.
[14] D.J. Blackiston, K.A. McLaughlin, M. Levin, Bioelectric controls of cell prolifera-tion: ion channels, membrane voltage and the cell cycle, Cell Cycle 8 (2009) 3527–3536.
[15] K.M. Block, H. Wang, L.Z. Szabo, N.W. Polaske, L.K. Henchey, R. Dubey, S. Kushal, C.F. Laszlo, J. Makhoul, Z. Song, E.J. Meuillet, B.Z. Olenyuk, Direct inhibition of hypoxia-inducible transcription factor complex with designed dimeric epidithio-diketopiperazine, J. Am. Chem. Soc. 131 (2009) 18078–18088.
[16] B.M. Bola, A.L. Chadwick, F. Michopoulos, K.G. Blount, B.A. Telfer, K.J. Williams, P.D. Smith, S.E. Critchlow, I.J. Stratford, Inhibition of monocarboxylate trans-porter-1 (MCT1) by AZD3965 enhances radiosensitivity by reducing lactate transport, Mol. Cancer Ther. 13 (2014) 2805–2816.
[17] G. Bonuccelli, D. Whitaker-Menezes, R. Castello-Cros, S. Pavlides, R.G. Pestell, A. Fatatis, A.K. Witkiewicz, M.G. Vander Heiden, G. Migneco, B. Chiavarina, P.G. Frank, F. Capozza, N. Flomenberg, U.E. Martinez-Outschoorn, F. Sotgia, M.P. Lisanti, The reverse Warburg effect: glycolysis inhibitors prevent the tumor promoting effects of caveolin-1 deficient cancer associated fibroblasts, Cell Cycle 9 (2010) 1960–1971.
[18] F. Bordeleau, B.N. Mason, E.M. Lollis, M. Mazzola, M.R. Zanotelli, S. Somasegar, J.P. Califano, C. Montague, D.J. LaValley, J. Huynh, N. Mencia-Trinchant, Y.L. Negron Abril, D.C. Hassane, L.J. Bonassar, J.T. Butcher, R.S. Weiss, C.A. Reinhart-King, Matrix stiffening promotes a tumor vasculature phenotype, Proc. Natl. Acad. Sci. U. S. A. 114 (2017) 492–497.
[19] P. Borys, On the biophysics of cathodal galvanotaxis in rat prostate cancer cells: Poisson-Nernst-Planck equation approach, Eur. Biophys. J. 41 (2012) 527–534.
[20] R.M. Bremnes, T. Donnem, S. Al-Saad, K. Al-Shibli, S. Andersen, R. Sirera, C. Camps, I. Marinez, L.T. Busund, The role of tumor stroma in cancer progression and prognosis: emphasis on carcinoma-associated fibroblasts and non-small cell lung cancer, J. Thorac. Oncol. : Off. Publ. Int. Assoc. Stud. Lung Canc. 6 (2011) 209–217.
[21] F. Broders-Bondon, T.H. Nguyen Ho-Bouldoires, M.E. Fernandez-Sanchez, E. Farge, Mechanotransduction in tumor progression: the dark side of the force, J. Cell Biol. 217 (2018) 1571–1587.
[22] K.M. Bussard, G.H. Smith, Human breast cancer cells are redirected to mammary epithelial cells upon interaction with the regenerating mammary gland micro-environment in-vivo, PLoS One 7 (2012) e49221.
[23] F. Cammarota, M.O. Laukkanen, Mesenchymal stem/stromal cells in stromal evolution and cancer progression, Stem Cell. Int. (2016) 4824573 2016.
[24] J.R. Cantor, D.M. Sabatini, Cancer cell metabolism: one hallmark, many faces, Cancer Discov. 2 (2012) 881–898.
[25] C. Carmona-Fontaine, M. Deforet, L. Akkari, C.B. Thompson, J.A. Joyce, J.B. Xavier, Metabolic origins of spatial organization in the tumor microenviron-ment, Proc. Natl. Acad. Sci. U. S. A. 114 (2017) 2934–2939.
[26] M. Cavo, M. Fato, L. Penuela, F. Beltrame, R. Raiteri, S. Scaglione, Microenvironment complexity and matrix stiffness regulate breast cancer cell activity in a 3D in vitro model, Sci. Rep. 6 (2016) 35367.
[27] M.E. Ciurea, A.M. Georgescu, S.O. Purcaru, S.A. Artene, G.H. Emami, M.V. Boldeanu, D.E. Tache, A. Dricu, Cancer stem cells: biological functions and therapeutically targeting, Int. J. Mol. Sci. 15 (2014) 8169–8185.
[28] W.H. Clark Jr., The nature of cancer: morphogenesis and progressive (self)-dis-organization in neoplastic development and progression, Acta Oncol. (Stockh.) 34 (1995) 3–21.
[29] E.C. Costa, A.F. Moreira, D. de Melo-Diogo, V.M. Gaspar, M.P. Carvalho, I.J. Correia, 3D tumor spheroids: an overview on the tools and techniques used for their analysis, Biotechnol. Adv. 34 (2016) 1427–1441.
[30] X. Cui, Y. Hartanto, H. Zhang, Advances in multicellular spheroids formation, J. R. Soc. Interface 14 (2017) 20160877.
[31] P. Cunnea, T. Gorgy, K. Petkos, S.A.N. Gowers, H. Lu, C. Morera, W. Wu, P. Lawton, K. Nixon, C.L. Leong, F. Sorbi, L. Domenici, A. Paterson, E. Curry, H. Gabra, M.G. Boutelle, E.M. Drakakis, C. Fotopoulou, Clinical value of bioelec-trical properties of cancerous tissue in advanced epithelial ovarian cancer patients, Sci. Rep. 8 (2018) 14695.
[32] C.H. Chang, J. Qiu, D. O'Sullivan, M.D. Buck, T. Noguchi, J.D. Curtis, Q. Chen, M. Gindin, M.M. Gubin, G.J. van der Windt, E. Tonc, R.D. Schreiber, E.J. Pearce, E.L. Pearce, Metabolic competition in the tumor microenvironment is a driver of cancer progression, Cell 162 (2015) 1229–1241.
[33] F. Chen, X. Zhuang, L. Lin, P. Yu, Y. Wang, Y. Shi, G. Hu, Y. Sun, New horizons in tumor microenvironment biology: challenges and opportunities, BMC Med. 13 (2015) 45.
[34] B. Chernet, M. Levin, Endogenous voltage potentials and the microenvironment: bioelectric signals that reveal, induce and normalize cancer, J. Clin. Exp. Oncol. Suppl 1 (2013) S1–S002.
[35] B.T. Chernet, M. Levin, Transmembrane voltage potential of somatic cells controls oncogene-mediated tumorigenesis at long-range, Oncotarget 5 (2014) 3287–3306.
[36] A. Chronopoulos, B. Robinson, M. Sarper, E. Cortes, V. Auernheimer,

D. Lachowski, S. Attwood, R. Garcia, S. Ghassemi, B. Fabry, A. Del Rio Hernandez, ATRA mechanically reprograms pancreatic stellate cells to suppress matrix re-modelling and inhibit cancer cell invasion, Nat. Commun. 7 (2016) 12630.
[37] S.M. Davidson, O. Jonas, M.A. Keibler, H.W. Hou, A. Luengo, J.R. Mayers, J. Wyckoff, A.M. Del Rosario, M. Whitman, C.R. Chin, K.J. Condon, A. Lammers, K.A. Kellersberger, B.K. Stall, G. Stephanopoulos, D. Bar-Sagi, J. Han,J.D. Rabinowitz, M.J. Cima, R. Langer, M.G. Vander Heiden, Direct evidence for cancer-cell-autonomous extracellular protein catabolism in pancreatic tumors, Nat. Med. 23 (2017) 235–241.
[38] D. Dong, G. Zhang, J. Yang, B. Zhao, S. Wang, L. Wang, G. Zhang, P. Shang, The role of iron metabolism in cancer therapy focusing on tumor-associated macro-phages, J. Cell. Physiol. 234 (2019) 8028–8039.
[39] I. Elia, M. Rossi, S. Stegen, D. Broekaert, G. Doglioni, M. van Gorsel, R. Boon, C. Escalona-Noguero, S. Torrekens, C. Verfaillie, E. Verbeken, G. Carmeliet, S.M. Fendt, Breast cancer cells rely on environmental pyruvate to shape the me-tastatic niche, Nature (2019) 117–121.
[40] B. Emon, J. Bauer, Y. Jain, B. Jung, T. Saif, Biophysics of tumor microenvironment and cancer metastasis - a mini review, Comput. Struct. Biotechnol. J. 16 (2018) 279–287.
[41] B.T. Finicle, V. Jayashankar, A.L. Edinger, Nutrient scavenging in cancer, Nat. Rev. Cancer 18 (2018) 619–633.
[42] C. Frantz, K.M. Stewart, V.M. Weaver, The extracellular matrix at a glance, J. Cell Sci. 123 (2010) 4195–4200.
[43] R.A. Gatenby, A.S. Silva, R.J. Gillies, B.R. Frieden, Adaptive therapy, Cancer Res. 69 (2009) 4894–4903.
[44] V. Gkretsi, T. Stylianopoulos, Cell adhesion and matrix stiffness: coordinating cancer cell invasion and metastasis, Front Oncol. 8 (2018) 145.
[45] D. Goehrig, J. Nigri, R. Samain, Z. Wu, P. Cappello, G. Gabiane, X. Zhang, Y. Zhao, I.S. Kim, M. Chanal, R. Curto, V. Hervieu, C. de La Fouchardiere, F. Novelli, P. Milani, R. Tomasini, C. Bousquet, P. Bertolino, A. Hennino, Stromal protein betaig-h3 reprogrammes tumour microenvironment in pancreatic cancer, Gut 68 (2019) 693–707.
[46] K. Gollapudi, C. Galet, T. Grogan, H. Zhang, J.W. Said, J. Huang, D. Elashoff, S.J. Freedland, M. Rettig, W.J. Aronson, Association between tumor-associated macrophage infiltration, high grade prostate cancer, and biochemical recurrence after radical prostatectomy, Am. J. Canc. Res. 3 (2013) 523–529.
[47] D.M. Graham, K. Burridge, Mechanotransduction and nuclear function, Curr. Opin. Cell Biol. 40 (2016) 98–105.
[48] K. Graham, E. Unger, Overcoming tumor hypoxia as a barrier to radiotherapy, chemotherapy and immunotherapy in cancer treatment, Int. J. Nanomed. 13 (2018) 6049–6058.
[49] Z. Granot, Z.G. Fridlender, Plasticity beyond cancer cells and the "im-munosuppressive switch, Cancer Res. 75 (2015) 4441–4445.
[50] D. Hanahan, L.M. Coussens, Accessories to the crime: functions of cells recruited to the tumor microenvironment, Cancer Cell 21 (2012) 309–322.
[51] D. Hanahan, R.A. Weinberg, Hallmarks of cancer: the next generation, Cell 144 (2011) 646–674.
[52] N. He, G. Feng, Y. Li, Y. Xu, X. Xie, H. Wang, Y. Wang, L. Ou, X. Pei, N. Liu, Z. Li, Embryonic stem cell preconditioned microenvironment suppresses tumorigenic properties in breast cancer, Stem Cell Res. Ther. 7 (2016) 95.
[53] E. Hirata, M.R. Girotti, A. Viros, S. Hooper, B. Spencer-Dene, M. Matsuda, J. Larkin, R. Marais, E. Sahai, Intravital imaging reveals how BRAF inhibition generates drug-tolerant microenvironments with high integrin beta1/FAK sig-naling, Cancer Cell 27 (2015) 574–588.
[54] P.C. Ho, J.D. Bihuniak, A.N. Macintyre, M. Staron, X. Liu, R. Amezquita, Y.C. Tsui, G. Cui, G. Micevic, J.C. Perales, S.H. Kleinstein, E.D. Abel, K.L. Insogna, S. Feske, J.W. Locasale, M.W. Bosenberg, J.C. Rathmell, S.M. Kaech, Phosphoenolpyruvate is a metabolic checkpoint of anti-tumor T cell responses, Cell 162 (2015) 1217–1228.
[55] A.W. Holle, J.L. Young, J.P. Spatz, In vitro cancer cell-ECM interactions inform in vivo cancer treatment, Adv. Drug Deliv. Rev. 97 (2016) 270–279.
[56] C.S. Hong, N.A. Graham, W. Gu, C. Espindola Camacho, V. Mah, E.L. Maresh, M. Alavi, L. Bagryanova, P.A.L. Krotee, B.K. Gardner, I.S. Behbahan, S. Horvath, D. Chia, I.K. Mellinghoff, S.A. Hurvitz, S.M. Dubinett, S.E. Critchlow, S.K. Kurdistani, L. Goodglick, D. Braas, T.G. Graeber, H.R. Christofk, MCT1 modulates cancer cell pyruvate export and growth of tumors that Co-express MCT1 and MCT4, Cell Rep. 14 (2016) 1590–1601.
[57] L. Ippolito, A. Morandi, M.L. Taddei, M. Parri, G. Comito, A. Iscaro, M.R. Raspollini, F. Magherini, E. Rapizzi, J. Masquelier, G.G. Muccioli, P. Sonveaux, P. Chiarugi, E. Giannoni, Cancer-associated fibroblasts promote prostate cancer malignancy via metabolic rewiring and mitochondrial transfer, Oncogene (2019).
[58] V. Izzi, J. Lakkala, R. Devarajan, E.R. Savolainen, P. Koistinen, R. Heljasvaara, T. Pihlajaniemi, Expression of a specific extracellular matrix signature is a favor-able prognostic factor in acute myeloid leukemia, Leuk. Res. Rep. 9 (2018) 9–13.
[59] M.K. Jena, J. Janjanam, Role of extracellular matrix in breast cancer development: a brief update, F1000Res. 7 (2018) 274.
[60] S.M. Jeon, E.A. Shin, Exploring vitamin D metabolism and function in cancer, Exp. Mol. Med. 50 (2018) 20.
[61] A. Jimenez-Sanchez, D. Memon, S. Pourpe, H. Veeraraghavan, Y. Li, H.A. Vargas, M.B. Gill, K.J. Park, O. Zivanovic, J. Konner, J. Ricca, D. Zamarin, T. Walther, C. Aghajanian, J.D. Wolchok, E. Sala, T. Merghoub, A. Snyder, M.L. Miller, Heterogeneous tumor-immune microenvironments among differentially growing metastases in an ovarian cancer patient, Cell 170 (2017) 927–938 e920.
[62] P. Jobling, J. Pundavela, S.M. Oliveira, S. Roselli, M.M. Walker, H. Hondermarck, Nerve-cancer cell cross-talk: a novel promoter of tumor progression, Cancer Res. 75 (2015) 1777–1781.
[63] J.V. John, S. Uthaman, R. Augustine, H. Chen, I.-K. Park, I. Kim, pH/redox dual stimuli-responsive sheddable nanodaisies for efficient intracellular tumour-trig-gered drug delivery, J. Mater. Chem. B 5 (2017) 5027–5036.
[64] J.V. John, S. Uthaman, R. Augustine, K. Manickavasagam Lekshmi, I.-K. Park, I. Kim, Biomimetic pH/redox dual stimuli-responsive zwitterionic polymer block poly(L-histidine) micelles for intracellular delivery of doxorubicin into tumor cells, J. Polym. Sci. A Polym. Chem. 55 (2017) 2061–2070.
[65] M.R. Junttila, F.J. de Sauvage, Influence of tumour micro-environment hetero-geneity on therapeutic response, Nature 501 (2013) 346–354.
[66] M. Kalli, T. Stylianopoulos, Defining the role of solid stress and matrix stiffness in cancer cell proliferation and metastasis, Front Oncol. 8 (2018) 55.
[67] J.J. Kamphorst, J.R. Cross, J. Fan, E. de Stanchina, R. Mathew, E.P. White, C.B. Thompson, J.D. Rabinowitz, Hypoxic and Ras-transformed cells support growth by scavenging unsaturated fatty acids from lysophospholipids, Proc. Natl. Acad. Sci. U. S. A. 110 (2013) 8882–8887.
[68] J.J. Kamphorst, M. Nofal, C. Commisso, S.R. Hackett, W. Lu, E. Grabocka, M.G. Vander Heiden, G. Miller, J.A. Drebin, D. Bar-Sagi, C.B. Thompson, J.D. Rabinowitz, Human pancreatic cancer tumors are nutrient poor and tumor cells actively scavenge extracellular protein, Cancer Res. 75 (2015) 544–553.
[69] G.S. Karagiannis, J.S. Condeelis, M.H. Oktay, Chemotherapy-induced metastasis: mechanisms and translational opportunities, Clin. Exp. Metastasis 35 (2018) 269 –284.
[70] J.K. Kular, S. Basu, R.I. Sharma, The extracellular matrix: structure, composition, age-related differences, tools for analysis and applications for tissue engineering, J. Tissue Eng. 5 (2014) 2041731414557112.
[71] P.M. Kulesa, J.C. Kasemeier-Kulesa, J.M. Teddy, N.V. Margaryan, E.A. Seftor, R.E. Seftor, M.J. Hendrix, Reprogramming metastatic melanoma cells to assume a neural crest cell-like phenotype in an embryonic microenvironment, Proc. Natl. Acad. Sci. U. S. A. 103 (2006) 3752–3757.
[72] D. Lachowski, E. Cortes, D. Pink, A. Chronopoulos, S.A. Karim, P.M.J, A.E. Del Rio Hernandez, Substrate rigidity controls activation and durotaxis in pancreatic stellate cells, Sci. Rep. 7 (2017) 2506.
[73] S.A. Langhans, Three-dimensional in vitro cell culture models in drug discovery and drug repositioning, Front. Pharmacol. 9 (2018) 6.
[74] M. Levin, Reprogramming cells and tissue patterning via bioelectrical pathways: molecular mechanisms and biomedical opportunities, Wiley Interdiscip. Rev. Syst. Biol. Med. 5 (2013) 657–676.
[75] M. Levin, Molecular bioelectricity: how endogenous voltage potentials control cell behavior and instruct pattern regulation in vivo, Mol. Biol. Cell 25 (2014) 3835–3850.
[76] M. Levin, C.J. Martyniuk, The bioelectric code: an ancient computational medium for dynamic control of growth and form, Biosystems 164 (2018) 76–93.
[77] M.V. Liberti, J.W. Locasale, The Warburg effect: how does it benefit cancer cells? Trends Biochem. Sci. 41 (2016) 211–218.
[78] S.B. Lim, S.J. Tan, W.T. Lim, C.T. Lim, An extracellular matrix-related prognostic and predictive indicator for early-stage non-small cell lung cancer, Nat. Commun. 8 (2017) 1734.
[79] M. Lobikin, B. Chernet, D. Lobo, M. Levin, Resting potential, oncogene-induced tumorigenesis, and metastasis: the bioelectric basis of cancer in vivo, Phys. Biol. 9 (2012) 065002.
[80] N.J. Mabjeesh, D. Escuin, T.M. LaVallee, V.S. Pribluda, G.M. Swartz, M.S. Johnson, M.T. Willard, H. Zhong, J.W. Simons, P. Giannakakou, 2ME2 inhibits tumor growth and angiogenesis by disrupting microtubules and dysregulating HIF, Cancer Cell 3 (2003) 363–375.
[81] T. Masuda, N. Hattori, T. Senoo, S. Akita, N. Ishikawa, K. Fujitaka, Y. Haruta, H. Murai, N. Kohno, SK-216, an inhibitor of plasminogen activator inhibitor-1, limits tumor progression and angiogenesis, Mol. Cancer Ther. 12 (2013) 2378–2388.
[82] M. Mazzone, D. Dettori, R.L. de Oliveira, S. Loges, T. Schmidt, B. Jonckx, Y.M. Tian, A.A. Lanahan, P. Pollard, C.R. de Almodovar, F. De Smet, S. Vinckier, J. Aragones, K. Debackere, A. Luttun, S. Wyns, B. Jordan, A. Pisacane, B. Gallez, M.G. Lampugnani, E. Dejana, M. Simons, P. Ratcliffe, P. Maxwell, P. Carmeliet, Heterozygous deficiency of PHD2 restores tumor oxygenation and inhibits me-tastasis via endothelial normalization, Cell 136 (2009) 839–851.
[83] P. Mesquida, D. Kohl, O.G. Andriotis, P.J. Thurner, M. Duer, S. Bansode, G. Schitter, Evaluation of surface charge shift of collagen fibrils exposed to glu-taraldehyde, Sci. Rep. 8 (2018) 10126.
[84] S.M. Mithieux, A.S. Weiss, Elastin, Adv. Protein Chem. 70 (2005) 437–461.
[85] F. Morais-Santos, S. Granja, V. Miranda-Goncalves, A.H. Moreira, S. Queiros, J.L. Vilaca, F.C. Schmitt, A. Longatto-Filho, J. Paredes, F. Baltazar, C. Pinheiro, Targeting lactate transport suppresses in vivo breast tumour growth, Oncotarget 6 (2015) 19177–19189.
[86] J.K. Mouw, G. Ou, V.M. Weaver, Extracellular matrix assembly: a multiscale de-construction, Nat. Rev. Mol. Cell Biol. 15 (2014) 771–785.
[87] A. Muir, M.G. Vander Heiden, The nutrient environment affects therapy, Science (New York, N.Y.) 360 (2018) 962–963.
[88] M.E. Mycielska, M.B. Djamgoz, Cellular mechanisms of direct-current electric field effects: galvanotaxis and metastatic disease, J. Cell Sci. 117 (2004) 1631–1639.
[89] M. Najafi, N.H. Goradel, B. Farhood, E. Salehi, S. Solhjoo, H. Toolee, E. Kharazinejad, K. Mortezaee, Tumor microenvironment: interactions and therapy, J. Cell. Physiol. 234 (2019) 5700–5721.
[90] S. Nath, G.R. Devi, Three-dimensional culture systems in cancer research: focus on tumor spheroid model, Pharmacol. Ther. 163 (2016) 94–108.
[91] M.R. Ng, J.S. Brugge, A stiff blow from the stroma: collagen crosslinking drives tumor progression, Cancer Cell 16 (2009) 455–457.

[92] K.M. Nieman, H.A. Kenny, C.V. Penicka, A. Ladanyi, R. Buell-Gutbrod, M.R. Zillhardt, I.L. Romero, M.S. Carey, G.B. Mills, G.S. Hotamisligil, S.D. Yamada, M.E. Peter, K. Gwin, E. Lengyel, Adipocytes promote ovarian cancer metastasis and provide energy for rapid tumor growth, Nat. Med. 17 (2011) 1498–1503.
[93] K.M. Nieman, I.L. Romero, B. Van Houten, E. Lengyel, Adipose tissue and adipo-cytes support tumorigenesis and metastasis, Biochim. Biophys. Acta 1831 (2013) 1533–1541.
[94] W. Palm, C.B. Thompson, Nutrient acquisition strategies of mammalian cells, Nature 546 (2017) 234–242.
[95] S. Pavlides, D. Whitaker-Menezes, R. Castello-Cros, N. Flomenberg, A.K. Witkiewicz, P.G. Frank, M.C. Casimiro, C. Wang, P. Fortina, S. Addya, R.G. Pestell, U.E. Martinez-Outschoorn, F. Sotgia, M.P. Lisanti, The reverse Warburg effect: aerobic glycolysis in cancer associated fibroblasts and the tumor stroma, Cell Cycle 8 (2009) 3984–4001.
[96] O.M.T. Pearce, R.M. Delaine-Smith, E. Maniati, S. Nichols, J. Wang, S. Bohm, V. Rajeeve, D. Ullah, P. Chakravarty, R.R. Jones, A. Montfort, T. Dowe, J. Gribben, J.L. Jones, H.M. Kocher, J.S. Serody, B.G. Vincent, J. Connelly, J.D. Brenton, C. Chelala, P.R. Cutillas, M. Lockley, C. Bessant, M.M. Knight, F.R. Balkwill, Deconstruction of a metastatic tumor microenvironment reveals a common matrix response in human cancers, Cancer Discov. 8 (2018) 304–319.
[97] H. Peinado, H. Zhang, I.R. Matei, B. Costa-Silva, A. Hoshino, G. Rodrigues, B. Psaila, R.N. Kaplan, J.F. Bromberg, Y. Kang, M.J. Bissell, T.R. Cox, A.J. Giaccia, J.T. Erler, S. Hiratsuka, C.M. Ghajar, D. Lyden, Pre-metastatic niches: organ-spe-cific homes for metastases, Nat. Rev. Cancer 17 (2017) 302–317.
[98] J.W. Pepper, C. Scott Findlay, R. Kassen, S.L. Spencer, C.C. Maley, Cancer research meets evolutionary biology, Evol. Appl. 2 (2009) 62–70.
[99] N. Pertega-Gomes, J.R. Vizcaino, J. Attig, S. Jurmeister, C. Lopes, F. Baltazar, A lactate shuttle system between tumour and stromal cells is associated with poor prognosis in prostate cancer, BMC Canc. 14 (2014) 352.
[100] F. Petitprez, C.M. Sun, L. Lacroix, C. Sautes-Fridman, A. de Reynies, W.H. Fridman, Quantitative analyses of the tumor microenvironment composition and orienta-tion in the era of precision medicine, Front Oncol. 8 (2018) 390.
[101] M.W. Pickup, J.K. Mouw, V.M. Weaver, The extracellular matrix modulates the hallmarks of cancer, EMBO Rep. 15 (2014) 1243–1253.
[102] A. Poggi, S. Varesano, M.R. Zocchi, How to hit mesenchymal stromal cells and make the tumor microenvironment immunostimulant rather than im-munosuppressive, Front. Immunol. 9 (2018) 262.
[103] L.M. Postovit, N.V. Margaryan, E.A. Seftor, D.A. Kirschmann, A. Lipavsky, W.W. Wheaton, D.E. Abbott, R.E. Seftor, M.J. Hendrix, Human embryonic stem cell microenvironment suppresses the tumorigenic phenotype of aggressive cancer cells, Proc. Natl. Acad. Sci. U. S. A. 105 (2008) 4329–4334.
[104] J. Pouysségur, F. Dayan, N.M. Mazure, Hypoxia signalling in cancer and ap-proaches to enforce tumour regression, Nature 441 (2006) 437.
[105] D.R. Powell, A. Huttenlocher, Neutrophils in the tumor microenvironment, Trends Immunol. 37 (2016) 41–52.
[106] N. Prevarskaya, R. Skryma, Y. Shuba, Ion channels and the hallmarks of cancer, Trends Mol. Med. 16 (2010) 107–121.
[107] D.F. Quail, J.A. Joyce, Microenvironmental regulation of tumor progression and metastasis, Nat. Med. 19 (2013) 1423–1437.
[108] S. Raab-Westphal, J.F. Marshall, S.L. Goodman, Integrins as therapeutic targets: successes and cancers, Cancers 9 (2017) 110.
[109] V.E. Rea, A. Lavecchia, C. Di Giovanni, F.W. Rossi, A. Gorrasi, A. Pesapane, A. de Paulis, P. Ragno, N. Montuori, Discovery of new small molecules targeting the vitronectin-binding site of the urokinase receptor that block cancer cell invasion, Mol. Cancer Ther. 12 (2013) 1402–1416.
[110] N. Riaz, J.J. Havel, V. Makarov, A. Desrichard, W.J. Urba, J.S. Sims, F.S. Hodi, S. Martin-Algarra, R. Mandal, W.H. Sharfman, S. Bhatia, W.J. Hwu, T.F. Gajewski, C.L. Slingluff Jr., D. Chowell, S.M. Kendall, H. Chang, R. Shah, F. Kuo, L.G.T. Morris, J.W. Sidhom, J.P. Schneck, C.E. Horak, N. Weinhold, T.A. Chan, Tumor and microenvironment evolution during immunotherapy with nivolumab, Cell 171 (2017) 934–949 e916.
[111] A.J. Rice, E. Cortes, D. Lachowski, B.C.H. Cheung, S.A. Karim, J.P. Morton, A. del Río Hernández, Matrix stiffness induces epithelial–mesenchymal transition and promotes chemoresistance in pancreatic cancer cells, Oncogenesis 6 (2017) e352.
[112] P. Roca-Cusachs, A. del Rio, E. Puklin-Faucher, N.C. Gauthier, N. Biais, M.P. Sheetz, Integrin-dependent force transmission to the extracellular matrix by alpha-actinin triggers adhesion maturation, Proc. Natl. Acad. Sci. U. S. A. 110 (2013) E1361–E1370.
[113] C. Roma-Rodrigues, R. Mendes, P.V. Baptista, A.R. Fernandes, Targeting tumor microenvironment for cancer therapy, Int. J. Mol. Sci. 20 (2019) 840.
[114] B. Ruffell, D. Chang-Strachan, V. Chan, A. Rosenbusch, C.M. Ho, N. Pryer, D. Daniel, E.S. Hwang, H.S. Rugo, L.M. Coussens, Macrophage IL-10 blocks CD8+ T cell-dependent responses to chemotherapy by suppressing IL-12 expression in intratumoral dendritic cells, Cancer Cell 26 (2014) 623–637.
[115] D. Saforo, L. Omer, A. Smolenkov, A. Barve, L. Casson, N. Boyd, G. Clark, L. Siskind, L. Beverly, Primary lung cancer samples cultured under micro-environment-mimetic conditions enrich for mesenchymal stem-like cells that promote metastasis, Sci. Rep. 9 (2019) 4177.
[116] C. Salvagno, M. Ciampricotti, S. Tuit, C.S. Hau, A. van Weverwijk, S.B. Coffelt, K. Kersten, K. Vrijland, K. Kos, T. Ulas, J.Y. Song, C.H. Ooi, D. Ruttinger, P.A. Cassier, J. Jonkers, J.L. Schultze, C.H. Ries, K.E. de Visser, Therapeutic tar-geting of macrophages enhances chemotherapy efficacy by unleashing type I in-terferon response, Nat. Cell Biol. 21 (2019) 511–521.
[117] I. San-Millan, G.A. Brooks, Reexamining cancer metabolism: lactate production for carcinogenesis could be the purpose and explanation of the Warburg Effect, Carcinogenesis 38 (2017) 119–133.
[118] L. Sapir, S. Tzlil, Talking over the extracellular matrix: how do cells communicate mechanically? Semin. Cell Dev. Biol. 71 (2017) 99–105.
[119] A. Schwab, C. Stock, Ion channels and transporters in tumour cell migration and invasion, Philos. Trans. R. Soc. Lond. B Biol. Sci. 369 (2014) 20130102.
[120] L. Seguin, J.S. Desgrosellier, S.M. Weis, D.A. Cheresh, Integrins and cancer: reg-ulators of cancer stemness, metastasis, and drug resistance, Trends Cell Biol. 25 (2015) 234–240.
[121] A.C. Shieh, Biomechanical forces shape the tumor microenvironment, Ann. Biomed. Eng. 39 (2011) 1379–1389.
[122] A.C. Shieh, M.A. Swartz, Regulation of tumor invasion by interstitial fluid flow, Phys. Biol. 8 (2011) 015012.
[123] T. Shiraishi, J.E. Verdone, J. Huang, U.D. Kahlert, J.R. Hernandez, G. Torga, J.C. Zarif, T. Epstein, R. Gatenby, A. McCartney, J.H. Elisseeff, S.M. Mooney, S.S. An, K.J. Pienta, Glycolysis is the primary bioenergetic pathway for cell mo-tility and cytoskeletal remodeling in human prostate and breast cancer cells, Oncotarget 6 (2015) 130–143.
[124] F. Sotgia, D. Whitaker-Menezes, U.E. Martinez-Outschoorn, N. Flomenberg, R.C. Birbe, A.K. Witkiewicz, A. Howell, N.J. Philp, R.G. Pestell, M.P. Lisanti, Mitochondrial metabolism in cancer metastasis: visualizing tumor cell mitochon-dria and the "reverse Warburg effect" in positive lymph node tissue, Cell Cycle 11 (2012) 1445–1454.
[125] A.M. Soto, C. Sonnenschein, The tissue organization field theory of cancer: a testable replacement for the somatic mutation theory, Bioessays 33 (2011) 332–340.
[126] J.P. Stains, R. Civitelli, Gap junctions regulate extracellular signal-regulated kinase signaling to affect gene transcription, Mol. Biol. Cell 16 (2005) 64–72.
[127] T. Sun, R. Patil, A. Galstyan, D. Klymyshyn, H. Ding, A. Chesnokova, W.K. Cavenee, F.B. Furnari, V.A. Ljubimov, E.S. Shatalova, S. Wagner, D. Li, A.N. Mamelak, S.I. Bannykh, C.G. Patil, J.D. Rudnick, J. Hu, Z.B. Grodzinski, Rekechenetskiy, V. Falahatian, A.V. Lyubimov, Y.L. Chen, L.S. Leoh, T.R. Daniels Wells, M.L. Penichet, E. Holler, A.V. Ljubimov, K.L. Black, J.Y. Ljubimova, Blockade of a laminin-411-notch Axis with CRISPR/Cas9 or a nanobioconjugate inhibits glioblastoma growth through tumor-microenvironment cross-talk, Cancer Res. 79 (2019) 1239–1251.
[128] T. Szoke, K. Kayser, J.D. Baumhakel, I. Trojan, J. Furak, L. Tiszlavicz, J. Eller, K. Boda, Prognostic significance of microvascularization in cases of operated lung cancer, Eur. J. Cardiothorac. Surg. : Off. J. Eur. Assoc. Cardio-thorac. Surg. 27 (2005) 1106–1111.
[129] D.P. Tabassum, K. Polyak, Tumorigenesis: it takes a village, Nature reviews, Cancer 15 (2015) 473–483.
[130] I. Tadeo, A.P. Berbegall, V. Castel, P. Garcia-Miguel, R. Callaghan, S. Pahlman, S. Navarro, R. Noguera, Extracellular matrix composition defines an ultra-high-risk group of neuroblastoma within the high-risk patient cohort, Br. J. Canc. 115 (2016) 480–489.
[131] I. Tadeo, A.P. Berbegall, L.M. Escudero, T. Alvaro, R. Noguera, Biotensegrity of the extracellular matrix: physiology, dynamic mechanical balance, and implications in oncology and mechanotherapy, Front Oncol. 4 (2014) 39.
[132] I. Tadeo, A.P. Berbegall, S. Navarro, V. Castel, R. Noguera, A stiff extracellular matrix is associated with malignancy in peripheral neuroblastic tumors, Pediatr. Blood Cancer 64 (2017) e26449.
[133] I. Tadeo, G. Bueno, A.P. Berbegall, M.M. Fernandez-Carrobles, V. Castel, M. Garcia-Rojo, S. Navarro, R. Noguera, Vascular patterns provide therapeutic targets in aggressive neuroblastic tumors, Oncotarget 7 (2016) 19935–19947.
[134] I. Tadeo, E. Gamero-Sandemetrio, A.P. Berbegall, M. Gironella, F. Ritort, A. Canete, G. Bueno, S. Navarro, R. Noguera, Lymph microvascularization as a prognostic indicator in neuroblastoma, Oncotarget 9 (2018) 26157–26170.
[135] I. Tadeo, M. Piqueras, D. Montaner, E. Villamon, A.P. Berbegall, A. Canete, S. Navarro, R. Noguera, Quantitative modeling of clinical, cellular, and extra-cellular matrix variables suggest prognostic indicators in cancer: a model in neuroblastoma, Pediatr. Res. 75 (2014) 302–314.
[136] J.R. Todd, K.A. Ryall, S. Vyse, J.P. Wong, R.C. Natrajan, Y. Yuan, A.C. Tan, P.H. Huang, Systematic analysis of tumour cell-extracellular matrix adhesion identifies independent prognostic factors in breast cancer, Oncotarget 7 (2016) 62939–62953.
[137] H.F. Tsai, A. Trubelja, A.Q. Shen, G. Bao, Tumour-on-a-chip: microfluidic models of tumour morphology, growth and microenvironment, J. R. Soc. Interface 14 (2017) 20170137.
[138] T. Ushiki, Collagen fibers, reticular fibers and elastic fibers. A comprehensive understanding from a morphological viewpoint, Arch. Histol. Cytol. 65 (2002) 109–126.
[139] M.G. Vander Heiden, R.J. DeBerardinis, Understanding the intersections between metabolism and cancer biology, Cell 168 (2017) 657–669.
[140] L. Vona-Davis, L.F. Gibson, Adipocytes as a critical component of the tumor mi-croenvironment, Leuk. Res. 37 (2013) 483–484.
[141] B. Waclaw, I. Bozic, M.E. Pittman, R.H. Hruban, B. Vogelstein, M.A. Nowak, A spatial model predicts that dispersal and cell turnover limit intratumour hetero-geneity, Nature 525 (2015) 261–264.
[142] J.C. Walrath, J.J. Hawes, T. Van Dyke, K.M. Reilly, Genetically engineered mouse models in cancer research, Adv. Cancer Res. 106 (2010) 113–164.
[143] C. Wei, C. Yang, S. Wang, D. Shi, C. Zhang, X. Lin, Q. Liu, R. Dou, B. Xiong, Crosstalk between cancer cells and tumor associated macrophages is required for mesenchymal circulating tumor cell-mediated colorectal cancer metastasis, Mol. Cancer 18 (2019) 64.
[144] Z. Werb, P. Lu, The role of stroma in tumor development, Cancer J. 21 (2015) 250–253.
[145] L. Wilde, M. Roche, M. Domingo-Vidal, K. Tanson, N. Philp, J. Curry, U. Martinez-

Outschoorn, Metabolic coupling and the Reverse Warburg Effect in cancer: implications for novel biomarker and anticancer agent development, Semin. Oncol. 44 (2017) 198–203.
[146] P.P. Wong, F. Demircioglu, E. Ghazaly, W. Alrawashdeh, M.R. Stratford, C.L. Scudamore, B. Cereser, T. Crnogorac-Jurcevic, S. McDonald, G. Elia, T. Hagemann, H.M. Kocher, K.M. Hodivala-Dilke, Dual-action combination therapy enhances angiogenesis while reducing tumor growth and spread, Cancer Cell 27 (2015) 123–137.
[147] L. Wullkopf, A.V. West, N. Leijnse, T.R. Cox, C.D. Madsen, L.B. Oddershede, J.T. Erler, Cancer cells' ability to mechanically adjust to extracellular matrix stiffness correlates with their invasive potential, Mol. Biol. Cell 29 (2018) 2378–2385.
[148] D. Yang, Y. Li, L. Xing, Y. Tan, J. Sun, B. Zeng, T. Xiang, J. Tan, G. Ren, Y. Wang, Utilization of adipocyte-derived lipids and enhanced intracellular trafficking of fatty acids contribute to breast cancer progression, Cell Commun. Signal. : CCS 16 (2018) 32.
[149] L. Yang, Y. Zhang, Tumor-associated macrophages: from basic research to clinical application, J. Hematol. Oncol. 10 (2017) 58.
[150] M. Yang, W.J. Brackenbury, Membrane potential and cancer progression, Front. Physiol. 4 (2013) 185.
[151] H. Ye, B. Adane, N. Khan, T. Sullivan, M. Minhajuddin, M. Gasparetto, B. Stevens, S. Pei, M. Balys, J.M. Ashton, D.J. Klemm, C.M. Woolthuis, A.W. Stranahan, C.Y. Park, C.T. Jordan, Leukemic stem cells evade chemotherapy by metabolic adaptation to an adipose tissue niche, Cell Stem Cell 19 (2016) 23–37.
[152] E.J. Yeo, Y.S. Chun, Y.S. Cho, J. Kim, J.C. Lee, M.S. Kim, J.W. Park, YC-1: a po-tential anticancer drug targeting hypoxia-inducible factor 1, J. Natl. Cancer Inst. 95 (2003) 516–525.
[153] M. Yin, S. Tan, Y. Bao, Z. Zhang, Enhanced tumor therapy via drug co-delivery and in situ vascular-promoting strategy, J. Control. Release : Off. J. Control. Release Soc. 258 (2017) 108–120.
[154] J. Yu, J. Li, Y. Chen, W. Cao, Y. Lu, J. Yang, E. Xing, Snail enhances glycolysis in the epithelial-mesenchymal transition process by targeting FBP1 in gastric cancer, Cell. Physiol. Biochem. : Int. J. Exp. Cell. Physiol. Biochem. Pharmacol. 43 (2017) 31–38.
[155] M. Zhang, J.S. Di Martino, R.L. Bowman, N.R. Campbell, S.C. Baksh, T. Simon-Vermot, I.S. Kim, P. Haldeman, C. Mondal, V. Yong-Gonzales, M. Abu-Akeel, T. Merghoub, D.R. Jones, X.G. Zhu, A. Arora, C.E. Ariyan, K. Birsoy, J.D. Wolchok, K.S. Panageas, T. Hollmann, J.J. Bravo-Cordero, R.M. White, Adipocyte-derived lipids mediate melanoma progression via FATP proteins, Cancer Discov. 8 (2018) 1006–1025.
[156] S. Zhang, X. Yang, L. Wang, C. Zhang, Interplay between inflammatory tumor microenvironment and cancer stem cells, Oncology Lett. 16 (2018) 679–686.
[157] Y. Zhang, M. Dang, Y. Tian, Y. Zhu, W. Liu, W. Tian, Y. Su, Q. Ni, C. Xu, N. Lu, J. Tao, Y. Li, S. Zhao, Y. Zhao, Z. Yang, L. Sun, Z. Teng, G. Lu, Tumor acidic microenvironment targeted drug delivery based on pHLIP-modified mesoporous organosilica nanoparticles, ACS Appl. Mater. Interfaces 9 (2017) 30543–30552.
[158] H. Zhao, Q. Duan, Z. Zhang, H. Li, H. Wu, Q. Shen, C. Wang, T. Yin, Up-regulation of glycolysis promotes the stemness and EMT phenotypes in gemcitabine-resistant pancreatic cancer cells, J. Cell Mol. Med. 21 (2017) 2055–2067.
[159] X.L. Zu, M. Guppy, Cancer metabolism: facts, fantasy, and fiction, Biochem. Biophys. Res. Commun. 313 (2004) 459–465

Article II: Vitronectin as a molecular player of the tumor microenvironment in neuroblastoma

Burgos-Panadero R, Noguera I, Cañete A, Navarro S, Noguera R.

BMC Cancer. 2019. 22;19(1):479. doi: 10.1186/s12885-019-5693-2.

Springer Nature BMC, London, ISSN: 1471-2407

Impact factor 2018: 2.933

5-year impact factor: 3.424

ARTICLE II

Burgos-Panadero et al. BMC Cancer (2019) 19:479
https://doi.org/10.1186/s12885-019-5693-2

BMC Cancer

RESEARCH ARTICLE Open Access

Vitronectin as a molecular player of the tumor microenvironment in neuroblastoma

Rebeca Burgos-Panadero[1,2], Inmaculada Noguera[3], Adela Cañete[4], Samuel Navarro[1,2] and Rosa Noguera[1,2*]

Abstract

Background: Vitronectin is a multifunctional glycoprotein known in several human tumors for its adhesive role in processes such as cell growth, angiogenesis and metastasis. In this study, we examined vitronectin expression in neuroblastoma to investigate whether this molecule takes part in cell-cell or cell-extracellular matrix interactions that may confer mechanical properties to promote tumor aggressiveness.

Methods: We used immunohistochemistry and image analysis tools to characterize vitronectin expression and to test its prognostic value in 91 neuroblastoma patients. To better understand the effect of vitronectin, we studied its in vitro expression using commercial neuroblastoma cell lines and in vivo using intra-adrenal gland xenograft models by immunohistochemistry.

Results: Digital image analysis allowed us to associate vitronectin staining intensity and location discriminating between territorial vitronectin and interterritorial vitronectin expression patterns. High territorial vitronectin expression (strong staining associated with pericellular and intracellular location) was present in tumors from patients with metastatic undifferentiating neuroblastoma, that were *MYCN* amplified, 11q deleted or with segmental chromosomal profiles, in the high-risk stratification group and with high genetic instability. In vitro studies confirmed that vitronectin is expressed in tumor cells as small cytoplasmic dot drops. In vivo experiments revealed tumor cells with high and dense cytoplasmic vitronectin expression.

Conclusions: These findings highlight the relevance of vitronectin in neuroblastoma tumor biology and suggest its potential as a future therapeutic target in neuroblastoma.

Keywords: Extracellular matrix, Vitronectin, Digital pathology, Migration, Neuroblastoma

Background

The composition, morphology and organization of the extracellular matrix (ECM) is key to both healthy and pathological environments. In healthy tissue, the ECM regulates development and homeostasis, whereas in tumors it displays mechanical properties such as stiffness that confer malignant characteristics to cell behaviour including proliferation, cell-death resistance, angiogen-esis, invasion and metastasis [1–3]. The interaction be-tween tumor cells and their surrounding elements is the first step in the development of metastasis, since cell movement requires firm cell-ECM adhesions to break down, as well as molecules to guide the migration.

Different cancer-promoting biological pathways of interest for further exploration are cell-cell or cell-ECM adhesions, proteases and chemokines [4]. In addition, recent studies show that cancer invasion and metastasis are driven by physical and chemical interactions between tumor cells and the ECM that translate into a stiff neo-plastic ECM and soft or deregulated tumor cells, which in turn lead to a more favorable microenvironment for cancer dissemination [5–8].

Vitronectin (VN) is an adhesive glycoprotein that acts as a link between cells and the ECM through several li-gands such as: integrins, plasminogen activator inhibitor-1(PAI-1) and urokinase plasminogen activator receptor (uPAR). VN is present in plasma as a mono-meric or dimeric structure (folded or native form) and in the ECM of several tissues as a multimeric formation (unfolded or active form) [9, 10]. It is mainly synthesized

* Correspondence: rnoguera@uv.es
[1]Pathology Department, Medical School, University of Valencia-INCLIVA, Valencia, Spain
[2]CIBERONC, Madrid, Spain
Full list of author information is available at the end of the article

by hepatocytes in the liver, although it has also been found in smaller amounts in extrahepatic tissues such as: brain, lung, kidney and vascular wall of adrenal gland [11–13]. It has also been observed that some tumor cells secrete VN as well as tumor-infiltrating T-lymphocytes (TIL) which bind to VN through TIL uPAR expression [14, 15]. The biological functions of VN, derived from its domains which bind several ligands in its activated form, are: preservation of vascular homeostasis (thrombosis and fibrinolysis), control of the innate immune system, facilitating cell adhesion and participation in migration in tissue repair and regeneration [16]. VN has a role in the provisional matrix of tumors, where it can promote cell adhesion and matrix degradation by binding to integrins, PAI-1 and uPAR [17]. In fact, in several hu-man neoplasms, VN is associated with tumor invasion, metastasis and angiogenesis [18–20].

Neuroblastoma (NB) originates from the neural crest in the Sympathetic Nervous System and is one of the most common pediatric solid tumors [21]. Although sev-eral clinical, biological and genetic markers define the risk of progression in NB patients [22], the mechanisms that control communication between tumor cells and the ECM, and can influence aggressiveness are not yet clear. Our group has already described the aggressive pattern of a stiff ECM defined as: ECM with cross-linked and disorganized reticulin fiber networks, scant amount of collagen type I fibers and glycosamino-glycans and large and abundant irregularly-shaped and high blood vessels, associated with a poor outcome in NB patients [23–26]. Hence, to better comprehend this tumor cell-ECM communication we searched for targets within the ECM elements. Previous studies in NB have noted VN expression in ganglion cells that could suggest

a differentiation role for this molecule [12] and its $\alpha_V\beta_3$ integrin receptor, which is highly expressed in high-risk NB [27].

In this study, we used digital image analysis to exam-ine the immunohistochemical expression of VN in NB to better understand the mechanical signals between neuroblasts and the ECM and their influence on tumor growth, differentiation and dissemination. In addition, we have done in vitro and in vivo experiments to assess if VN present in tumor or host microenvironments shows any modification on NB behavior since previous research showed the relationship between VN and me-tastasis and tumor progression in several human neoplasms.

Methods

Patient samples

A total of 91 primary NB tumors (at least two represen-tative cylinders of 1 mm) included in tissue microarrays (TMAs) were chosen according to NB genetic instability criteria [28], and classified into the following categories: very low instability (numerical chromosomal aberration (NCAs) profiles, defined as gains or losses of a whole chromosome), low instability (≤3 typical segmental chromosomal aberrations (SCAs), excluding 11q deleted (11qD) profiles, defined as gains or losses of chromo-somal fragments), medium instability (profiles with *MYCN* amplified (MNA) or 11qD, both genetic markers of worse prognosis or > 3 typical SCAs) and high in-stability (profiles with chromothripsis, defined as a local breaking with subsequent aleatory reassembly of frag-ment in a single event [28], or > 3 gene amplifications), these categories were dichotomized as low instability (very low and low groups) versus high instability (medium and high groups). All samples had been re-ferred to the Spanish Reference Centre for NB Biological and Pathological studies (Department of Pathology, Uni-versity of Valencia-INCLIVA) from 2000 to 2015. The samples were also classified according to INRG clinico-biological parameters [22] (Additional file 1: Table S1). This study was approved by the Ethical Committee of the University of Valencia (reference B.0000339 29/01/ 2015). Participants or their family members/legal guard-ians provided written informed consent for histological and genetic studies performed in our laboratory. Clinical data were provided by the pediatric oncologists in charge or by the Reference center for NB clinical studies.

Immunohistochemistry

One 3 μm section of each TMA was cut and immuno-stained with rabbit monoclonal antibody against VN (EP873Y, Clone; ab45139, Abcam, Cambridge, MA, USA) at 1:100 using OptiView Amplification Kit (Ven-tana Medical Systems Inc., Tucson, EE.UU.) in the BenchMark XT automated slide staining system (Ven-tana Medical Systems Inc., Tucson, USA). To determine the optimal antibody dilution, normal liver tissue and whole NB sections were used. As controls we stained several normal tissues (liver, kidney, salivary gland, smooth muscle, striated muscle, trachea, pancreas, spleen, adrenal gland, colon and placenta). Immunoreac-tivity was assessed by two researchers. VN immunoreac-tion was rated as no staining (0), and weak (1+), moderate (2+), and strong (3+). This category was di-chotomized as weak to moderate vs strong. This was used to determine the adequacy of a further image ana-lysis and help setting the image analysis parameters.

Image analysis

All immunostained slides were digitized with the whole-slide Pannoramic MIDI scanner (3DHISTECH Ltd., Budapest, Hungary) at 20x magnification. We used two applications to quantify VN in NB samples: Image Pro-Plus (IPP) software v.6.0 (Media Cybernetics Inc.,

Silver Spring, MD, USA) and DensitoQuant module (DensitoQ), Pannoramic viewer software 1.15 (3DHISTECH Ltd., Budapest, Hungary). The second was used as a validation tool of the first as it allows quick segmentation based on immunohistochemical staining intensity. The steps used for IPP and DensitoQ macro customization are described in Additional file 2: Table S2. Examples of how these two applications work are pro-vided in Additional file 3: Figure S1.

IPP: To characterize VN expression, a macro was customized using control tissues through RGB color segmentation; restrictive values were used to distinguish between VN staining intensity and location. We quanti-fied VN staining as weak to moderate or strong, and VN distribution was identified as intercellular only or pericellular plus intracellular location. In addition, the percentage of VN stained area (%SA) per cylinder and the mean of the two cylinders belonging to the same case were calculated as the area positive for VN divided by the total area of the cylinder, multiplied by 100. The %SA and density (number of objects/mm^2) of cell nuclei of each case were also quantified.

DensitoQ: The measures obtained were: negative, weak, moderate and strong pixels intensity and H-score. The H-score (or "histo" score), is a score that indicates if the sample can be considered positive or negative on the basis of a specific discriminatory threshold, ranging from 0 to 300 [29].

Statistical methods

All data were analyzed using SPSS statistical analysis software (version 24). The consistency between the subjective assessment and the VN image analysis was analyzed using the non-parametric Kruskal-Wallis test. Samples with no immunoreactivity for VN were ex-cluded from the statistical analysis. The VN numerical continuous variables derived from the morphometric analysis that did not follow a normal distribution were related to the INRG prognostic categories using the non-parametric Mann-Whitney and Kruskal-Wallis tests and were dichotomized using the third quartile (Q_3) to perform a survival analysis using the Kaplan-Meier curves and log-rank test. Cox survival regression using Wald (step back) test was used to estimate the influence of VN linked to INRG prognostic factors as independent variables on event-free and overall survival (EFS and OS, respectively). We considered p-values less than 0.05 as statistically significant.

In vitro and in vivo models

In vitro and in vivo models were used to evaluate the changes in neuroblasts VN expression independently of the hepatic/extrahepatic VN synthesis.

SH-SY5Y and SK-N-BE (2) NB cell lines were a generous gift from Miguel F. Segura (Laboratory of Translational Research in Child and Adolescent Cancer, Hospital Universitari Vall d'Hebron) and were grown, since VN is a fetal bovine serum component, in complete and serum-free media as indicate in Additional file 4: Table S3. To detect VN expression, cells were detached by Trypsin/EDTA 0.25% (Gibco; Thermo Fisher Scientific Inc.), deposited onto poly L-lysine coated (Sigma) slides using Shandon CytoSpin

III Cytocentrifuge at 1200 rpm for 10 min, fixed with methanol/acetone (1:1) for 10 min at room temperature and stained as indicated previously.

Mice deficient in $VN^{-/-}$ (B6.129S2 (D2)-Vtn^{tm1Dgi}/J) and $RAG1^{-/-}$ (B6.129S7-$Rag1^{tm1Mom}$/J) were obtained from Jackson Laboratory (USA) and Charles River Laboratories (France) and interbred to homozygosis for both alleles. Four-to six-week-old female or male $RAG1^{-/-}$ $VN^{+/+}$ (control) and $RAG1^{-/-}$ $VN^{-/-}$ (experimental) mice were used for left adrenal injection of 1×10^6 SH-SY5Y (n = 20) and SK-N-BE (2) (n = 20) NB cells lines in 30 μl of (1:1) Dulbecco's phosphate-buffered saline (DPBS; Gibco; Thermo Fisher Scientific Inc.) and Matrigel (Corning; Cultek S.L.U, Barcelona, Spain). Mice were anaesthetised using 4–5% isoflurane in a glass chamber for induction and anesthetic plan was main-tained by face mask with 1–2% isoflurane and subse-quently buprenorphine (0.1 mg/kg) was administered subcutaneously as analgesia. All experiments were car-ried out in accordance with the standards and care approved by the institutional ethical animal care com-mittee (reference 2015/VSC/PEA/00083). Tumor growth was checked visually weekly and mice were sacrificed by overdose of isoflurane at 8 weeks after taking blood from anaesthetised mice (as described previously) via the car-diac puncture method. After fixing in formaldehyde 4% and embedding in paraffin, xenograft tumors and mice organ samples were stained with Hematoxylin-eosin (HE) and with anti-VN as indicated previously. The Discovery anti-rabbit HQ reagent (Ventana Medical Systems Inc., Tucson, EE.UU.) was only used to detect VN expression in human NB cells.

Results

VN is present in NB samples

Positive VN immunoreactivity was observed in 85 out of 91 samples (93.4%). A good consistency between subjective and digital image analysis was observed (p-value = 0.000). The subjective assessment of VN pattern was weak to moderate (61 samples) and strong, (24 samples) (Fig. 1). Using digital image analysis, we found that: 1) Strong VN intensity was associated with a pericellular and intracellular location; it is mostly present in the pericellular region and stored intracellularly to a lesser

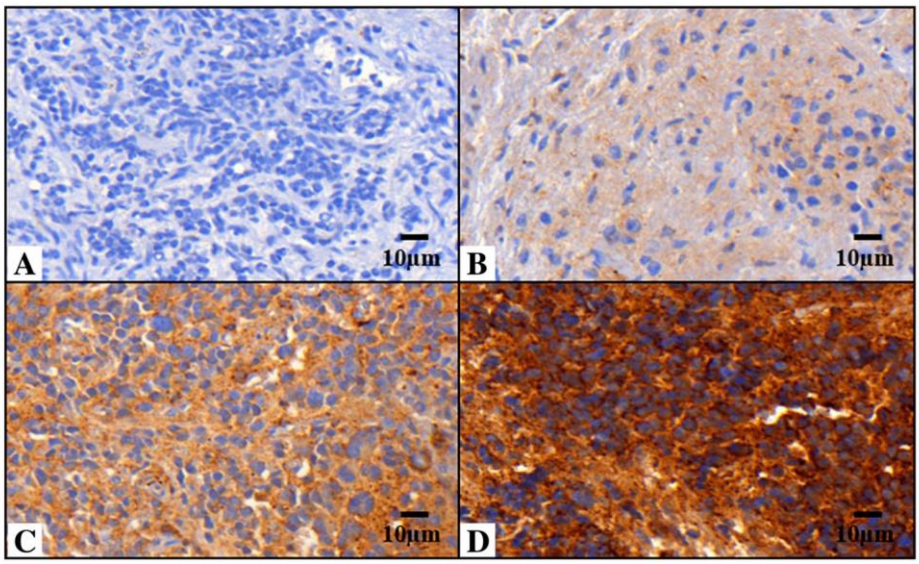

Fig. 1 Vitronectin pattern in neuroblastic tumors. Images immunostained with antibody anti-vitronectin (VN) at 40X. **a** Sample corresponding to negative VN. **b** and **c** Samples corresponding to weak to moderate VN expression and ECM distribution only (defined as interterritorial VN). **d** Sample with strong VN expression with pericellular and intracellular location (defined as territorial VN)

extent. The pericellular region concerned two tiny sites: the matrix adjacent to the cell membrane like a capsular territory, and a layer surrounding the capsular matrix of each cell or nests of grouped cells; we labeled this expression pattern territorial VN. 2) Weak to moderate VN intensity was associated with intercellular location (peripherally to territorial matrix); we named this expression interterritorial VN (Fig. 1).

The objective quantification patterns were considered as the %SA of interterritorial VN, territorial VN and H-score. We noted that the %SA of interterritorial VN and H-score was low in control tissues, high in liver tis-sues and intermediate in NB samples. Nevertheless, the highest %SA of territorial VN was found in NB samples. All VN and nuclei morphometric measurements are shown in Table 1. Median values of VN and nuclei quantity in relation to the INRG clinicopathological cri-teria are shown in Additional file 1: Table S1.

High territorial VN expression pattern is associated with poor prognostic factors

Mann-Whitney and Kruskal-Wallis tests demonstrated that strong VN intensity, territorial VN and high H-score were statistically associated with unfavorable prognostic factors. These VN features were present in tumors from patients with metastatic stage (excluding high H-score), uNB/pdNB histopathology, MNA, SCA profile, 11qD (excluding high H-score), high-risk pre-treatment stratification group and high genetic instabil-ity. No significant statistical relationship was observed between VN quantity and ploidy or histopathology category. The quantity of cell nuclei was higher in sam-ples from patients aged ≥18 months, metastatic stage, uNB/pdNB histopathology, MNA, high-risk pretreat-ment stratification and high genetic instability. p-values for the relationship between VN patterns and INRG pre-treatment risk classification are shown in Table 2.

The highest territorial VN expression pattern is related to poor survival

Samples with the highest VN levels and corresponding to strong staining intensity, territorial location and H-score ≥ Q_3 were associated with poorer 5-year EFS and lower 5-year OS, compared to patients whose sam-ples presented a low VN level (<Q_3), (p-value< 0.05). Furthermore, samples with nuclei density ≥ Q_3 were re-lated to poorer 5-year EFS and lower 5-year OS (Fig. 2). To perform the multivariate survival analysis using Cox proportional hazards regression, we considered all INRG variables together with the VN morphometric variables considered as statistically significant by the log-rank test (Kaplan-Meier curves). This test showed that age ≥ 18 months, uNB/pdNB histopathology and 11qD remained significant predictors for EFS. OS was influenced by age ≥ 18 months, 11qD (p-value< 0.05), MNA and terri-torial VN expression (p-value< 0.1) (Table 3).

In vitro and in vivo studies demonstrate VN expression by malignant neuroblasts

Regarding VN expression in malignant neuroblasts, we observed low amounts of cytoplasmic VN dot drops expression in around 50% of cells in both growth conditions

Table 1 Description of the vitronectin and nuclei morphometric measurements of control tissues and NB primary tumors

Parameter			Median	Mean	SD	Range	Q_3
Normal control tissues other than liver (n = 12)							
IPP	Nuclei	Density	308.10	305	99.75	94.10–477.70	355
		%SA	7.30	7.90	3.35	4–14	8.80
	Inter. VN	%SA	1.57	3.92	5.70	0.42–17	3.67
	Terr. VN	%SA	0.04	0.07	0.07	0–0.20	0.15
Densito	VN ratio of pixels	Weak	0.04	1	1.50	0–4	1.75
		Moderate	2.25	10.95	13	0.06–35	22.90
		Strong	1	2	2.60	0–9	2.95
	H-score		20.45	46.40	52.51	0.16–163	82.50
Liver samples (n = 5)							
IPP	Nuclei	Density	616	1846.70	2384.30	472–6051.70	3767.80
		%SA	4	3.80	2.05	2–7	5.50
	Inter. VN	%SA	20	19	11.40	3–31	29.50
	Terr. VN	%SA	3	2.50	1.30	0.65–4	3.50
Densito	VN ratio of pixels	Weak	2.50	2.85	2.30	0.30–6	5.15
		Moderate	67	64.55	8.30	50–71	69.50
		Strong	12.75	13.50	2.70	10–17	16
	H-score		175.80	172.60	11.60	152.25–181.35	179.55
Primary tumors (n = 91)							
IPP	Nuclei	Density	560	1074.25	1455.80	95–6793	739
		%SA	11.75	11.70	6.30	0.35–29.70	15.50
	Inter. VN	%SA	9.35	12.25	10.95	0.02–40.97	18.20
	Terr. VN	%SA	0.71	2.95	4.45	0.01–20.70	4.50
Densito	VN ratio of pixels	Weak	0.80	1.60	2.40	0.01–14.65	2.10
		Moderate	35	36.10	24.70	0.05–88.10	56.75
		Strong	3.55	12.85	17.85	0.01–61.85	20.40
	H-score		110.91	112.85	78.55	1.07–257.60	183.80

Descriptors of vitronectin (VN) immunoreactivity and nuclei according to their morphometric measurements are shown. IPP: Image Pro-Plus; Densito: DensitoQuant; Inter.VN: Interterritorial VN; Terr.VN: Territorial VN. Density: number of objects/mm^2; %SA: percentage of stained area. SD: Standard deviation; Q_3: third quartile

Table 2 p-values and relationship between vitronectin and nuclei morphometric measurements and poor prognostic factors

Parameter			Age: ≥18 months	Stage: M	Hist.D: uNB/ pdNB	MYCN: MNA	Gen. profile: SCA	11q: 11qD	Risk group: high-risk	Gen. Instab.:High
IPP	Nuclei	Dens.	–	0.005↑	0.007↑	0.001↑	–	–	0.001↑	0.003↑
		%SA	0.004↑	–	–	–	0.018↓	–	–	–
	Inter.VN	%SA	–	–	–	–	–	–	–	–
	Terr.VN	%SA	–	0.010↑	0.001↑*	0.024↑	0.001↑	0.035↑	0.008↑	0.000↑
Densito	VN ratio of pixels	Weak	–	–	–	–	–	–	–	–
		Mod.	–	–	–	–	–	–	–	–
		Strong	–	0.037↑	0.010↑*	0.011↑	0.002↑	0.021↑	0.004↑	0.010 ↑
	H-score		–	–	0.019↑	0.040↑	0.011↑	–	0.008↑	0.001↑

Only morphometric variables for vitronectin (VN) expression and nuclei having a statistically significant relationship with pre-treatment risk stratification factors are shown (p-value< 0.05). IPP: Image Pro-Plus; Densito: DensitoQuant; Dens. Density (number of objects/mm2); %SA: percentage of stained area; Inter. VN: Interterritorial VN; Terr.VN: Territorial VN; Mod.: moderate. M: metastatic; Hist.D: histopathologic differentiation; uNB: undifferentiated neuroblastoma; pdNB: poorly differentiated neuroblastoma; NOS was excluded from statistical analysis; Gen. Profile: genetic profile; SCA: segmental chromosomal aberration; MNA: MYCN amplified; 11qD: 11q deletion; Gen. Instab.: genetic instability. -: not statistically significant, ↑/↓: higher or lower median value for the poor-prognostic group(s). *There are statistically significant differences between pdNB and uNB, within Strong VN (p-value< 0.05) and %SA Territorial VN (p-value< 0.1) morphometric variables

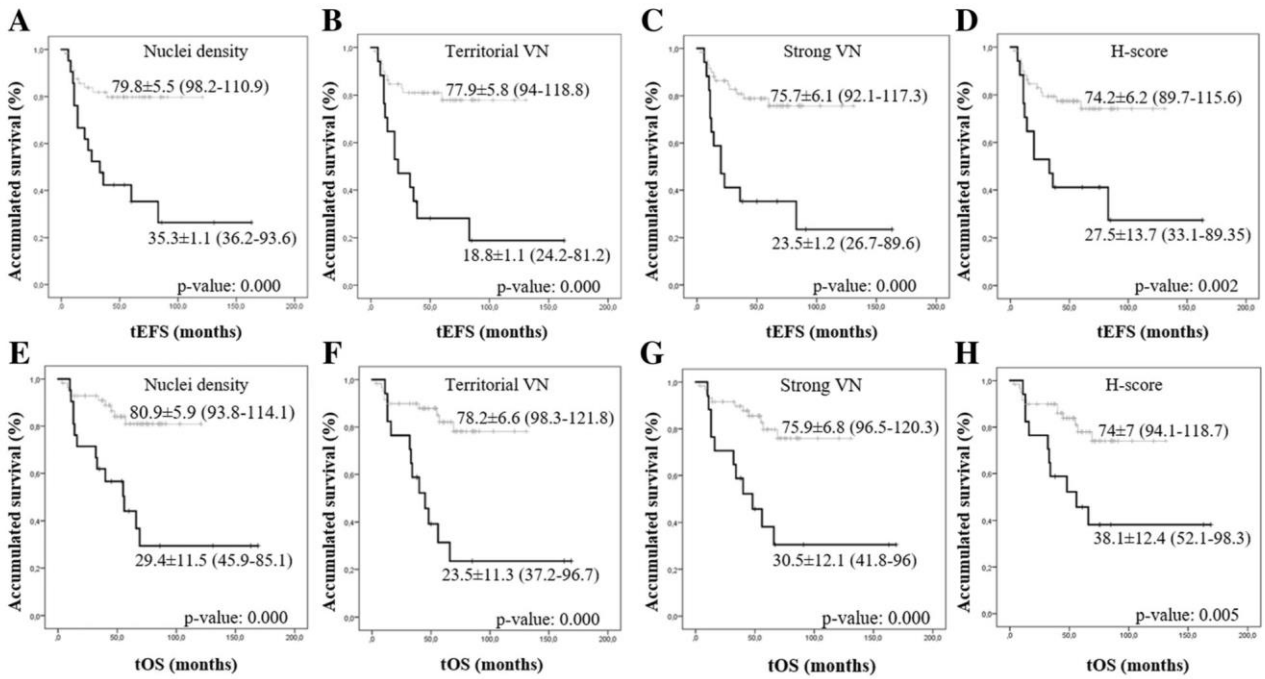

Fig. 2 Kaplan–Meier graphs showing the EFS (**a-d**) or OS (**e-h**) depending on different variables. In all cases, the black and grey lines correspond to the group above and below the third quartile (Q_3) used for dichotomization, respectively. Only morphometric variables for vitronectin (VN) quantity with a statistically significant relationship with event-free survival (EFS) and/or overall survival (OS) are shown (p-value< 0.05). p-values and 5-year survival rates are shown. **a** and **e** Nuclei density. **b** and **f** Territorial VN. **c** and **g** VN Strong ratio of pixels. **d** and **h** H-score

(complete and serum-free media) of both cell lines (Fig. 3). Tumor development after SH-SY5Y and SK-N-BE (2) inoculation was observed in RAG1$^{-/-}$ VN$^{+/+}$ mice (SH-SY5Y = 7/10 and SK-N-BE (2) = 10/10) and RAG1$^{-/-}$ VN$^{-/-}$ mice (SH-SY5Y = 9/10 and SK-N-BE (2) = 9/10).

Table 3 Cox Regression of morphometric vitronectin variables and INRG prognostic factors

Variable	B	S.E	Wald	Exp (B) (95% CI)	p-value
EFS					
Age (≥18 month)	1.361	0.526	6.696	3.898 (1.39–10.92)	0.010
Hist.D (uNB/pdNB)	1.073	0.411	6.806	2.924 (1.30–6.54)	0.009
11q status (11qD)	0.883	0.424	4.332	2.418 (1.05–5.55)	0.037
OS					
Age (≥18 month)	1.320	0.603	4.797	3.745 (1.14–12.20)	0.029
11q status (11qD)	1.309	0.469	7.785	3.702 (1.47–9.28)	0.005
*MYCN (MNA)	0.857	0.472	3.296	2.357 (0.94–5.94)	0.069
*Terr. VN_Q_3	0.852	0.480	3.154	2.344 (0.92–6)	0.076

Significant INRG prognostic parameters and morphometric vitronectin (VN) measurements predictive of poor outcome in neuroblastoma (NB) patients based on event-free survival (EFS) and overall survival (OS) with p-value < 0.05 and *p-value < 0.1. Hist.D: histopathologic differentiation; uNB: undifferentiated neuroblastoma; pdNB: poorly differentiated neuroblastoma; 11qD: 11q deletion; MNA: MYCN amplified; Terr.VN_Q_3: Territorial vitronectin dichotomized at the third quartile. B: Beta coefficient; S.E: Standard Error; CI: Confidence interval. Coefficients Exp (B) > 1 indicate that high values of this parameter increase the probability of it being an independent poor prognostic factor

We found no significant differences between tumor growth in control compared to experimental RAG1$^{-/-}$ VN$^{-/-}$ in any of the cell lines. Tumors displayed small and limited intra-adrenal, and large abdominal solid masses with a heterogeneous macroscopic appearance, as well as moderate infiltrative growth into surrounding tissues such as perirenal fat, pancreas and liver, both in animal models and in NB cell lines. Regarding histopathology, solid tu-mors from the SH-SY5Y cell line presented 30–90% undif-ferentiated neuroblastic cells, non-evident nucleolus, high mitosis-karyorrhexis index (IMK) and between 5 and 50% necrosis. With respect to the samples derived from cell line SK-N-BE (2), these were characterized by being uNB with a mean of 40–70% neuroblasts with evident nucle-olus, high IMK, and 5–50% necrosis. Highly dense cyto-plasmic VN staining was similar in control and experimental mice derived from both cell lines (Fig. 3).

Discussion

VN is an attachment glycoprotein that directs cell migration, progression, adhesion and differentiation in many biological and pathological processes [13, 15, 30, 31]. By introducing advanced morphometric methodology, we have been able to demonstrate and robustly quantify VN as an important ECM component in aggressive NB synthetized by undifferentiated neuroblasts. We have found two VN expression patterns which reflect the

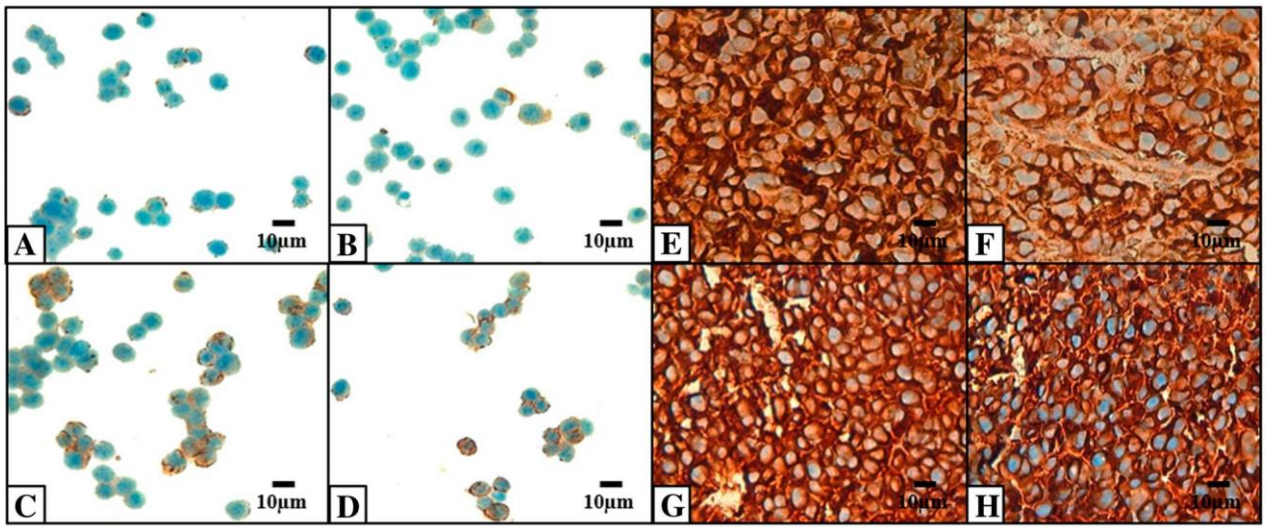

Fig. 3 Examples of in vitro (**a-d**) and in vivo (**e-h**) vitronectin expression. Vitronectin (VN) expression in SK-N-BE (2) cells maintained in: **a** Complete medium. **b** Serum-free medium. VN expression in SH-SY5Y cells maintained in: **c** Complete medium. **d** Serum-free medium. VN expression in orthotopic neuroblastoma (NB) mice after SK-N-BE (2) injection. **e** $RAG1^{-/-}$ $VN^{+/+}$ mice. **f** $RAG1^{-/-}$ $VN^{-/-}$ mice. VN expression in orthotopic NB mice after SH-SY5Y injection. **g** $RAG1^{-/-}$ $VN^{+/+}$ mice. **h** $RAG1^{-/-}$ $VN^{-/-}$ mice

secretion time and role of this glycoprotein that has typic-ally been described for ECM constituents in cartilage: the territorial VN pattern, where VN is synthetized and re-cently incorporated to the newly formed matrix facilitating mechanical stresses of tumor cells, and the interterritorial VN pattern, where VN has been integrated some time ago to the matrix contributing to metabolic and biomechan-ical properties of several tumor tissue elements.

Some contradictory studies of VN expression in NB have been described [12, 27, 32]. Gladson et al. 1997, showed VN expression in differentiating neuroblastic tu-mors and noted its attachment role in retinoic-acid dif-ferentiated neuroblastic cells stimulating in vivo differentiation [12]. Later NB studies detected an overex-pression of $\alpha_v\beta_3$ integrin and uPAR, both of which are important VN ligands, in high-risk NB [27, 32]. From a larger cohort of neuroblastic tumors, our immunohisto-chemical results revealed VN expression in NB and GNB, with a high territorial VN expression in undiffer-entiated neuroblasts. Our findings are in agreement with the most recent studies mentioned above and the differ-ences from the earlier study [12] could be explained by cohort size. Using digital pathology techniques, we were able to accurately provide a connection between inten-sity and location. These techniques assure the standardization of all measurements and minimize inter-observer differences [33, 34] and can easily be reproduced in future studies. We are currently carrying out topological analysis on the histopathological images to evaluate non-cellular VN distribution features related to the tumor microenvironment. Our topological ap-proach will capture different aspects of the VN distribution to improve the classification of biopsy sam-ples from NB samples.

The in vitro and vivo preliminary results in the present study mainly focused on human NB, were to emphasize the VN secretion by both NB cell lines and highlight the tumor and/or host microenvironment influence in their VN synthesis. We found that in vitro NB cells expressed a low quantity of VN as a small cytoplasmic dot drops pat-tern and that the in vivo experiments revealed a high amount of VN as a dense cytoplasmic pattern with no dif-ferences in VN staining pattern or tumor growth rate be-tween $RAG1^{-/-}$ $VN^{+/+}$ and $RAG1^{-/-}$ $VN^{-/-}$ mice. The increased VN secretion by tumor cells, which produces mechanical stress, generates an initial stiff matrix and re-sults in disrupted cell-cell and cell-ECM interactions, pro-moting tumor proliferation in both mice strains, as described in ovarian cancer, through the breakdown of VN bonds to improve metastasis [35]. We confirmed that:

a) Fetal bovine serum (FBS) does not contribute to a higher amount of VN in tumor cells as reported by Glad-son et al. [36] and b) the importance of VN in NB tumor growth due to its high presence in vivo. These findings reinforce the previously described VN role in improving the migratory ability of tumor cells in NB and suggest that in vivo tumor cells produce VN to achieve greater migra-tory capacity. Furthermore, given the importance of VN in breast cancer [37], we are developing experiments to clar-ify the role of VN in vivo in NB tumor growth. Serial tumor passages will allow VN secretion by neuroblasts to be modified in relation to a host microenvironment, af-fecting tumor growth and genetic instability, as occurs in hormone-dependent tumors [38]. Therefore, although

xenotranplanted neuroblastic cells continue to synthe-tize VN, the absence of liver VN in the host would have a subtle role in the secretory ability of malignant neuro-blasts, but some long-term influence on cell proliferation and tumor aggressiveness.

We stress that a high territorial VN expression pattern could contribute to tumor cell adhesion, thus promoting invasion and metastasis in NB, suggesting that VN or its ligands could be used as targets when developing therapeutic strategies for modulating the relationship between tumor cells and the ECM. In fact, the highest presence of territorial VN protein in the present cohort is related to unfavorable independent prognostic INRG variables. The high presence of territorial VN staining in tumors from patients with metastasic stage and unfavorable histology, would lead to higher migration ability of tumor cells by anchorage to fibers and proteoglycans, as well as disrupted cell adhesion and spreading via interactions with specific $\alpha_V\beta_3$ and $\alpha_V\beta_5$ integrins, uPAR and PAI-1 in a stiff matrix. In the case of tumors with genetic instability, a huge presence of territorial VN would generate mechanical alterations in ECM, which would be transmitted to the nuclear matrix and would modulate the response of intracellular signals activating genetic and epigenetic mechanisms of instability in these tumors [39].

The main therapeutic goal would be to focus on decreasing VN expression or to inhibit its joining with $\alpha_V\beta_3$ integrin, uPAR or PAI-1, thus depriving the tumor cells of the mechanical forces necessary to create the ap-propriate environment for invasion [40–42]. Via its li-gands, VN has a role in biochemical cell-ECM pathways which could be used as therapeutic targets; however, no drug against cell-ECM interactions has yet been approved, although some trials are ongoing as described below.

$\alpha_V\beta_3$ and $\alpha_V\beta_5$ integrins bind to the arginine-glyci-ne-aspartate (RGD) VN sequence and are key factors in angiogenesis. It has been observed that VN activates vascular endothelial growth factor receptor 2 (VEGFR-2) via $\alpha_V\beta_3$, thus contributing to angiogenesis [43]. As anti-$\alpha_V\beta_3$ integrin targeted drugs: Vitaxin, Intetumubab (CNTO 95) and 17E6 (EMD 525797) are in different phases of clinical trials [44], also in vitro melanoma re-search has displayed metastasis retardation using IH1062, an $\alpha_V\beta_3$ integrin inhibitor that blocks the bind-ing of this integrin to VN [45].

uPAR is a protease that binds to VN in the RGD motif or N-terminal somatomedin B (SMB) domain. It has been observed that this union initiates integrin pathways that promoting migration [46, 47]. In addition, when uPAR binds to urokinase plasminogen activator (uPA), it causes the cleaving of plasminogen to produce plasmin that mediates the degradation of the ECM [48]. An in vivo study into a monoclonal anti-uPAR antibody (ATN-658) reported that this antibody inhibits tumor cell proliferation in prostate cancer [49].

Finally, PAI-1 is a protease inhibitor of the serpins family that binds to the SMB domain of VN where its main function is uPA inhibition. Thus, PAI-1 partici-pates in the uPA/uPAR proteolytic cascade, as well as interfering in the binding of uPAR and α_V integrins fam-ily in the SMB domain and RGD motif to VN, respect-ively [50]. In fact, an in vivo study of NB using PAI-1 deficient mice showed a reduction in tumor size [51]. In vitro and in vivo studies on the inhibition of PAI-1 using compounds such as TM5441, TM5275 and SK-216 have demonstrated toxic effects in cancer cells [52, 53].

Conclusions

In conclusion, NB samples of patients with poor prognostic factors are characterized by the highest territorial VN expression pattern. Our findings suggest the importance of extensive studies on VN as a possible target for inhibiting interactions in NB.

Additional files

Additional file 1: **Table S1**. Descriptors and median values of vitronectin and nuclei morphometric variables in the present cohort. (DOCX 19 kb)

Additional file 2: **Table S2**. Description of the image analysis process. (DOCX 15 kb)

Additional file 3 **Figure S1**. Examples of how these applications work in vitronectin samples. A. Liver sample image immunostained for vitronectin (VN) without segmentation. B. Image of liver control sample segmentation with the DensitoQuant module (Pannoramic viewer software). C. Image of liver control sample segmentation with Image Pro-Plus software. D. Primary neuroblastoma (NB) sample immunostained for VN without segmentation. E. Image of NB sample segmentation with the DensitoQuant module (Pannoramic viewer software). F. Image of NB sample segmentation with Image Pro-Plus software. (ZIP 8306 kb)

Additional file 4: **Table S3**. Growth conditions of NB human cell lines. (DOCX 14 kb)

Abbreviations

%SA: Percentage of stained area; 11qD: 11q deleted; 11qND: 11q non-deleted; DensitoQ: DensitoQuant; dNB: Differentiating neuroblastoma; ECM: Extracellular matrix; EFS: Event-free survival; GNB: Ganglioneuroblastoma; INRG: International Neuroblastoma Risk Group; IPP: Image Pro-Plus; MNA: MYCN amplified; MNNA: MYCN non-amplified; NB: Neuroblastoma; NCAs: Numerical chromosomal aberrations; OS: Overall survival; PAI-1: Plasminogen activator inhibitor-1; pdNB: Poorly differentiated neuroblastoma; Q3: Third quartile; RGD: Arginine-glycine-aspartate motif; SCAs: Segmental chromosomal aberrations; SMB: Somatomedin B domain; TMAs: Tissue microarrays; uNB: Undifferentiated neuroblastoma; uPA: Urokinase plasminogen activator; uPAR: Urokinase plasminogen activator receptor; VN: Vitronectin

Acknowledgments

The authors would like to thank Elisa Alonso for technical support, Francisco Santonja for statistical assistance and Kathryn for English correction. We also thank the Spanish Society of Pediatric Hemato-Oncology (SEHOP) for patient data management.

Funding

This study was supported by the FAECC (contract 2015, FAECC2015/006), CIBERONC (CB16/12/00484) and FIS (PI17/01558, Institute of Health Carlos III,

Madrid/ERDF). The funders had no involvement in the research process or the preparation and submission of the article.

Availability of data and materials
The datasets used and analyzed in the current study are available from the corresponding author on reasonable request.

Authors' contributions
RB-P carried out the in vitro and in vivo experiments, the image and statistical analyses of the samples, and wrote the original draft of the manuscript. IN: contributed to in vivo experiments and suggested draft changes. AC provided the pediatric clinical data used for this study. SN carried out the histopathological analyses of the samples and reviewed the paper and suggested draft changes. RN elaborated the concept and designed the study, reviewed the paper and suggested draft changes. All authors read and approved the final manuscript.

Ethics approval and consent to participate
This study was approved by the Ethical Committee of the University of Valencia (reference B.0000339 29/01/2015). Participants or their family members/legal guardians provided written informed consent for histological and genetic studies performed in our laboratory. The animal experiments were carried out in accordance with the standards and care approved by the institutional ethical animal care committee (reference 2015/VSC/PEA/00083).

Consent for publication
Not applicable

Competing interests
The authors declare that they have no competing interests.

Publisher's Note

Author details
[1]Pathology Department, Medical School, University of Valencia-INCLIVA, Valencia, Spain. [2]CIBERONC, Madrid, Spain. [3]Central Support Service for Experimental Research (SCSIE), University of Valencia, Valencia, Spain. [4]Pediatric Oncology Unit, University and Polytechnic Hospital La Fe, Valencia, Spain.

Received: 19 June 2018 Accepted: 8 May 2019
Published online: 22 May 2019

References
1. Xiong G, Xu R. Function of cancer cell-derived extracellular matrix in tumor progression. J Cancer Metastasis Treat. 2016; 2:357–64.
2. Pickup MW, Mouw JK, Weaver VM. The extracellular matrix modulates the hallmarks of cancer. EMBO Rep. 2014;15(12):1243–53.
3. Wells RG. The role of matrix stiffness in regulating cell behavior. Hepatology. 2008;47(4):1394–400.
4. Wirtz D, Konstantopoulos K, Searson PC. The physics of cancer: the role of physical interactions and mechanical forces in metastasis. Nat Rev Cancer. 2011;11(7):512–22.
5. Iozzo RV, Sanderson RD. Proteoglycans in cancer biology, tumour microenvironment and angiogenesis. J Cell Mol Med. 2011;15(5):1013–31.
6. Oskarsson T. Extracellular matrix components in breast cancer progression and metastasis. Breast. 2013;22(Suppl 2): S66–72.
7. Vincent T, Mechti N. Extracellular matrix in bone marrow can mediate drug resistance in myeloma. Leuk Lymphoma. 2005;46(6):803–11.
8. Lin HH, Lin HK, Lin IH, Chiou YW, Chen HW, Liu CY, et al. Mechanical phenotype of cancer cells: cell softening and loss of stiffness sensing. Oncotarget. 2015;6(25):20946–58.
9. Preissner KT. Structure and biological role of vitronectin. Annu Rev Cell Biol. 1991; 7:275–310.
10. Schvartz I, Seger D, Shaltiel S. Vitronectin. Int J Biochem Cell Biol. 1999;31(5): 539–44.
11. Seiffert D. Constitutive and regulated expression of vitronectin. Histol Histopathol. 1997;12(3):787–97.
12. Gladson CL, Dennis C, Rotolo TC, Kelly DR, Grammer JR. Vitronectin expression in differentiating neuroblastic tumors: integrin alpha v beta 5 mediates vitronectin-dependent adhesion of retinoic-acid-differentiated neuroblastoma cells. Am J Pathol. 1997;150(5):1631–46.
13. Dimova T, Georgieva R, Petlov D, Lazarova S. Comparative study on the expression of fibronectin, vitronectin, $\alpha_5\beta_1$, β_3 and α_v integrins in goat and pig adrenal glands. Comptes rendus de l'Academie bulgare des Sciences. 2005; 12:1457–62.
14. Edwards S, Lalor PF, Tuncer C, Adams DH. Vitronectin in human hepatic tumours contributes to the recruitment of lymphocytes in an alpha v beta3-independent manner. Br J Cancer. 2006;95(11):1545–54.
15. Yasumitsu H, Seo N, Misugi E, Morita H, Miyazaki K, Umeda M. Vitronectin secretion by hepatic and non-hepatic human cancer cells. In Vitro Cell Dev Biol Anim. 1993;29A(5):403–7.
16. Preissner KT. The role of vitronectin as multifunctional regulator in the hemostatic and immune systems. Blut. 1989;59(5):419–31.
17. Madsen CD, Ferraris GM, Andolfo A, Cunningham O, Sidenius N. uPAR-induced cell adhesion and migration: vitronectin provides the key. J Cell Biol. 2007;177(5):927–39.
18. Gladson CL, Cheresh DA. Glioblastoma expression of vitronectin and the alpha v beta 3 integrin. Adhesion mechanism for transformed glial cells. J Clin Invest. 1991;88(6):1924–32.
19. Schneider G, Bryndza E, Poniewierska-Baran A, Serwin K, Suszynska M, Sellers ZP, et al. Evidence that vitronectin is a potent migration-enhancing factor for cancer cells chaperoned by fibrinogen: a novel view of the metastasis of cancer cells to low-fibrinogen lymphatics and body cavities. Oncotarget. 2016;7(43):69829–43.
20. Shi K, Lan RL, Tao X, Wu CY, Hong HF, Lin JH. Vitronectin significantly influences prognosis in osteosarcoma. Int J Clin Exp Pathol. 2015;8(9):11364–71.
21. Cheung NK, Dyer MA. Neuroblastoma: developmental biology, cancer genomics and immunotherapy. Nat Rev Cancer. 2013;13(6):397–411.
22. Cohn SL, Pearson AD, London WB, Monclair T, Ambros PF, Brodeur GM, et al. The international neuroblastoma risk group (INRG) classification system: an INRG task force report. J Clin Oncol. 2009;27(2):289–97.
23. Tadeo I, Berbegall A, Castel V, García-Miguel P, Callaghan R, Påhlman S, et al. Extracellular matrix composition defines an ultra-high-risk group of neuroblastoma within the high-risk patient cohort. Br J Cancer. 2016;115(4): 480–9.
24. Tadeo I, Berbegall A, Navarro S, Castel V, Noguera R. A stiff extracellular matrix is associated with malignancy in peripheral neuroblastic tumors. Pediatr Blood Cancer. 2017;64(9). https://doi.org/10.1002/pbc.26449.
25. Tadeo I, Bueno G, Berbegall A, Fernández-Carrobles M, Castel V, García-Rojo M, et al. Vascular patterns provide therapeutic targets in aggressive neuroblastic tumors. Oncotarget. 2016;7(15):19935–47.
26. Tadeo I, Gamero-Sandemetrio E, Berbegall AP, Navarro S, Cañete A, Noguera R. 1p36 deletion results in a decrease in glycosaminoglycans which is associated with aggressiveness in neuroblastic tumors. Histol Histopathol. 2018; 33:487–95.
27. Erdreich-Epstein A, Shimada H, Groshen S, Liu M, Metelitsa LS, Kim KS, et al. Integrins alpha(v)beta3 and alpha(v)beta5 are expressed by endothelium of high-risk neuroblastoma and their inhibition is associated with increased endogenous ceramide. Cancer Res. 2000;60(3):712–21.
28. Ambros IM, Brunner C, Abbasi R, Frech C, Ambros PF. Ultra-high density SNParray in neuroblastoma molecular diagnostics. Front Oncol. 2014; 4:202.
29. Lavorato-Rocha AM, Akagi EM, de Melo Maia B, Rodrigues IS, Botelho MC, Marchi FA, et al. An integrative approach uncovers biomarkers that associate with clinically relevant disease outcomes in vulvar carcinoma. Mol Cancer Res. 2016;14(8):720–9.
30. Niu Y, Zhang L, Bi X, Yuan S, Chen P. Evaluation of Vitronectin expression in prostate Cancer and the clinical significance of the Association of Vitronectin Expression with prostate specific antigen in detecting prostate Cancer. Urol J. 2016;13(1):2527–32.
31. Ortega-Martinez I, Gardeazabal J, Erramuzpe A, Sanchez-Diez A, Cortes J, Garcia-Vazquez MD, et al. Vitronectin and dermcidin serum levels predict the metastatic progression of AJCC I-II early-stage melanoma. Int J Cancer. 2016;139(7):1598–607.
32. Li P, Gao Y, Ji Z, Zhang X, Xu Q, Li G, et al. Role of urokinase plasminogen activator and its receptor in metastasis and invasion of neuroblastoma. J Pediatr Surg. 2004;39(10):1512–9.
33. Nast CC, Lemley KV, Hodgin JB, Bagnasco S, Avila-Casado C, Hewitt SM, et al. Morphology in the digital age: integrating high-resolution description of

structural alterations with phenotypes and genotypes. Semin Nephrol. 2015;
35(3):266–78.
34. Mulrane L, Rexhepaj E, Penney S, Callanan JJ, Gallagher WM. Automated image analysis in histopathology: a valuable tool in medical diagnostics. Expert Rev Mol Diagn. 2008;8(6):707–25.
35. Kenny HA, Kaur S, Coussens LM, Lengyel E. The initial steps of ovarian cancer cell metastasis are mediated by MMP-2 cleavage of vitronectin and fibronectin. J Clin Invest. 2008;118(4):1367–79.
36. Gladson CL, Wilcox JN, Sanders L, Gillespie GY, Cheresh DA. Cerebral microenvironment influences expression of the vitronectin gene in astrocytic tumors. J Cell Sci. 1995;108 (Pt 3:947–56.
37. Pirazzoli V, Ferraris GM, Sidenius N. Direct evidence of the importance of vitronectin and its interaction with the urokinase receptor in tumor growth. Blood. 2013;121(12):2316–23.
38. Chang C, Lee SO, Yeh S, Chang TM. Androgen receptor (AR) differential roles in hormone-related tumors including prostate, bladder, kidney, lung, breast and liver. Oncogene. 2014;33(25):3225–34.
39. nGraham DM, Burridge K. Mechanotransduction and nuclear function. Curr Opin Cell Biol. 2016;40:98–105.
40. Sloan EK, Pouliot N, Stanley KL, Chia J, Moseley JM, Hards DK, et al. Tumor-specific expression of alphavbeta3 integrin promotes spontaneous metastasis of breast cancer to bone. Breast Cancer Res. 2006;8(2):R20.
41. Mauro CD, Pesapane A, Formisano L, Rosa R, D'Amato V, Ciciola P, et al. Urokinase-type plasminogen activator receptor (uPAR) expression enhances invasion and metastasis in RAS mutated tumors. Sci Rep. 2017;7(1):9388.
42. Harbeck N, Kruger A, Sinz S, Kates RE, Thomssen C, Schmitt M, et al. Clinical relevance of the plasminogen activator inhibitor type 1--a multifaceted proteolytic factor. Onkologie. 2001;24(3):238–44.
43. Li R, Luo M, Ren M, Chen N, Xia J, Deng X, et al. Vitronectin regulation of vascular endothelial growth factor-mediated angiogenesis. J Vasc Res. 2014; 51(2):110–7.
44. Holle AW, Young JL, Spatz JP. In vitro cancer cell-ECM interactions inform in vivo cancer treatment. Adv Drug Deliv Rev. 2016;97:270–9.
45. Zhang Y, Yang M, Ji Q, Fan D, Peng H, Yang C, et al. Anoikis induction and metastasis suppression by a new integrin alphavbeta3 inhibitor in human melanoma cell line M21. Investig New Drugs [Internet. 2011;29(4):666–73.
46. Montuori N, Pesapane A, Rossi FW, Giudice V, De Paulis A, Selleri C, et al. Urokinase type plasminogen activator receptor (uPAR) as a new therapeutic target in cancer. Transl Med UniSa. 2016;15:15–21.
47. Noh H, Hong S, Huang S. Role of urokinase receptor in tumor progression and development. Theranostics. 2013;3(7):487–95.
48. Smith HW, Marshall CJ. Regulation of cell signalling by uPAR. Nat Rev Mol Cell Biol. 2010;11(1):23–36.
49. Rabbani SA, Ateeq B, Arakelian A, Valentino ML, Shaw DE, Dauffenbach LM, et al. An anti-Urokinase plasminogen activator receptor antibody (ATN-658) blocks prostate Cancer invasion, migration, growth, and experimental skeletal metastasis in vitro and in vivo. Neoplasia. 2010;10:778–88.
50. Andreasen PA, Egelund R, Petersen HH. The plasminogen activation system in tumor growth, invasion, and metastasis. Cell Mol Life Sci. 2000;57(1):25–40.
51. Bajou K, Peng H, Laug WE, Maillard C, Noel A, Foidart JM, et al. Plasminogen activator inhibitor-1 protects endothelial cells from FasL-mediated apoptosis. Cancer Cell. 2008;14(4):324–34.
52. Masuda T, Hattori N, Senoo T, Akita S, Ishikawa N, Fujitaka K, et al. SK-216, an inhibitor of plasminogen activator inhibitor-1, limits tumor progression and angiogenesis. Mol Cancer Ther. 2013;12(11):2378–88.
53. Placencio VR, Ichimura A, Miyata T, DeClerck YA. Small molecule inhibitors of plasminogen activator Inhibitor-1 elicit anti-tumorigenic and anti-Angiogenic activity. PLoS One. 2015;10(7):e0133786.

Additional file 1: Table S1. Descriptors and median values of vitronectin and nuclei morphometric variables in the present cohort.

Variable and category		Nº cases	Nuclei		Inter. VN	Terr. VN	VN ratio of pixels			H-score
			Density	%SA	%SA	%SA	Weak	Mod.	Strong	
Age	<18months	51	534.15	12.95	10	0.66	0.70	34	3.20	95.40
	≥18months	40	614.20	9.45	7.95	0.85	0.82	37.80	3.90	131.30
Stage	L1,L2,MS	65	527.25	12	9.90	0.55	0.82	34.30	2.50	80.80
	M	23	669.40	9.90	9.10	2.65	0.60	37.90	13.45	143.40
Hist. C.	GNB	9	219	6.50	2	0.50	1	44.25	4	80.10
	NB	82	570.60	12.20	9.90	0.75	0.75	34.60	4.39	111.30
Hist.D.	dNB	10	456.25	13.90	5.95	0.20	0.85	30.25	2	71.25
	pdNB	57	563.94	12.20	9.90	0.80	0.80	36.40	3.55	110.70
	uNB	13	1567	8.60	11.80	6.30	0.60	34.30	24.60	198
MYCN	MNNA	71	534.15	12.20	11.80	0.50	0.80	34.30	2.25	97.30
	MNA	19	2173.90	8.60	9	2.30	0.60	37.70	17.12	156.80
11q	ND	65	563.95	12.50	10	0.60	0.95	34.95	2.85	110.90
	D	19	603.40	9.60	13.10	2.90	0.75	38.35	16	143.75
Ploidy	Hiperp.	48	570.60	12.10	9.95	1.35	0.60	38	5.25	112.95
	Dip+tetrap	11	739	9.80	10.50	0.90	0.95	36.35	5.60	137
Gen. profile	NCA	26	551.40	14.10	5.80	0.30	1.10	21.60	1.60	69.80
	SCA	57	600.60	11.60	11.80	1.30	0.80	37.90	7.10	143.40
Risk group	Non-HR	64	530.70	12.60	9.10	0.50	0.80	32.30	2.20	81.60
	HR	27	1120	9.40	9.90	2.30	0.80	38.37	13.45	163.70
Gen. Instab.	Low	46	538.60	13.60	9.20	0.43	1	27	1.70	75.70
	High	26	793	9.10	10.85	2.87	0.70	38.36	16.57	169.87

Density: number of objects/mm^2; Inter. VN: Interterritorial VN; Terr.VN: Territorial VN; %SA: percentage of stained area. L1 and L2: localized and MS: special metastatic; M: metastatic; Hist. C.: histopathologic category; GNB: ganglioneuroblastoma; NB: neuroblastoma; Hist. D: histopathologic differentiation; dNB: differentiating neuroblastoma; pdNB: poorly differentiated neuroblastoma; uNB: undifferentiated neuroblastoma; NOS was excluded from statistical analysis; MNNA: *MYCN* non-amplified; MNA: *MYCN* amplified; ND: non deletion; D: deletion; Gen. Profile: genetic profile; NCA: numerical chromosomal aberration; SCA: segmental chromosomal aberration; Hiperp.: Hiperploid; Dip.: diploid; Tetrap.:tetraploid; HR: High-risk; Gen. Instab.:genetic instability.

Additional file 2: Table S2. Description of the image analysis process.

Element	Material	Software	Algorithm segmentation
VN	-Individual images -JPEG format, quality 80 -RGB colour model	Image Pro-Plus (IPP) software v.6.0 (Media Cybernetics Inc., Silver Spring, MD, USA)	<u>Customized macro:</u> -Image pre-processing: contrast enhancement to better distinguish between blue and brown hues, in the following values: 50, 70, and 1 and for the high intensity VN cases: 70,70,1. -Morphological filters: Erode/Dilate and the enhancement HiGauss filter. In this step, an optimization of the appearance of the image without altering the true immunoreactivity of the cases was got to facilitate the segmentation process. -RGB channel segmentation: • The values for nuclei segmentation were R: 0-169, G: 0-214 and B: 82-255 (R: 0-202, G: 0-214 and B: 43-255 for high intensity VN cases). To a proper nuclei separation we used Autosplit and Watershed, followed by a restriction area $>10\mu m^2$. • The color ranges for interterritorial VN were R:166-255, G:4-193 and B:0-135 (R:166-255, G:39-123 and B:0-135 for high intensity VN cases) and for territorial VN R:0-90, G:0-90 and B:0-90 (R:0-136, G:0-90 and B:0-90 for high intensity VN cases). A restriction area > $5\mu m^2$ was used in both cases.
	-Whole-digitized slide (identification of cylinders corresponding to the different samples) -TIFF format -RGB color model	Pannoramic viewer software1.15 (3DHISTECH Ltd., Budapest, Hungary)	<u>DensitoQuant module:</u> -Color adjustments: Blue detection: 0.8 and brown tolerance: 1. (In high VN intensity images the brown tolerance changes to 1.8). -The score levels were: 6.41, 15.13, and 44.28. (In case of high VN intensity images, the last score level 44.28 changes to 56.14).

VN: Vitronectin; JPEG: joint photographic expert group format; RGB: R=red, G=green and B=blue color model; TIFF: tagged image file format.

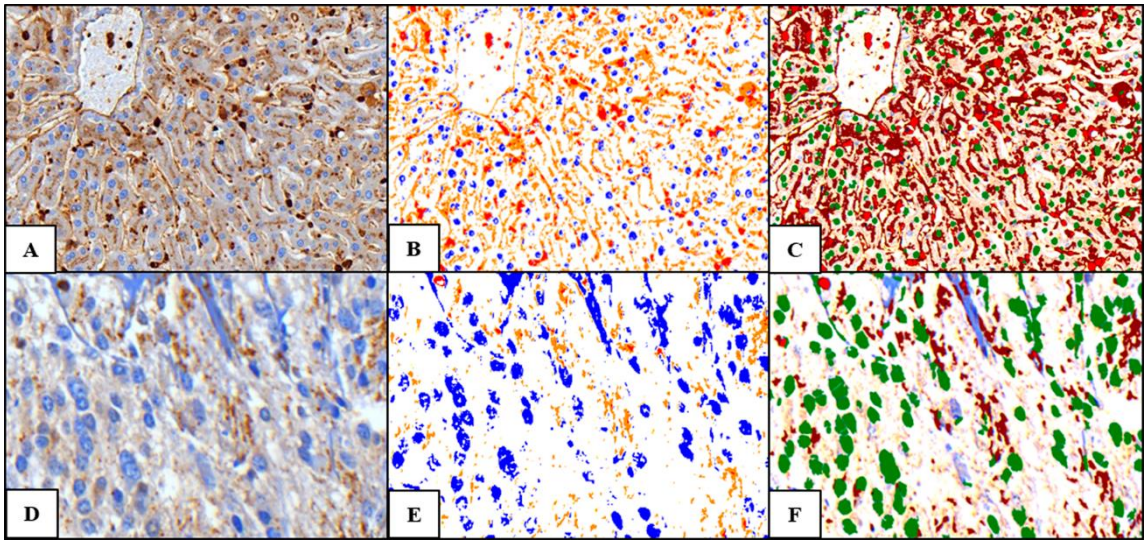

Additional file 3: Figure S1. Examples of how these applications work in vitronectin samples. **A**. Liver sample image immunostained for vitronectin (VN) without segmentation. **B**. Image of liver control sample segmentation with the DensitoQuant module (Pannoramic viewer software). **C**. Image of liver control sample segmentation with Image Pro-Plus software. **D.** Primary neuroblastoma (NB) sample immunostained for VN without segmentation. **E.** Image of NB sample segmentation with the DensitoQuant module (Pannoramic viewer software). **F.** Image of NB sample segmentation with Image Pro-Plus software. Color coding of VN analysis: in DensitoQuant segmented image, blue=negative, yellow=weak, orange= moderate and red=strong; in Image Pro-Plus segmented image, green=nuclei, brown= weak to moderate (interterritorial VN) and red=strong (territorial VN).

Additional file 4: Table S3. Growth conditions of NB human cell lines.

Complete medium	Serum-free medium
Iscove's Modified Dulbecco's Medium (IMDM; Gibco; Thermo Fisher Scientific Inc., Waltham, MA, USA).	Iscove's Modified Dulbecco's Medium (IMDM; Gibco; Thermo Fisher Scientific Inc., Waltham, MA, USA).
10% Fetal bovine serum (FBS; Gibco; Thermo Fisher Scientific Inc.).	F-12 (F-12 Nutrient Mix, GlutaMAX™; Gibco; Thermo Fisher Scientific)
Insulin-transferrin-selenium (ITS; Gibco; Thermo Fisher Scientific, Inc.).	Insulin-transferrin-selenium (ITS; Gibco; Thermo Fisher Scientific, Inc.).
100 U/mL penicillin/100 µg/mL streptomycin (Gibco; Thermo Fisher Scientific Inc.).	100 U/mL penicillin/100 µg/mL streptomycin (Gibco; Thermo Fisher Scientific Inc.).
Plasmocin (Ibian Technologies, S.L., Zaragoza, Spain) to prevent mycoplasma contamination.	Plasmocin (Ibian Technologies, S.L., Zaragoza, Spain) to prevent mycoplasma contamination.

Article III: The topology of vitronectin: A complementary feature for neuroblastoma risk classification based on computer-aided detection

Vicente-Munuera P*, **Burgos-Panadero R*,** Noguera I, Navarro S, Noguera R, Escudero LM.

*Equal colaboration

Int J Cancer. 2020 Jan 15; 146(2):553-565. doi: 10.1002/ijc.32495

Wiley Switzerland, ISSN: 1097-0215

Impact factor 2018: 4.982

5-year impact factor: 6.210

ARTICLE III

IJC
International Journal of Cancer

The topology of vitronectin: A complementary feature for neuroblastoma risk classification based on computer-aided detection

Pablo Vicente-Munuera[1,2]*, Rebeca Burgos-Panadero[3,4]*, Inmaculada Noguera[5], Samuel Navarro[3,4], Rosa Noguera[3,4] and Luis M. Escudero[1,2]

[1]Departamento de Biología Celular, Instituto de Biomedicina de Sevilla (IBiS), Hospital Universitario Virgen del Roció/CSIC/Universidad de Sevilla, Seville, Spain

[2]Biomedical Network Research Centre on Neurodegenerative Diseases (CIBERNED), Madrid, Spain

[3]Department of Pathology, Medical School, University of Valencia/INCLIVA, Valencia, Spain

[4]Biomedical Network Research Centre on Oncology (CIBERONC), Madrid, Spain

[5]Central Support Service for Experimental Research (SCSIE), University of Valencia, Valencia, Spain

Tumors are complex networks of constantly interacting elements: tumor cells, stromal cells, immune and stem cells, blood/lympathic vessels, nerve fibers and extracellular matrix components. These elements can influence their microenvironment through mechanical and physical signals to promote tumor cell growth. To get a better understanding of tumor biology, cooperation between multidisciplinary fields is needed. Diverse mathematic computations and algorithms have been designed to find prognostic targets and enhance diagnostic assessment. In this work, we use computational digital tools to study the topology of vitronectin, a glycoprotein of the extracellular matrix. Vitronectin is linked to angiogenesis and migration, two processes closely related to tumor cell spread. Here, we investigate whether the distribution of this molecule in the tumor stroma may confer mechanical properties affecting neuroblastoma aggressiveness. Combining image analysis and graph theory, we analyze different topological features that capture the organizational cues of vitronectin in histopathological images taken from human samples. We find that the Euler number and the branching of territorial vitronectin, two topological features, could allow for a more precise pretreatment risk stratification to guide treatment strategies in neuroblastoma patients. A large amount of recently synthesized VN would create migration tracks, pinpointed by both topological features, for malignant neuroblasts, so that dramatic change in the extracellular matrix would increase tumor aggressiveness and worsen patient outcomes.

Key words: neuroblastoma, vitronectin, topology, computational biology, networks

Abbreviations: ECM: extracellular matrix; INRG: International Neuroblastoma Risk Group; MNA: MYCN amplified; NB: neuroblastoma; SCAs: segmental chromosome aberrations; VN: vitronectin

Additional Supporting Information may be found in the online version of this article.

Conflict of interest: No potential conflict of interests were disclosed by the authors.

Grant sponsor: Centro de Investigación Biomédica en Red Cancer; Grant number: CB16/12/00484; Grant sponsor: Fundación Científica Asociación Española Contra el Cáncer; Grant number: FAECC2015/006; Grant sponsor: Instituto de Salud Carlos III; Grant number: FIS (PI17/01558); Grant sponsor: Ministerio de Economía y Competitividad; Grant numbers: BFU2016-74975-P, Ramón y Cajal program (PI13/01347); Grant sponsor: Nico contra el cancer infantil; Grant sponsor: Universidad de Sevilla; Grant number: V plan propio *P.V.-M. and R.B.-P. contributed equally to this work

DOI: 10.1002/ijc.32495

History: Received 25 Jan 2019; Accepted 27 May 2019; Online 7 Jun 2019

Correspondence to: Rosa Noguera, Department of Pathology, Medical School, University of Valencia/INCLIVA/CIBERONC, Avda. Blasco Ibáñez, 15. 46010, Valencia, Spain, Tel.: +34-963983948, E-mail: rnoguera@uv.es; or Luis M. Escudero, Edificio IBiS, Lab 117. H.U. Virgen del Rocío. Avda. Manuel Siurot s/n. 41013 Seville, Spain, Tel.: +34-655772838, E-mail: lmescudero-ibis@us.es

What's new?
The tumor microenvironment has a strong influence on cancer malignancy. Here, the authors investigate whether the organization of the extracellular matrix glycoprotein vitronectin in the tumor stroma may confer mechanical properties affecting neuroblastoma aggressiveness. Combining image analysis and graph theory, they identify two topological features of vitronectin that could potentially be used to improve patient pre-treatment risk stratification. The data also point to the creation of vitronectin migration tracks for malignant neuroblasts, so that dramatic changes in the extracellular matrix would increase tumor stiffness and aggressiveness and worsen patient outcomes.

Introduction

The interplay between different fields of basic science has been revealed as an efficient way to advance in medicine. Physics and mathematics-related terms like tensegrity, topology and tessellations (see Glossary) are now used to improve understanding of biology and biomedicine.[1–3] In parallel, a robust and efficient analysis of histopathological images is required due to their increasingly accepted use. Image analysis land-scape has enormous potential to improve the quality of histo-logical image interpretation, supporting without overruling pathologists in decision-making.[4,5] In the oncology field, a plethora of computational tools is being designed to capture medical information with the help and supervision of a variety of professionals such as pathologists, biologists or physicists.[6–8] Morphometric analysis has often been used as a first approach, successfully highlighting new prognostic indicators.[9–11] However, more sophisticated techniques are needed to model highly complicated diseases like cancer. In particular, computerized image analysis has proven useful to find relevant features in different types of cancer.[12–14] For instance, features related to texture analysis, which is based on the intensity and colors of the images, or morphological fea-tures considering the shape of the detected elements, are broadly used. These approaches did not consider the spatial relationship between its components[12,13] or were restricted to nuclei.[14] However, morphometric techniques assure the standardization of all measurements and minimize interobserver differences.[15,16] Understanding how biopsy elements are organized is important to find potential new markers for improv-ing treatment strategies and outcome prediction.

There is an increasing emergence of network theory methods in biology.[17–20] In cancer, graph theory (see Glossary) is commonly used to analyze gene networks.[21,22] In the case of histopathological images, three reconstructions have recurrently been used to obtain a graph that connects the elements of the image: Delaunay triangulation, Voronoi diagram (see Glossary) and minimum spanning tree.[23–25] However, these approaches did not consider the importance of the spa-tial context of the extracellular matrix (ECM) for patient out-comes. Likewise, small nonisomorphic induced subgraphs (graphlets, see Glossary) have been used as a means to charac-terize biological networks,[26–28] but as yet they have not been used to topologically characterize histopathological samples regarding outcomes.

The tumor microenvironment, particularly ECM, has a strong influence on cancer malignancy.[29,30] Specifically, vitronectin (VN), a glycoprotein belonging to the ECM, is considered to promote angiogenesis and vascular permeability, aiding tumor migration.[31–33] In particular in neuroblastoma (NB), a heterogeneous tumor in childhood with widely vary-ing prognosis according to several clinical and genetic factors in the International Neuroblastoma Risk Group (INRG) classification,[34] the role of VN remains incompletely defined, although our previous studies suggested a connection to tumor progression.[35] Despite efforts to fully characterize the impact of the NB microenvironment on patient pretreatment risk evaluation and tumor genetic instability, it still remains unclear how ECM topology and the interplay of its elements affect patient prognosis.[9,36,37] Our hypothesis is that tumor cells affect the organization of the different elements surrounding them, including ECM elements such as VN. Working from this, our aim is to identify independent tumor tissue parameters, like VN topology, which could help to assess the risk group of NB patients and/or tumor genetic instability.

Materials and Methods

Material

Ninety-one primary NB tumors (at least two representative cylinders of 1 mm^2 from each tumor) included in eight tissue microarrays were chosen according to INRG classification parameters and/or tumor genetic instability criteria related to segmental chromosome aberrations (SCAs)[34,38] (Supplementary Table 1). Tissue microarray slices of 3 μm were stained with anti-VN (1/100) (clone EP873Y, isotype IgG, code ab45139, Abcam), scanned at 20x with Pannoramic MIDI (3DHistech Ltd., Budapest, Hungary), and analyzed objectively with Image Pro-Plus v.6.0 (Media Cybernetics, Inc., Rockville, MD 20850 USA) and DensitoQuant module from Pannoramic viewer software 1.15 (3DHistech Ltd.). For each biopsy (Figs. 1a and 1b), we obtained three markup images (area of each image: 1 mm^2, see Glossary) and their morphometric data: hematoxylin stained nuclei (Fig. 1c); territorial VN location (Fig. 1d), strongly stained intensity; and interterritorial VN location (Fig. 1e), represented by low and medium intensity. These biopsy results were classified as high-risk group (≥18 months and stage M or <18 months, stage M/MS and MYCN amplified [MNA]) and non-high-risk

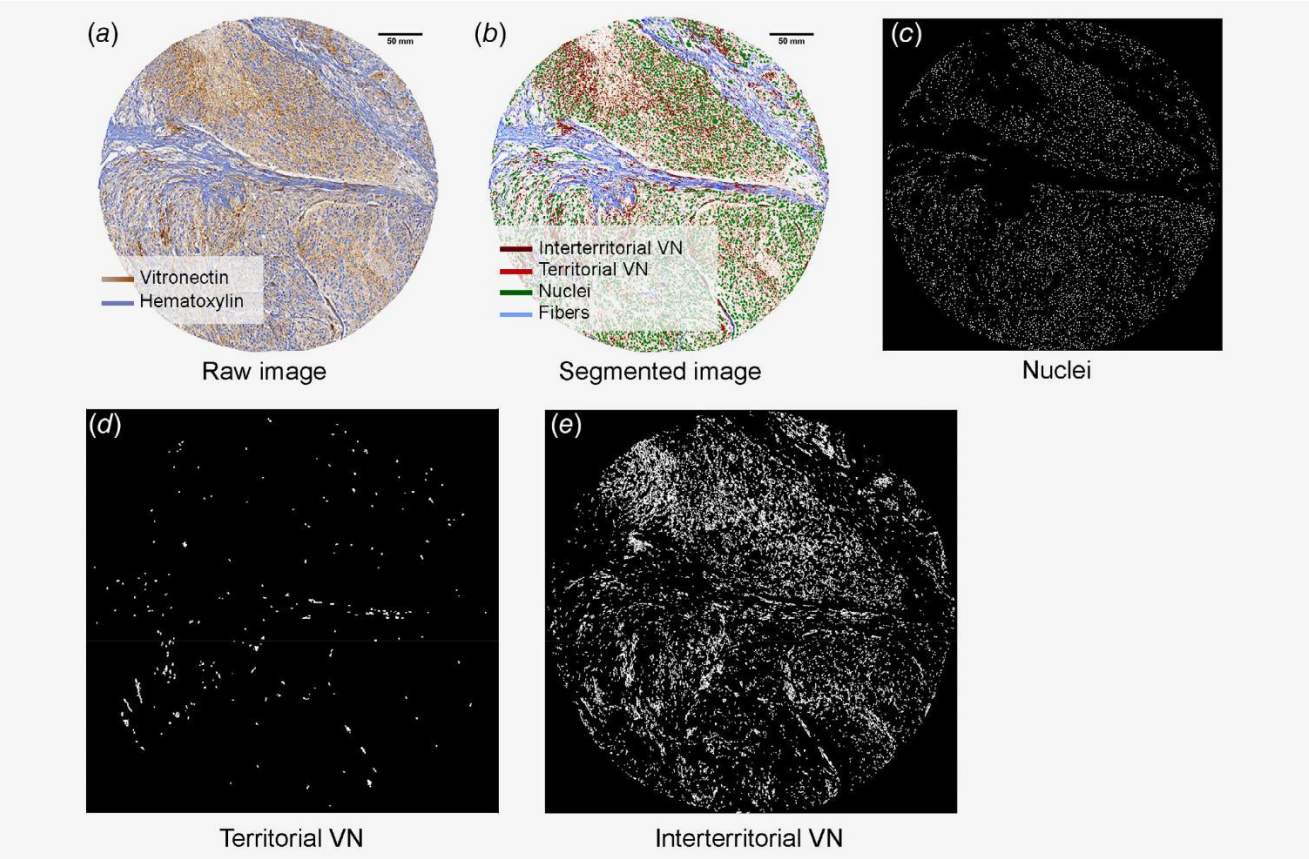

Figure 1. Segmentation of biopsy images from neuroblastoma (NB) patients. (a) Image of an immunohistochemical biopsy stained to detect vitronectin (VN) (brown scale). Hematoxylin is highlighted in blue, corresponding to nuclei and fibers of extracellular matrix. (b) Segmented image differentiating between territorial VN (red) and interterritorial VN (brown). The cell nuclei are also shown in the resulting image (green). (c–e) Markup images showing the segmented elements separately, but all in white: cell nuclei (c), territorial VN (d) and interterritorial VN (e). Scale bar in black, 50 mm.

group (very low, low and intermediate categories following the INRG classification) patient material (additional Table 2). Regarding tumor genetic instability criteria, results were also grouped as higher SCA patient material (genetic profiles with >3 typical SCAs plus MNA or 11q deleted or >3 gene amplifications or with hyperrearranged chromosomal segments) and lower SCA patient material (genetic profiles with numerical chromosomal aberration or ≤3 typical SCAs, excluding 11q SCA).[35] Our study was approved by the Ethics Committee (reference B.0000339 29/01/2015). Participants or their family members/legal guardians provided written informed consent.

Topological features

To characterize our biopsies, we have extracted a set of 47 features, where 25 captured the organization of both types of VN (territorial and interterritorial), separately. First, considering the impossibility of measuring VN as if it were individual objects in our black-and-white markup images (Figs. 1c–1e), we decided to discretize the space in hexagonal regions of a fixed side of, approximately, 8.05 mm (50 pixels) (Fig. 2 and Fig. S1b). Considering that hexagonal regions filled with VN staining represented by nodes (see Glossary), we quantified the following parameters (Table 1a): (i) quantity of VN staining inside it (features with ID 4, 5, 16 and 17). (ii) Euler number (see Glossary): defined as the number of objects minus the number of holes within a region (7, 8, 19 and 20). (iii) Branching (see Glossary): We measured the number of crosslinks (11, 12, 23 and 24). (iv) Difference in quantity between interterritorial and territorial VN (feature with ID 25).

To get the final value of the features, we calculated the average of each parameter considering all the regions (fea-tures with suffix "per region," Table 1a) or only the nodes (suffix "per node," Table 1a) of the Euler number and branching, while the deviance (standard deviation [std]) of either the nodes or all the regions were computed to all the parameters. In addition, we computed a series of features that did not consider the hexagonal region (Table 1a): the holes inside VN staining regions and the deviance of their area (features with ID 9, 10, 21 and 22). We also computed the Euler number per VN staining area of the whole image (6 and 18). All the topological features were extracted with Matlab R2014b (MathWorks).

Pure topological features. We used graph theory to obtain a subset of "pure topological" features. Briefly, to extract this set of characteristics, we collected the position and number of the hexagonal regions of our images (Fig. 2). In our network (graph), hexagonal regions filled with VN staining stand for nodes. To connect the nodes with a link (edge, see Glossary), we considered the "ordinary" (Euclidean) distance between them. We, therefore, started with all the nodes having no connections amid them. Aiming to model how the regions are distributed throughout the sample, we linked the nodes to

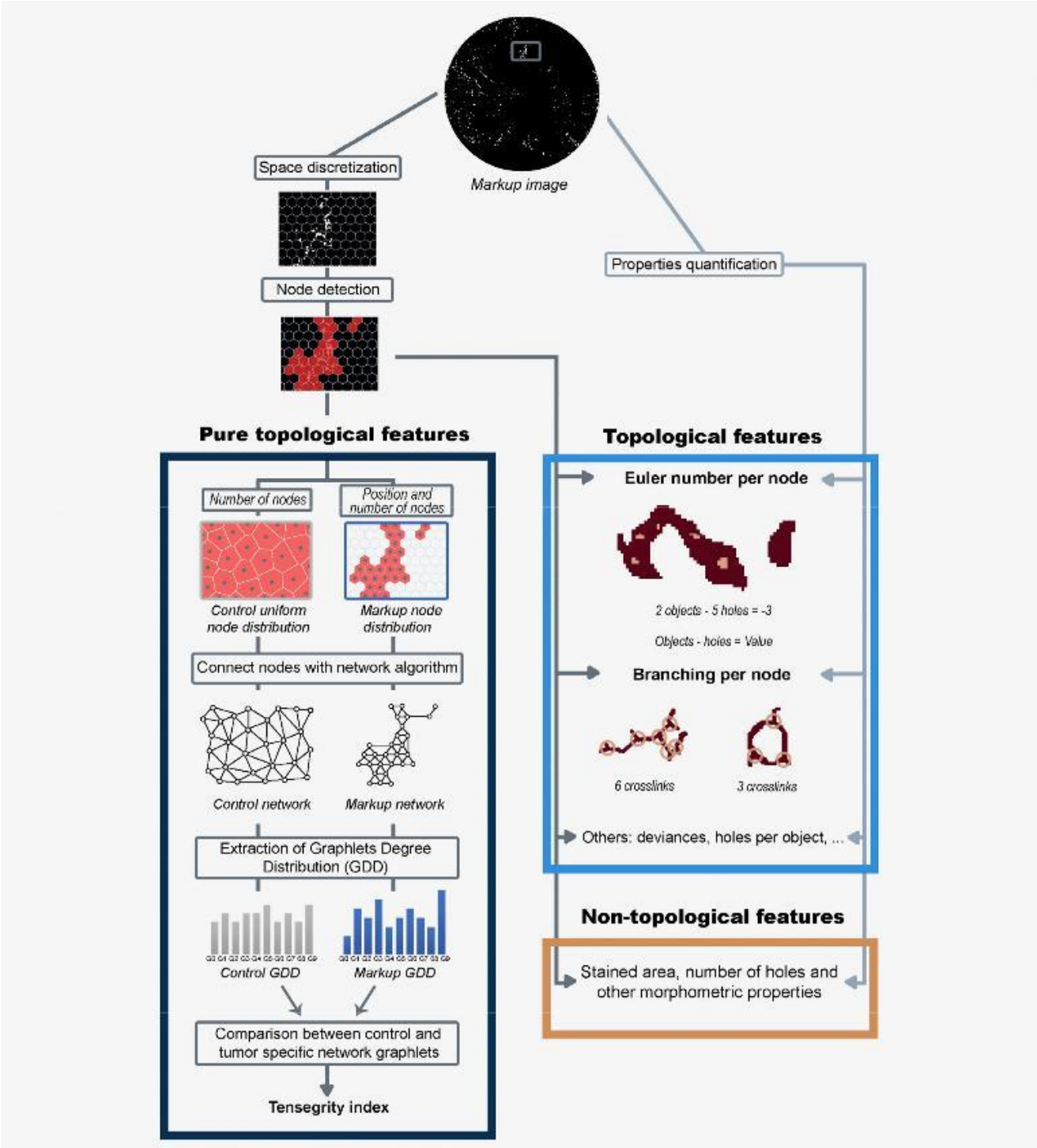

Figure 2. Legend on next page.

obtain a connected network (i.e., any node can reach any node using the edges as a vehicle) using three different algorithms (iteration, sorting or minimum spanning tree, Supplementary Methods). Note that, for a given markup image, we will have three networks with the same number of nodes (one per algorithm).

Once we had the networks, which connect the regions filled with VN, we extracted the different configurations that can be achieved with a small number of nodes (graphlets[26] of up to five nodes). Specifically, we used the ORCA (Orbit Cou-nting Algorithm) computer program for graphlet identifica-tion and calculation,[39] to extract the different graphlets of each network. In order to obtain the final tensegrity index (see Glossary) features, we compared, using the graphlet degree distribution distance,[40] the graphlets obtained from the biopsy markup image with an in silico control, which tries to mimic a sample where the VN is equally distributed through-out the sample (represented by a homogeneous Voronoi tes-sellation, Supplementary Methods).

We computed the average distance between ten in silico generated controls with its tumor markup image specific net-work. Therefore, a tensegrity index represents how the real distribution of territorial or interterritorial VN differs from a homogeneous distribution. Finally, we obtained the six tensegrity indices (Table 1a): three algorithms from two loca-tions (features 1, 2, 3, 13, 14 and 15). The whole pipeline is explained in Figure 2.

Nontopological characteristics

We captured an additional set of nontopological features (Fig. 2), which involve morphometric characteristics:

1. Nuclei (Fig. 1c). We obtained the number, area, ratio and percentage of hematoxylin stained nuclei (from non-VN secretory cells) and the total nuclei number (from non-secretory and VN secretory cells) from the total markups.
2. Percentage of stained area (Fig. S1b). We quantified the VN stained areas in each delimited hexagonal area. We cal-culated the mean and std of the whole grid. In addition, we computed this mean and std using only the nodes. In the total markups, we also calculated VN location (percentage of stained area and number/mm^2), pixel intensity ratio (ratio of positive stained pixels), positive or negative H-score (based on a specific discriminatory threshold, ranging from 0 to 300) and number of VN secretory cells (percent-age of VN positive cells).
3. Number of holes. We also identified the holes in an image.
4. Difference between interterritorial and territorial VN. We computed the average difference between interterritorial and territorial VN per region. For each hexagonal area, we operated territorial minus interterritorial.

Statistical analysis

We have adapted the pipeline shown in past studies[41,42] to obtain complementary features to refine the risk-group assign-ment for NB treatment stratification and genetic instability in the present cohort. In particular, we have performed a multi-variate analysis using logistic regression to collect these relevant features. See Supplementary Information for more details.

Data availability

The data set used and analyzed in the current study is avail-able upon request.

Code availability

The code is available at: https://github.com/Complex OrganizationOfLivingMatter/NeuroblastomeIntegration.

Results

Capturing organization from NB biopsy images

We processed and analyzed 91 histological images taken from human samples stained with anti-VN antibody to visualize VN distribution (Figs. 1a and 1b, Methods). Using these images, we obtained the hematoxylin stained nuclei markup image for each biopsy (Fig. 1c). We also distinguished two dif-ferent localizations of VN according to intensity, as previously described[35]: strong intensity was assigned to a territorial VN, whose location is pericellular and intracellular (Fig. 1d); and the intercellular location (peripherally to territorial matrix), which was named interterritorial VN, corresponded to low

Figure 2. Pipeline overview of how the features are extracted. The process starts with the initial markup image, which in this example corresponds to territorial VN. A region of interest (ROI) from the initial image was selected (in dark gray) to show the space discretization and further operations. Below, the nodes (in red) are identified when a hexagon has VN inside. This information is used to obtain the pure topological features (dark blue, left side), a subset of the topological characteristics. In particular, the number of nodes is used to create the control with a uniform node distribution, while the position and number of nodes are utilized to gain the markup node distribution. Thereafter, each distribution of nodes is connected using a network algorithm (sorting, iteration or minimum spanning tree methods) and the graphlets degree distribution (GDD) is computed for both control and markup networks. To obtain the tensegrity index, the distance between the control GDD and the markup GDD is calculated. For topological characteristics (blue, right side), excluding the pure topological ones, two sources of information are used: the hexagonal grid and detected nodes (arrows in darker gray), and properties quantification performed directly on the markup image (lighter gray arrows). Two topological features are highlighted: Euler number per node, where the Euler number is calculated by subtracting the two objects (in brown) against the five holes within them (in light brown) resulting in a Euler number of minus three; and Branches per node in which the crosslinks (circles in light brown) from territorial VN shapes (in brown) were detected. Likewise, the nontopological features (orange, bottom right) use information extracted directly from the markup image and from the space discretization.

Table 1. Statistically significant features. (a) Index of feature name and identifier used in the study, divided into topological (in white) or nontopological (gray). Topological features are the ones who capture organization, while the nontopological characteristics are morphometric measurements and other nonorganizational quantifications. (b) Results from the univariate analysis performed for tumor genetic instability criteria and high-risk pretreatment stratification group. Only statistically significant characteristics ($\chi^2 < 0.05$) are shown. The features are ranked by their p-values obtained on the chi-square test, in ascending order. The selected features to be used in the next steps are underlined. The characteristics of territorial vitronectin (VN) are marked in bold (12/21 in the risk group and 15/27 in tumor genetic instability criteria). Highly statistically significant common features in tumor genetic instability criteria and risk group were marked with an asterisk. MST, minimum spanning tree; std, standard deviation

(a) Definition of features		(b) Univariate analysis			
ID	**Characteristics**	**Rank**	**ID**	**Characteristics**	**Chi-square**
Topological		**Tumor genetic instability criteria**			
1	Interterritorial—sorting tensegrity index	**1**	**20**	**Territorial—Euler number per node***	**8.20E-07**
2	Interterritorial—iteration tensegrity index	**2**	**24**	**Territorial—mean quantity of branches per node***	**4.03E-06**
3	Interterritorial—MST tensegrity index	**3**	**37**	**Territorial—percentage of stained area***	**6.58E-05**
4	Interterritorial—std percentage of VN stained area per region	4	16	Interterritorial—std percentage of VN stained area per region	9.05E-05
5	Interterritorial—std percentage of VN stained area per node	5	39	Total nuclei	1.27E-04
6	Interterritorial—Euler number per VN stained area	**6**	**29**	**Territorial—mean percentage of VN stained area per node**	**1.75E-04**
7	Interterritorial—Euler number per region	**7**	**16**	**Territorial—std percentage of VN stained area per region**	**2.74E-04**
8	Interterritorial—Euler number per node	**8**	**45**	**Territorial—ratio of strong positive pixels to total pixels**	**2.74E-04**
9	Interterritorial—number of holes per VN stained area	**9**	**27**	**Territorial—mean percentage of VN stained area per region**	**3.87E-04**
10	Interterritorial—std area of holes	**10**	**23**	**Territorial—mean quantity of branches per region**	**3.87E-04**
11	Interterritorial—mean quantity of branches per region	**11**	**7**	**Territorial—Euler number per region**	**5.34E-04**
12	Interterritorial—mean quantity of branches per node	12	40	Percentage of hematoxylin stained nuclei area	6.11E-04
13	Territorial—sorting tensegrity index	**13**	**22**	**Territorial—std area of holes**	**8.44E-04**
14	Territorial—iteration tensegrity index	14	43	Interterritorial—ratio of weak positive pixels to total pixels	1.46E-03
15	Territorial—MST tensegrity index	15	47	H-score	0.002
16	Territorial—std percentage of VN stained area per region	**16**	**38**	**Territorial—VN stained area/mm^2**	**0.002**
17	Territorial—std percentage of VN stained area per node	17	46	Ratio of all positive pixels	0.004
18	Territorial—Euler number per VN stained area	**18**	**31**	**Territorial—mean area of holes**	**0.005**
19	Territorial—Euler number per region	19	42	Ratio of hematoxylin stained nuclei pixels to total pixels	0.006
20	Territorial—Euler number per node	20	36	Interterritorial—VN stained area/mm^2	0.009
21	Territorial—number of holes per VN stained area	21	12	Interterritorial—mean quantity of branches per node	0.014
22	Territorial—std area of holes	22	34	Hematoxylin stained nuclei/mm^2	0.016
23	Territorial—mean quantity of branches per region	23	2	Interterritorial—iteration tensegrity index	0.017
24	Territorial—mean quantity of branches per node	**24**	**19**	**Territorial—Euler number per region**	**0.024**
25	Std difference territorial and Interterritorial	**25**	**21**	**Territorial—number of holes per VN stained area**	**0.030**
Non-topological		26	9	Interterritorial—number of holes per VN stained area	0.034
26	Interterritorial—mean percentage of VN stained area per region	27	6	Interterritorial—Euler number per VN stained area	0.045
27	Interterritorial—mean percentage of VN stained area per node	**Risk pretreatment stratification group**			
28	Interterritorial—mean area of holes	**1**	**20**	**Territorial—Euler number per node***	**0.001**

(Continues)

Table 1. Statistically significant features. (a) Index of feature name and identifier used in the study, divided into topological (in white) or nontopological (gray). Topological features are the ones who capture organization, while the nontopological characteristics are morphometric measurements and other nonorganizational quantifications. (b) Results from the univariate analysis performed for tumor genetic instability criteria and high-risk pretreatment stratification group. Only statistically significant characteristics ($\chi^2 < 0.05$) are shown. The features are ranked by their p-values obtained on the chi-square test, in ascending order. The selected features to be used in the next steps are underlined. The characteristics of territorial vitronectin (VN) are marked in bold (12/21 in the risk group and 15/27 in tumor genetic instability criteria). Highly statistically significant common features in tumor genetic instability criteria and risk group were marked with an asterisk. MST, minimum spanning tree; std, standard deviation (Continued)

(a) Definition of features		(b) Univariate analysis			
ID	**Characteristics**	**Rank**	**ID**	**Characteristics**	**Chi-square**
29	Territorial—mean percentage of VN stained area per region	**2**	**24**	**Territorial—mean quantity of branches per node***	**0.003**
30	Territorial—mean percentage of VN stained area per node	3	39	Total nuclei	0.003
31	Territorial—mean area of holes	**4**	**37**	**Territorial—percentage of stained area***	**0.006**
32	Mean difference territorial and Interterritorial	**5**	**16**	**Territorial—std percentage of VN stained area per region**	**0.010**
33	Percentage of hematoxylin stained nuclei area	**6**	**22**	**Territorial—std area of holes**	**0.010**
34	Hematoxylin stained nuclei/mm^2	7	34	Hematoxylin stained nuclei/mm^2	0.010
35	Interterritorial—percentage of stained area	8	36	Interterritorial—VN stained area/mm^2	0.010
36	Interterritorial—VN stained area/mm^2	**9**	**45**	**Territorial—ratio of strong positive pixels to total pixels**	**0.010**
37	Territorial—percentage of stained area	10	43	Interterritorial—ratio of weak positive pixels to total pixels	0.014
38	Territorial—VN stained area/mm^2	11	17	Interterritorial—std percentage of VN stained area per node	0.016
39	Total nuclei	**12**	**29**	**Territorial—mean percentage of VN stained area per region**	**0.019**
40	Percentage of hematoxylin stained nuclei	**13**	**23**	**Territorial—mean quantity of branches per region**	**0.019**
41	Percentage of VN positive cells	**14**	**19**	**Territorial—Euler number per region**	**0.019**
42	Ratio of hematoxylin stained nuclei pixels to total pixels	15	47	H-score	0.019
43	Interterritorial—ratio of weak positive pixels to total pixels	**16**	**27**	**Territorial—std percentage of VN stained area per node**	**0.019**
44	Interterritorial—ratio of moderate positive pixels to total pixels	**17**	**38**	**Territorial—VN stained area/mm^2**	**0.019**
45	Territorial—ratio of strong positive pixels to total pixels	18	33	Percentage of haematoxylin stained nuclei area	0.028
46	Ratio of all positive pixels	19	42	Ratio of haematoxylin stained nuclei pixels to total pixels	0.028
47	H-score	**20**	**30**	**Territorial—mean percentage of VN stained area per node**	**0.033**
		21	46	Ratio of all positive pixels	0.033

The asterisk indicated three features that presented low values of chi-square in both categories.

and medium intensity (Fig. 1e). In this way, we detected the objects (VN stained areas) in the markup images, and over-lapping a hexagonal grid with the related markup image, we divided the image into regions. In addition, we detected which hexagons were filled with VN objects becoming our nodes of the future graph (Figs. S1a and S1b, Methods). Using the infor-mation from the overlapped images and markup images, we studied the organization of the two locations of VN, by obtaining 25 features characterizing the topology of VN (Table 1a and Fig. 2). In particular, we quantified (i) the general topology of the distribution of cells with interterritorial (features with ID 1, 2 and 3) or territorial (13, 14 and 15) VN; (ii) the variance in quantity of VN per hexagonal region (characteristics 4, 5, 16 and 17); (iii) the Euler number, which corresponds to the number of objects minus the holes (6, 7, 8, 18, 19 and 20 (Fig. S1b); (iv) the number of holes per object (9 and 21) and the variation of the area of the holes (10 and 22); (v) branching, representing how many crosslinks are found (11, 12, 23 and 24) and (vi) the variation on the difference between interterritorial VN and territorial VN in terms of its quantity (25).

The values for the pure topological features (network characteristics 1, 2, 3, 13, 14 and 15) were obtained in three steps

(Fig. 2). First, we used the superimposed images and its nodes to build a graph using different methods to connect these nodes (with edges). Specifically, we developed three different algorithms that consider the distance between the nodes: sorting, connecting all the closest distances between nodes, obtaining a highly-linked graph (Fig. S1c); iteration, which links the closest neighbors of the nodes emphasizing local topologies (Fig. S1d); and minimum spanning tree, which connects all the nodes together minimizing the total edge distance, creating a minimum topological structure (Fig. S1e). The three algorithms were designed to construct a connected graph, meaning that no nodes were isolated (Methods). Sec-ond, for each original markup image of a given VN location (Figs. 1d and 1e), ten control images were generated by taking the number of nodes in a biopsy (Fig. S1b) and distributing them homogenously in the regions where it was possible to find VN (i.e., tears of the tissue were discarded) (Figs. S1f and S1g). The nodes of the control images were connected to obtain a corresponding control graph (Methods and Figs. S1f and S1g). Third, to get the final value of these features (the tensegrity indices), we calculated a descriptor of the similarity between each graph and its control (Fig. 2). To this end, we used the graphlet degree distribution distance[26] (Methods). As a result, we obtained six tensegrity indices for each biopsy (three types of algorithms from two different locations of VN).

A combination of morphometric and topological features

In addition to the topological features, we captured 22 non-topological characteristics (Table 1a), 7 of them obtained using the information from the hexagonal grid overlapped with the original markup image (Fig. 2): (i) percentage of VN (features 26, 27, 29 and 30); (ii) area of holes of the VN objects (28 and 31) and (iii) difference between territorial and interterritorial VN regarding their quantity (32). The remaining 15 morphometric features (33–47) did not consider the hexagonal grid and were acquired in a previous study.[35]

Altogether, we had 47 VN characteristics (Table 1a and Supplementary Table 1): 19 came from interterritorial VN, 18 from territorial VN, 5 from both VN location, 4 from nuclei and 1 from total cells presented in their related markup images. We combined all this information to see if we could obtain a new supporting feature to enhance our two possible criteria: pretreatment risk stratification group (high-risk vs. non-high-risk, 91 cases) and tumor genetic instability (higher vs. lower, 82 cases).

The pattern of VN is more homogeneous in patients with higher tumor genetic instability

As a preliminary analysis of the relation between the pure topology of the VN in the biopsy and the risk group of the patients or tumor genetic instability, we compared the distribution of our six tensegrity indices in high-risk vs. non-high-risk groups and higher vs. lower tumor genetic instability. Regarding risk criteria, no feature was statistically significant between different prognoses. On the contrary, for the tumor genetic instability, both Iteration algorithms, interterritorial (lower instability: 0.22 0.08; higher instability: 0.18 0.10, $p < 0.01$) and territorial VN (lower instability: 0.26 0.08, higher instability: 0.21 0.09, $p < 0.01$), were statistically sig-nificant to divide between lower and higher genetic instability (Methods). Even though only the two mentioned results (2 out of 12) were statistically relevant, a trend was found among all the tensegrity indices: higher risk group or higher tumor genetic instability was associated with lower values in tensegrity indices, that is, differences between biopsy and con-trols (Fig. 3a and Table S2). This means that using these indi-cators, low-risk group and low tumor genetic instability cases were distributed more heterogeneously than low-risk group patients and higher tumor genetic instability.

The territorial Euler number could enhance the prediction of poor risk group-related prognosis

Next, considering the whole data set (47 features), we looked for variables that could improve the current tumor-tissue predictors of patients' risk group or tumor genetic instability. For this purpose, we used a multivariate logistic regression pipe-line based on the statistical analysis previously performed.[41,42] The first step of the pipeline was a univariate logistic regres-sion analysis. This test checked whether the individual contri-bution of each feature was statistically significant for each criterion. Then, we retained only the features with statistical significance ($p < 0.05$) that could be independent factors in the study cohort (Table 1b). Among them, the three most sta-tistically significant in tumor genetic instability were related to territorial VN features and they also presented low chi-square values predicting the high-risk pretreatment stratification group. In addition, the majority of possible independent fac-tors were characteristics of territorial VN (12/21 in high-risk pretreatment stratification group and 15/27 in tumor genetic instability criteria, Table 1b).

The second step of the pipeline was a multivariate logistic regression analysis, whose outputs are characteristics that should generate new insights; thus, they cannot overlap with variables that have known predictive power. Therefore, we coupled all the INRG variables, with values known to assess patient prognosis, with the top eight VN features of each criterion considered as the most statistically significant (nine features with $p < 0.011$ in risk group; eight characteristics with $p < 3e\text{-}04$ for tumor genetic instability) by the univariate anal-ysis (Methods and Table 1b). Thereafter, we performed the multivariate logistic regression, which yielded a set of characteristics formed by age ≥18 months, Euler number per node from territorial VN, MYCN status (MNA) and metastatic stage (M) (Table 2), which was the best model characterizing the INRG pretreatment risk classification (nagelkerke R^2: 0.47).Using these four features, we obtained a significant model ($\chi^2 < 0.005$) with a specificity of 0.89 (non-high-risk

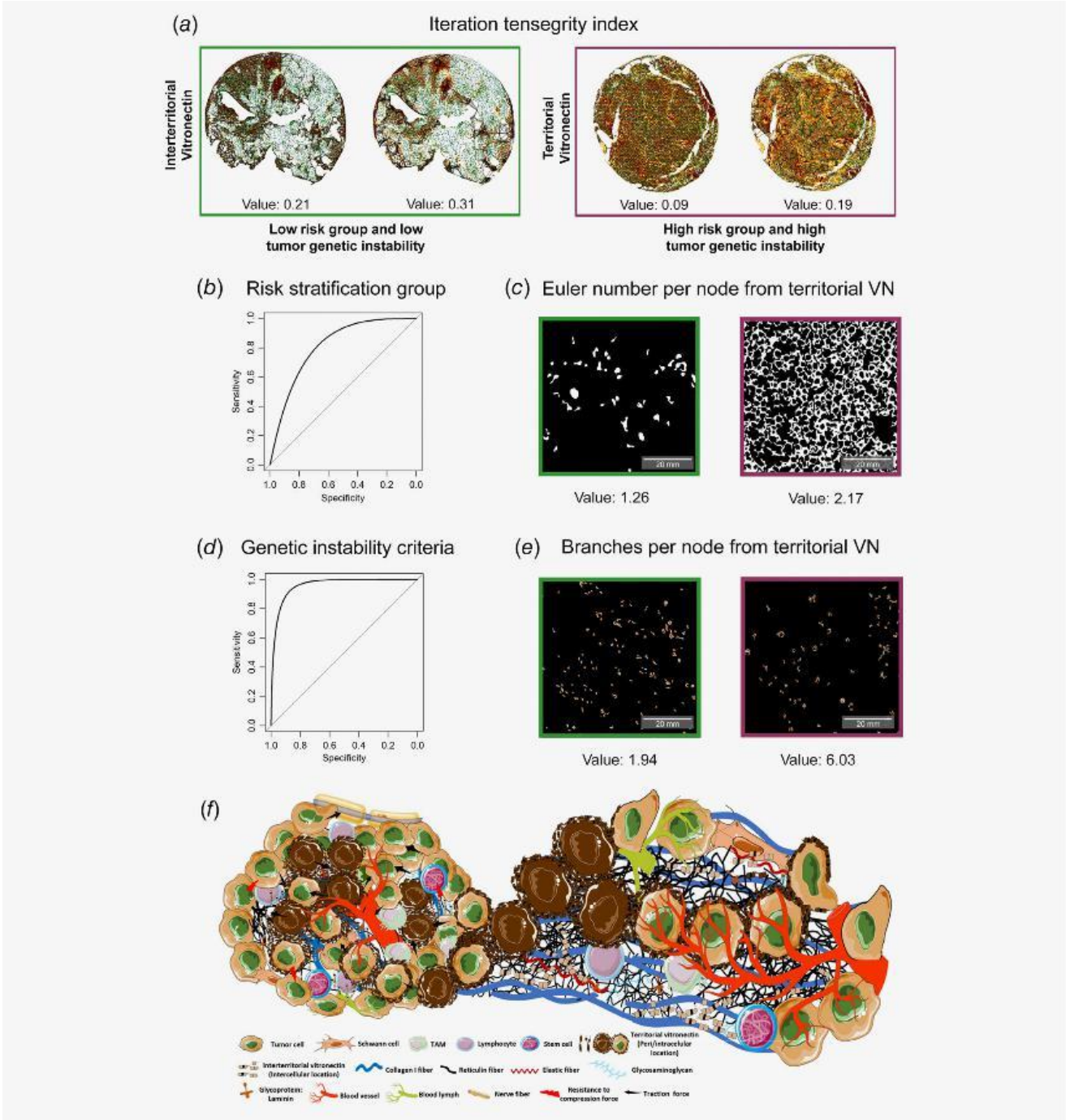

Figure 3. The topology of territorial vitronectin (VN) is relevant to patient outcome. (a) Iteration tensegrity index values for the biopsies shown. For the same case, both VN locations are illustrated: interterritorial (top, connecting brown hexagonal areas) and territorial (bottom, connecting red hexagonal regions). (b) Region of interest (ROC) curve for the final model of risk pretreatment stratification group. (c) Territorial VN Euler number per node feature. Values are for the whole image, but the representative image is from a ROI. (d) ROC curve resulting from the model of tumor genetic instability criteria. (e) Branches per node from territorial VN. ROI taken from an image stained with territorial VN. The branches found are presented in dark orange. The skeletonized region of the marker is in light orange. Scale bar, 20 mm. Note that images from patients related to the non-high-risk group and lower tumor genetic instability are represented in green. Burgundy shows examples of cases belong to high-risk group and higher tumor genetic instability. (f) Representative drawing of neuroblastoma microenvironment. Tumor with a close-up of a stiff area: rich territorial vitronectin regions (dark brown) were associated with a desmoplastic extracellular matrix (represented by a low amount of glycosaminoglycans, crosslinked reticulin fibers, collagen I fibers and interterritorial vitronectin), tortuous blood and lymph vessels as a scaffold of tumor and stromal cells.

Table 2. Multivariate logistic regression. The models using the final set of features for each criterion. Each model is defined by the different coefficients (B column) of the intercept and independent variables (features). For tumor genetic instability criteria, both regular logistic regression and Firth's logistic regression are shown. SE stands for standard error. The odds ratio and confidence score are presented (exp(B) 95% CI column). In regular logistic regression, Z-score and its associated p-value are represented, while in Firth's logistic regression chi-squared and its p-value are presented

Features	B	SE	Exp (B) (95% CI)	Z-value	Pr(>|z|)
Risk pretreatment stratification group					
(Intercept)	−3.95	0.91	0.019 (0.003–0.114)	−4.36	1.32E-05
Territorial—Euler number per node	0.65	0.26	1.92 (1.15–3.20)	2.49	0.013
Age (≥18 month)	2.66	0.61	14.36 (4.34–47.50)	4.36	1.28E-05
Stage	−6.05E-03	0.01	0.99 (0.97–1.02)	−0.51	0.610
MYCN (MNA)	−5.45E-03	0.01	0.99 (0.97–1.02)	−0.50	0.620
Tumor genetic instability criteria					
Regular logistic regression					
(Intercept)	−23.64	2,914.00	5.45E-11 (0–Inf)	−0.01	0.994
Territorial—mean quantity of branches per node	1.50	0.58	4.46 (1.44–13.80)	2.60	0.009
SCA	19.89	2,914.00	4.37E+08 (0–Inf)	0.01	0.995
MYCN (MNA)	22.58	3,245.00	6.43E+09 (0–Inf)	0.01	0.994
Ploidy	−2.83E-03	1.32E-03	1.00 (0.99–1.00)	−2.15	0.032
Firth's logistic regression					
Features	**B**	**SE**	**Exp (B) (95% CI)**	**Chi-square**	**p**
(Intercept)	−6.53	2.10	1.42E-04 (4.58E-06–4.64E-02)	21.99	2.73E-06
Territorial—mean quantity of branches per node	1.24	0.47	3.45 (1.42–10.96)	8.00	0.005
SCA	3.45	1.58	31.45 (3.04–4.45)	10.20	0.001
MYCN (MNA)	5.26	1.95	192.31 (9.81–4764.41)	20.04	7.56E-06
Ploidy	−2.21E-03	1.04E-03	1.00 (1.00–1.00)	5.46	0.019

group) and a sensitivity of 0.74 (high-risk group) (Fig. 3b). The selected independent prognostic predictor was based on the Euler number for territorial VN (Fig. 2). It stands for the number of objects in a sample minus the number of holes within those objects. Although the feature Euler number per node from territorial VN is related to the quantity of peri-cellular VN, it also takes into account the compactness of the territorial VN stained area including intracellular VN. More-over, it considers the hematoxylin-stained nuclei of active VN secretory cells with intracellular VN accumulation. In particu-lar, we found that a greater number of objects and a lesser number of holes (a higher Euler number per node) from terri-torial VN was associated with the high-risk pretreatment stratification group ($p < 0.05$) (Fig. 3c).

Territorial crosslinks can assess tumor genetic instability

We repeated the second step of the pipeline to obtain the most relevant independent factors in the study cohort for tumor genetic instability. The final set was composed of the mean quantity of branches per node of territorial VN and the INRG variables: genetic profile (SCA), MYCN status (MNA) and ploidy (diploid and tetraploid) (nagelkerke R^2: 0.84), although it yielded quasi-completion separation odd ratios, as can be seen in the standard errors of the results (Table 2). To avoid this issue, we performed a Firth's logistic regression.

The output of this logistic regression was a penalized model ($\chi^2 < 0.005$) with a specificity of 0.91 and a sensitivity of 0.89 (Fig. 3d). For tumor genetic instability, the mean quantity of branches per node of territorial VN was selected as an individual predictor in the study cohort. It considers the number of crosslinks after skeletonizing the image, taking into account only the filled hexagons (Figs. 2, 3e and Supplementary Fig. S1b). This feature highlights the proximity of VN secretory cells with merged areas of recent VN secretion, mainly located per-icellularly. We found that a higher number of branches corre-lated with higher tumor genetic instability. In addition, we also found a trend with the four defined levels from the genetic instability of the tumors (very low: 1.81 0.8; low: 2.30 1.6; medium: 2.43 1.1; high: 7.05 5.4; Table S1).

Discussion

In this work, we show that capturing VN organization can help improve understanding of how VN, essential to the structure of the ECM, affects or is affected by tumor progres-sion, and thus patient prognosis. To acquire the characteristics for this purpose, we used two defined VN expression patterns that indicate the duration of time in the ECM:[35] a territorial pattern indicates VN that has just been synthesized (also, intracellular) and/or was recently secreted into the surround-ing matrix (pericellular); interterritorial VN has been present

for a while in the intercellular space. In the same study, the optical analysis was used to determine the adequacy of further image analysis and to set the image analysis parameters. A good consistency (in terms of intensity) between the visual analysis and the digital image analysis quantification was observed using Kruskal-Wallis test ($p < 1e\text{-}4$). Our automatic image analysis approach can capture relevant information, which could be missing with traditional methods, to improve the classification of biopsy samples from NB patients. As a result, our different sets of experiments using different types of features indicate that territorial VN is relevant to evaluate the risk group of patients affected by NB and their tumor genetic instability.

The preliminary results of the pure topological features highlighted the iteration tensegrity index for both territorial and interterritorial VN with respect to tumor genetic instabil-ity (Fig. 3a). In addition, the tensegrity index for inter-territorial VN is the only relevant attribute of our novel features classifying tumor genetic instability (Table 1b). Nei-ther sorting nor minimum spanning tree tensegrity index appeared relevant to capture the patient's outcome. A possible reason could be the density of the resulting networks. The sorting graph (Fig. 2 and Supplementary Fig. S1c) is likely too dense, while the network of minimum spanning tree (Fig. 2 and Supplementary Fig. S1e) may be insufficiently connected for the graphlets to find differences between cases and con-trols. Thus, the intermediate graph of Iteration tensegrity index (Fig. 2 and Supplementary Fig. S1d), neither too dense nor too sparse, has the correct attributes to characterize the topology of the VN in these samples.

Although only one of our defined pure topological features was an independent factor in the study cohort, we found a trend in all the tensegrity indices: more homogeneous territo-rial and interterritorial VN patterns in node distribution emerged where patient prognosis was worse (Table S2 and Fig. 3a). Here, rather than the direct quantity of VN, homoge-neous reflects that VN is equally distributed throughout the sample: VN is spread over the tissue without restrictions in patients with poor prognosis. This is consistent with recent studies on the matter,[35,43] suggesting that VN enhanced the migratory capacity of tumor cells located in focal areas, thus associating VN with intratumor heterogeneity, tumor inva-sion, angiogenesis and metastasis.[44] It could also be the case that endothelial cells migrate to a fibronectin and VN-rich environment as a way to create new blood vessels in the pro-cess of neoangiogenesis.[31,33,45,46]

We found an individual independent predictor in the study cohort for each of the criteria analyzed (pretreatment risk stratification group and tumor genetic instability). Both are topological features that can predict prognosis without over-lapping with the existing known variables (age, stage, MYCN status and genetic profile). In the risk stratification group, the Euler number per node from territorial VN, which was a com-pendium between VN quantity and organization, came out as a remarkable feature. In our topological feature Euler number per node, we only consider the regions with information and computed the Euler number of each region separately. There-fore, a higher number of this feature, related to tumors with MNA from high-risk patients, stage M and ≥18 months, might indicate that existing territorial VN is compacted with stretch marks in focal areas, as previously indicated. In sum-mary, our results suggest that the topology of territorial VN would aid tumor cell migration, mechanically altering the ECM, which translates into disrupted tumor cell adhesion and easier spreading into a stiff matrix. It has been shown that the Euler number is able to characterize the aggressiveness of prostate cancer, distinguishing between tubular and cribriform growth patterns associated with lower and higher aggressive behaviors, respectively.[47] These organization patterns resemble the ones we encounter in territorial VN, where a higher Euler number is related to worse prognosis (Fig. 3c). One possibility is that the territorial VN forms cribriform-like structures that try to surround the cancer cells with a stiff ECM, allowing migration. VN-rich territorial regions would facilitate the dis-ruption of ECM–cell or cell–cell interactions (Fig. 3f). Inter-estingly, this pattern is similar to the fibrosis areas previously described in human lung cancer.[48]

For the tumor genetic instability criteria, we obtained the topological feature branches per node from territorial VN, related to the shape of VN and its number of crosslinks, as an individual independent factor. Irregular shapes (not straight), which may be surrounding the cells (Fig. 3e, right), appeared in tumors with higher genetic instability. The displacement of malignant neuroblasts in a stiff ECM could be mediated by cycles of formation and rupture of binding glycoproteins, VN and/or fibronectin, as described in these studies in ovarian and oral squamous carcinoma tumor cells.[32,49] Likewise, VN branching could represent migration tracks with a large amount of VN, connecting integrins and fiber elements of the ECM. Furthermore, these irregular territorial VN branches would represent migrating tracks facilitating invasion by acti-vating nuclear intracellular signaling pathways that would modify genetic and epigenetic mechanisms, increasing tumor instability in these patients (Fig. 3f).

The digital analysis tools are increasingly numerous and powerful as a result of the growing demand for an automatic objective method that allows rapid and effective analysis (reduce inter and intraobserver variability) of the huge num-ber of tumor samples required at a routine clinical diagnosis and research.[50,51] In particular, previous works had used tex-tural analysis to improve the current methods of grading pros-tate cancer[24] or malignancy detection in breast tumors,[12] among others.[13,23] Although these studies achieved accurate results, the features they got did not directly unlock biological mechanisms. NB is considered a heterogeneous and complex cancer dependent on many known variables, such as age and MYCN oncogene amplification,[37,52] but there are still unknown biological factors. Thus, interpret and relate features

with biology are essential to extract new insights. Likewise, most of the works using computerized image analysis rely on recognizable objects to capture the morphology or topology, such as the nuclei of the cells within the sample.[14,24,25] In our case, VN cannot be captured as an object due to its variability in size and shape (Figs. 1d and 1e). We propose that these automatic methods can be enhanced with the use of mathematical tools that can capture the organization of the elements identified in the biopsies. Our approach discretizes the space to extract different topological and morphological features avoiding these two issues while obtaining statistically significant characteristics.

Overall, our conclusion is that the particular organization of territorial VN markedly changes the constitution and mechanics of the ECM by the rapid addition of new synthesized VN creating migration tracks, which may lead to more aggressive NB. However, the molecular mechanism behind these results remains unclear. In conclusion, combining topology and morphometric features seems an effective strategy to find complementary factors that could obtain a more precise pretreatment risk stratification to guide treatment strategies. We have shown that VN may play a greater role than previously assumed in prognostic assessment of human patients, in agreement with our previous work that suggested the importance of territorial VN.[35] There remains a wealth of information to be captured from these biopsies. Human samples are an excellent source of information that should be thoroughly analyzed. On this sense, our topological approach requires long computational processing to obtain high-quality and reliable markups. However, once the markup images have been validated, their topological properties can be easily extracted using our pipeline. Our mathematical approach shows a big potential in histopathological images of NB samples. In the near future, the integration of histopathological consecutive slices will be the first step to approach the 3D tumor's structure. These studies will be needed to reveal the true role of VN in NB to test whether the results of our study are consistent.

Glossary

Tensegrity: Stabilization of structures constituted by continuous elements of tension and discontinuous elements resistant to compression. **Topology:** How a set of elements are struc-tured and connected in a given space. **Tessellation:** A sur-face covered by geometric components (or tiles) with no gaps and without overlapping. **Graph/network:** A set of elements connected between them following determined rules that represent binary relations. A graph is formed by nodes (the elements) and edges that link them. **Voronoi diagram**: A particular tessellation formed by convex polygons. Each convex polygon is a Voronoi cell. Every Voronoi cell emerges from a seed. All the points of a Voronoi cell are closer to its own seed that to any other seed of the surface. **Graphlets:** Graphs with a small number of nodes extracted from a larger network. A network can be quantitatively characterized by its graphlets composition. **Markup image**: A binary immunohistochemistry microscopic image in which the white regions represent detected objects, and the black ones, the background. **Euler number feature:** In an image where a set of objects has been identified, the Euler number is the value of the number of objects minus the number of holes inside them. **Branching feature:** In an image where a set of objects has been identified, the Branching is the value of the number of crosslinks that are found on the objects. **Node**: A representation of an object. In our case, it stands for a hex-agonal area filled with vitronectin. **Edge:** The link between nodes. Two nodes connected by one edge are considered adjacent. **Tensegrity index***:* Represents how different is the VN (interterritorial or territorial) organized in the biopsy compared to a homogenous distribution.

Acknowledgements

The authors thank Juan Francisco Martín-Rodríguez for useful guidance on statistical analysis and Kathryn Davies for English correction. The authors also thank the Spanish Society of Pediatric Hemato-Oncology (SEHOP) for patient data management.

Financial support

L.M.E. is supported by the Ramón y Cajal program (PI13/01347). The work of L.M.E. and P. V.-M. is funded by the Ministry of Economy, Industry, and Competitiveness grant BFU2016-74975-P cofunded by FEDER funds. P.V.-M. and R.B.-P. are supported by a contract by the Asociación Fundación Española contra el Cáncer. P.V.-M. contract is also supported by Seville University (V plan propio). This work was funded by the FAECC (contract 2015, FAECC2015/006), CIBERONC (CB16/12/00484) and FIS (PI17/01558, Institute of Health Carlos III, Madrid/ERDF), NEN Association (Nico contra el cancer infantil 2017). The funders had no involvement in the research process or the preparation and submis-sion of the article.

References

1. Tsuboi A, Ohsawa S, Umetsu D, et al. Competition for space is controlled by apoptosis-induced change of local epithelial topology. Curr Biol 2018;28:2115–28.
2. Fiorino S, Bacchi-Reggiani L, Pontoriero L, et al. Tensegrity model hypothesis: may this paradigm be useful to explain hepatic and pancreatic carcinogenesis in patients with persistent hepatitis B or hepatitis C virus infection? JOP 2014;15:151–64.
3. Gómez-Gálvez P, Vicente-Munuera P, Tagua A, et al. Scutoids are a geometrical solution to three-dimensional packing of epithelia. Nat Commun 2018;9:2960.
4. Clunie D, Hosseinzadeh D, Wintell M, et al. Digital imaging and communications in medicine whole slide imaging connectathon at digital pathology association pathology visions 2017. J Pathol Inform 2017;8:1–12.
5. Bueno G, Fernández-Carrobles MM, Deniz O, et al. New trends of emerging technologies in digital pathology. Pathobiology 2016;83:61–9.
6. Furler R, Nixon D, Brantner C, et al. TGF-β sustains tumor progression through biochemical and

mechanical signal transduction. Cancers (Basel) 2018;10:199.
7.Shi Z, Yu J, Shao H, et al. Exploring the molecular pathogenesis associated with t-cell prolymphocytic leukemia based on a comprehensive bioinformat-ics analysis. Oncol Lett 2018;16:301–7.
8.Carleton NM, Lee G, Madabhushi A, et al. Advances in the computational and molecular understanding of the prostate cancer cell nucleus. J Cell Biochem 2018;119:7127–42.
9.Tadeo I, Piqueras M, Montaner D, et al. Quantita-tive modeling of clinical, cellular, and extracellular matrix variables suggest prognostic indicators in cancer: a model in neuroblastoma. Pediatr Res 2014;75:302–14.
10.Tambasco M, Eliasziw M, Magliocco AM. Mor-phologic complexity of epithelial architecture for predicting invasive breast cancer survival. J Transl Med 2010;8:140.
11.Lam WA, Cao L, Umesh V, et al. Extracellular matrix rigidity modulates neuroblastoma cell dif-ferentiation and N-myc expression. Mol Cancer 2010;9:35.
12.Veta M, Pluim JPW, Van Diest PJ, et al. Breast cancer histopathology image analysis: a review. IEEE Trans Biomed Eng 2014;61:1400–11.
13.Belsare AD, Mushrif MM. Histopathological image analysis using image processing techniques: an overview. Int J Signal Image Process 2012;3:23–36.
14.MacAulay C, Keyes M, Hayes M, et al. Quantifica-tion of large scale DNA organization for predicting prostate cancer recurrence. Cytometry A 2017;91:1164–74.
15.Nast CC, Lemley KV, Hodgin JB, et al. Morphol-ogy in the digital age: integrating high-resolution description of structural alterations with pheno-types and genotypes. Semin Nephrol 2015;35:266–78.
16.Stålhammar G, Fuentes Martinez N, Lippert M, et al. Digital image analysis outperforms manual biomarker assessment in breast cancer. Mod Pathol 2016;29:318–29.
17.Sanchez-Gutierrez D, Tozluoglu M, Barry JD, et al. Fundamental physical cellular constraints drive self-organization of tissues. EMBO J 2016; 35:77–88.
18.Binchi J, Merelli E, Rucco M, et al. iHoles: a tool for understanding biological complex networks via clique weight rank persistent homology. Elec-tron Notes Theor Comput Sci 2014;306:5–18.
19.Barabási AL, Oltvai ZN. Network biology: under-standing the cell's functional organization. Nat Rev Genet 2004;5:101–13.
20.Sáez A, Rivas E, Montero-Sánchez A, et al. Quan-tifiable diagnosis of muscular dystrophies and neurogenic atrophies through network analysis. BMC Med 2013;11:77.
21.Frost JJ, Pienta KJ, Coffey DS. Symmetry and symmetry breaking in cancer: a foundational approach to the cancer problem. Oncotarget 2017; 9:11429–40.
22.Pan Y, Duron C, Bush EC, et al. Graph complex-ity analysis identifies an ETV5 tumor-specific network in human and murine low-grade glioma. PLoS One 2018;13:e0190001.
23.Angel Arul Jothi J, Mary Anita Rajam V. A survey on automated cancer diagnosis from histopathol-ogy images. Artif Intell Rev 2017;48:31–81.
24.Doyle S, Agner S, Madabhushi A, et al. Automated grading of breast cancer histopathology using spectral clustering with textural and architectural image features. In: 2008 5th IEEE International Symposium on Biomedical Imaging: From Nano to Macro, Proceedings, ISBI. IEEE, 2008. 496–9.
25.Yao J, Ganti D, Luo X, et al. Computer-assisted diagnosis of lung cancer using quantitative topol-ogy features. Lecture notes in computer science (including subseries lecture notes in artificial intel-ligence and lecture notes in bioinformatics). Cham, Switzerland: Springer, 2015. 288–95.
26.Pržulj N, Corneil DG, Jurisica I. Modeling inter-actome: scale-free or geometric? Bioinformatics 2004;20:3508–15.
27.Yaveroglu ÖN, Malod-Dognin N, Davis D, et al. Revealing the hidden language of complex net-works. Sci Rep 2014;4:1–9.
28.Vicente-Munuera P, Gomez-Galvez P, Tetley RJ, et al. EpiGraph: an open-source platform to quan-tify epithelial organization. bioRxiv 2018;217521.
29.Pickup MW, Mouw JK, Weaver VM. The extra-cellular matrix modulates the hallmarks of cancer. EMBO Rep 2014;15:1243–53.
30.Gilkes DM, Semenza GL, Wirtz D. Hypoxia and the extracellular matrix: drivers of tumour metas-tasis. Nat Rev Cancer 2014;14:430–9.
31.Li R, Ren M, Chen N, et al. Vitronectin increases vascular permeability by promoting VE-cadherin internalization at cell junctions. PLoS One 2012;7: e37195.
32.Kenny HA, Kaur S, Coussens LM, et al. The initial steps of ovarian cancer cell metastasis are medi-ated by MMP-2 cleavage of vitronectin and fibro-nectin. J Clin Invest 2008;118:1367–79.
33.Orr FW, Podor TJ, Buchanan MR, et al. Up-regulated biosynthesis and expression of endothelial cell vitronectin receptor enhances cancer cell adhesion. Cancer Res 1992;52:2202–8.
34.Cohn SL, Pearson ADJ, London WB, et al. The International Neuroblastoma Risk Group (INRG) classification system: an INRG task force report. J Clin Oncol 2009;27:289–97.
35.Burgos-Panadero R, Noguera I, Cañete A, et al. Vitronectin as a molecular player of the tumor microenvironment in neuroblastoma. BMC Cancer 2019;19:479.
36.Tadeo I, Berbegall AP, Navarro S, et al. A stiff extracellular matrix is associated with malignancy in peripheral neuroblastic tumors. Pediatr Blood Cancer 2017;64:e26449.
27.Tadeo I, Gamero-Sandemetrio E, Berbegall AP, et al. Lymph microvascularization as a prognostic indicator in neuroblastoma. Oncotarget 2018;9: 26157–70.
38.Ambros IM, Brunner C, Abbasi R, et al. Ultra-high density SNParray in neuroblastoma molecular diagnostics. Front Oncol 2014;4:202.
39.Hocevar T, Demšar J. A combinatorial approach to graphlet counting. Bioinformatics 2014;30:559–65.
40.Pržulj N. Biological network comparison using graphlet degree distribution. Bioinformatics 2007; 23:177–83.
41.Martín-Rodríguez JF, Cervera-Barajas A, Madrazo-Atutxa A, et al. Effect of bariatric surgery on microvascular dysfunction associated to metabolic syndrome: a 12-month prospective study. Int J Obes (Lond) 2014;38:1410–5.
42.Martín-Rodríguez JF, Madrazo-Atutxa A, Venegas-Moreno E, et al. Neurocognitive function in acromegaly after surgical resection of GH-secreting adenoma versus naïve acromegaly. PLoS One 2013;8:e60041.
43.Schneider G, Bryndza E, Poniewierska-Baran A, et al. Evidence that vitronectin is a potent migration-enhancing factor for cancer cells chaperoned by fibrinogen-a novel view of the metastasis of cancer cells to low-fibrinogen lym-phatics and body cavities. Oncotarget 2016;7: 69829–43.
44.Zhou A, Huntington JA, Pannu NS, et al. How vitronectin binds PAI-1 to modulate fibrinolysis and cell migration. Nat Struct Biol 2003;10:541–4.
45.Isogai C, Laug WE, Shimada H, et al. Plasmino-gen activator inhibitor-1 promotes angiogenesis by stimulating endothelial cell migration toward fibronectin. Cancer Res 2001;61:5587–94.
46.DeClerck YA, Mercurio AM, Stack MS, et al. Pro-teases, extracellular matrix, and cancer: a work-shop of the path B study section. Am J Pathol 2004;164:1131–9.
47.Wittke C, Mayer J, Schweiggert F. On the classifi-cation of prostate carcinoma with methods from spatial statistics. IEEE Trans Inf Technol Biomed
2007;11:406–14.
48.Sieren JC, Smith AR, Thiesse J, et al. Exploration of the volumetric composition of human lung cancer nodules in correlated histopathology and computed tomography. Lung Cancer 2011; 74:61–8.
49.Ali MRK, Wu Y, Tang Y, et al. Targeting cancer cell integrins using gold nanorods in photothermal therapy inhibits migration through affecting cytoskeletal proteins. Proc Natl Acad Sci U S A 2017;114:E5655–63.
50.Rojo MG, Bueno G, Slodkowska J. Review of imaging solutions for integrated quantitative immunohistochemistry in the pathology daily practice. Folia Histochem Cytobiol 2010;47:
349–54.
51.Callau C, Lejeune M, Korzynska A, et al. Evaluation of cytokeratin-19 in breast cancer tissue samples: a comparison of automatic and manual evaluations of scanned tis-sue microarray cylinders. Biomed Eng Online 2015;14:S2.
52.Tadeo I, Berbegall AP, Castel V, et al. Extracellular matrix composition defines an ultra-high-risk group of neuroblastoma within the high-risk patient cohort. Br J Cancer 2016;115: 480–9.

SUPPLEMENTARY INFORMATION

Algorithms of the pure topological features

To model how the VN is organized in the biopsy, we have created a graph in which nodes represent the hexagonal regions with VN. How these nodes are linked (by edges) depends on the rules we use. For this reason, we computed three algorithms to obtain three different connected networks:

a) *Iteration* (**Supplementary Fig. 1D**). Obtains a network connecting its closest regions. It reviews all the neighbours of each node, connecting the closest ones until the network is fully connected. The algorithm follows these steps: 1) Create a matrix, whose rows and columns are the detected nodes of the image (the first row and the first column correspond to the same node) representing the distance between any two nodes. 2) Perform an iteration that involves going through all the rows and 2.1) getting the smallest distance of each row; 2.2) adding the column's node and row's node as edges. 2.3) Remove that same edges from the distance matrix. 3) Once an iteration is over, check if the network is connected. Step 2 begins again if there are still isolated nodes.

b) In contrast to *Iteration*, *Sorting* algorithm (**Supplementary Fig. 1C**) entails ordering all the distances and connecting them one at a time until the output network is connected. The algorithm follows this flow: 1) Sort from closest to furthest all the distances between any pair of regions. 2) Take as a threshold, the largest distance of the closest node of every node from the list. 3) Add all the edges with a distance smaller or equal to the previously defined threshold. 4) Remove the added edges and distances from the list. 5) Perform steps 2 to 4 until the output graph is connected.

c) Minimum Spanning Tree (**Supplementary Fig. 1E**). Although the two previous algorithms were designed for this study, the last algorithm, Minimum Spanning Tree (MST), has already been used in other studies [1]. It was already implemented on a Matlab function named *graphminspantree* (Matlab R2014b, MathWorks). The resulting network of the MST is a network with the minimum possible number of edges. Moreover, this network is a tree, whose particularity is that any two nodes are connected by exactly one path.

Building the controls

The pipeline of control creation follows these steps: 1) Collect the number of nodes from the mark-up image. 2) Randomly place that number of seeds inside an image. The seeds should avoid the regions of the original image where it was not possible to find the marker (i.e. tears of the tissue). 3) Create a Voronoi partitioning space into regions starting from the seeds. In a Voronoi, every point of the image is associated with a seed and all the points will be closest to its seed than to any other seed. 4) Perform Lloyd's algorithm ten times, homogenizing the Voronoi cells to become more hexagonal [2,3]. As a result, we obtained a control in which the regions are homogeneously spread throughout the mark-up image of the biopsy. Once the nodes were distributed, we computed the algorithm of Sorting and Iteration for the controls, whose output is a graph (**Supplementary Fig. 1F-G**). These graphs were compared with the tumor specific network. Iteration control network served as a control to MST. Note that the control is not overlapped with a hexagonal grid; instead, a Voronoi is created with the same number of seeds as the original.

Statistical analysis

We first performed a Shapiro test to check if the tensegrity indices came from a normal distribution. Next, we performed the non-parametric Mann-Whitney test using Wilcoxon R function [4] to test if the distribution of the tensegrity indices were statistically different, as a preliminary experiment.

Thereafter, we computed the pipeline to obtain individual independent factors (based on previous works [5,6]) from our dataset of features that could not overlap with known predictive variables (INRG variables like age or *MYCN* status). First, we categorized the continuous variables regarding the quartiles preparing them to perform the logistic regression. Due to a large number of features, when performing the logistic regression with all the values we did not know what features were contributing more. Therefore, in the second step, we computed a univariate analysis with each variable and calculated an ANOVA chi-square (chi-sq, which refers to how the addition of a new feature differs significantly from the expected outcome), keeping only the statistically significant features (**Table 1A**). Third, using the results from the univariate analysis, we performed a multivariate logistic regression (**Table 2**), with a 'best subset' approach. We gathered the eighth and ninth characteristics with a lower p-value in the high-risk pre-treatment stratification group and tumour genetic instability criteria, together with the known INRG variables, to perform this first step. To do this, initially, we applied an exploratory analysis of what probabilities the selected variables have, to obtain a good subset using *mplot* [7]. Afterwards, we performed one main subset selection using *glmulti* [8], and a second selection to check for the

most relevant features with *bestglm* [9]. Both obtained a model with a minimum Akaike Information Criterion (AIC) and we reported nagelkerke R^2 as a measure of fitness of the model. Using the 'VIF' function in the *car* library in R [10], we removed the most redundant features (collinearities, when two features can be represented, approximately, with the same regression line), retaining all the features with a value below three (we ran the function each time after removing a feature). Since we encountered with coefficients of one of the final models converging to infinity (p-values nearly 1, very large coefficients and standard errors larger than its own coefficients), we used the library of R *logistf*, which implements Firth's logistic regression [11], to avoid this issue. Firth's method let us obtain real odds ratio by penalized profile likelihood. The results of the multivariate analysis are variables that can independently and individually classify the prognosis of NB patients (**Fig. 3C, E**). Therefore, the outputs of the pipeline are complementary features that cannot overlap and which add new insights to the existing ones (INRG variables) refining both classification criterion.

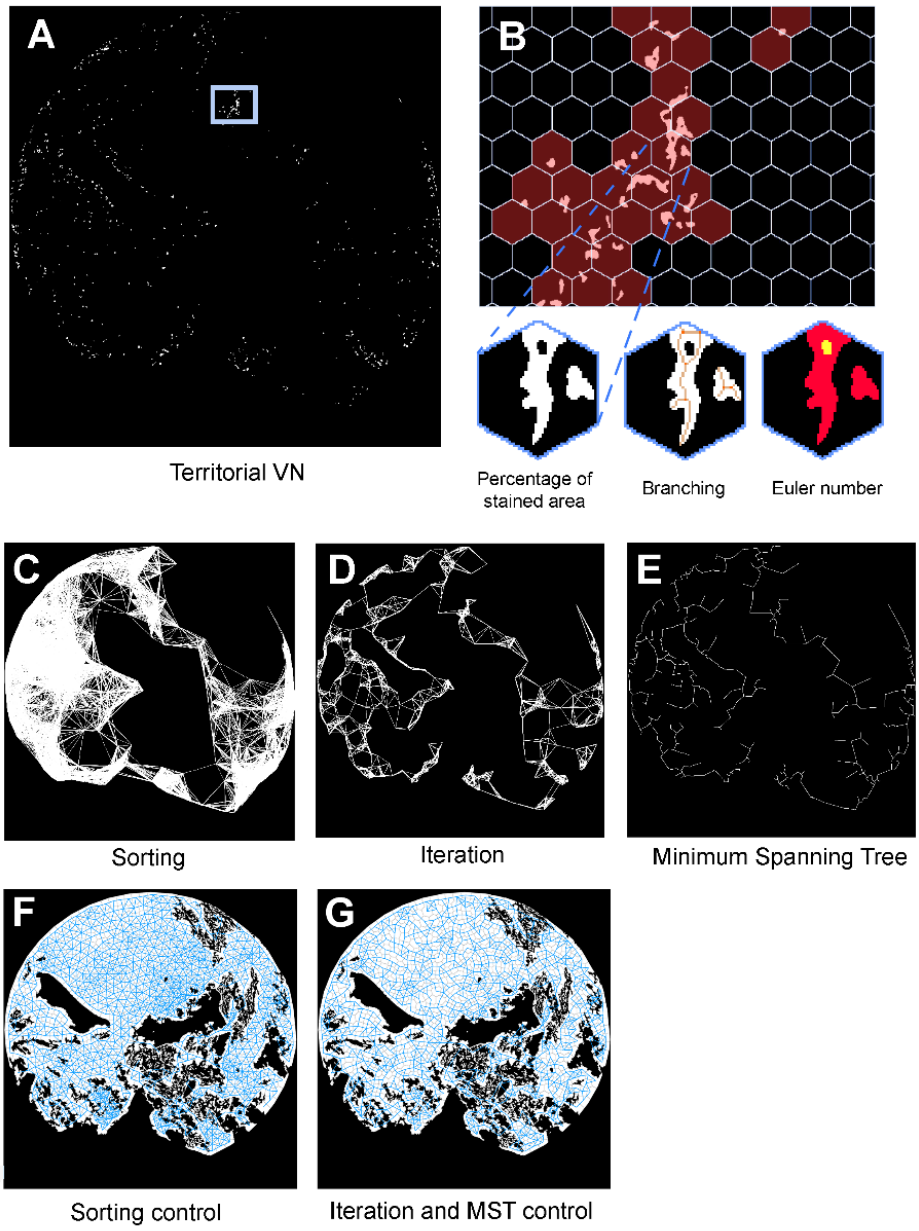

Supplementary figure 1. Features derived from the mark-up images of a neuroblastoma (NB) biopsy. A) A segmented image representing territorial vitronectin (VN), the same as in **Fig. 2**. Coloured in light blue is a ROI that represents the region of (B). **B)** A cropped region from (A), where the regions with information become the nodes of the graphs in (C-E). A single hexagonal cell from the light blue grid is selected to characterize: the *percentage of stained area* (left hexagon), which is the number of white pixels found on it divided by the total area of the hexagon; *branching* (central hexagon), after skeletonizing (light orange), crosslinks (7 in orange) are identified; and the *Euler number* (right hexagon), that needs to recognise the objects (2 in red) and the holes (1 in yellow). Note that a hole should be inside an object (the background of the image is not a hole). **C-E)** Networks or graphs resulting from applying the algorithms in the (A) mark-up image: Sorting (C), Iteration (D) and Minimum Spanning Tree (E). **F-G)** A Voronoi control generated using the same number of nodes as in the original case (A), covering the biopsy homogenously. Regions where the marker could not be found are in black, while in

hexagonal white areas represent the uniform node distribution. Blue represents the graph computed with the algorithm Sorting (F) and Iteration (G). The control for the MST algorithm was the same as in Iteration (G).

Supplementary table 1. Raw data of topological and non-topological vitronectin (VN) features. Risk groups and tumour genetic instability criteria for each case are indicated. Note that tumour genetic instability criteria includes cases with no data, corresponding to atypical genetic profiles with unknown clinical implication marked as -. The identification (ID) list of topological and non-topological VN features is enumerated in **Table 1A**. See online: IJC-146-553-s003.xlsx

Supplementary Table 2. Tensegrity indices per criteria and prognosis. Mean and standard deviation for each tensegrity index. In addition, results from Shapiro normality test and Mann-Whitney test. In bold, distributions that are statistically different regarding risk group or tumour genetic instability criteria. std: standard deviation. See online: IJC-146-553-s004.xlsx

Papers as a co-author not included in this thesis

I. Integrating the Tumor Microenvironment into Cancer Therapy. Sanegre S, Lucantoni F, **Burgos-Panadero R**, de la Cruz-Merino L, Noguera R, Álvaro Naranjo T. Cancers 2020, 12, 1677.

II. A three-dimensional bioprinted model to evaluate the effect of stiffness on neuroblastoma cell cluster dynamics and behavior. Monferrer, E., Martín-Vañó, S., Carretero, A., García-Lizarribar, A., **Burgos-Panadero, R.**, Navarro, S., Samitier, J., & Noguera, R. Scientific reports, 2020; 10(1), 6370.

III. An integral view of cancer (III). Evaluation of new biomarkers and treatment strategies. Noguera R, **Burgos-Panadero R**, Lucantoni F, de la Cruz-Merino L, Álvaro Naranjo T. Rev Esp Patol. 2020;53(2):88-99.

IV. An integral view of cancer (II). Fields of investigation and emerging biomarkers. Noguera R, **Burgos-Panadero R**, Gamero-Sandemetrio E, de la Cruz-Merino L, Álvaro Naranjo T. Rev Esp Patol. 2019; 52(4):222-233.

V. An integral view of cancer (I). The study, classification and reprogramming of the tumoral microclimate. Noguera R**, Burgos-Panadero R**, Gamero-Sandemetrio E, de la Cruz-Merino L, Álvaro Naranjo T. Rev Esp Patol. 2019 Apr - Jun;52(2):92-102. D

VI. High Oct4 expression: implications in the pathogenesis of neuroblastic tumors. Monferrer E, **Burgos-Panadero R,** Blanquer-Maceiras M, Cañete A, Navarro S, Noguera R. BMC Cancer. 2019 Jan 3;19(1):1

VII. Fibronectina: Estructura y Función. Análisis cuantitativo con imagen microscópica. **Burgos-Panadero R**, Tadeo Cervera I, Blanquer-Maceiras M, Benito Jardón M, Costell Rosselló M, Noguera Salvá R. Heridas y Cicatrización, SEHER. 2015. 5(20):6-11.

CHAPTER 1. Introduction

1.1 Neuroblastoma (NB)

1.1.1. General aspects

Neuroblastoma (NB) is an extracranial malignancy in childhood that belongs to the peripheral neuroblastic tumors group being the most common and aggressive form of these neoplasms. It is found among the largest diagnosed tumors in patients younger than 15 years of age after leukemia, CNS neoplasms, and lymphomas, accounts for 7% of pediatric cancers worldwide and 15% of children related-deaths. NB is the greatest prevalent solid tumor in kids younger than 5 years, being the median age of presentation between 17 and 22 months [1-4]. In a cohort of Spanish NB patients between 1980-2016, 86.7% of the 1,964 diagnosed patients presented less than five-year age, and only 2.3% with a 10-14 years age [5]. Moreover, this neoplasia may appear also in adolescents and young adults, this patient group has a poor outcome [6-8]. The general 5-year survival rate for NB is around 80% being only 36% in adolescents and adults [9, 10].

NB is an embryonic neoplasm that derives from progenitor cells of the sympathoadrenal lineage of the neural crest. This assumption is reinforced by the expression of neuronal differentiation markers and the characteristics of self-renew and migration that is found in the NB cells [11-13]. NB can appear in any location throughout the sympathetic nervous system, being the most common primary place in the adrenal gland, followed by the thoracic, cervical, and pelvic ganglia [14-16]. Metastatic disease is mainly found in bone marrow, bone, lymph nodes, and liver, and rarely in the skin, lungs, or brain [17]. The clinical symptoms vary according to the location of this primary neoplasm, the site of its metastatic spread, and in a less frequency depending on paraneoplastic manifestations such as opsoclonus-myoclonus syndrome [18]. In the case that the primary tumor appears in the abdomen some normal manifestations are abdominal distension, diarrhea, constipation, and abdominal pain. Thoracic NB presents scoliosis or compression of the airway. If the NB develops in the chest may cause signs like wheezing and chest pain. Some general symptoms can be bone pain, fever, and unexplained weight loss [19, 20].

Since the symptoms are variable, there are some standards for the diagnostic of NB such as the imaging study through computed tomography, magnetic resonance, and metaiodobenzylguanidine scan, that determines the place and size of the primary tumor and even the existence of metastasis, the screening of catecholamines or their derived metabolites

in urine or serum, however, the key in the diagnosis is the histopathological analysis after acquiring a biopsy of the primary tumor and bone marrow aspiration to evaluate the extent of this neoplasm [21-23].

A remarkable feature of NB is its high heterogeneity that depends on clinical presentation and several biological features, existing a possibility of spontaneous regression and a better outcome in the youngest children than a more aggressive disease and worse prognosis in older ones [24]. Indeed, we have to keep in mind that the prognosis depends on many factors, particularly on the risk stratification group of the tumor. Considering that, the survival rate in high-risk (HR) patients is characterized by 50%, whereas low- or intermediate-risk patients have a long-term survival between 85-90% [25, 26].

NB represents an enigmatic and complex entity due to its clinical, molecular, and genetic variability generating an influence on the progression and treatment response. Its tumor heterogeneity can derive from cellular clonal evolution changes that originate the acquisition of higher plasticity and molecular characteristics by neuroblastic cells or to the presence of diverse genomic alterations such as the status of *MYCN* oncogene, ploidy, deletion (D) of 1p or 11q and gain of 17q [27-29]. In addition, although NB is known by a low rate of mutations, it has been described some genetic mutations in paired-like homeobox 2B (*PHOX2B*) and anaplastic lymphoma kinase (*ALK*) that are related to familiar NB [30, 31].

1.1.2 Clinical, histological and genetic factors according to INRG classification system

As NB is an intricate disease to perform a proper and established risk stratification of the patients the International Neuroblastoma Risk Group (INRG) classification system has been developed. This system provides a pre-treatment categorization based on imaging of the disease extent and image defining risk factors rather than postsurgical grading that was used by the previous staging system (INSS). The INRG classification system has into account factors like clinical traits (age and stage), tumor histology, and genetic aberrations to classify the patients into very low, low, intermediate, or HR categories (**table 1**). In this way, this system facilitates comparisons across international clinical trials and is used to predict the clinical behavior of the tumor and how it will respond to treatment [32, 33].

Table 1. INRG pre-treatment classification system, established by consensus in 2009 [32].

INRG Stage	Age (months)	Histologic Category	Grade of Tumor Differentiation	*MYCN*	11q Aberration	Ploidy	Pretreatment Risk Group
L1/L2		GN maturing; GNB intermixed					A Very low
L1		Any, except GN maturing or GNB intermixed		NA			B Very low
				Amp			K High
L2	< 18	Any, except GN maturing or GNB intermixed		NA	No		D Low
					Yes		G Intermediate
	≥ 18	GNB nodular; neuroblastoma	Differentiating	NA	No		E Low
					Yes		H Intermediate
			Poorly differentiated or undifferentiated	NA			
				Amp			N High
M	< 18			NA		Hyperdiploid	F Low
	< 12			NA		Diploid	I Intermediate
	12 to < 18			NA		Diploid	J Intermediate
	< 18			Amp			O High
	≥ 18						P High
MS	< 18			NA	No		C Very low
					Yes		Q High
				Amp			R High

GN, ganglioneuroma; GNB, ganglioneuroblastoma; Amp, amplified; NA, not amplified; L1, localized tumor confined to one body compartment and with an absence of image-defined risk factors (IDRFs); L2, locoregional tumor with the presence of one or more IDRFs; MS, metastatic disease confined to skin, liver and/or bone marrow in children < 18 months of age; M, distant metastatic disease (except stage MS).

Clinical factors

Age

Age at the time of diagnosis was one of the first prognostic indicators identified. Older patients are associated with poor outcome. After several analyses in different patient's cohort with an age range between 15-18 months, the established age cutoff by the task force was 18 months. Nonetheless, for the group of patients with diploid, stage M, *MYCN* non-amplified tumors, the Task Force proposed an age cutoff of 12 months [32, 34].

Stage

The new INRG staging system (INRGSS) distinguishes between localized tumor which is defined by the absence or presence of image-defined risk factors (L1 and L2, respectively) [33, 35]. Metastatic disease, that corresponds to distant metastatic disease (stage M). Special metastatic disease (stage MS), when the metastases are restricted to the skin, liver, and/or bone marrow in patients younger than 18 months and is normally related to favorable biological features including spontaneous regression [33].

Tumor histology

The currently used International Neuroblastoma Pathology Classification (INPC) was suggested by Shimada *et al*. and considered a histological typing of tumors into favorable and unfavorable categories based on the age at diagnosis, the amount of Schwannian stromal content, the grade of tumor differentiation and the mitosis-karyorrhexis index (MKI). Then, the neuroblastic tumors are classified into four histological types: 1) NB (Schwannian stroma-poor), 2) intermixed ganglioneuroblastoma (iGNB) (Schwannian stroma-rich), 3) nodular Ganglioneuroblastoma (nGNB) (composite Schwannian stroma-rich/stroma-dominant and stroma-poor) and 4) Ganglioneuroma (GN) (Schwannian stroma-dominant). Besides, there are three grades of tumor differentiation: undifferentiated (u), poorly differentiated (pd) and differentiating (d) [36, 37].

Genetic aberrations

MYCN status

MYCN is an oncogene located on the chromosome 2p24 involved in cell growth, proliferation, and apoptosis. *MYCN* amplification (MNA), defined as more than 10 gene copies, appears in 20% of primary NB being considered a high specific biomarker in the routine management of NB for that it was incorporated as the first genomic factor in the risk classification. MNA is associated with poor outcome independently on the status of the rest of the prognostic factors. Patients with MNA tumors are classified as HR-NB. Nowadays the Society of Paediatric Oncology Europe Neuroblastoma (SIOPEN), as well as the Children´s Oncology Group (COG), uses fluorescent in situ hybridization to determine the status of *MYCN* [38, 39]. A remarkable feature of MNA, is the presence of intratumoral heterogeneous MNA (hetMNA), it is referring to exist together MNA clones and *MYCN* non-amplified clones, this is an infrequently feature with poorly defined clinical consequences [40, 41].

DNA ploidy

The DNA index has a prognostic value in NB patients younger than 18 months with metastatic disease and *MYCN* non-amplified (MNNA) tumors. Diploid and tetraploid tumors are correlated with poorer outcomes causing more structural rearrangements [42, 43].

11q

Loss of chromosome 11q is a relevant molecular marker that remains in 30% of primary NB associated with unfavorable prognosis defining the HR tumor group [44]. Normally it is inversely correlated with MNA which involves different genetic categories of clinically aggressive NB, although some exceptions have been described [45].

Other genetic markers

Pangenomic studies have acquired a great role to improve the staging of the patients, being incorporated in the genomic profiles recently to the risk classification system [46]. Molecular analysis of NB defined that the appearance and also a high amount of segmental (SCA) versus numerical chromosome aberrations (NCA) has been related to a non-favorable clinical behavior of the tumors [46, 47]. Therefore, these results denoted a presence of chromosomal instability in neuroblastic cells playing a major role in NB tumorigenesis [48, 49]. In fact, in MNNA tumors, the appearance of SCA has been related to a major probability of relapse and it was observed that tumors of patients older than 18 months and 11q deleted tumors have a high number of SCAs [50, 51]. Besides MNA and 11qD, other typical SCAs that are frequently seen in NB are deletions of 1p, 3p, and 4p and gains of 1q, 2p, and 17q. Loss of 1p chromosome has been found in 30% of the cases [52] and gain of 17q is the most common alteration observed in 50% of the NB patients; both aberrations associated with poor prognosis in MNA tumors [53].

The application of next-generation techniques as whole exome or genome sequencing to identify gene mutations has been developed to establish a targeted therapy. Although NB is defined by a low mutation rate, it has been observed the presence of some somatic gene mutations with a frequency of 12% as much. Some of these genes are *ARID1A* and *ARID1B* (related to chromatin regulation that implicates a nonsense or missense alteration improving NB oncogenesis), *ALK* (where F1174 and F1245 mutations are exclusive of this NB form), *PTPN11* (plays a role in growth factor signaling and missense mutations has been associated with developmental diseases), *TIAM1* (results in a loss of function that controls neuritogenesis) and *ATRX* (involves a loss of function that results in lengthened telomeres and is normally found in NB of adolescents and young adults) [53-55]. Another frequent somatic genetic alteration implicates structural rearrangements in *TERT* that is related to poor prognosis, besides it has been observed coexistence of MNA, *TERT,* and *ATRX* mutations in HR-NB [56]. Another curious phenomenon associated with a poor outcome that is found in 18% of the high NB stage is called chromothripsis, which is a random organization along a chromosome of chromosomal fragments [53]. All these molecular disorders together with the rest of the genetic alterations

above mentioned belonging to the sporadic NB group that is the most prevalent form in NB patients.

Familiar NB is only found in 1-2% of patients and the vast majority of the cases are represented by mutations in *ALK* or *PHOX2B* genes. The *ALK* receptor tyrosine kinase is the most common mutated gene representing 80% of hereditary NB where a gain of function increases the proliferation rate. One aspect of this gene is that not all *ALK* mutations are related to familiar NB since 8% of *ALK* mutations are associated with sporadic NB. An infrequent activation mechanism of *ALK* implicates the amplification of this gene, although the coexistence of mutation and amplification of this gene in the same tumor is rare [57]. The *PHOX2B* accounts for 6,4% and is the main regulator gene of the neural crest development. The *PHOX2B* mutations in NB implicate a loss of function of the gene [54].

Sequencing studies between primary and relapse tumors, suggest an association of mutations in RAS-MAPK pathway with a significant increase to relapse in NB patients and implicate genes such as *ALK, NRAS*, and *HRAS*; also new recurrent mutations genes like *CHD5*, *DOCK8* and *PTPN14* have been found in relapsed NB [58]. These data evidences a complexity on the NB genomics events that have to be considered for the design of future therapeutic approaches.

1.1.3. Therapy and novel targets

Clinical strategies in NB patients are based on the INRG patient stratification system (**table 1**) due to the molecular and clinical features of NB, exist a variety in the treatment standards. Patients with very low, low, and intermediate-risk are characterized by a good outcome. Then, the ordinary treatment plan for very and low-risk patients is only surgery. However, in some exceptions such as a difficulty in the tumor elimination process or presence of remaining tumor cells, minimal chemotherapy is applied. Even, the peculiar MS stage with some molecular markers as MNNA and children younger than 18 months do not need any treatment caused by spontaneous tumor regression [59]. Patients belonging to the intermediate-risk receive surgery plus moderate-chemotherapy [54]. On the other hand, as it is mentioned above, HR NB patients present the lowest survival rate and the treatment approach is classified into three main steps: 1) intensive chemotherapy induction that consists in vincristine, doxorubicin, cyclophosphamide, cisplatin, and etoposide [60](COJEC) which is followed up by surgery; in certain clinical trials some little modifications as the incorporation of topotecan were

introduced, 2) the consolidation phase aims to eliminate the persisting tumor cells with a myeloablative dose of chemotherapy followed by a reinfusion of stem cell and local radiation therapy, and 3) the maintenance phase that includes the 13-cis retinoic acid administration to prevent the relapse since is a clinical marker in the majority of HR patients. Currently, to improve the overall survival (OS) in this group of patients also received the anti-ganglioside immunotherapy in addition to granulocyte-macrophage colony-stimulating factor and interleukin-2 (IL-2) [54, 61, 62]. A recent study of the chemoimmunotherapy approach has observed that an antitumor activity in patients with relapsed/refractory NB [63].

Regarding some progress as immunotherapy, in contrast with other tumors, NB expresses a scant quantity of neoantigens that restrict the chances for immunotherapeutic strategies; nonetheless, clinical trials are using novel strategies as the combination of chemotherapeutics and dinutuximab, a chimeric anti-GD2 antibody, or even inducing the expression of chimeric antigen receptors (CAR) targeting GD2 by effector T cells [64, 65].

The principle of targeted therapy is the replacement of the cytotoxic effect of chemotherapy for a cytostatic effect. Some targeted therapies can include: crizotinib, that is an *ALK* inhibitor, this treatment has been approved for lung cancer, and it was observed an effective response in NB cell lines that express R1275Q-mutated *ALK* or present the *ALK* amplification [66]. Nowadays, new *ALK* targeted therapies have emerged as entrectinib, ceritinib, and alectinib, showing better efficacy than rizotinib [59, 67]. The elevated presence of MNA in HR patients drives in other key elements for determining a goal therapy such as PI3K/AKT/mTOR and Aurora A kinase inhibitors to destabilize N-Myc protein [59, 68]. Besides, some studies have shown that the inactivation of *CDK2* works in MNA tumors [69]. On the other hand, p53 mutations that derive in an increased *MDM2* expression are related to the half cases of NB relapses, then inhibitors of *MDM2* have demonstrated optimistic preclinical results in NB *in vitro* and *in vivo* models [59]. The RAS-MAPK pathway occurs in 78% of relapsed NB being another good objective; some studies show that MEK inhibitor and retinoic acid treatment can be useful [70]. Another important signaling pathway in NB involves the TrkA and TrkB neurotrophin receptors and, the anti-tumor role has been demonstrated using GNF-4256 and AZD6918, two Trk inhibitors [59]. NK1R belongs to neurokinin receptors and plays a role in several adult and childhood cancers; the use of NK1R inhibitor in NB *in vitro* and *in vivo* models showed a reducing effect in tumor growth [70].

In another way, as chemotherapy implicates high toxicity driving in future complications or cognitive dysfunctions for children, new treatment strategies are being developed as the use of

nanomedicines that have benefits as having control in drugs releasing [71]. Some researches in NB found a decrease in the toxicity using encapsulated cisplatin or SN-38 (an active metabolite of irinotecan) and also the precise advantage of the application of anti-GD2 conjugated nanoparticles [71-73]. The outcome for NB patients has been improved during the last years, however, a considerable group of patients is distinguished by poor survival and recurrent relapses. For that, is necessary to identify new biomarkers for developing novel treatment methodologies. **Articles I, II,** and **III** included in this thesis are focused on the investigation of a novel framework to look for targets and a specific target molecule included on it, related to the tumor microenvironment.

1.2. Tumor microenvironment

1.2.1. General aspects

A tumor is a functional and interconnected tissue where malignant cells proliferate uncontrollably being dependent on their tumor niche or microenvironment (TME). The TME is composed of cellular and noncellular components to provide support and a proper scaffold for cell proliferation and migration playing a relevant role in the progression of several malignancies [74, 75]. The elements that comprised this intricate network are the cellular components as tumor and stromal cells (fibroblasts, adipocytes, endothelial and immune cells) and the non-cellular part constituted by the extracellular matrix (ECM), growth factors, cytokines and chemokines (**figure 1**) [76]. The cross-talk between neoplastic cells and their surrounding elements is the first step in the initiation of a tumor [77]. This reciprocal communication derives in the activation of biological and molecular events where tumor cells are sculpting their convenient TME. Understanding the nature of these interactions will allow the discovering of specific targets inside of the TME. It has been demonstrated that dialogs between tumor and stromal cells like mesenchymal cells have a relevant role in NB progression [78]. The importance of the TME study in tumorigenesis is reflected in the **article I***: The tumour microenvironment as an integrated framework to understand cancer biology,* where we presented a classification of the tumor stroma according to the structural and mechanical changes in the TME elements according to tumor dynamics, prognosis and treatment responses.

Tumor tissues required cellular and ECM biophysical forces originating a mechanical balance between compression and tension stimuli to keep the framework architecture stability. The architectural principle, known as tensegrity, was conceived by Buckminster Fuller in the 1960s which can be applied to every level of the human body with the term of biotensegrity, defined

by Donald Ingber [79, 80]. According to this principle, the ECM can be treated as a dynamic and multifunctional controller with its biotensegral system composed of fibers and fundamental amorphous substance [81].In the TME the biotensegral network between cells and ECM can modify the cellular and molecular functions triggering a rigidity tumor scaffold. Rigidity or stiffness is defined as the resistance deformation degree after applying a force. It has been found that stiffness of primary tumors is higher than normal tissue and also has been related to cancer progression and metastasis, which becomes it in a potential therapeutic target [82-84].

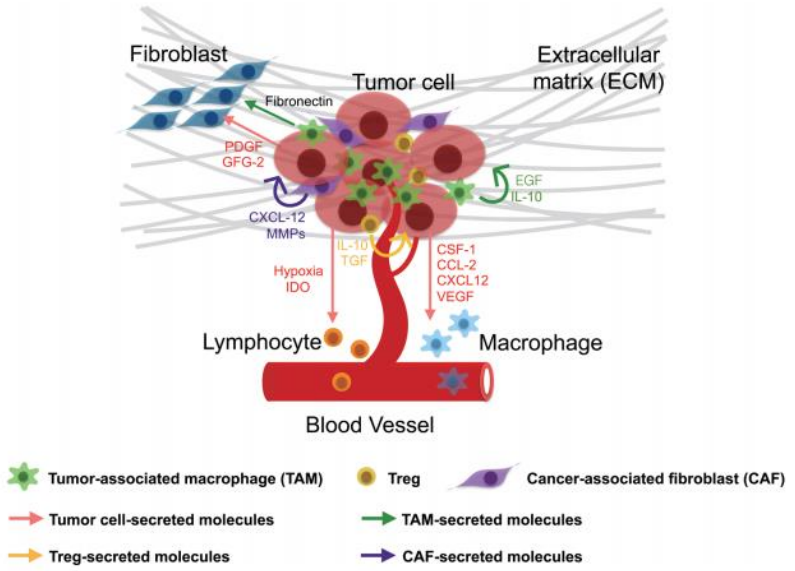

Figure 1. Representation of the interplay among the tumor microenvironment components [76].

1.2.2. Cellular components

Tumor cells do not exist in isolation, they interact with themselves via molecules that have been mentioned in the above subsection, residing in a proper scaffold together to other non-malignant host cells such as immune cells, fibroblasts, blood and lymphatic endothelial cells, pericytes, adipocytes and stem cells [85].

The immune system has a central role in cancer through the inflammation link, and consequently, diverse immune cells infiltrate the TME due to the secretion of cytokines and chemokines by cancer cells. Within the TME, exist a co-development of cancer cells and immune cells through an interaction where tumor cells can be recognized by immune cells and suffer cell death (immunosurveillance), or on the other hand, tumor cells can escape by avoiding immune checkpoints [86].

One of the main immune cells, that are charged with this selective stress are the T lymphocytes. Exist different T cell populations in the TME that are located inside tumor core or in the invasive area; it has been observed that a high amount of CD8+ T and CD4+ T (TH1 helper) cells in the TME are associated with good prognosis. The CD4+(TH2 helper) cells are related to promoting tumor growth, being the immunosuppressive CD4+ cells (T regulatory, Treg) the cells most implicated in this event. Regarding B lymphocytes, which are usually located in the invasive margin, there is a controversy about their role in tumor prognosis [85].

Natural killer (NK) cells take also part in tumor cell interactions. The NK cells present a cytotoxic ability and carry out this function through the recognition of MHC class I absence in response to infections and, are also involved in tissue remodeling homeostasis and morphogenesis. In cancer, the NK cells can control tumor growth thanks to its cytotoxic ability; however, tumor cells have developed some mechanisms to evade NK cell immunosurveillance [87]. Besides, it has been observed in some neoplasias that NK cells tend to place in the stroma, rather than in direct contact with malignant cells, a low NK activity has been correlated with poor outcome [88].

Macrophages are crucial elements in the immune system; there are two different phenotypes according to the cytokines production and the environment type where they are embedded: M1 (classically activated, pro-inflammatory) and M2 (alternatively activated, anti-inflammatory). The M1 presents an antitumor activity whereas the M2 phenotype is associated with immunity suppression, ECM remodeling, and angiogenesis that drives to tumor invasion. In cancer, we found tumor-associated macrophages (TAMs) that are typically related to pro-tumorigenic behavior and functionally mostly closer to the M2 macrophages [89]. Although in the early stages of tumorigenesis there is a presence of M1 macrophages, they change to an M2 phenotype in the advanced stages [90]. The M2 phenotype, in solid tumors, presents an inverse correlation with treatment success and longer survival rates. Also, hypoxia that is a common feature of solid tumors, leads to aggressive features in tumor cells reprogramming the phenotype towards M2 [91].

Dendritic cells (DCs), together with macrophages and B lymphocytes, belong to the antigen-presenting cells (APC) and are vital for the activation of T lymphocytes. The DCs, that are presented in the TME, are usually damaged so they are unable to recognize the tumor-associated antigens, contributing to the immune suppression [92]. However, their function in the tumor is controversial, since DCs can act to improve anti-tumor immunity or may suppress mechanisms that promote tumorigenesis [93]. Furthermore, the maturation stage of DCs could

be key for its role in the TME. It has been found a slower maturation rate of DCs in patients with lung cancer than in control patients [94]. Regarding NB, the immune system plays a critical role since the spontaneous regression observed in the MS stage is related to immunity [95]. Indeed, it has been observed that NB presents CD8+ T cells activated by survivin being able to act by IFN-ɣ, which influences on the caspase-8 expression inducing the apoptosis of neuroblastic cells and avoiding the tumoral evasion [96, 97]. Besides, another important NB feature is the immune escape pathway, such as a defective expression of the HLA class I avoiding the T cells (mainly cytotoxic lymphocytes) function [98].

Fibroblasts are support elements, representing one of the most abundant stromal cells that constitute the tumors and have a role in ECM remodeling and deposition. In cancer, the fibroblasts change their phenotype to cancer-associated fibroblasts (CAFs), due to stimuli (transforming growth factor (TGF-β) expression by malignant cells existing robust crosstalk)[99]. And it correlates with a modification of this function resulting in an increment of matrix proteins secretion and defective production of proteolytic enzymes that aid tumor invasion. CAFs can enhance tumor growth and cell survival by the production of molecules such as vascular endothelial growth factor (VEGFA), CXCL12, and IL-6 [100]. A notable characteristic of CAFs is their heterogeneous markers expression that leads both suppressing and promoting tumor abilities [99].

It is known that tumors need the creation of vascular networks to cover the essential nutritional and metabolic needs for growth and also for tumor dissemination. For these vital supplies, tumors have created two main strategies, one is angiogenesis that consists of the sprouting of new blood vessels from preexisting ones that are promoted by the secretion of pro-angiogenesis factors like VEGF-A or TGF-α by malignant cells or inflammatory cells. The second one is lymphangiogenesis which is the growth of lymphatic vessels supported by the production of VEGF-C and VEGF-D pro-lymphangiogenic factors by tumor cells or macrophages[85]. Then, malignant cells can spread via blood or lymphatic vessels; the path chosen depends on the location of the primary tumor, the presence of factors in the environment, and the cell adhesion molecules produced by blood and lymph endothelial cells establishing a cross-talk between both cells [101]. The hematogenous spread implicates the seeding directly into body cavities whereas the lymphatic spread involves an intermediated step that consists of the invasion of lymph nodes [102].

Moreover, it is observed that pericytes, which are perivascular cells that provide structural support and maintenance to blood vessels, acquire properties that contribute directly or indirectly to tumor growth, metastatic spread, and resistance to therapy [103, 104].

The adipose tissue is defined by being energy storage, although presents a regulatory role in the endocrine signaling, as well as in hematopoiesis and lymphopoiesis. Its role in tumor progression is not well known yet. It has been described that adipocytes can support the metabolic requirements of malignant cells that allow tumor growth. Besides, it has been established a connection between dysfunction of the adipose system (obesity/adiposity) and elevated risk of cancer appearance [90, 105].

Stem cells are characterized by self-renewal ability and the capacity to differentiate into several specialized cell types. These features are acquired by the cancer stem cells that reside in the TME contributing to the tumorigenesis and non-treatment response [106, 107].

In conclusion, the TME related with non-malignant cell component plays a relevant role in cancer; researches show that the cellular components of NB microenvironment could be considered for inclusion in optimal treatment determination [108, 109].

1.2.3. Non-cellular components: extracellular matrix (ECM) and vitronectin (VN)

The ECM is composed of water, minerals, proteins, proteoglycans (PGs), and glycoproteins (GPs) making a structure where malignant and non-malignant cells, neural fibers, vascular, and accompanied elements reside. A notable feature is that the ECM constitution and organization are highly dynamic, ranging from regulating tissue homeostasis and development to participate in disease processes like cancer or fibrosis when their elements are dysregulated [81]. Among structural ECM of the TME, we found all these components as well as cytokines, chemokines growth factors, matrix and inflammatory enzymes that guide the cell-cell and cell-ECM interactions. These elements and molecules are relevant in cancer since tumor cells need physical contacts through receptor-ligand synergies or secreted stimuli from surrounding stromal cells and/or matrix elements to orchestrate the behavior of the tumor [82]. Besides, biochemical features also have an influence on this interaction like the metabolic status, such as the deprivation of oxygen (hypoxia) or nutrients (lack of energy) [110]. The huge variety of ECM elements act as a structural scaffolding to cells and control biochemical and biophysical characteristics that influence cell proliferation, adhesion, migration, polarity, differentiation, and apoptosis [111].

The major structural protein of the ECM is the collagen which provides architectural support and directs cell migration and chemotaxis. There are 28 subtypes of collagen, distinguishing between fibrillar (collagen types I, II, III, V, and XI) and non-fibrillar collagens. The type I collagen is the most abundant in the human body, found in bones and skin, among other locations. The type III collagen is known as the component of reticulin fibers and is the main collagen form within the walls of blood vessels and also is found connected to the thicker type I collagen fibers [112]. The reticulin fibers are fine fibers that form a branching network in certain tissues and organs working as a support for the cells and playing a relevant adhesive role. Another structural protein is elastin that forms part of the elastic fibers closely linked with collagen, involved in the elasticity of our tissues. It provides support and may regulate cell communication [112, 113].

In tumors, the collagen scaffold is transformed showing a chaotic organization and an increase in the number of fibers resulting in desmoplasia (collagen type I and reticulin fibers accumulation). This deregulation appears in several malignancies and offers a suitable environment for tumor cells to successfully establish metastasis and, activate therapy resistance programs [114, 115]. It has been found a messy and remodeling of the fibrous component associated with more anaplastic and aggressive forms of several cancers as in prostate tumors [116].

PGs constitute the ground substance in the ECM and are composed of a core protein attached to glycosaminoglycans (GAGs) by covalent bonds. GAGs are long, linear, and anionic polymers made up of repeating disaccharide units. GAGs are classified into: hyaluronic acid, dermatan sulfate, keratan sulfate, chondroitin sulfate, and heparan sulfate or heparin. The great quantity of PGs confers to the ECM a hydrophilic attribute due to the negative charges of GAGs producing a network that acts as a diffusion barrier resisting compression stresses and enduring deformation. The PGs constitute a gel-like skeleton in which the fibrillary proteins are embedded. Also, PGs interact with growth factors, chemokines, and cell surface receptors, presenting a regulatory role in cell signaling and biological processes, including angiogenesis [81, 117]. Furthermore, PGs have a role in cancer pathogenesis, as the hyalectan, versican, and perlecan as pro-angiogenic factors or serglycin that is overexpressed in several malignancies [118, 119].

GPs are matricellular proteins finding in a minor amount in the ECM, some of them are laminin (LN), fibronectin (FN), thrombospondin (TSP), tenascin (TN) and vitronectin (VN). These GPs are characterized by an adhesive function [111, 120]. Besides, they participate in ECM assembly, in ECM-cell interactions by acting as a link between cells and ECM elements and

connecting the ECM to soluble molecules within the extracellular space. These bridge elements tend to present several domains in their structure that contain binding motifs for other ECM proteins, growth factors, and cell surface receptors [120]. The best-known receptors in the ECM are the integrins, transmembrane proteins that connect cells to the ECM detecting chemical and mechanical cues from the ECM and promote the activation of intracellular signaling pathways [121]. Due to this adhesion function derived from the integrin-binding, the GPs participate in some phases of tumorigenesis as FN and their $\alpha_5\beta_1$ integrin ligand, overexpressed in breast cancer and also this interaction participates in metastasis in ovarian cancer. In pancreatic cancer tissues, it has been observed increased levels of FN, VN, and LN or even the pro-migratory effect of VN in driving metastasis [122-125]. Therefore, GPs play an important role in tumors. Since, to allow the contact between ECM and tumor cells, focal adhesions are needed, and integrins are the molecules responsible for carrying it out. Among the various ECM GPs, VN as a multifunctional protein has particular importance in physiological and pathological states due to its role in the regulation of pericellular proteolysis, vascular hemostasis, cell adhesion, and migration. These functions of VN derived from the multiple ligands that bind to its four domains [126, 127]. The main domain for VN cell adhesion is the RGD (arginine-glycine-aspartate) sequence located adjacent to the somatomedin B domain. These three amino acids form a loop to which some integrins as $\alpha_v\beta_1$, $\alpha_v\beta_3$, $\alpha_v\beta_5$, $\alpha_v\beta_6$, $\alpha_v\beta_8$, and $\alpha_{IIb}\beta_3$ can join strongly. The α_v integrin family is related to angiogenesis; besides abundant experimental data suggest that $\alpha_v\beta_3$ and $\alpha_v\beta_5$ integrins are found in blood vessels associated with tumors, so they can be used as therapeutic targets to inhibit angiogenesis processes and therefore tumor metastasis [128]. Furthermore, VN presents more binding sites, such as for uPAR and PAI-1, both bind to the somatomedin B domain and also uPAR binds to the RGD sequence [129]. The study of VN in the cancer field is important since it is involved in functions such as cell adhesion, ECM remodeling, and tumor cell migration, through three main ligands as uPAR, PAI-1, and integrins. From those functions derive its role in processes such as tumor growth, angiogenesis, and metastasis in several malignancies [130-132].

Also, the ECM includes the interstitial fluid where the cells and secreted molecules are disposed. The ECM can store and capture inside of the interstitial fluid: growth factors, cytokines, and chemokines, establishing concentration gradients and regulating spatially and temporally their bioavailability [81]. Growth factors, cytokines, and chemokines are molecules that promote growth signals to activate the proliferation in normal tissues. In cancer, they are secreted by stromal and malignant cells and may be captured by the ECM, where provide these spreading stimuli taking part as tumor-promoting components. These molecules increase the

risk of cancer since they promote cell survival signals to avoid apoptosis, proangiogenic factors, and epithelial-mesenchymal transition (EMT) by metalloproteinases (MMPs) [133]. It has been observed an association of overexpression of the epidermal growth factor (EGF) and the TGF-α with poor prognosis in colon cancer [134] or a pleiotropic role of TGF-β in cancer [135]. The therapeutic importance of these molecules is reflected by the presence of mutations in EGFR, a ligand of EGF, in pancreatic cancer, and non-small cell lung cancer [136, 137]. Likewise, the inflammatory process is another important factor in the initiation of a tumor, where also growth factors, cytokines and chemokines have an attraction role. Among the variety of cytokines that are related to tumor progression, the necrosis factor and IL-6 are the best characterized pro-tumorigenic cytokines in several neoplasias [138]. Regarding chemokines, some of the most cancer-related are CXC and CC families [139]. For example, CXCR4 is the most common chemokine receptor expressed in several malignancies or CCR8 is overexpressed in non-small cell lung cancer [140].

There are several types of proteolytic enzymes which substrates are collagens and other ECM elements such as MMPs, the most predominant, ADAMs family proteins (a disintegrin and metalloproteases), ADAM with thrombospondin motifs (ADAMTS), and also proteases such as cathepsin G and elastase. They play a vital role in physiological events, including development, tissue remodeling, or repair. In pathological events, like cancer, MMPs perform the ECM degradation which is associated with invasion facilitation by breaking the ECM physical barriers, releasing molecules as active growth factors or active ECM fragments, and exposing signaling components like integrins [141]. Another derived consequence is the activation of the inflammatory response via specific cytokines induction. MMPS aims to create an environment conducive to tumor development, for that could be promising therapeutic targets [141, 142]. Indeed, several MMPs are over-expressed in different types of tumors such as MMP2 in gliomas or MMP1 in breast cancer [143, 144]. Another relevant enzyme is lysyl oxidase (LOX) which is necessary for the mechanical integrity of the collagen. Then, LOX acts in the ECM stabilization and its deregulation is related to fibrotic processes, tumor progression, and metastasis [145].

As we can summarize the mesh of the ECM turns into a stiff ECM that derives in an increased deposition of matrix proteins and activates integrins generating a cytoskeleton tension promoting adhesion, cell motility, and cell interactions. The rigidity of the ECM support tumor progression and increase the aggressiveness in NB, liver, and pancreatic cancer [142, 146, 147].

1.2.4. Use of this knowledge for treating patients

According to Weinberg *et al.*, [148] the hallmarks of cancer are defined by the increase of proliferation, growth induction, death resistance, replicative immortality, angiogenesis, activation of invasion and metastasis, metabolism deregulation and the escape of immune response which are caused by the cell-cell and cell-ECM interactions. These strategies together with the heterogeneous composition of the TME suggest that targeting the TME elements can be relevant for the development of more specific treatments that could be used to supplement the conventional therapies applied currently, which involve severe side effects and therapeutic resistance [90]. Then, the goal of the therapeutic approach against TME is a multitargeted effect, where tumor cells and the TME are simultaneously inhibited to normalize the TME for preventing the formation of premetastatic niches in a tumor-friendly environment.

There are several studies whose aim is targeting directly ECM components; nonetheless, it is a difficult task due to the complexity of components interplay. Below, we present a review mainly focus on diagnostic strategies and therapies related to the ECM elements studied in this compendium.

An important fact is that in tumor progression exists a chaotic ECM in terms of the composition and organization of its elements. Collagen is one of the predominant elements and therefore an important target; in fact, the inhibition of the TGF-β signaling pathway results in a low presence of this element and it decreases desmoplasia; since this factor stimulates CAFs to produce collagen [149]. It is also known that MMPs degrade collagen inducing angiogenesis; then the combination of an anti-MMP-9 antibody plus nab-paclitaxel (as standard cytotoxic therapy) showed a decrease of type I collagen in tumors [150]. Regarding the importance of GAGs as a target in cancer, derived from its interaction with multiple ligands. For that function, several types of research aim to target GAGs through some drugs, as non-anticoagulant heparin analogs (SST0001 or Roneparstat) with a decrease of tumor size, already used in preclinical studies; non-anticoagulant hexasaccharide sequence of heparin (HS06) presenting a specificity in GAGs-protein interactions and inhibitors of the activity of heparanase (PI-88) that has already been used in phase III clinical trials for hepatocellular carcinoma [151].

Integrins are significant receptors involved in cell-cell and cell-ECM communication integrating extracellular and intercellular signals. They are ligands to several proteins and GPs of the ECM such as collagen, FN, LN, and VN through recognition of the RGD sequence and other sites like LVD motif that are present in vascular cell adhesion molecule 1 and FN. Indeed, all α_v integrins present the capacity to find ECM elements that contain this RGD sequence [152]. These

α_v integrins play a key role in tumor growth, invasion, and metastasis, and although therapeutic approaches are mainly focused on the inhibition of these integrins, several studies using anti-integrins have experimented success and others failed in preclinical studies. Two pan-α_v integrin antibodies that have been evaluated in late-stage clinical trials: abituzumab (DI17E6, EMD 525797) and intetumumab (CNTO95), showing an anti-metastasis activity[153]. Also, $\alpha_v\beta_3$ and $\alpha_v\beta_5$ integrins have been involved in tumor angiogenesis, for this reason, inhibitors as vitaxin (MEDI-523) and etaracizumab, (abegrin; MEDI-522) have been applied with high specific results. Cilengitide (EMD121974) is a peptide that inhibits both integrins; preclinical studies in breast cancer supported its efficacy reducing bone metastasis. However, phase III clinical studies in late-stage glioblastoma did not show any effect [153]. The anti-$\alpha_v\beta_3$ antibody etaracizumab (MEDI-522) has been used in phase I and II clinical studies and showed good tolerability, also in combination with chemotherapy, but without anti-angiogenesis evidence. Another integrin that showed a fundamental therapeutic profit in cancer as a target is the $\alpha_5\beta_1$ integrin; the antibody M200/volociximab was shown to inhibit angiogenesis in preclinical studies [154]. To improve the targeting of integrins in cancer, new treatment methodologies are being developed as the use of nanotechnology to overcome some known limitations. Some examples are the production of liposomes nanoparticles coating with polyethylene glycol (PEG), which are RGD based peptides, with a major specificity for targeting integrins, or with cilengitide that showed improvement against the conventional cilengitide treatment in glioblastoma [155, 156].

Several efforts have been made to target ECM-modifying enzymes such as MMPs and LOXs. Due to the relevance of MMPs in tumor progression, synthetic inhibitors have been developed as neovastat (Benefin/AE-941) that blocks MMPs-2, 9, and 12, which is well tolerated by cancer patients in phase I/II clinical trials. Regarding LOXs, there are some clinical trials using tetrathiomolybdate in breast cancer patients [157]. In the TME occurs an immune cell adaptation to the metabolic needs of cancer cells and therefore the immune cells take part in resistance to treatments being important as targets for immunotherapy [158, 159]. Some common types of immunotherapy include: 1) Immune checkpoint inhibitors, such as anti-CTLA4 or PD-1/PD-L1 (that are based on T cells suppression) by using monoclonal antibodies. Indeed, ipilimumab, an anti-CTLA-4 antibody, was approved by the Food and Drug Administration (FDA) in 2011 for melanoma patients with metastatic disease and antibodies targeting PD1 or PD-L1, that include pembrolizumab nivolumab (anti-PD1), were approved by the FDA for melanoma and non-small-cell lung carcinoma. Other checkpoints in preclinical studies include lymphocyte activation gene 3 (LAG3) proteins and mucin domain-containing protein 3 (TIM3). 2) T-cell transfer therapy, which consists of the transference of immune cells for the initiation of systemic

antitumor immunity, increasing the number of active tumor-infiltrating lymphocytes (TILs) in the tumor. In this category, the CAR T-cell is also an important therapy; in fact, Kymriah has been approved in hematologic neoplasias. 3) Cancer vaccines, whose aim is specific immunologic responses against tumor antigens; however, some obstacles as inducing immune tolerance appear to be challenged as the proper tumor antigen definition and understanding the role of DCs. 4) Combination therapies as the association of immune checkpoint inhibitors (combination of anti-CTLA-4 and anti-PD1) therapies have been demonstrated a synergic effect; integration of immune checkpoint inhibitors, conventional therapies (like the combination of ipilimumab with dacarbazine) and VEGF, due to the latter acts in immunity by enhancing the number of Treg cells in several clinical trials [159, 160]. Besides, one example of immunotherapy in NB is the use of an anti-GD2 monoclonal antibody, since the GD2 is a ganglioside expressed by NB and other tumors. In clinical studies with HR-NB patients, the combination of anti-GD2 plus cytokines as IL-2 and GM-CSF and retinoic acid therapy showed good results and, the generation of CAR T-cells that express anti-GD2 was also tested in clinical trials [161, 162].

As mentioned previously, CAFs are another possible target since are the most abundant cell types in TME. The fibroblast activation protein (FAP), is a protease that contributes to the fibroblast phenotype, being more specific to the tumor stroma. Several attempts to target FAP have failed, nevertheless, there are ongoing studies that are using RO6874281, an IL-2 variant that recognizes and also binds to FAP, in combination with other drugs as atezolizumab, an anti-PD-L1 antibody, gemcitabine, and vinorelbine, in solid tumors [158].

Tumor vessels are abnormal, with a chaotic structure as a consequence of endothelial disorganization; this vascular alteration is related to a low effect of chemotherapy. The defective formation of tumor blood vessels is due to irregular levels of growth factors like VEGF, angiopoietins, platelet-derived growth factor (PDGF-B), and TGF-β. Another aspect to keep in mind is the ‘‘vascular mimicry’’ (VM) that refers to tumor cells which behave as endothelial cells expressing several markers and forming vessels-like structures. Modifying this unsuitable tumor vasculature can prevent tumor invasion and improves the power of antitumor treatments [163]. For that reason, although new anti-angiogenic therapies are needed, several approaches and drugs have been developed, such as a) VEGF signaling inhibitors, bevacizumab, humanized anti-VEGF-A monoclonal antibody, that had a potential synergy with conventional treatments; however this treatment was defined by side effects and drug resistance [164, 165]; b) ramucirumab, a fully human monoclonal antibody that targets VEGFR2 by blocking its interaction with VEGF, that is currently in a phase III trial; c) angiopoietin inhibitors, as the antibody MEDI3617, impeding the angiopoietin function or AMG-386 (trebananib) preventing

angiogenesis by blocking the joining of angiopoietin 1 and 2 to their Tie2 receptor, that is in phase I trials for advanced solid tumors; d) PDGF-B/PDGFR interaction involved in the pericyte coverage in new blood vessels. Some PDGF-B inhibitors, CR002 and IMC-2C5 or CDP860 have been used. The use of PDGFR inhibitors like imatinib, sunitinib, regorafenib, and pazopanib which also present an anti-VEGFR function showed an improvement in anti-angiogenesis therapies as well as the combination of Ang-2 and VEGF inhibitors as vanucizumab; e) and finally an optimized human monoclonal antibody targeting the C-type lectin-like domain of CLEC14a inhibits VEGF microvessel formation, CLEC14a is a marker that is exclusively expressed on tumor blood vessels in several neoplasias [165]. Moreover, it is known that the VEGF-C/VEGF-D/VEGFR-3 signaling pathway is a key regulator of tumor lymphangiogenesis. Some anti-lymphangiogenic therapies that include monoclonal antibodies to VEGF-C and VEGF-D, which block VEGFR-2 and VEGFR-3 binding and small molecules (sorafenib, sunitinib, pazopanib, and axitinib) that go inside the cell such as inhibitors of the VEGFR-3 tyrosine kinase, are in clinical trials [166, 167].

In conclusion, the TME participates in tumorigenesis and the crosstalking between its components has to be taken into account to get achieving anticancer therapy and for seeking future targets. The use of experimental models to advance in this field is needed.

1. 3. Experimental models in cancer

1.3.1. General aspects

Cancer represents serious healthcare defiance worldwide, being the understanding of cell-cell and cell-ECM interactions that occurs in the TME one of the main limitations to fight against this disease. For the comprehension of the cancer mechanisms, several approaches have been developed over time. Due to the complexity of this malignancy and its intra-and inter-tumor heterogeneity, reliable models are required; however, only one model is not enough to simulate all the cancer features. For that fact, a broad spectrum of preclinical models that include *in vitro* and *in vivo* prototypes have been implemented for the detection of therapeutic targets and biomarkers or testing and assessing drug effects and response. The final aim of these models is to supply knowledge that improves the development of better treatment strategies and patient's prognosis [168, 169]. We have reviewed those that we have used.

1.3.2. *In vitro* models

The range of *in vitro* models has progressed from cancer cell lines that grew on monolayer to the generation of 3D models that have emerged in the last decades. The purpose of these models is to provide information about the behavior of cells to observe how they mediate a role in tumor progression, invasion, and drug resistance [168].

Established human cell lines have been used for decades in the cancer field and are essential for the comprehension of the basic biological and molecular principles of cancer. Indeed, today they are the most common tool used in cancer research [169]. Cancer cell lines are normally maintained in culture for a long time which derives in the adaptation of *in vitro* conditions through the acquisition of reversible and irreversible phenotypic and genotypic alterations [170]. These changes induce the appearance of clonal evolution, since the cell clones that grow faster, control the culture leading in a modification of cell behavior [171]. Nonetheless, it has been observed that molecular features of colon cancer cell lines are equal that those described *in vivo* colon models [172]. Another issue of handling cell lines is the cross-contamination or misidentification of cells that can influence on getting controversial results [173, 174]. To avoid this drawback is recommendable to authenticate the identity of each cell line, as employing genotypic identification through short tandem repeats [174]. These aspects normally imply a controversy for the utility of cell lines as a preclinical model in cancer. However, the benefits of cell lines are their availability, low cost, and easy manipulation to study cellular roles in cancer.

Stable cell lines as tools in preclinical studies represent a broad platform for multidrug screening or functional studies through the use of a panel of cancer cell lines, using them as standards, that allow the comparison of researches worldwide [171].

Regarding NB, there are a wide range of available cell lines, that are classified into three phenotypes according to their origin, morphology and genetic alterations: neuroblastic, N-type as SH-SY5Y and LA1-55n, are sympathoadrenal neuroblasts; the substrate-adherent, S- type like LA1-5s and SH-EP1, resembles non-neuronal precursor cells; and the intermediate, I-type as SK-N-Be(2)C and SH-I, because its morphology is intermediate between N and S phenotypes, and this type restrains the abilities of stem cells. A comparison study among the tumorigenic ability of these three cell phenotypes showed that the I-type may be the most aggressive due to their stem cell features [172]. On the other hand, the culture media is also a critical key for the molecular and biological features of cell lines. Indeed, there are pieces of evidence that support that NB cell lines grown in serum-free medium retain the genetic and phenotypic characteristics of primary NB tumors in comparison to serum complete medium [175, 176].

Cancer cell lines continue being the first step in the scale of preclinical trials, and then achievements in the application of these *in vitro* systems are ongoing. One example is the co-culture of cancer cell lines and stromal cells like fibroblasts, endothelial and immune cells. Nevertheless, the 2D *in vitro* culture does not recapitulate entirely the biophysical and mechanical properties of the TME since monolayer cell lines cannot simulate the intricate network of cells and non-cellular elements of the TME [168].

To resemble the complexity of TME architecture, some 3D prototypes have been developed to overcome some limitations of 2D cultures. It has been observed that when cells are in 3D respond to drugs differently than cells in 2D, giving results more similar to those observed *in vivo*. 3D models are more suitable prototypes for drug screening because they can recapitulate physical barriers, so drugs do not penetrate as easily as in 2D cultures. Besides, the 3D migration models are more comparable to *in vivo* spreading being in all directions as well as restrain its interaction with their surrounding elements [169, 177]. Also, the gene expression profiles in 3D models are more similar to *in vivo* systems finding some differences regarding 2D systems [178]. The use of a scaffold in 3D systems also acts as a support and can be adjusted to the stiffness or pore size to replicate the TME. In general, we can say that 3D cellular morphology and the interactions with its 3D environment is more like *in vivo* [179].

There are several types of 3D *in vitro* models, one typical are spheroids that are clusters of cells without a tissue structure; in case that they derived from tumor cells are known as tumor

spheroids. Spheroids can be generated using hanging drop methods [180, 181]. Cells inside of spheroids replicate the *in vivo* features found in tumors since in the center, due to the decrease of nutrients and oxygen, they usually become hypoxic and necrotic. However, due to their sphere shape, they present some limitations such as not being able to simulate vascularized tumors or not mimicking some types of metastasis initiation [182-184].

Other *in vitro* 3D models recreated the TME by combining malignant and non-malignant cells over a supporting scaffold based on natural or synthetic materials that act as ECM. A key point is the choice of a proper scaffold that depends on the TME you want to get. Generally, natural scaffolds are proteins that form the ECM like collagen, fibrin, and hyaluronic acid, or other natural biomaterials as gelatin or silk. A remarkable feature of natural scaffolds is its biodegradability that can limit the duration of the study, causing uncontrolled effects [185]. On the other hand, synthetic scaffolds are made of polymers, bioactive glasses, or self-assembled peptides. The essential profit of using these scaffolds is, due to their defined composition, their reproducibility. Another different approach to classify scaffolds is discerning between hydrogels and solid scaffolds, which can be generated through natural or engineered structures. Normally cells are mixed or encapsulated in a soft tissue-like environment in hydrogels, while in solid scaffolds they can be fibrous or porous [185, 186]. An emerging method to generate naturally derived scaffolds consists of decellularizing ECM from the tissues; this approach keeps the natural architecture and removes the allogenic cellular antigens, however, it is a hard technique [187]. Another novel methodology is the combination of microfluidic technology with 3D culture to create an entire system called organ-on-a-chip that constitutes a complex and dynamic model. It has been used to recreate several neoplasms as breast cancer tissue [188].

Recently, some 3D strategies to simulate the TME in NB have been developed. Research showed that tumor cells retrain their nature proliferative features in bioprinted type I collagen scaffolds [189]. In another study, after building NB models through two different collagen frames, discovered that the treatment response in these 3D culture prototypes was much more similar to *in vivo* models [190]. Our group described a study analyzing the effects of the surrounding biomaterial stiffness over time and defining how aggressiveness increases in SK-N-BE (2) NB cell line [191].

Summarising, the main advantage of *in vitro* studies is that they offer a high control of the cellular and biochemical constituents of the tumor network, representing reliable tools. 3D *in vitro* systems recreate more real models in comparison to 2D. However, it is desirable to use simultaneously both systems, since the 2D models are an easy way to start experiments and

changing to 3D culture models should be a progressive procedure since it is required more complex technologies [178].

1.3.3. *In vivo* models

Investigations using *in vivo* models improve the comprehension of cellular processes in a physiological and entirely natural TME, being relevant in the oncology field to assess different therapies and to identify possible targets and potential side effects easier than employing *in vitro* models [192]. However, we have to keep in mind that some animal models displayed discrepancies regarding human physiology. This fact explains the high proportion of drug failure on humans which presented a good response in animal models. Nonetheless, the divergence issue is being solved by the application of humanized animals [193]. For cancer research, the most powerful *in vivo* models are rodents such as rats and mice, emerging the usage of complementary animals like zebrafish [194]. Nowadays, the dominant employment of mice is due to the high homology sharing with humans, and the substantial contribution of clinical animal models have derived in the existence of a wide range of mouse models for cancer studies [193, 195].

One of the straightforward and most normally used *in vivo* model system is based on the engraftment of established human cell lines to generate cell-line-derived xenografts (CDX). Another enhanced *in vivo* strategy consists in the creation of patient-derived xenografts (PDX). In the latter case, the human tumor material excised from the patient or primary cells derived from the disintegration of the tumor into single cells is implanted/injected directly into the mice [196, 197]. For this purpose, immunodeficient models are needed to allow the acceptance of human cell lines or tissue, permitting the development of tumors. Exist a large variety of immunocompromised mouse strains from the athymic nude mice, SCID, *Rag*, to highly immunodeficient mice as NOG and NSG [195, 198]. NOG and NSG represent excellent recipients with the highest human tissue engraftment [199].

Both CDX and PDX models can be engrafted heterotopically or orthotopically. In the heterotopic implantation, cells or tissue are implanted into a different location unrelated to the original tumor site, generally subcutaneously. This procedure has benefits as easy as implantation and tumor growth monitoring [200]. Orthotopic models involve the implantation of cell lines or tissue into the proper place where the primary tumor is commonly developed. The generation of these models is more technically challenging and time-consuming and it is required the use of precise imaging techniques to control tumor development. However,

orthotopic models recapitulate more accurate aspects of the original TME being more clinically relevant than heterotopic models [201].

The traditional CDX possesses some disadvantages as they do not acquire the heterogeneity that characterized the tumors. As well, the generation of orthotopic CDX models have the drawback that the stromal component is murine, despite this, are used as initial screening tools of drug toxicity and efficacy [202, 203]. A study using orthotopic CDX NB models showed a rigorous invasion behavior and vascularization features with spontaneous metastasis in places like bone marrow and liver that recapitulate common characteristics in NB [204]. Another research with orthotopic NB models displayed different invasion tropism patterns in different established NB cell lines [205].

PDX models were developed to overcome some CDX limitations, such as decreasing the risk of cells *in vitro* adaptation. During the last years, PDXs are becoming the preferred preclinical tools being platforms of characterized PDX models [206]. This is supported by numerous pieces of evidence where are suggested that PDXs retrain original features of tumor patients, as histology traits, genetic aberrations, and malignant phenotypes in several malignancies, like colorectal cancer, breast cancer and NB [207-209]. Besides, stable PDXs tumors can be serially passaged *in vivo* without molecular or phenotypical modifications, however, it is recommendable to keep relatively low passage number (<10) [210].

Despite the potential benefit of PDX models in the cancer field, it has been observed some limitations [211]. One is, due to host mice are immunocompromised, PDXs do not resemble the immune system that normally appears in TME. For solving this problem, the generation of humanized mice, as well as the emerging of different approaches, is being developed to simulate the human immune system such as the transplantation of human hematopoietic stem cells in NOG and NSG mouse strains [212, 213]. Another disadvantage is the gradual replacement of human stromal components by murine stromal elements like ECM, fibroblasts and endothelial cells that it has been observed in NB and colorectal PDX models [214, 215]. It can be explained by the recruitment of murine stromal cells though cytokines production by human tumor cells and also to Matrigel substrate, a murine basement membrane, that is commonly used to increase the engraftment rate in PDX models. Then, some strategies like the co-injection of human stromal cells may be used to simulate and study the TME interactions [216]. The last issue is the lack of intratumor heterogeneity related to the fact that PDX establishment is based on a small representation of the whole tumor and to the selection pressure of specific clones that also occurs during the engraftment and passaging. In fact, this heterogeneity has been demonstrated after the generation of NB PDXs using tumor pieces with different locations [217].

Therefore, the implantation of several samples derived from distinct tumor places may be a potential solution.

Another point is that the establishment of PDX models will take considerable time. A wide range of growth time has been reported, between one to ten months [218]. This difficulty is influenced by the aggressively of tumor, implant location, and strain of immunodeficient mice utilized [199]. An association between successful engraftment with adverse clinicopathological features in the pancreatic PDX model has recently shown [219]. Moreover, the median rate of engraftment in NB PDX models is around 50%, exhibiting a major successful rate the HR-NB tumors [217].

As we mentioned above, the generation of PDX can come from two inputs: the non-dissociated tumor fragments, which is the preferred way since trying to avoid the molecular and phenotypic modifications from cell culturing or cell suspension from tumor dissociation and culturing. Some NB studies had established several 3D spheroids in serum-free medium from orthotopic PDX models (known as patient-derived cell lines models) demonstrating that cells, up to at least 30 passages, recapitulate the features of the original tumor [175, 176]. Another strategy used is to get patient-derived organoids (PDOs), which consists of patient-derived cell lines that grow embedded in a scaffold-like Matrigel or collagen. A recent study has established various NB PDOs demonstrating that these cells preserve histological, genetic, and heterogeneity features of the original tumor [220]. These 3D human tumor cells are a relevant tool to replace animals in experimentation.

On the other hand, *in vivo* strategies as the genetically engineered mouse models (GEMM) represent an important tool in cancer that has the benefit of spontaneous tumor development in the proper site, with an effective immune system; however, tumors consist of murine cancer and stromal cells. As other model systems have limitations as tumor usually takes a long time to develop and because the majority of GEMMs only have few genes modified they present a less cellular heterogeneity [196, 221]. One of the common GEMM NB models is the TH-*MYCN* that demonstrated the *MYCN* role in NB pathogenesis and is important for preclinical studies of *MYCN* therapies. Another model, TH-*MYCN/ALK*(F1174), examines the role of *ALK* mutation to provide drug *ALK* inhibitors [213].

For the progression of effective therapies, preclinical studies need to employ several models. They must integrate the challenges of biology and genetics to achieve successful results by improving patient prognosis and guiding clinical trials. To do this, it is important to be aware of

the use of the right model for research, and the most objective tools to analyze tumor biomarkers such as the computer-aid image analysis.

1.4. Digital pathology in cancer

1.4.1. General aspects

Tumor growth and metastasis are well-known processes in the tumor biology field derived from communication signals that tumor cells exchange with their surrounding microenvironment. [222, 223]. In the development of these processes, some of the attractive activities to consider their study are: how to act tumor cells clones to create a phenotypic and genetic heterogeneity, stromal and immune cells to be required as companion constituents, the ECM elements to establish and remodeling an appropriate scaffolding and finally, vascular elements to provide crucial nutrients [110, 224, 225].

For the understanding of these processes, not only *in vitro* and *in vivo* models are used to study the underlying mechanisms that cause tumor progression, but many computational approaches can be also found nowadays in the literature [226-229]. Digital pathology, a sub-field of pathology that focuses on data management based on information generated from digitized specimen slides, uses virtual microscopy and computer-based technology. Glass slides are converted into digital slides that can be viewed, managed, shared and analyzed on a computer monitor. Mathematical modeling, dynamic methods, and the application of equations have shown how is possible to simulate physical and biological alterations that occur in tumor invasion such as adhesion or migration [230, 231]. Current computational strategies are not only focused on recreating the context of a tumor, allowing the identification of tumor growth patterns in cervical cancer [232] or the tumor cells ability to spread in non-small cell lung cancer [233], nonetheless these methodologies go beyond being able to detect therapeutic drugs through a virtual examination in lung cancer [234]. This multidisciplinary network gives us information to detect key targets and simulates the mechanisms that take place in tumor growth and metastasis events. Indeed, the application of novelty image tools provides complementary information to be functional to clinical practice [235]. Morphometric techniques through the use of computer-automated segmentation algorithms attempt to decrease human error. These techniques intend to increase assessment efficiency, due to the huge amounts of tumor samples that are generated in the diagnostic routine and create reproducible results since they decrease the subjectivity in the analysis allowing standardization of the measurements [236-238]. The use

of morphometric quantitative image analysis to determine the nuclear role in breast cancer evidenced an association between nuclear shape and clinicopathological features [239]. Also, the employment of image analysis tools observed differences in nuclear characteristics between benign and malignant squamous neoplasms, being the nuclear pleomorphism the most useful feature [240]. On the other hand, topological approaches like network analysis in combination with Vonoroi tessellations are useful in quantifying the risk of developing a disease through the detection of associated clusters at the molecular level [241]. The use of Voronoi Diagram and its subgraphs showed the ability to assess the tissue architecture extracting structural features being able to discriminate between normal and cancerous oral mucosa and the outcome in patients with prostatic and cervical carcinoma [242]. Also, the application of topological characteristics can potentially identify predictive biomarkers through network-based classification in breast cancer [243].

Another relevant approach is the development of machine-learning algorithms to be applied as a computer-aided tool in cancer research. Its purpose is to discover different patterns based on clinical, proteomic, genomic, epidemiological, or histological information to establish datasets according to the best combination. These datasets can discriminate for example among prognostic outcomes or risk of cancer, in several malignancies as breast and liver cancer [244-246].

Regarding the wide positive aspects of using image tools for cancer modeling, its application in routine diagnosis is being implemented. All these novel approaches required a global validation to be used in the clinical diagnostics routine [247]. With the practice of Whole-Slide Imaging, which is another name for virtual microscopy, the field of digital pathology is growing and has applications in diagnostic medicine, to achieve efficient and cheaper diagnoses, prognosis, and prediction of diseases.

1.4.2. Computer-aided analysis in NB

Over the last decades, the survival rate has improved due to the application of an international NB pre-treatment risk classification system, however, HR and relapsed patients are characterized by the need for innovative therapies or strategies to enhance their outcome [14, 62]. The biological pathways that are hidden in these patients are some weaknesses share by the NB studies. In this way, novel approaches as computer tools are needed to complement the conventional pre-treatment strategies and to discover potential biomarkers or targets that could imply in NB pathogenesis and therapies.

Indeed, image analysis algorithms applied to hematoxylin-eosin (HE) stained NB whole-sections have been used to discriminate the grade of neuroblastic differentiation automatically, through the selection of representative features such as cytoplasm and neuropil [248]. NB belongs to the small round cell tumors family, being the uNB category a diagnostic challenge to the rest of tumors because of morphological similarities, requiring the use of specific immunohistochemical markers. The application of morphometric image tools to discriminate among this tumor family showed that Ewings/PNET presented more tumor necrosis and mitosis compared to the rest of related tumors [249].

Greater efforts in NB using mathematical approaches allowed the characterization of TME elements; our group has described that tumor patients with poor prognosis presented a firm scaffold between neoplastic cells described as crosslinked and branching reticulin fibers, scarcity of collagen type I fibers and GAGs [147, 250, 251]. Regarding the vascular elements, large and abundant irregularly-shaped blood vessels and a high amount of irregular intermediate lymphatic capillaries and irregular small collector vessels were present in tumors from patients with metastatic stage, undifferentiating neuroblasts and/or classified as HR [252, 253]. This tumor architecture reflects a chaotic situation that promotes the spreading of tumor cells. In this way, novel methodologies are needed for a better understanding of the ECM elements and their interplay with tumor cells. Therefore, in **articles *II* and III**, computational tools were used to define novel features related to the morphometric characteristics and organization between tumor cells and ECM elements. These recent tumor modeling systems emerge as techniques to add detail diagnostic information as well as an attempt to study the significance of new markers in NB tumorigenesis.

CHAPTER 2. Hypothesis, aims and justification of article compendium

2.1. Hypothesis

We consider the microenvironment of neuroblastoma to be a complex network of stromal cells and surrounding non-cellular elements, which influences and is influenced by the behavior of neuroblastic cells. In fact, malignancies often precipitate intensive remodeling of the extracellular matrix, as well as increased rigidity, which confers reciprocal biotensegral mechanical stress between continuous cell traction forces and discontinuous compression resistance presented by extracellular matrix elements, all of which facilitate the aggressiveness of the malignant cell. We hypothesize that vitronectin, an extracellular matrix glycoprotein characterized by its linking role between cells and elements of the extracellular matrix and/or soluble molecules within extracellular space, is a key molecular player in the aggressive tumor environment and should be studied in neuroblastoma with digital pathology.

2.2. Aims

General

In this thesis, our general purpose is to define vitronectin as a crucial connector within the extracellular matrix which helps modulate of the physical and chemical signaling between tumor cells and their surrounding elements, hence designating vitronectin ligands as new therapeutic candidates.

Specifics

- *Studies in neuroblastoma human samples:*
    1. Morphometrical and topological characterization of vitronectin expression through the design and use of various algorithms, to uncover its role.
    2. Correlate vitronectin and vitronectin ligands binding expression to clinical characterisitics of patients and biological features of tumors with known prognostic value, to determine different degrees and/or histological patterns of aggressiveness.
    3. Associate vitronectin expression and distribution with other biotensegral elements of the tumor microenvironment such as reticular fibers, type I collagen, glycosaminoglycans, blood/lymphatic vessels and immune cells, in order to establish an extracellular matrix pattern related to aggressiveness.

- *2D studies in neuroblastoma cell lines:*
    1. Identify vitronectin and its binding ligands such as $\alpha_v\beta_3$ integrin, uPAR and PAI-1 in several established neuroblastoma cell lines.
    2. Define the contribution to tumor aggressiveness of vitronectin patterns and binding ligands by comparing their expression with that obtained in human neuroblastoma samples.

- *In vivo neuroblastoma xenografts*
    1. Generate xenografts using a selection of the established neuroblastoma cell lines in knockout vitronectin and *Rag1* immunodeficient mice to determine the influence of the tumor macroenvironment.
    2. Characterize several tumor microenvironment elements such as reticular fibers, type I collagen fibers, glycosaminoglycans, blood/lymph vessels and immune cell infiltration along with those obtained from vitronectin and its ligands, to determine their histological patterns of aggressiveness. Comparison with results obtained in human tumor samples for suitability as therapeutic targets.
    3. Describe the genetic characteristics of the tumors obtained to gain insight into the impact of extracellular matrix properties on neuroblastoma genomic heterogeneity, particularly as regards the vitronectin role as an element of the tumor macroenvironment.

2.3. Justification of the thesis as publication compendium

The present doctoral thesis research is presented as a compendium of three publications and newly obtained relevant data to advance current understanding of the mechanical interplay between neuroblastic cells and extracellular elements, pinpointing the adhesive glycoprotein vitronectin as a key contact point inside the extracellular matrix.

All the findings of these papers have the same point of convergence: the search for therapeutic targets at the contact points of the tumor cell with its extracellular matrix in neuroblastic tumors, as is summarized briefly below.

The objective of the review carried out in article I, **The tumour microenvironment as an integrated framework to understand cancer biology**, and indeed the main focus of this dissertation, is to highlight the importance of tumor microenvironment interactions

underpinning tumor aggressiveness and patient prognosis, and identify possible biomarkers and targets with which to modulate the tumor niche and response to treatment. We highlight a proposed classification of tumor stroma into three grades of aggressiveness based on new data obtained in human tumor samples.

In article II, **Vitronectin as a molecular player of the tumor microenvironment in neuroblastoma**, we seek to characterize vitronectin as an extracellular matrix target molecule in a cohort of neuroblastoma patients grouped by diagnosis of tumor genetic instability, including an initial description of the *in vivo* study. Our thesis defense has centered on extending the *in vitro* and *in vivo* analyses of the vitronectin protein and its ligands to reinforce our conclusions regarding its importance as a future therapeutic target.

The objective of research summarized in article III, **The topology of vitronectin: A complementary feature for neuroblastoma risk classification based on computer-aided detection**, is to detect vitronectin distribution patterns in tumor stroma that could explain the behavior of neuroblastic cells in the cohort previously described in article II. Our dissertation centers on comparative analysis between non-topological and topological features of the various extracellular matrix elements, which generate complex stress forces to the cells, conducting a more in-depth exploration of this area.

CHAPTER 3. Results and Discussion

Several NB tumorigenesis studies have been performed to unravel how the cooperation is carried out between tumor cells and the surrounding elements being focusing preferentially on tumor cells (malignant neuroblasts and/or cancer stem cells) as the main players [108, 254]. However, other strategies that are mainly based on the TME elements have to gain interest as more physiopathological approaches to study common problems in NB such as metastasis or drug resistance. Therefore, discover new predictive markers to understand the interactions between all tumor elements is an option to locate specific therapeutic targets [78, 255, 256].

To describe how is the communication inside of the NB tumor ecosystem, we have paid attention to the study of VN, a glycoprotein of the ECM that supports cell adhesion. Since the attachment is a critical attribute that allows cell mobility, VN carried out its functions through the interaction with several ligands. It is recognized by cells or elements that express VN ligands or present binding sites along with its structure, promoting the adherence to other cells or ECM elements. The cell recognition and their communications are elemental steps that may promote migration in physiological processes [257-259] and even triggering pathological processes such as metastasis [260-262].

The main objective of our investigation is to focus on the study of VN and its ligands as well as its relationship with other NB microenvironment elements, to guide specific VN therapeutic assays shortly. For that purpose, we carried out the morphometric and topological characterization of VN in human NB, and link the emerging VN data to image analysis information of microenvironment elements, that we have previously obtained and published, to better define a tumor stroma classification. We have used 2D *in vitro* and *in vivo* experimental NB models, to also define the different expression patterns of VN in NB cell lines, to understand the influence of VN secretion related to microenvironmental and/or macroenvironmental factors, respectively.

In this chapter, we describe and discuss the updated and expanded results of the present thesis by article compendium related to the expression studies of VN and its ligands, the morphometric and topological measurements used and the ECM patterns found in three types of NB samples (human, cell cultures and xenografts) as well as the translational application of research studies.

3.1 Human NB samples

We have analyzed 8 tissue microarrays (TMAs) containing at least two representative cylinders of 1mm of 198 NB cohort, comprised between 2004 and 2015, which were referred to the Spanish Reference Centre for NB Biological and Pathological studies (Department of Pathology, University of Valencia/Incliva Biomedical Institute). In most cases (n=154), the tumor material belong to primary tumors, and in 127 cases, the tissue included in the cylinders was representative of the histology of the primary NB observed in the whole tumor section; the artifacts or non-evaluable samples were eliminated of the study. The present study was approved by INCLIVA's Clinical Research Ethics Committee (ref. B.0000339).

The morphometric and topological quantification was focused on the 91 samples out of 127 with previous single nucleotide polymorphisms array (aSNP) results, to carry out the classification according to genetic instability criteria. Genomic instability is a known cancer hallmark [263, 264] and our goal for routine future diagnosis is to link ECM stiffness with chromosomal instability; the SCAs have a known impact in NB [265]. The genomic instability criteria [based on structural chromosomal changes: very low (profiles without SCAs); low (≤3 typical SCAs, excluding 11qD; medium (profiles with 11qD or MNA or >3 typical SCAs); high (profiles with chromothripsis, or > 3 gene amplifications)] that we have applied, has a relationship with the prognosis in the NB patient's cohort; in fact, patients grouped in medium and high categories presented worse prognosis being worst when both groups come together (**figure 2**).

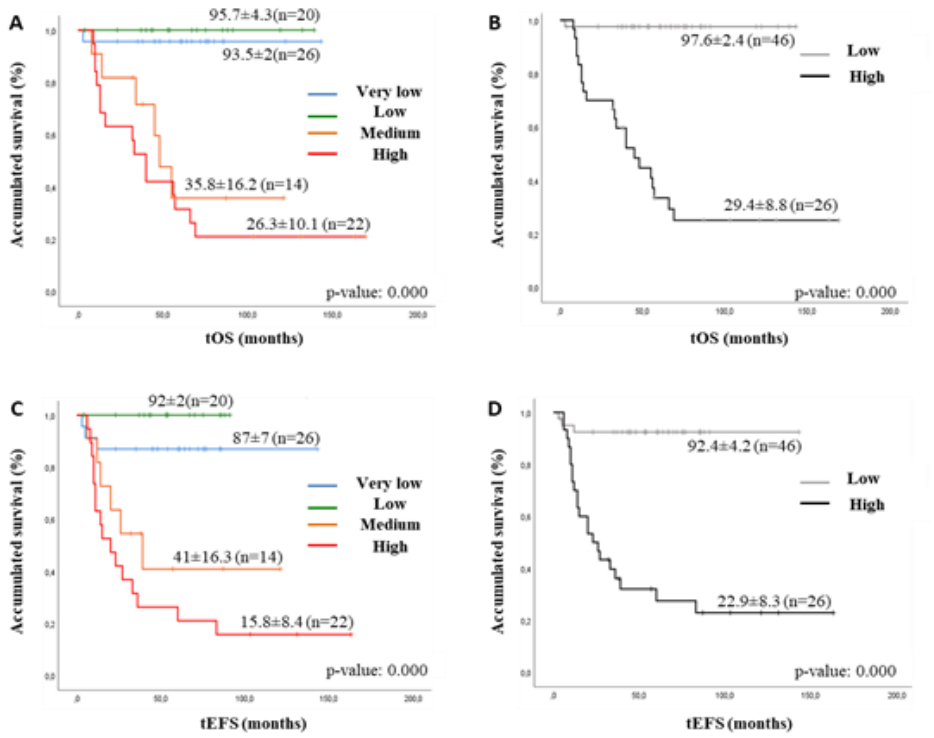

Figure 2. Kaplan-Meier graphs showing the EFS (C, D) or OS (A, B) depending on the genetic instability category. A and C. These graphs show the four categories of the genetic instability and their association with EFS and OS. B and D. These graphs show the dichotomized relationship between genetic instability categories and their relation to EFS and OS. EFS: event-free survival; OS: overall survival.

3.1.1 The importance of an adequate biopsy in the era of personalized treatment

We verified that the patient cohort analyzed in this research accomplish the clinicobiological and genetic features defined by the INRG classification [32]. We confirmed that the different risk factors defined by the INRG (age, stage, the grade of tumoral differentiation, genetic profile, *MYCN*, 11q, 1p, and 17q status) were in agreement with the patient survival described in the bibliography [32, 33, 262] (**tables 2-4, appendix**).

Nonetheless, the histopathology category and ploidy do not match the published patterns. The difference may be due to an increased number of included cases with the GN plus iGNB histopathology category (13%) and an underrepresented diploid category (13%); the cohort included in 2009 to elaborate the INRG classification, considered 4% and 29%, respectively. We have also to keep in mind that we have only around 70% of ploidy data from the total cohort. Finally, a recent INRG project, concludes that replacing INPC with individual histologic features in the COG risk classification will eliminate confounding, facilitate international harmonization of risk classification, and provide a schema for more precise prognostication and refined therapeutic approaches [266].

3.1.2. Expression studies of VN and its ligands highlight its relevance in NB biology

We have observed VN expression in tumor cells (as differentiated and undifferentiated neuroblastic cells) and stromal cells as some lymphocytes. Focusing on tumor cell staining intensity, we have distinguished 113 (89%) positive samples: 82 with weak-moderate staining and 31 with strong staining; and 14 (11%) negative samples (**figure 3**). The subjective assessment of VN was used to validate the subsequent customization of the algorithms, and positive control samples were used to verify its known location (e.g., specific cell type, intracellular compartment, among others) and whose histomorphology and cytomorphology can be visualized by a "stain". This stain intensity distinction allows us to detect a significant statistical association of strong VN presence in M stage (p-value:0.030), undifferentiated tumors (p-value:0.022), SCAs presence (p-value:0.010) and in HR patient subgroup (p-value:0.010), finding only a statistical tendency regarding the expression of strong VN and high frequency of relapses and poor OS (p-values:0.09 and 0.07, respectively). The abovedescription and other specific information were collected in **article II** of the current compendium.

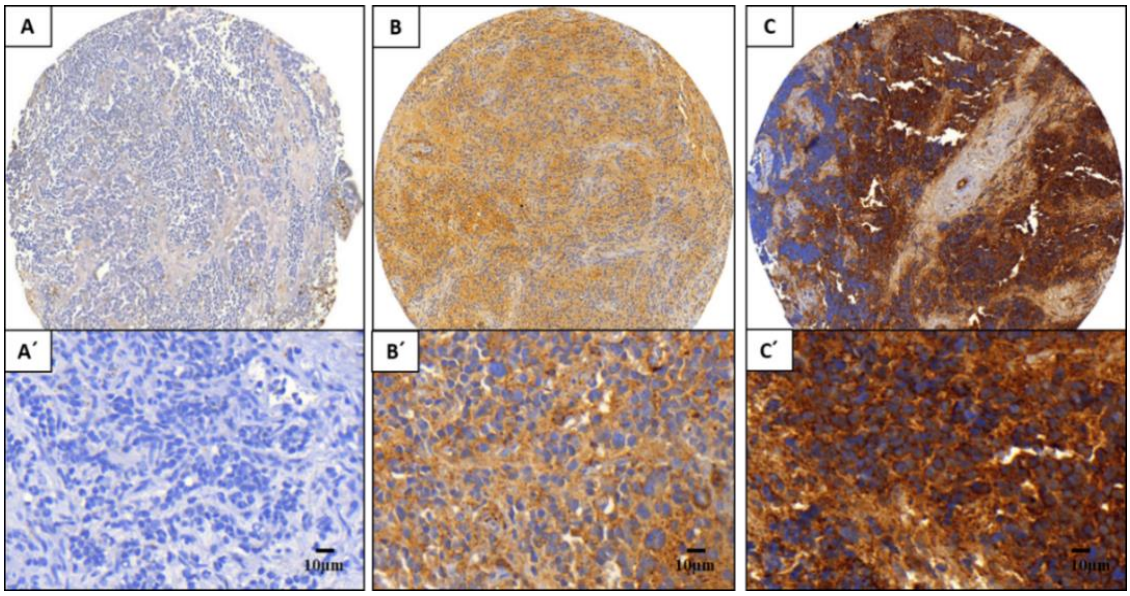

Figure 3. VN expression pattern in neuroblastic tumors. A. Image cylinder of negative VN sample. B. Image cylinder of the sample corresponding to weak to moderate VN expression. C. Image cylinder of the sample with strong VN expression. A´, B´ and C´. Immunostained images at 40x.

Going deeper into the VN structure (**figure 4**), this glycoprotein presents several domains, that are recognized for specific ligands to carry out adhesion and dissemination functions.

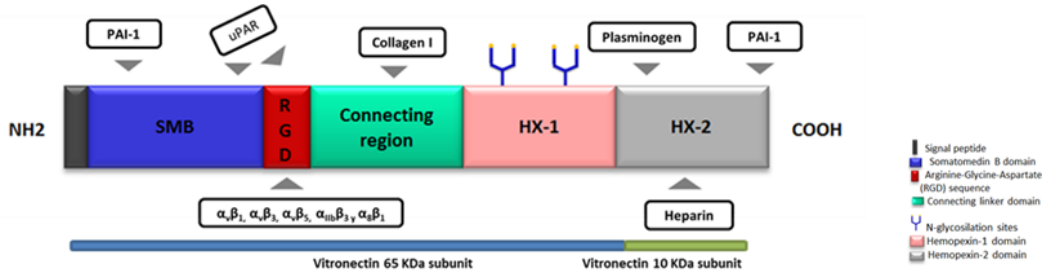

Figure 4. Structure of VN adapted from [127].

We have subjectively characterized the expression of some VN ligands using immunohistochemical methodology; employing the same NB cohort that has been stained for VN (127 samples). Nevertheless, due to those TMAs have been cut several times, the number of available cases for VN ligands decreased. We have focused on both, the study of three ligands: uPAR, PAI-1, and α_vB_3 integrin and their contribution through a proteolytic cascade and/or over the mechanical transmission of intracellular signaling pathways have been described to reinforce the adhesive role of VN to promote tumor growth and metastasis in several neoplasias, including NB [267-270]. Specifically, in NB, a previous study showed that uPAR is expressed by tumor cells, being elevated in HR patient's samples and tumors with unfavorable histology and with high invasiveness [271]. Controversially, it was observed in primary NB tumors that the uPAR mRNA expression was weak, whereas PAI-1 was presented in biopsies of patients with metastatic stage, being expressed by endothelial and stromal cells around tumor cells [272]. Also, Sugiura *et al*., demonstrated that increased PAI-1 expression by endothelial cells in tumor tissue stimulates metastasis, through the detachment of tumor cells from VN [272]. This last event was also confirmed by other investigations that demonstrated coexpression among PAI-1, VN, and α_vB_3 in blood vessels, which will explain its modulatory effect in angiogenesis. Furthermore, the authors observed that PAI-1 inhibits α_vB_3 integrin mediating cell adhesion to VN and promotes migration facilitated by binding α_5B_1 integrin to FN [273]. From all integrins that recognize the RGD VN domain, we have chosen the α_vB_3 integrin due to its role as a marker for angiogenesis and as a target for the treatment of various cancer entities [274-276]. Erdreich-Epstein *et al.,* evidenced a high expression of α_vB_3 integrin by microvessels in NB patients with metastatic stage remarking that the inhibition of the RGD integrin-binding site would avoid the attachment of endothelial cells to VN or FN [277]. Gladson *et al.*, in 1996 observed an expression of α_v and B_3 integrin subunits in undifferentiated NB, outlining that in these unfavorable tumors the α_vB_3 integrin would be produced by tumor cells [278]. Besides, in posterior research carried out by Erdreich-Epstein *et al.,* confirmed a high α_vB_3 integrin expression in blood vessels and an association with poor prognosis features (patients with stage 3, MNA and unfavorable tumor histology), inversely correlated with low *PTEN* in tumor cells. This tumor suppressor gene is

associated with the PI3K/AKT pro-survival pathway. They also demonstrated that the use of an RGD-conjugated pan PI3K inhibitor blocked tumor growth and tumor angiogenesis in NB xenografts [279].

Regarding uPAR expression, we observed that its expression was limited to immune stromal cells, 73% of the samples (55/75) showed no positivity, and 27% of the samples (20/75) were positive, of which, 18 samples presented positive stromal immune cells staining pattern with some positive stromal endothelial cell. We also found 2 samples with positive ganglion cells, nevertheless, for statistical analysis, we did not consider these 2 samples since ganglion cells normally presented a nonspecific immunoreactivity being able to disrupt the results (**figure 5**). Despite we were not able to confirm the results obtained in the above-mentioned NB study [271], our data are similar to those obtained in other cancers. Dohn *et al*. characterized the uPAR expression in terms of the number of positive cells and location patterns that discern between the tumor core and the tumor periphery in the bladder neoplasm. The authors observed that uPAR was expressed mainly in macrophages and myofibroblasts, finding a low percentage of positive cancer cells. They also found a significant relationship between uPAR expression in the above mentioned stromal cells at the two locations correlated with advanced the tumor stage and grade [280]. Another study on uPAR expression, matching our results, showed its expression in tumor cells (being low) and in stromal cells (macrophages, endothelial cells, and myofibroblasts) and observed a significant association between the survival of the patient with colorectal cancer and the uPAR expression in stromal cells [281]. Our observations are in line with these findings; however, we find no statistical association with INRG prognostic features, despite having grouped all the positive samples.

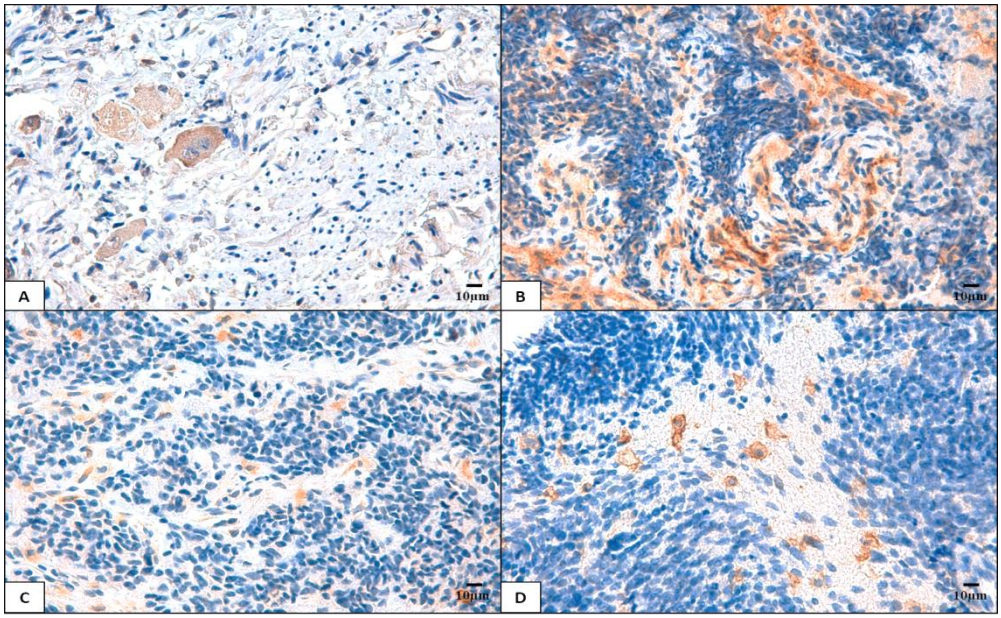

Figure 5. uPAR expression patterns in neuroblastic tumors using the antibody (ab218106,1:500 Abcam). A. Image with positive ganglion cells. B. Image with positivity in endothelial cells. C and D. Image with positive stromal immune cells. Immunostained images at 40x.

With PAI-1 staining, we observed that 73% of the samples (57/78) were negative and for the rest, 27% (21/78) were positive: 11 cases in tumor cells (nuclear and prolongation staining) and 10 cases in endothelial and blood cells (leukocytes and erythrocytes) (**figure 6**). Using the Chi-square test, we found a statistical association between PAI-1 expression in MNA tumor cells (p-value: 0.037) and HR patients (p-value: 0.015). As for survival, using the log-rank test we found a significant statistical relationship between the expression of PAI-1 in tumor cells and a higher rate of relapse (**figure 7**). The results of the PAI-1 expression in our NB analyzed cohort, showed a heterogeneous cell expression pattern, and therefore different from the previously mentioned NB study that only found the expression of PAI-1 in stromal cells [272]. However, in both studies, an association between increased PAI-1 expression and NB poor prognosis factors has been shown. We observed low PAI-1 expression in tumor cells following the results found in other neoplasias [282]. The role of PAI-1 in tumors is intricate and its proteolytic and non-proteolytic activity should be taken into account [283]. Some researches have described that PAI-1 inhibits cell adhesion and migration by blocking VN binding to integrins or by detaching the VN-uPAR connection [284, 285]; other studies reported that PAI-1 promotes cell adhesion of cancer cells [286, 287]. Research in oral squamous cell cancer found a predominantly PAI-1 expression in cancer cells and a low expression in stromal cells (fibroblast-like cells). In the same study, the expression of uPAR was observed, preferably in stromal cells, stating the low presence of uPAR in some cancer cells. These findings suggest that these two molecules are involved in the cascade of plasminogens promoting invasive characteristics in this neoplasm [282]. Other research on PAI-1 in ovarian cancer showed that strong expression of this molecule by cancer cells was

associated with shorter progression-free survival time, and also that *in vitro* use of the anti-PAI-1 compound reduced the expression of this molecule, resulting in the inhibition of signaling cascades related to cell adhesion to VN in those cells with PAI-1 expression [288]. Additional PAI-1 research showed that this serpin is also predominantly expressed in myofibroblasts, endothelial cells, and cancerous cells in invasive ductal breast cancer [289], with a special colocalization in the ECM close to VN positive cells [289, 290]. Henceforth, we could take into account that in a similar way to other neoplasms, the expression of PAI-1 in NB, would be related to the over-regulation of the plasminogen system involved in tumor invasion and angiogenesis.

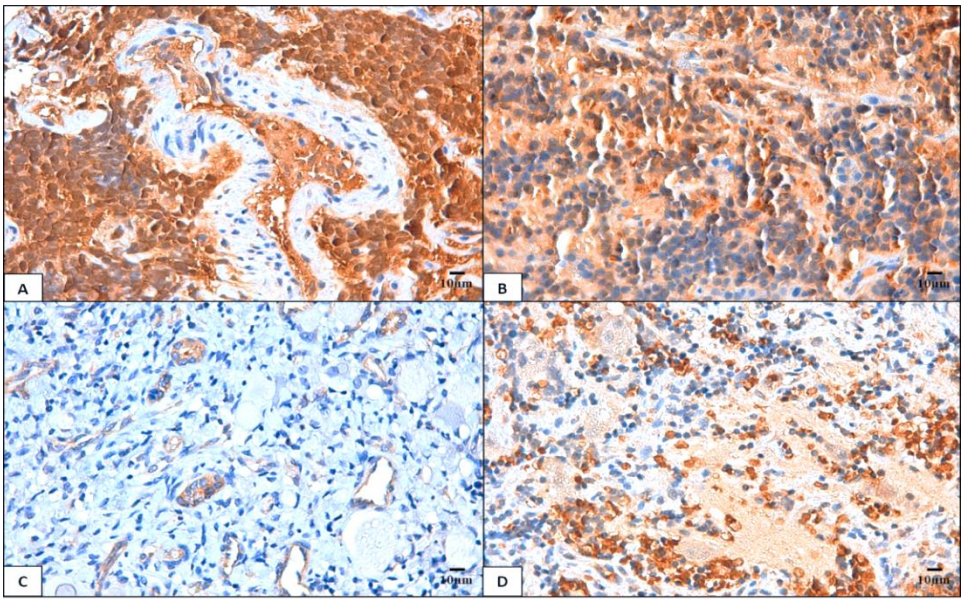

Figure 6. PAI-1 expression patterns in neuroblastic tumors using the antibody (ab125687, 1:200, Abcam). A and B. Image with positive tumor cells, nuclear and neuropile, respectively. C. Image with positivity in endothelial cells. D. Image with positive blood cells. Immunostained images at 40x.

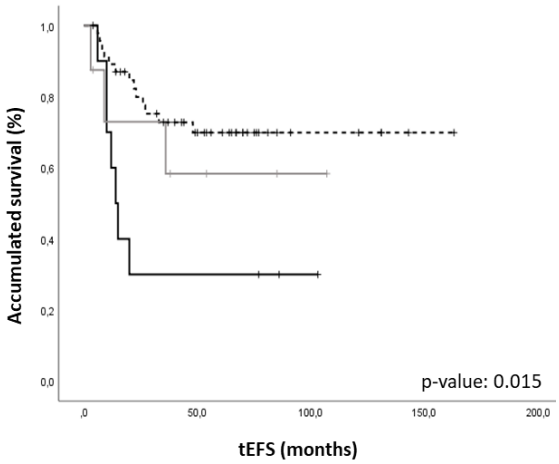

Figure 7. Kaplan Meier curves showing the relation among the PAI-1 expression patterns in neuroblastic tumors and EFS. The discontinuous line corresponds to negative samples, the grey line to positivity in endothelial and blood cells, and the black line positivity in tumor cells. EFS: Event-free survival.

Concerning the expression of α_vB_3 integrin, we found that 57% of the samples (43/75) showed no positivity and 43% of the samples (32/75) were positive in endothelial cells and monocyte/macrophage lineage cells (**figure 8**)**.** Using the Chi-square test, we found a statistical association between α_vB_3 integrin expression in endothelial cells and 17q gain (p-value: 0.028). Our findings of predominant expression in endothelial cells are following the findings described in NB, as mentioned before [277, 279], and in other neoplasms [291-293]. A research carried out on prostate cancer showed that the expression of this integrin was in the intratumoral blood vessels, being tumor cells mainly negative [291]. However, a study in glioblastoma found that the expression of this integrin was not limited to endothelial cells; the authors discovered that tumor cells cooperate with their secretion, being its expression increased in both types of cells in high-grade gliomas compared to low-grade gliomas [292]. Other research on breast cancer demonstrated an important expression of α_vB_3 integrin in blood vessels, stressing that in very few samples it also appeared in tumor cells [293].

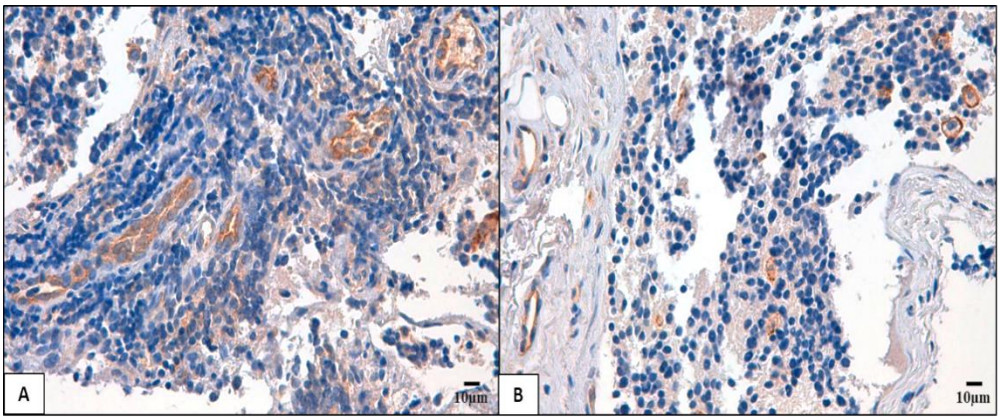

Figure 8. α_vB_3 integrin expression patterns in neuroblastic tumors using (ab7166, 1:50, Abcam). A. Image with positivity in endothelial cells. B. Image with positive monocyte/macrophage and endothelial cells. Immunostained images at 40x.

Using Kendall's Tau correlation coefficient, we observed a tendency to a positive correlation between VN and α_vB_3 integrin (0.066) and a negative correlation between VN and uPAR/PAI-1 expression patterns (-0.052 and -0.078, respectively). However, a trend was found to be positively correlated when we associate VN ligands: α_vB_3 integrin and uPAR (0.007), αvB3 integrin, and PAI-1 (0.166), and uPAR and PAI-1 (0.111). The positive but not significant correlation found between VN and α_vB_3 integrin could be explained by the fact that in the analyzed samples, we observed that some endothelial or macrophage cells are positive for both molecules (**figure 9**, **appendix**). A study in meningiomas showed an association between VN and α_vB_3 integrin expression in microvessels located in the tumor margin [294]. Another study has

recently described coexpression between uPA (that is the main ligand of uPAR) and PAI-1 in stromal cells also related to poor prognosis in early breast cancer [295]. **Figure 10** shows a NB biopsy with positive cells for VN, α_vB_3 integrin, and PAI-1 associated with negativity for the uPAR marker. We want to highlight the evidence that VN is a relevant molecule in aggressive NB mainly secreted by non-differentiated neuroblastic cells. Related with the potential implication of our results, through the application of morphometric and topological tools, we will get a more defined characterization of the expression and organizational pattern of VN in neuroblastic tumors.

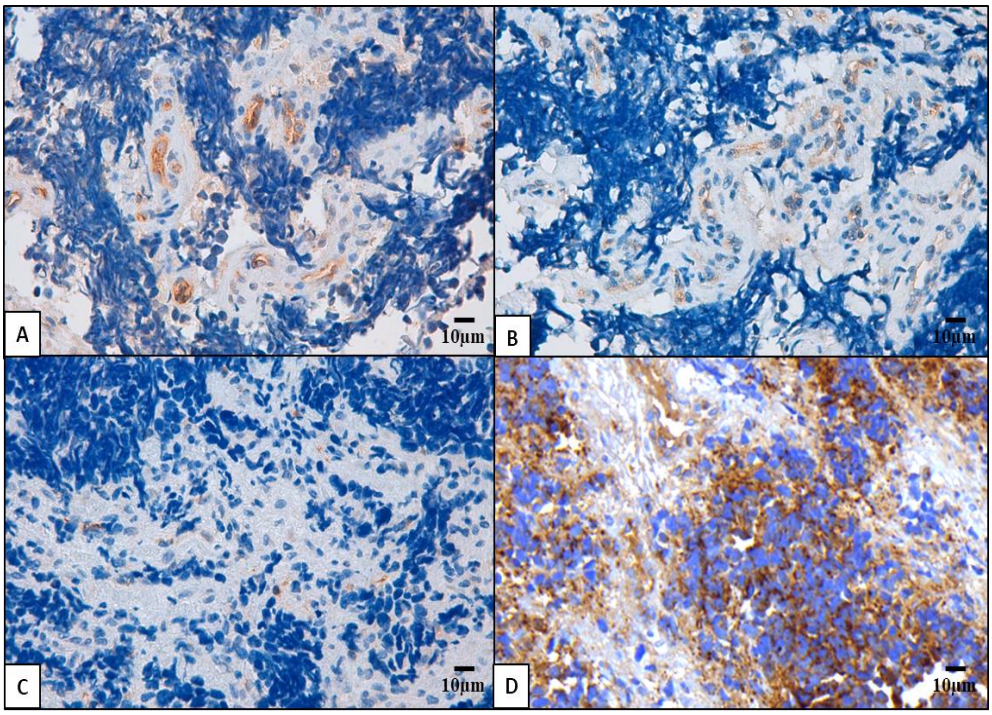

Figure 10. Immunohistochemically stained images for VN and their ligands belong to the same NB biopsy. A. α_vB_3 integrin positive expression in endothelial cells. B. PAI-1 positive expression in endothelial cells. C. Negative uPAR expression. D. VN positive expression in tumor cells. Immunostained images at 40x.

3.1.2.1 Morphometric measurements generate knowledge about tissue biotensegral responses

Using morphometric measurements, we concluded that the VN patterns are related to the secretion time of this glycoprotein and its integration into the ECM: territorial pattern, defined by newly VN synthesized (intracellular location) and recently integrated to the matrix (pericellular location) characterizing by strong staining; and interterritorial pattern, denoted to VN that has been incorporated to the ECM some time ago, distinguishing by weak-moderate staining. This means that the territorial VN would participate in linking the biomechanical properties of the tumor cells and the surrounding elements, facilitating the migration of tumor cells (**article II**).

Our findings showed that a high presence of territorial VN was associated with unfavorable INRG independent variables (**figure 11**) and the highest expression of this pattern was related to poor Event-free survival (EFS) and low OS, therefore we included it as a complementary predictor factor in the studied NB cohort. **Figures 12- 13 (appendix)** showed how the morphometric parameters were distributed in the subcategories of the clinical and biological INRG variables.

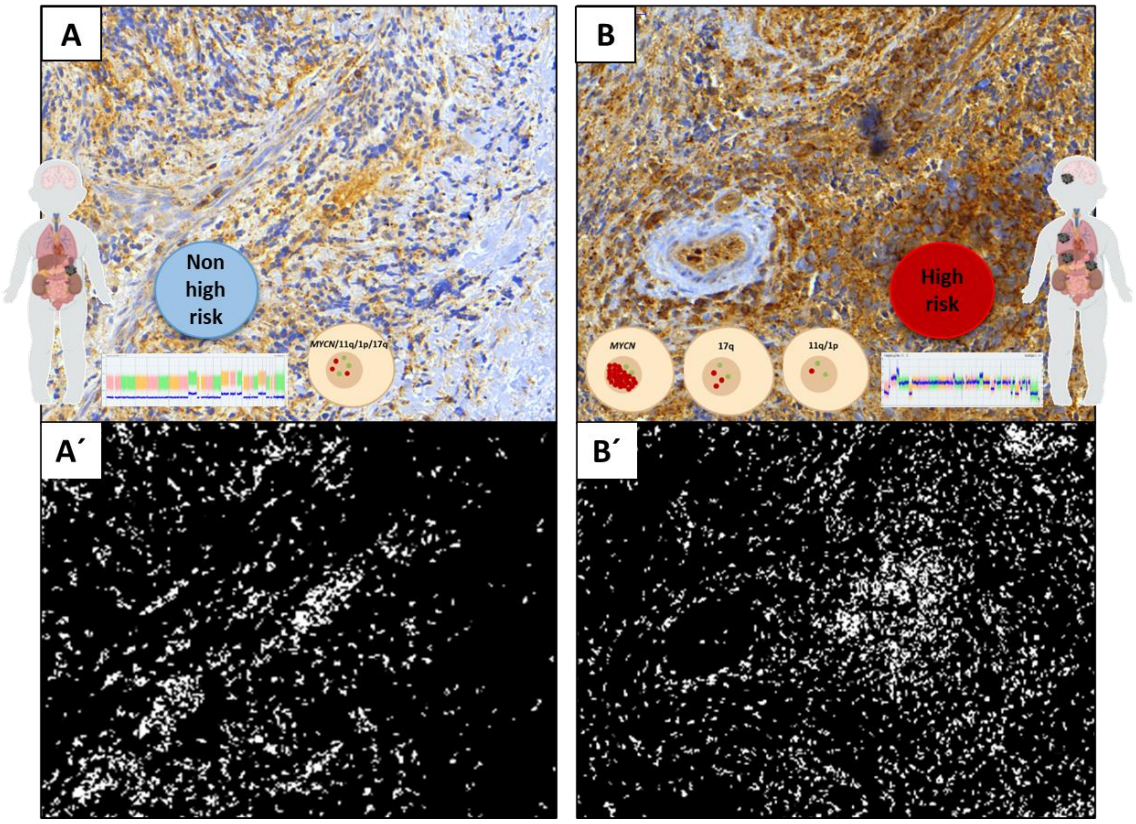

Figure 11. Summary representation of the main associations between VN morphometric features and the INRG parameters. A. Immunohistochemical sample lacking territorial VN, with interterritorial VN that was presented as VN pattern in tumors with differentiated histopathology, NCA profile, MNNA, and included as low genetic instability tumors groups related to non-high-risk patient subgroups. A´. Binarized image (markup image) to better distinguish interterritorial VN staining in A. B. Immunohistochemical sample of high territorial VN expression that was the VN pattern often found in tumors with non-differentiated histopathology, SCAs profiles, including MNA,11qD and 1pD and included as high genetic instability tumors belonged to HR patient subgroup and metastatic stage. B´) Binarized image (markup image) to highlight the territorial VN in B.

The use of digital analysis tools in pathological processes, such as in cancer, are becoming more frequent and the results more robust. This occurs as a need to have an automatic objective method that allows a quick and efficient analysis of the huge amount of tumor samples that must be analyzed in routine clinical diagnosis and the field of research [237, 296, 297]. Indeed, these approaches have been applied to get a better knowledge of tumor stroma interactions. Using morphometric analysis, it has been demonstrated the existence of changes in some

stromal elements that are part of the TME such as reticular and collagen fibers, and blood vessels in colon cancer [298]. A study performed in oral squamous cell carcinoma observed that the metastatic samples presented a high amount of tortuous lymph vessels after their quantification [299]. Several kinds of research carried out by our group using digital image analysis techniques, revealed the importance of using these tools for studying how is the organization of ECM to define different tumor stroma architecture of HR and ultra-HR NB patients [147, 251] or clarifying vascular and lymphatic morphometric patterns to provide targets related to NB prognosis [252, 253]. These studies statement the intricate communication between the tumor cells and the surrounding stromal elements or tissues that can be modified to promote proactive tumor behavior.

To obtain some relevant results included in the present compendium, we have used two different software (Image Pro-plus (IPP, Media Cybernetics) and DensitoQuant module (DensitoQ), Pannoramic viewer (3DHISTECH). It was the approach to find a more accurate image segmentation. An advantage of IPP software is that presents a range of image pre-processing tools to solve different problems derived from the pre-analytical processes. However, it is always necessary to validate the used image tools and standardize all the parameters obtained for a faithful representation of reality [300, 301]. In our study, we have been able to validate the objective method based on the subjective evaluation, comparing the results obtained in both methods. The tests performed indicate that the algorithms were standardized, correlated with subjective assessment, and reproducible to be applied in different samples with minimal algorithm customization (**tables 5 and 6, appendix**). It is important to note that for a good reproducibility of this study it is advisable to maintain the same software configurations. It is also advisable to perform the staining and scanning images under similar conditions.

Using morphometric approaches, we have defined two specific VN patterns in NB, remarking that an increase of the territorial one is found in tumors with non-differentiated histopathology. However, there are some controversial investigations related to our VN results in NB. C. L. Gladson *et al*., described the presence of VN in differentiated NB biopsies, but non or weak expression in undifferentiated NB, suggesting that it plays a role in neural differentiation. They also evidenced *in vitro,* that VN mediates attachment through $\alpha_v B_5$ integrin of retinoic-acid-differentiated and undifferentiated neuroblastic cells, being lower in undifferentiated cells. Since both types of cells produce this integrin, it proposed that the production of VN by differentiated neuroblastic cells could lead them to an adhesive phenotype. The same study described that VN has a role in neurite formation and polarization of neural progenitor cells during development [302]. The last phenomenon was confirmed by research carried out by *Pons*

et al., which informed that VN contributes to the regulation of proliferation, differentiation, and neurite elongation in mouse cerebellar granule cell precursors [303]. Also, a recent study confirmed that mouse cerebellar granule cell precursors differentiation is promoted by the recognition of VN through α_vB_5 integrin [304]. S. Shimizu *et al*. evidenced a possible mechanism mediated by Foxa for explaining the increased VN presence during differentiation in mouse NB cells (Neuro2a) stimulated by retinoic acid [305]. In recent research, using the same cells, as a retinoic acid-induced neurogenesis model demonstrated that VN regulates the transition from multipolar to bipolar morphology and the cell cycle exit, remarking that Par6 (a cell polarity regulator) and α_vB_5 cooperated in the morphological transition [306].

3.1.2.2 Topological measurements facilitate architectural tissue findings

One of the bases of topology is to know how objects are linked. Taking into account tumor proliferation, as a non-static process in which neoplastic cells and cellular/non-cellular elements have to cooperate and gradually change to obtain a significant growth rate, the topological methodology is beneficial for detecting key points in tumor organization and tumor elements behavior [307]. Topological analysis in NB, described by Marinaro G *et al*., revealed that N2A cells exhibited organizational changes in designed networks depending on the culturing substrate to acquire an effective formation influenced by cellular communication [308]. The nuclear topology of the *MYCN* gene was also subjected to topological analysis focused on distinguishing the location when this gene is amplified and forms double minutes (dmins) or homogeneously staining regions (HSRs) [309].

The application of topological analysis (widely described in the doctoral thesis of Pablo Vicente-Munuera, University of Sevilla) allowed us to understand how the distribution of VN affects the ECM scaffolding in NB (**article III**). Results after applying pure topological features showed that the iteration tensegrity index for both VN patterns was the only significant pure topological characteristic to classify NB patients concerning tumor genetic instability. Regarding topological characteristics, we identify that the Euler number per node of territorial VN, a feature that mixes its quantity and organization, as a notable attribute to improve the established pre-treatment risk classification. We noted that a high index was related to tumors of HR NB patients, which meant that territorial VN had been compacted into focal areas. These findings suggest that this VN distribution could alter the ECM structure, leading to tumor cell adhesion perturbation and tumor cell spreading. It has been shown in cervical cancer that Euler's number is related to aggressiveness being able to discriminate between metaplasia, or cell

adaptation, and neoplasia, abnormal and excessive cell growth that can invade vessels and migrate to different places [310].

Moreover, we noted that branches per territorial VN node were related to tumor instability; this feature considers the VN structure in terms of intersections number. Therefore, we showed that tumors with high genetic instability had a high territorial VN branching, in other words, presented a non-solid VN distribution around cells. So, this topological feature could represent migratory pathways with a huge amount of VN that promote clonal expansion with limited genetic variability and significant adaptive advantage, by activating nuclear pathways that alter genetic machinery generating high genomic instability. For the study and measurement of networks in other biological events, such as vasculogenesis, non-static approaches based on topological methodologies have also been applied that consider branching parameter relevant [311]. In fact, in the study of several organs, such as the small bowel, mammary gland or pancreas due to the need to exchange nutrients, metabolic products, and chemical or physical signals have developed structures that follow branching mechanisms to facilitate these processes [312]. Then, extrapolating this information to our branching results, we can suggest that this modification in the VN organization pattern could also be the selective cost of adaptation to achieve an effective proliferation and migration, which are two key pieces in tumor aggressiveness.

3.1.3 ECM elements generate complex stress forces to cells

To find how tumor stroma progressively transforms as the malignant phenotype progresses, in the current cohort of NB patients (91 samples) we obtained different patterns (categories) of previously analyzed TME elements (**article I**). This was achieved thanks to the extraordinary experience of our group after several published articles [147, 250-253, 313], doctoral theses [314, 315], and descriptions presented in national and international conferences (some included in my CV), and in the available literature. A huge amount of morphometric data on TME components (reticulin fibers, type I collagen, GAGs, VN, blood/lymph cells, immune cells, and stem cells), which have had an association with the patient prognosis of NB is available. Some categories that we have described come from analyzed variables from different elements that constitute models of morphometric patterns that had been found after performing a univariate and multivariate linear regression of dichotomized variables (GAGs, reticulin fibers, and blood/lymph vessels) in a cohort of 400 primary NB samples (**table 7**).

Table 7. Variables that compose models of morphometric patterns.

Variable	B	S.E.	Wald	Exp(B)	(95% CI)	p-value
Reticulin Length	-0,72	0,36	3,92	0,49	0,24 0,99	0,05
Reticulin Width	1,14	0,37	9,39	3,12	1,51 6,47	0,00
Reticulin Dendrites	-1,01	0,29	12,11	0,36	0,21 0,64	0,00
%SA Glycosaminoglycans	-0,57	0,27	4,45	0,57	0,34 0,96	0,03
% SA 15_20 Lymph vessels	1,78	0,69	6,70	5,92	1,54 22,73	0,01
Roundness 20_50 Lymph vessels	1,40	0,51	7,64	4,07	1,51 11,02	0,01
Area 5_15 Blood vessels	2,15	0,60	13,01	8,58	2,67 27,58	0,00
PerRatio 20_50 Blood vessels	1,41	0,50	8,14	4,11	1,56 10,86	0,00
Perimeter 50_200 Blood vessels	1,76	0,51	11,77	5,82	2,13 15,94	0,00

SA: stained area

These models allowed predicting probability to define patterns of varying degrees of aggressiveness according to the state of several variables (**article I**). Collagen type I was not taken into account for this statistical analysis in NB, since in nerve tissues (both central and peripheral) it is scarce, however in the tumor stroma classification that we have designed was taken into account, and its data were extracted from results previously obtained in other tumors [147]. As for the rest of the variables, we have chosen those according to our previous results presented a significant statistical relationship with the worst prognosis in NB patients. From VN, we selected the %SA of territorial VN, from immune cells we chose several markers (the % of macrophages associated with tumors -using anti-CD68, a broad marker of monocytes/macrophages and anti-CD163, which is expressed predominantly in M2-type macrophages - and % of DCs -using CD11c marker-), from stem cells we also chose several markers (the % of positive cells to CD133, OCT4, S100A6, and CD105). As several elements had different measured parameters, we compiled them to differentiate between categories of different prognosis (good, intermediate, and poor). The distribution of samples within the different categories of data available for each item is found in **table 8.** Appendix section (morphometric and topological features to obtained and ECM patterns) provides more detailed information on how to achieve these categories.

Table 8. Descriptive data of analyzed parameters from each element grouped in stromal alteration grades according to patient outcome.

TME element	Category		
	Good	Intermediate	Bad
Glycosaminoglycans	34	33	23
Reticulin fibers	32	12	47
Blood vessels	7	11	64
Lymph vessels	46	10	33
Vitronectin	44	23	22
Immune system	44	23	15
Stem cells	18	46	27

TME: tumor microenvironment

We have found that reticulin fibers, VN and immune cells grades were significant according to survival results (EFS and OS), regarding blood vessels grade we only observed a significant relation with OS (**figures 14 and 15**).

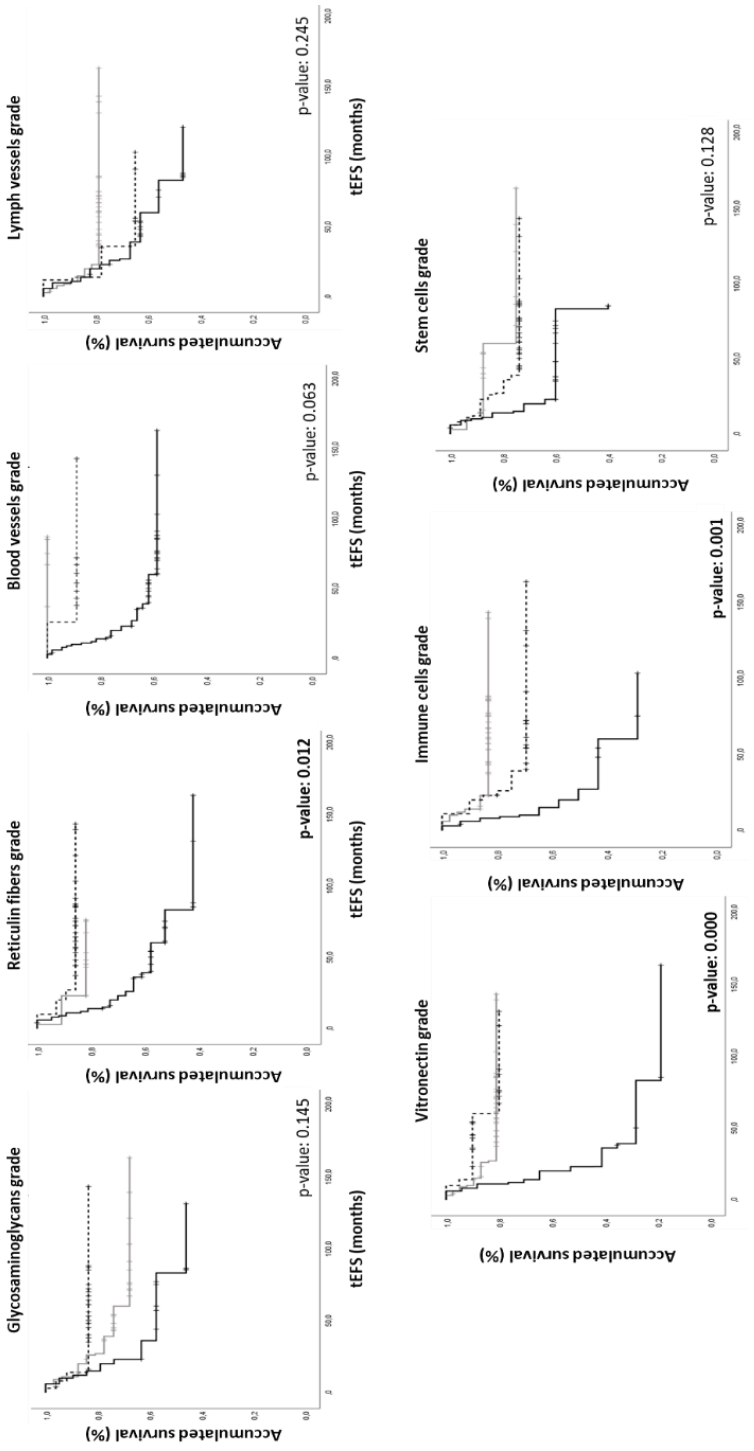

Figure 14. Kaplan Meier curves of the categories from each element that constitutes models of morphological TME patterns associated with the prognosis (EFS). The black line corresponds to the bad prognosis, discontinuous line belongs to intermediate prognosis and grey line to good prognosis. EFS: Event-free survival.

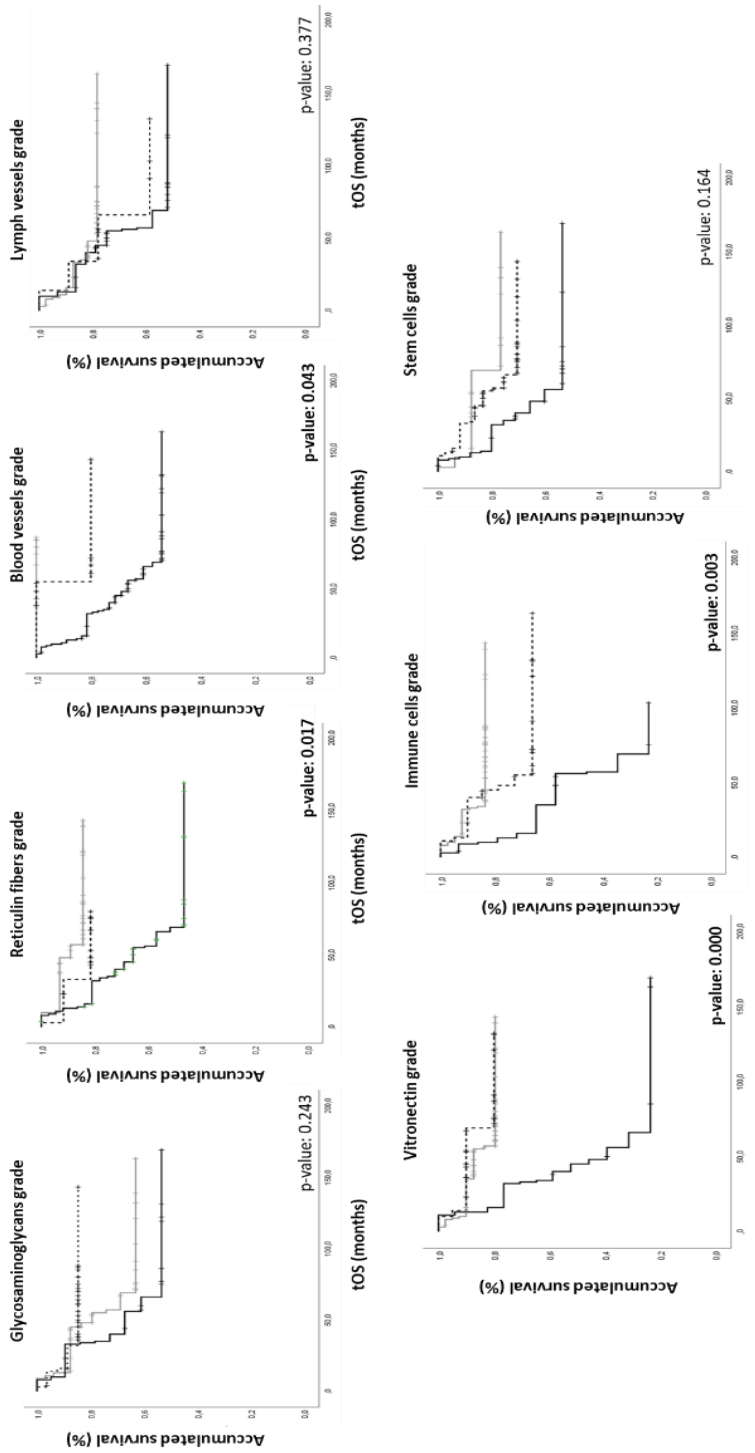

Figure 15. Kaplan Meier curves of the categories from each element that constitutes models of morphological TME patterns associated with the prognosis (OS). The black line corresponds to the bad prognosis, discontinuous line belongs to intermediate prognosis and grey line to good prognosis. OS: overall survival.

The overall results invite us to propose a classification of tumor stroma changes at three levels: grade I, defined by minimal changes in the biotensegrity of the tumor stroma and characterized by the presence of variables related to good prognosis; grade II, represented by slight changes given some rigidity to the stroma and with the characteristics of the variables associated with indeterminate prognosis; and grade III, characterized by stiff stroma, where the elements that form this category are associated with poor prognosis. We have found that some

categories are not significant according to survival results (EFS and OS) or there is even a trend where the intermediate category might be better than a good prognosis (as in GAGs). The first problem can be explained by the low proportion of samples examined since we have analyzed 91 samples, and as can be shown in **table 8**, however, we do not have that total for many elements due to the lack of some variables. The second situation can be clarified by the fact that we have obtained three different categories derived from the combination of several variables of each element. In the case of GAGs, in previous publications we showed that a low amount of this element was correlated with a poor prognosis in NB patients, then we have followed this criterion to generate the category [250]. As can be seen in **figures 14** and **15**, the poor category presents a significant rate of relapse and worse OS.

This proposed classification aims to provide information on the complexity of the tumor milieu, underscore the knowledge about the neoplastic and non-neoplastic cells, ECM elements, and vascular networks that are necessary to determine targeted therapies. Therefore, this integrative vision tries to decipher what remodeling events occur in tumor stroma during tumorigenesis leading to the search for new treatments that could serve as a benefit for cancer patients. Some publications reinforce that interactions through mechanical and biophysical forces can influence the tumor framework. Kumar and Weaver in 2009, described this process as a transformation event involving remarkable modifications in the phenotype of tumor cells and their surrounding environment [316]. Similarly, a later study showed that the transformation ranging from a soft stroma until a stiff tumor has a relationship to metastatic progression [82]. Rakesh *et al*. evidenced how mechanotransduction cues exchanged within the tumor entity have significant implications to improve treatments through the normalization of the abnormal tumor environment [317]. A more recent investigation also showed the importance of communication between crucial stromal cells in breast cancer microenvironment and the progression of this neoplasia [318].

We faced all the mentioned grades, which we obtained from clinical and biological studies, to know which one has the greatest influence on the outcome of NB patients. Our results detailed that the VN and immune cell grades had more influence to define a poor EFS and OS (**table 9**). Also, we determined the statistical power of these categories compared to clinical variables with a known independent prognostic value in NB as age, stage, histological classification, *MYCN* status, and 11q aberration. We found that reticulin fibers grade is the only morphometric category together with age/stage, MNA, and 11qD that had a strong influence on poor EFS and OS, respectively (**table 10**). In both models, blood vessel grade also reached until the last step without statistically significant association.

Table 9. Cox regression of the morphometric categories of TME elements.

Variable	B	S.E.	Wald	Exp (B)	(95% CI)	p-value
EFS						
Vitronectin grade (Bad category)	1.01	0.28	12.95	2.76	1.58-4.80	0.000
Immune cells grade (Bad category)	0.92	0.31	8.75	2.51	1.36-4.63	0.003
OS						
Vitronectin grade (Bad category)	0.92	0.28	10.99	2.52	1.49-4.35	0.001
Immune cells grade (Bad category)	0.74	0.30	6.06	2.10	1.16-3.79	0.014

Significant predictive morphometric measurements of poor outcome in NB patients based on EFS and OS with p-value<0.05. S.E: standard error; CI: confidence interval. EFS: event-free survival; OS: overall survival.

Table 10. Cox Regression of the morphometric categories and INRG prognostic factors.

Variable	B	S.E.	Wald	Exp (B)	(95% CI)	p-value
EFS						
*Age (≥18 months)	1.12	0.65	2.97	3.08	0-85-11.10	0.085
11q status (11qD)	1.34	0.54	7.09	3.82	1.42-10.28	0.008
MYCN (MNA)	1.38	0.55	6.30	4.01	1.35-11.83	0.012
Reticulin fibers grade (Bad category)	0.68	0.31	4.85	1.99	1.074-3.67	0.028
OS						
*Stage (M)	0.69	0.39	3.10	2.01	0.92-4.33	0.078
MYCN (MNA)	2.04	0.52	15.26	7.71	2.76-21.48	0.000
11q status (11qD)	1.23	0.49	6.30	3.44	1.32-9.05	0.012
Reticulin fibers grade (Bad category)	0.66	0.32	4.18	1.95	1.02-3.70	0.041

Significant predictive morphometric measurements of poor outcome in NB patients based on EFS and OS with p-value<0.05 and *p-value<0.1. S.E: standard error; CI: confidence interval; 11qD: 11q deletion; MNA: *MYCN* amplified; M: metastatic; EFS: event-free survival; OS: overall survival.

These findings reveal the idea that reticulin fibers, VN, and immune cells have to be considered as important targets in NB stroma. Since their statistical significance is maintained after the integration of the stromal elements and clinicobiological features of the INRG classification. Some researches also noted the importance to develop tumor classifications according to standards similar to those criteria presented in this doctoral thesis. A triple-negative breast cancer study evidenced that the generation of an immune model focused on the expression phenotype of these specific cells is an independent prognostic indicator for this malignancy [319]. A model constructed through the detection of stromal features in hepatocellular carcinoma, and the combination of this data with clinicopathological

characteristics resulted in two categories of this neoplasia with robust discrimination of patient´s outcome [320]. A study focusing on tumor heterogeneity of hepatocellular carcinoma also identified a classification of this tumor in three types representing diverse clinical situations in patients [321]. Wartenberg *et al*. demonstrated that the integration of immune patterns and data from molecular features also resulted in the distinction of three biologically relevant pancreatic ductal adenocarcinoma subtypes [322].

For this reason, the next step was to use a set of different morphometric variables from TME components in NB (GAGs, reticulin fibers, collagen type I fibers, VN, blood, and lymph vessels) to know if some of them could improve the results obtained with the topological characteristics of VN to classify NB samples according to the pre-treatment risk stratification or tumor genetic instability criteria. We used the morphometric parameters of all these elements, and also the two relevant VN topological features described previously (Euler's number per node of territorial VN and number of branches per node of the territorial VN). Regarding tumor genetic instability, firstly we performed a selection of statistically significant morphometric features (% SA and relative density of capillaries, roundness, deformity, and shape of post-capillaries/metarterioles and shape of sinusoids). Next, we combined these significant morphometric variables with the known INRG classification variables (age, presence of SCAs, stage, histology *MYCN* status, 11q aberration, and ploidy) plus VN topological variables. Using Discriminant analysis (DA) characteristics selection, the deformity of the post-capillaries/metarterioles variable could be added to the patient classification. After logistic regression, the variables that better predicted the different groups of high and low tumor genetic instability were: *MYCN* status, age, number of branches per node of the territorial VN, presence of SCAs, and deformity of post-capillaries/metarterioles (**figure 16A**). This model improved specificity (0.96 vs 0.91) with equal sensitivity (0.89).

As for risk criteria, we followed the same approach, described above. The morphometric variables that were previously statistically significant (length, perimeter-ratio, vertices, %SA, and relative density of capillaries, roundness, and shape of post-capillaries/metarterioles and shape of sinusoids) were joined to INRG factors and VN topological features. We noted that the resulting variable, which could potentially be used for classification is the shape of sinusoids. Through logistic regression, the variables that best predicted the different risk pre-treatment groups were in the order of importance: age, the shape of sinusoids, stage, Euler number of territorial VN, and *MYCN* status (**figure 16B**). This model improved specificity (0.89%) according to the model that takes into account only the VN topological feature being now 0.94 but decrease sensitivity (0.70 vs 0.75).

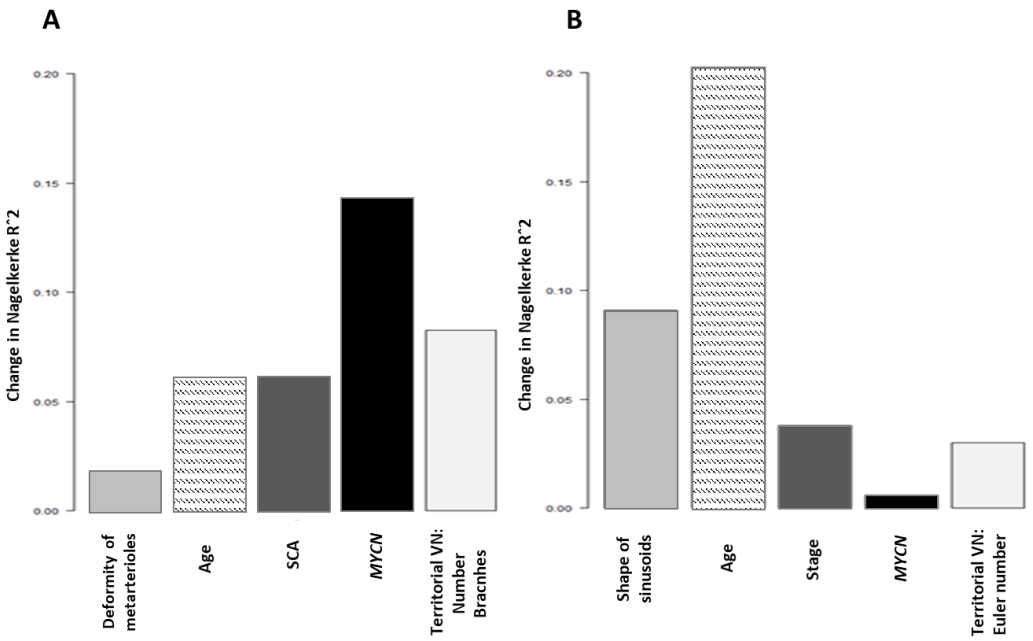

Figure 16. Graphs of the best predictor variables associated with A) tumor genetic instability and B) risk stratification in NB patients.

3.1.4. Studies to strengthen clinically relevant biomarkers or therapeutic targets

The vast majority of NB investigations are focused on the VN role in cell differentiation processes, which is one of the cellular functions promoted by the interaction of its binding domains to multiple receptors [257]. However, VN acts not only in differentiation processes in NB but also in other cellular pathways, including spreading, adhesion, and migration [129, 323]. Our findings in tumor samples from patients with poor prognosis indicate that the synthesis of VN by neuroblastic cells could reflect the formation of pathways to facilitate cell leakage and invasion by allowing easy attachment-detachment cycles between cells and reticulin fibers and/or mucopolysaccharides with neoplastic cells. The role of VN in this interaction has been demonstrated by several studies in different malignancies [260, 261, 324, 325]. Other studies also showed increased expression of VN receptors related to poor prognosis in NB patients [271-273, 277-279]. The expression results of VN and its ligands by tumor and/or stromal cells imply that these molecules could develop a multifunctional role in NB, which reinforces the protagonism that has the tumor stroma in tumorigenesis, prognosis and in the search for specific therapeutic targets. Findings in biopsy samples of the present compendium of researches suggest that although there is no significant correlation between the expression of VN and its ligands, they could provide a synergy effect with the secretion of VN in aggressive NB, as has

been observed in other malignancies [267-270]. The communication between cancer cells and the surrounding environment can trigger essential signaling cues that determine cell fate and influence the evolution of the malignant phenotype; several studies have described that TME plays a supporting role acting as a major contributor in the onset of tumorigenesis [77, 326, 327].

We combined quantitative and topological morphometric features since beyond the morphology of the components it is interesting to know how the elements of the biopsy are organized. To this end, we wanted to find new independent individual factors to generate a model that will help us to establish new and multidisciplinary forms of cancer research. The use of mathematical approaches results in the generation of models that represent predictive patterns to improve patient outcomes, relying on different algorithms. Some researches have been carried out in this field; for example, a NB study that has used deep neural networks to analyze genomic and transcriptomic data has been able to identify topological characteristics that support predictive clinical outcomes [328]. Radhakrishnan *et al*. also established a morphometric platform in combination with genomic methods to detect nuclear-level alterations that are important for cancer diagnosis [329]. These researches that applied mathematical models bring out the underlying biological mechanisms to offer new therapeutic strategies. Our results, along with the previously published references, determine that identifying specific markers of TME, as VN and its ligands would help establish an individualized treatment approach for NB patients.

Our histological characterization VN results together with previous studies that extended the prognostic role of this glycoprotein in tumors [129, 130, 132, 304, 324, 325] lead us to search for a more specific VN pattern using digital analysis tools. In this way, we can better understand how VN acts in different tumor context and look for new therapeutic approaches by sensitizing tumors to anti-VN therapy through suppressing its metastatic phenotype. In fact, in breast cancer research, the unification of nuclear morphometry data and tissue topology characteristics resulted in a better assessment of the tumor margin to distinguish between normal and tumor tissue [330]. Similarly, in a renal carcinoma study, after using these approaches was possible the characterization of different types of cells within the TME and the description of the topological characteristics of tumor cells and stroma [331]. Therefore, the use of digital analysis of microscopic images is a relevant tool for finding new therapeutic targets in the context of TME to understand the interactions that occur within a malignancy and improve the patient's outcome [332-334].

The combination of morphometric and topological methodologies is useful for describing the characteristics of various VN-related molecules, which are associated with unfavorable prognostic factors and could lead to the detection of new therapeutic targets using in *vitro* and *in vivo* models.

3.2 In vitro NB models

Cell cultures are accessible experimental models widely used for biological research and drug improvement. We have used *in vitro* models to describe the presence and characteristics of the VN and its links in a wide set of NB cell lines. It is a great challenge for knowledge to identify and validate multiple biological molecules that can be applied in an extensive variety of tumors, including VN and its links, as new therapeutic agents for the progression of cancer medicine.

3.2.1. Cell lines used

The following table shows the human NB cell lines panel that has been used with their main features:

Table 11. Summary of NB cell lines.

Cell line	Stage	Age (months)	*MYCN* status	Chromosomal aberrations
SK-N-BE (2)	4	24	Amplified	1p- ((cnLOH pter- p21.3), (p21.3-p12)), +1q(q11-qter), 3p-(pter-p14.2), +11q(q13.1-qter), +17q (q12-qter), *ALK* WT, p53 (p.C135F)
SK-N-BE (2)c	4	24	Amplified	1p- (cnLOH pter-p21.3), 3p-(pter-p14.2), + 11q (LOH q11-qter; q13.4-qter), +17q (q12-qter) ALK WT, p53 (p.C135F)
NGP	Unknown	30	Amplified	1p- (cnLOH pter-p32.3), 3p- (Gain pter-p25.3), 11q- (q22.1-qter), +17q (q21.1-qter), *ALK* WT, p53 (p.A159D, p.C141W)
NB-5 (SJNB-5)	3	24	Amplified	1p- (LOH)
SH-SY5Y	4	48	Non amplified	+1q (q12-q44), +2p (pter-p16.3), +17q (q21.31-qter), *ALK* (F1174L), p53 WT
SK-N-SH	4	48	Non amplified	+2p (pter-p16.3), +17q (q21.31-qter), *ALK* (p.F1174L), p53 WT
CHLA-90	4	102	Non amplified	p53 not functional, *ALK* (p.F1245V)
NBL-S	3	42	Non amplified	11q- (q14.1-qter), *ALK* WT, p53 WT

cnLOH=copy neutral loss of heterozygosity; WT: wild type. Information obtained from references:[335-340].

We have used this group of NB cell lines for the characterization of VN and its ligands. The reason to use this *in vitro* cell lines panel is to have a range representation of candidates for morphological and molecular features of HR-NB. They represent different clinical features like age, origin site of the tumor, and stage (although they are predominantly metastatic stage)

[335]. Moreover, we have to keep in mind that heterogeneity is a key point in neuroblastic tumors and it implies to test several cell lines [28]. The NB cell lines used in this study were kindly provided by Miguel F. Segura (Laboratory of Translational Research in Child and Adolescent Cancer, Hospital Universitari Vall d´Hebron) purchased from the ATCC (American Type Culture Collection).

3.2.2. Expression of VN and its receptors by neuroblastic cells

We have grouped and compared in **table 12** since *MYCN* oncogene status is a prognostic relevant factor in NB, the immunocytochemical results of VN, uPAR, PAI-1, and $\alpha_v\beta_3$ integrin, in MNA vs MNNA cell lines [32, 33].

Table 12. Summary of VN, uPAR, PAI-1, and $\alpha_v\beta_3$ integrin expression in NB cell lines.

Biomarker/ Analyzed feature		Cell lines							
		SK-N-BE (2)	**SK-N-BE(2)c**	**NGP**	**NB5**	**SH-SY5Y**	**CHLA-90**	**SK-N-SH**	**NBL-S**
VN	% positive cells	70%	75%	80%	10%	70%	50%	50%	30%
	Intensity	+++	+++	70% (++) 10% (+++)	+	++	30% (++) 20% (+++)	+	+
	Location	Cell membrane and neuritic projections		Cytoplasm				Cell membrane	
uPAR	% positive cells	15%	30%	30%	30%	90%	80%	Negative	
	Intensity	++	++	++	++	+++	50% (+++) 30 (++)		
	Location	Cytoplasm		Cytoplasm and Golgi pattern		Golgi pattern	Cytoplasm		
PAI-1	% positive cells	20%	10%	10%	10%	40%	20%	Negative	
	Intensity	+	+	+	+	++	+		
	Location	Cytoplasm							
$\alpha_v B_3$	% positive cells	10%	10%	10%	50%	85%	50%	20%	20%
	Intensity	+	+	+	++	80% (++) 5% (+++)	++	++	+
	Location	Cytoplasm. In case of NB5 and CHLA-90, also in cell membrane.							

MNA and MNNA identification cell lines are marked in dark and light gray, respectively. The staining intensity was graded as high (+++), medium (++), and low (+). The immunocytochemistry of VN was performed with and without serum medium. No differences in VN expression was found.

The range of positive cells for VN was 70-80% and 30-70% with a medium-high and low-medium staining intensity, in MNA and MNNA cell lines, respectively. The location was predominantly in the cytoplasm, cell membrane, and dendritic prolongations. This pattern was a rule for all NB cell lines regardless of *MYCN* status, except for the NB5, MNA cell line, where only 10% of positive cells were observed with low-intensity staining. In the case of uPAR, 15-30%

and 80-90% of positive cells were observed, with a medium and high intensity in almost all MNA and MNNA cell lines, respectively; uPAR staining presented a diffuse cytoplasmic and paranuclear (Golgi-like pattern) expression pattern predominantly. However, two MNNA cell lines (SK-N-SH and NBL-S) were negative for this molecule. Regarding PAI-1 staining, it was positive at 10-20% and 40-50% in MNA and MNNA cells, with a low staining intensity and diffuse cytoplasm location. Remarking that two MNNA cell lines were negative (SK-N-SH and NBL-S). Finally, $\alpha_v\beta_3$ was found in about 10-50% and 20-85% of positive cells in all MNA and MNNA cell lines, with a low-medium staining intensity that was characteristically found as a diffuse pattern cytoplasm and cell membrane locations. **Table 12** shows more detailed information about each cell line and **figure 17** shows the *in vitro* patterns of the biomarkers analyzed.

In conclusion, both cell lines presented high expression of VN, marked differences in the percentage of positive cells, intensity and ubication of uPAR and α_vB_3 expression (lower in MNA cells than in MNNA) and little dissimilarities of PAI-1 expression, being PAI-1 the less abundant VN receptor in the neuroblastic cells analyzed. However, the characterization of these molecules shows their intra culture heterogeneity with different degrees of expression in 2D NB models, confirming our previous results [272, 341, 342].

Taking these aspects into account, we have chosen SK-N-BE (2) and SH-SY5Y to perform a deeper description analysis through the generation of xenografts; the selection criteria is based on the fact that both cell lines had the morphological feature as a predominance of N-type cells [343] and presented specific genetic characteristics each one related to HR-NB patients (MNA and *ALK* mutation, respectively). The molecular aspects of SK-N-BE (2) cell line derive in simulating a tumor situation found in HR-NB patients with relapse, whereas SH-SY5Y represents a tumor relevant condition of 20% of HR-NB patients at the time of initial diagnosis [344]. Comparing these findings with those obtained in human samples, where VN ligands are predominantly expressed by non-tumoral cells is remarkable. The fact that tumor cells expressed these molecules during *in vitro* conditions could be explained because cells have to survive in an environment that is not the natural human macroenvironment forcing them to synthesize the mentioned molecules to promote and support essential needs as an attachment. Moreover, the expression level of PAI-1 that in 2D NB cells is low or even negative, in patients with a metastatic stage was observed that malignant neuroblasts are stimulated to express PAI-1 by adjacent endothelial and stromal cells. The level of PAI-1 increased when coculture NB cell lines with endothelial cells [272] as evidence that the reciprocal interaction between cancer cells and TME determines the recruitment, activation, and reprogramming of stromal, inflammatory and immune cells.

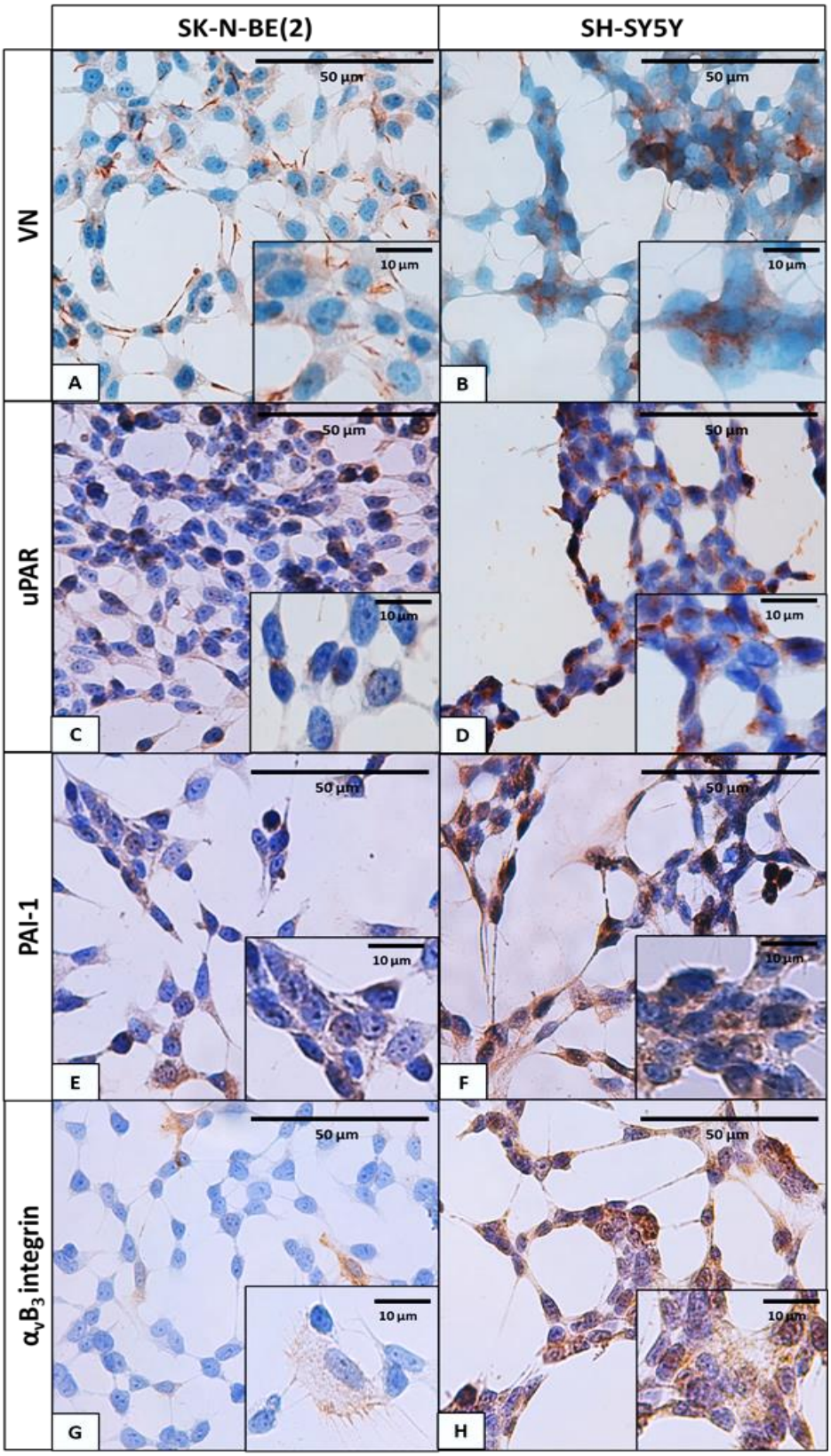

Figure 17. Examples of VN and receptors expression in 2D NB models. 1) SK-N-BE (2), MNA cell line expression patterns A. VN, C. uPAR, E. PAI-1, G. α_vB_3 integrin. 2) SH-SY5Y, MNNA cell line expression patterns: B. VN, D. uPAR, F. PAI-1, H. α_vB_3 integrin. Images at 40x in the overviews and 63x in the close-ups.

3.3. *In vivo* NB models (orthotopic xenografts)

The therapeutic approaches currently used in the treatment of metastatic NB, unfortunately, show limited effectiveness. Modest therapeutic progress, especially in the most aggressive cases of NB, highlights the urgent need for identifying predictive preclinical models to propose more effective therapeutic strategies. Orthotopic xenograft models are relevant tools for *in vivo* drug testing in the early stages against aggressive NB. The main reason is their clinical relevance since they may retain biological characteristics of the tumors [204] and it is a clear advantage to the classic *in vitro* models used for the development of treatments, which are questionable due to the low success rate [345]. Then, we have chosen orthotopic models for studying and targeting molecules that could promote *in vivo* invasion and metastasis since targeted therapy rather than conventional treatment approaches would be more likely to be curative for HR-NB patients. However, as we have recently reported, 3D bioprinting technology can contribute to the standardization of NB-targeted therapies by further reducing the use of laboratory animals [191].

3.3.1. Excellent growth adaptation in deficient VN mice

We have generated orthotopic NB xenografts using the two established cell lines mentioned previously in four-to six-week-old RAG1$^{-/-}$ VN$^{-/-}$ (experimental or VN knockout) and RAG1$^{-/-}$ VN$^{+/+}$ (control or VN wildtype) mice. Several studies affirmed that xenograft tumors for at least two passages can be considered established by observing consistent morphological and molecular characteristics and a good engraftment rate, being from the third generation normally used for pharmacological treatment [346, 347]. Our experimental study arrived until passage 5 to become cells adapted to experimental *in vivo* conditions. The serial passages consisted in choosing 4 representative tumors for each mouse model and cell line of the 10 animals, those that had tumor growth in passage 0 (after local inoculation of cell lines), implanting them in at least two mice successively up to passage 5, to compare tumor growth and morphological and genetic modifications between experimental and control models. All experiments were carried out under the standards and care approved by the institutional ethical animal care committee (reference 2015/VSC/PEA/00083). The *in vivo* experiment described in this research was performed using homozygous mice (the detailed procedure appears in the appendix, *in vivo* experiments section).

The animals that belonged to passage 0 were sacrificed at 8 weeks, allowing a maximum of 16 weeks between the rest of the passages to obtain a morphological, immunophenotypic, and

molecular characterization. In the MNA cell line, we detected tumors in 18 out of 38 mice in the VN-KO group, with a tumor success of 47.4%, compared to 24 out of 37 tumors detected in the VN WT-group (65% success). Regarding, the MNNA cell line, we observed tumors in 25 out of 41 mice in the VN-KO group, which accounts for 61% of engraftment, related to 10 out of 30 in the VN-WT group, that is a 33% of tumor success. Detail information of tumor engraftment is shown in **figures 18-19**.

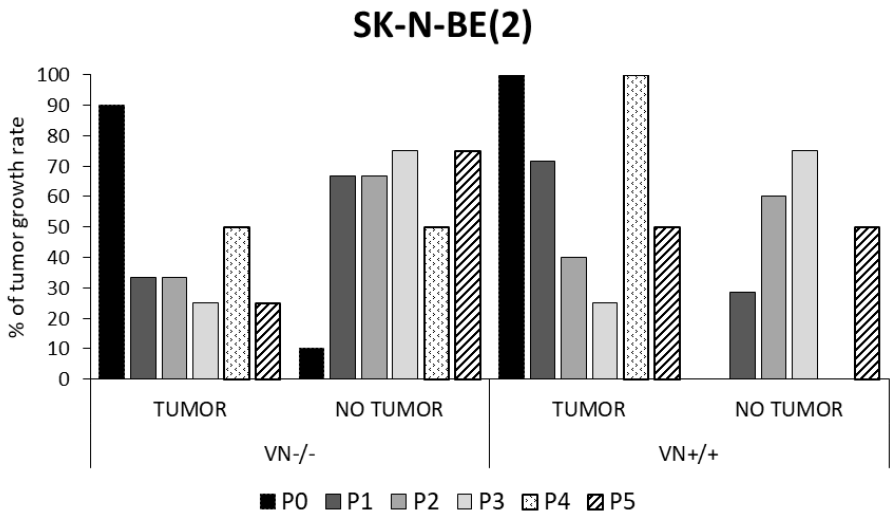

Figure 18. Bar diagrams of percentage (%) tumor growth rate in the MNA-derived xenografts.

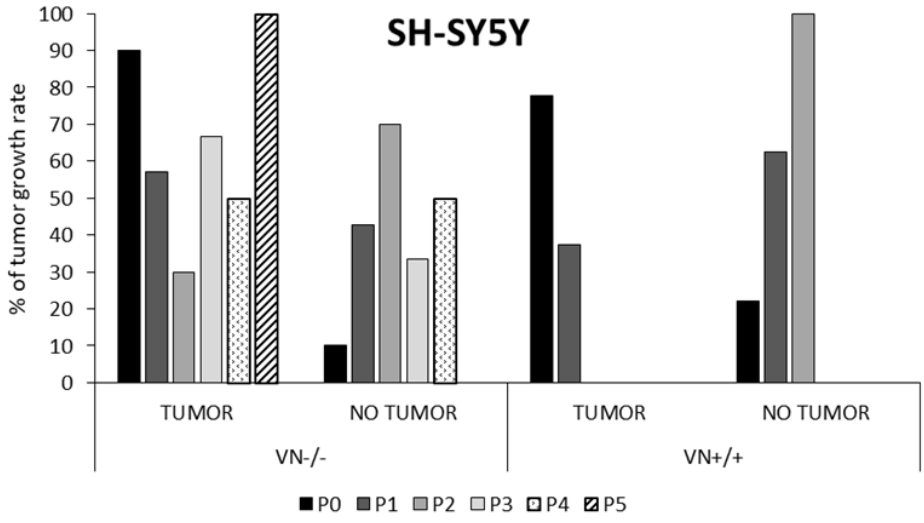

Figure 19. Bar diagrams of percentage (%) tumor growth rate in the MNNA-derived xenografts.

To assess tumor growth rate, tumor volume was measured using a modified ellipsoid formula, [344, 348] in control and experimental models. All tumor volumes were classified

according to the five groups of passages (**figure 20 A-B**) and the three times of necropsy (at 8, 12, and 16 weeks) (**figure 20 C-D**).

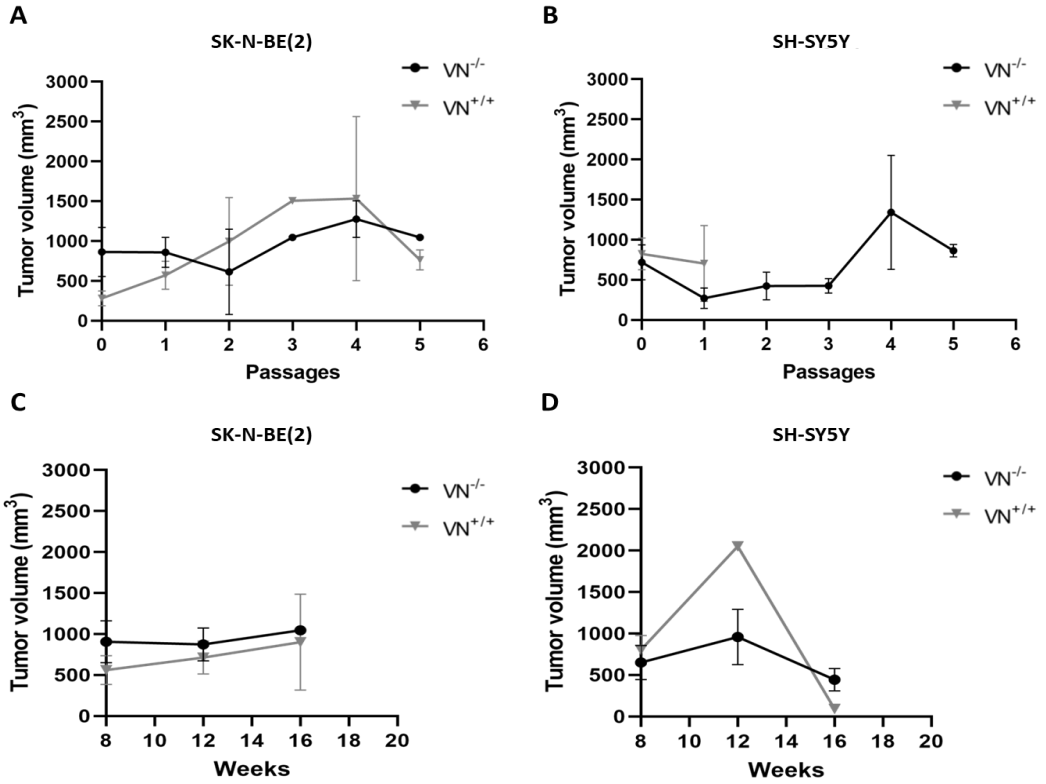

Figure 20. Tumor growth curves. A-C Representation of the MNA cell line, SK-N-BE (2); B-D Illustration of of the MNNA cell line, SH-SY5Y. A-B Volumes according to tumor passage; C-D Volumes according to necropsy time. $VN^{-/-}$: black lines, $VN^{+/+}$: grey lines. Error bars represent the SEM (standard error of the mean). Each passage (p) and weeks (w) had a diferent number (n) of mice with tumor growth. A.$VN^{-/-}$: p0 (n=9), p1 (n=2), p2 (n=2), p3 (n=2), p4 (n=2), p5 (n=1); $VN^{+/+}$: p0 (n=10), p1 (n=5), p2 (n=4), p3 (n=1), p4 (n=2), p5 (n=2). B. $VN^{-/-}$: p0 (n=9), p1 (n=4), p2 (n=3), p3 (n=4), p4 (n=3), p5 (n=2); $VN^{+/+}$ p0 (n=7), p1 (n=3). C. $VN^{-/-}$: 8 w (n=11), 12 w(n=5), 16 w (n=2); $VN^{+/+}$: 8 w (n=14), 12 w(n=6), 16 w (n=4). D. $VN^{-/-}$: 8 w (n=10), 12 w (n=6), 16 w (n=9); $VN^{+/+}$: 8 w (n=8), 12 w (n=1), 16 w (n=1).

For SK-N-BE (2) tumor passages, we observed that significant tumor volume was reached in passage 4 in both mouse models (**figure 20A**). The growth time pattern was constant in both tumor models, presenting a higher tumor volume in the $VN^{-/-}$ model than in the $VN^{+/+}$ (**figure 20C**). Regarding SH-SY5Y tumor passages, we also observed a high tumor volume at passage 4 in the $VN^{-/-}$ model (**figure 20B**). Concerning the growth time pattern of this cell line in $VN^{-/-}$ showed stable growth, while an exponential pattern was observed followed by a contraction pattern in $VN^{+/+}$ (**figure 20D**). Although both cell lines showed high tumor volume in passage 4, we observed a slowdown in tumor growth in the SH-SY5Y cell line in $VN^{-/-}$ mice, which could be related to the non-presence of *MYCN* amplified. The lack evidence of statistically significant results can be explained by the wide range of dispersion of the tumor volume, as well as by the

size of the sample analyzed, since we have not had such as a high graft success rate as that described by Pirazzoli *et al*., [268] (**figures 18, 19 and 20**).

The cellular composition of a tumor greatly influences the growth, spread, immune activity, and other aspects of the xenografts. Reasons, why we did not observe increased tumor growth, include the histological heterogeneity of the selected NB tissue with non-viable areas or presence of minor aggressive subclones, the state of the tumor tissue used (mainly cryopreserved) fueling resistance to growth, not detection of a small tumor growth followed by tumor regression and/or the murine strain (*Rag1*) used with lower susceptibility of tumor growth. Our results showed a similar success rate of tumor growth from fresh/ cryopreserved tissue in MNA xenografts of 50%/45% and in MNNA xenografts of 33%/40%, which agreed with described studies [349, 350]. Related to the issue of the murine strain used, several kinds of research showed that the type of immunodeficient murine host should not affect tumor growth [268, 351]. The low engraftment rate of SH-SY5Y in the control background, although several types of research showed an adequate tumor rate in similar immunodeficient strains [352, 353], could be explained by some reasons mentioned above or by the inconsistent growth behavior and the observed regression event observed in xenografts generated from their parental SK-N-SH cell line [354].

3.3.2. Maintaining cell morphology of patient tumors

Macroscopically, xenograft tumors derived from MNA and MNNA cell lines, both in control and experimental mice models, were limited to the adrenal gland or generated large abdominal solid masses with heterogeneous areas, being MNA tumors more hemorrhagic than MNNA (**figure 21**). We differentiated between metastasis and adjacent implants (invasion versus cancer cells that grew in surrounding tissues such as the spleen, kidney, pancreas, liver, mesentery, or perirenal fat without penetrating them) [355]. Both types of growth can be explained by the propagation behavior found in orthotopic models to specific organs [356]. Tumors showed moderate implant growth in surrounding tissues. The number of metastases that we found in these models was low, located mainly in the liver. As for implants, we find a high number in p0 MNA-derived tumors in $VN^{-/-}$ with statistical significance (p-value: 0.023) compared to p1-5, and no statistical significance in xenografts derived from MNNA (**table 13, appendix**). Regarding metastasis, we observed no significant differences in xenografts derived from the MNA cell line, while xenografts derived from MNNA in the $VN^{-/-}$ model showed a higher state of metastases in p0 compared to p1-5 (p-value: 0.014) nonetheless, in $VN^{+/+}$ the number of metastasis was greater in p1-5 (p-value: 0.016). Detailed data are shown in **table 13** (**appendix**).

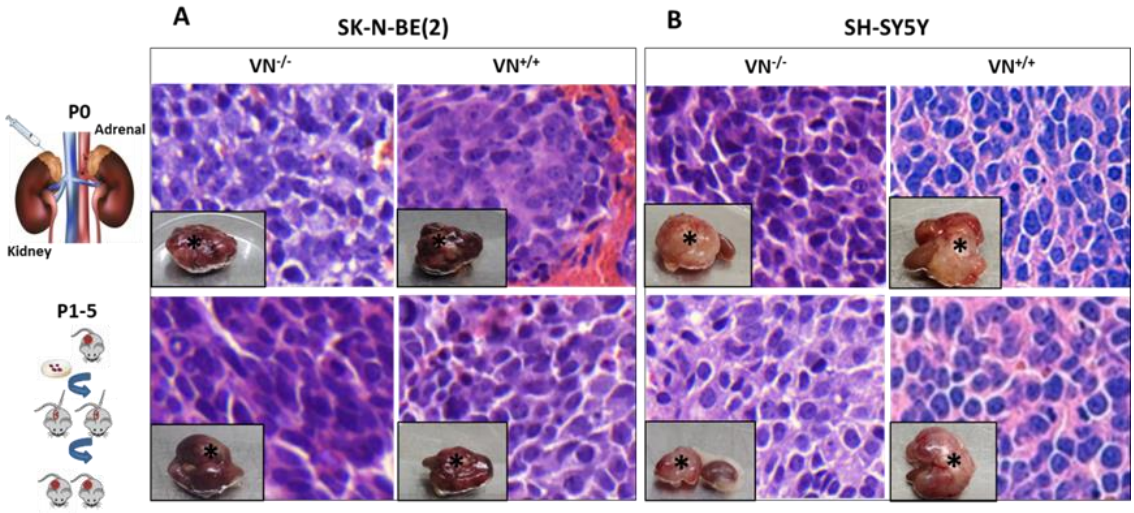

Figure 21. Representative tumor masses (*) and HE stain images of MNA (A) and MNNA-derived xenografts (B) to passages classification (p0 vs p1-5).

We characterized these tumors histologically by HE stain. All tumor xenografts showed the same histological category and grade of differentiation standing out for a uniform pattern of small round blue tumor cells with scant cytoplasm, none or minimal schwannian stroma, no neuropil and numerous mitotic figures and classified as undifferentiated NB category following the INPC system (**figure 21**). To perform the subsequent statistical analysis related to histopathological characterization, we grouped all the tumor-mice into initial (belonged to the passage 0), and subsequent passages (from 1 to 5) keeping a similar sample size per group (SK-N-BE (2) cell line: in $VN^{-/-}$ (p0, n=9; p1-5, n=9) and in $VN^{+/+}$ (p0, n=10; p1-5, n=14); SH-SY5Y cell line: in $VN^{-/-}$ (p0, n=9; p1-5, n=16) and in $VN^{+/+}$ (p0, n=7; p1-5, n=3)). We subjectively assessed the percentage of neuroblastic cells, necrosis, and hemorrhagic areas without finding any statistically significant variation (**tables 14-16, appendix**). SK-N-BE (2) tumors present a minor amount of neuroblasts and a greater percentage of necrosis and hemorrhage in $VN^{-/-}$ p0 and p1-5 compared to $VN^{+/+}$ tumors. These results could indicate that this cell line tends to be more aggressive at initial passages to adapt to a VN deficient environment. SH-SY5Y, presented a minor amount of neuroblasts in $VN^{-/-}$ p0 tumors, however, the number of neuroblasts increases in p1-5 tumors in comparison to $VN^{+/+}$ in those tumor passages. The percentage of necrosis is higher in $VN^{+/+}$ tumors and the hemorrhage decreases respect to $VN^{-/-}$ tumors in p0 and p1-5. Comparison of both cell lines evidenced that the percentage of neuroblastic cells is quite similar, existing a higher amount of necrosis and hemorrhage in xenograft tumors derived from SK-N-BE (2), mainly in the $VN^{-/-}$ model. Since these two features are hallmarks related to poor prognosis in tumors [148], it would indicate higher tumor cell proliferation and aggressive behavior in SK-N-BE (2) cells than in SH-SY5Y cells. These findings are confirmed by other studies, where the

authors observed an association of tumor necrosis and hemorrhagic phenotype with MNA [357, 358].

3.3.3. Hallmarks of microenvironmental components

Taking into account the relevant role of the TME in tumor progression, metastasis, and treatment responses, we investigated different stromal elements (VN and other ECM components, vascular structures, and immune cell infiltration) and cellular receptors (uPAR, $\alpha_v\beta_3$ integrin, and PAI-1) in xenografts derived from MNA and MNNA cell lines, grouping them as p0 vs p1-5. We performed a subjective assessment following the staining criteria below: negative = no presence or <5% of stained area; positive 1 + = weak staining, 5-10% of stained area; positive 2 + = moderate staining, 10-50% of stained area and positive 3 + = strong staining,> 50% of stained area.

Neuroblastic cells increased *in vivo* VN expression compared to *in vitro* conditions. This data emphasizes the secretory ability of the malignant neuroblasts related to the previous evidence defined by us in human NB (**article II**). VN staining was found as a pattern of the cell membrane and cytoplasmic stains, without observing differences between the two mice models or cell lines; these findings suggest, at least when we subjectively analyzed the VN amount, that VN deficiency of the host macroenvironment does not influence tumor synthesis of VN; (**figures 22 and 23**). Besides, we performed inoculations of the two cell lines cultivated over a period of 3-7 days in serum-free medium and found that the xenografts obtained showed no differences in the VN staining pattern.

uPAR staining was found in stromal immune cells as described above in human NB samples, also characterized by a Golgi-like staining pattern (**figures 22 and 23**). In MNA-derived xenografts we observed a statistically significant increase in the expression level of this molecule in both mouse models: uPAR was negative in p0 tumors (100% of the cases, 9/9), being positive in p1-5 tumors, (33% of the cases, 3/9) in $VN^{-/-}$; $VN^{+/+}$ p0 tumors were not positive (100% of the samples, 10/10), and in tumors p1-5 (36%, 5/14) were positive (**figures 23 and 24**). Xenografts derived from the MNNA cell line were characterized by a positive expression also characterized by a Golgi-like pattern without discrepancies in the four groups analyzed (**figures 22 and 24**).

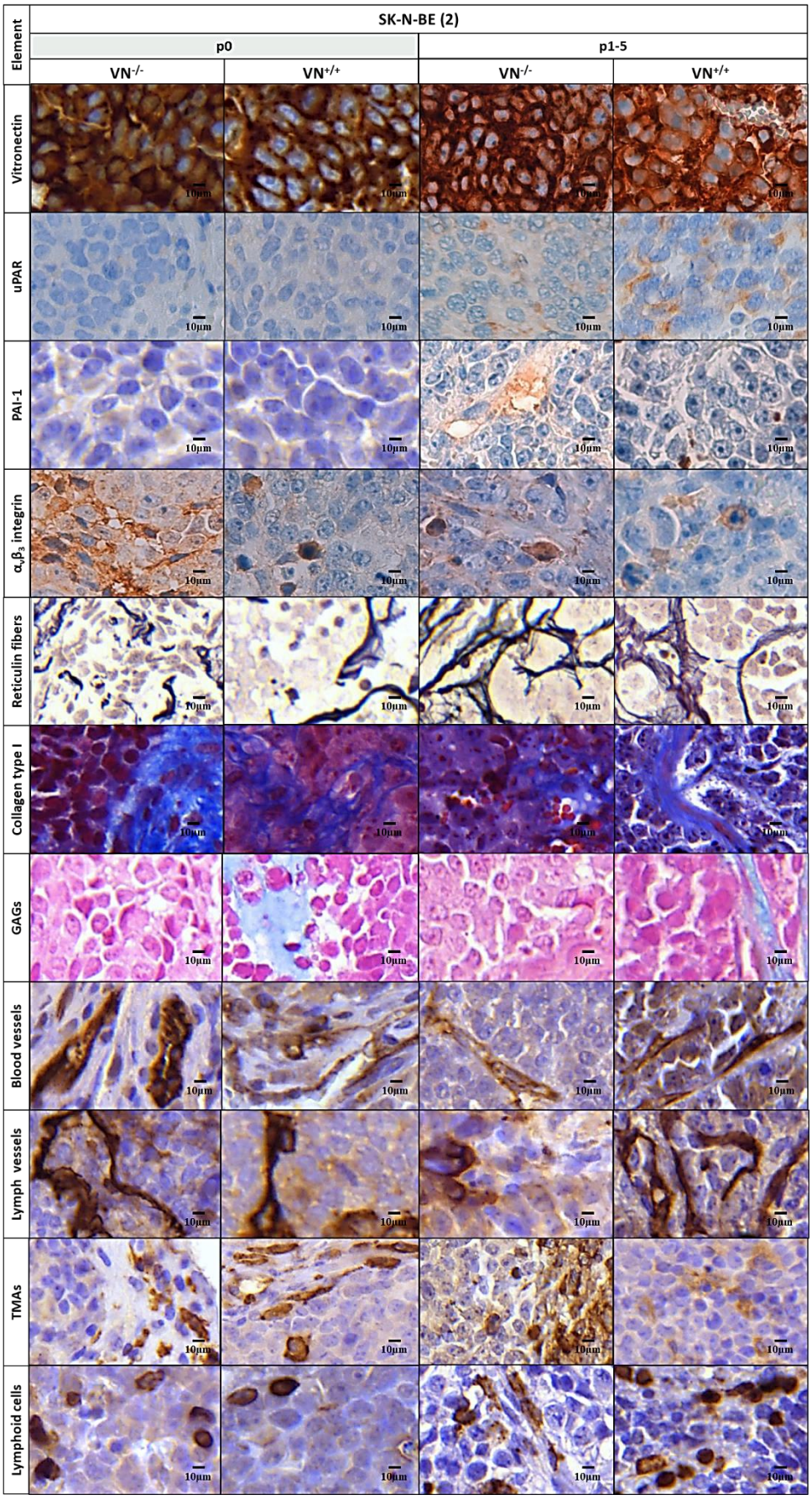

Figure 22. Histological sections of different stains of TME elements in MNA-derived xenografts. Images at 63x.

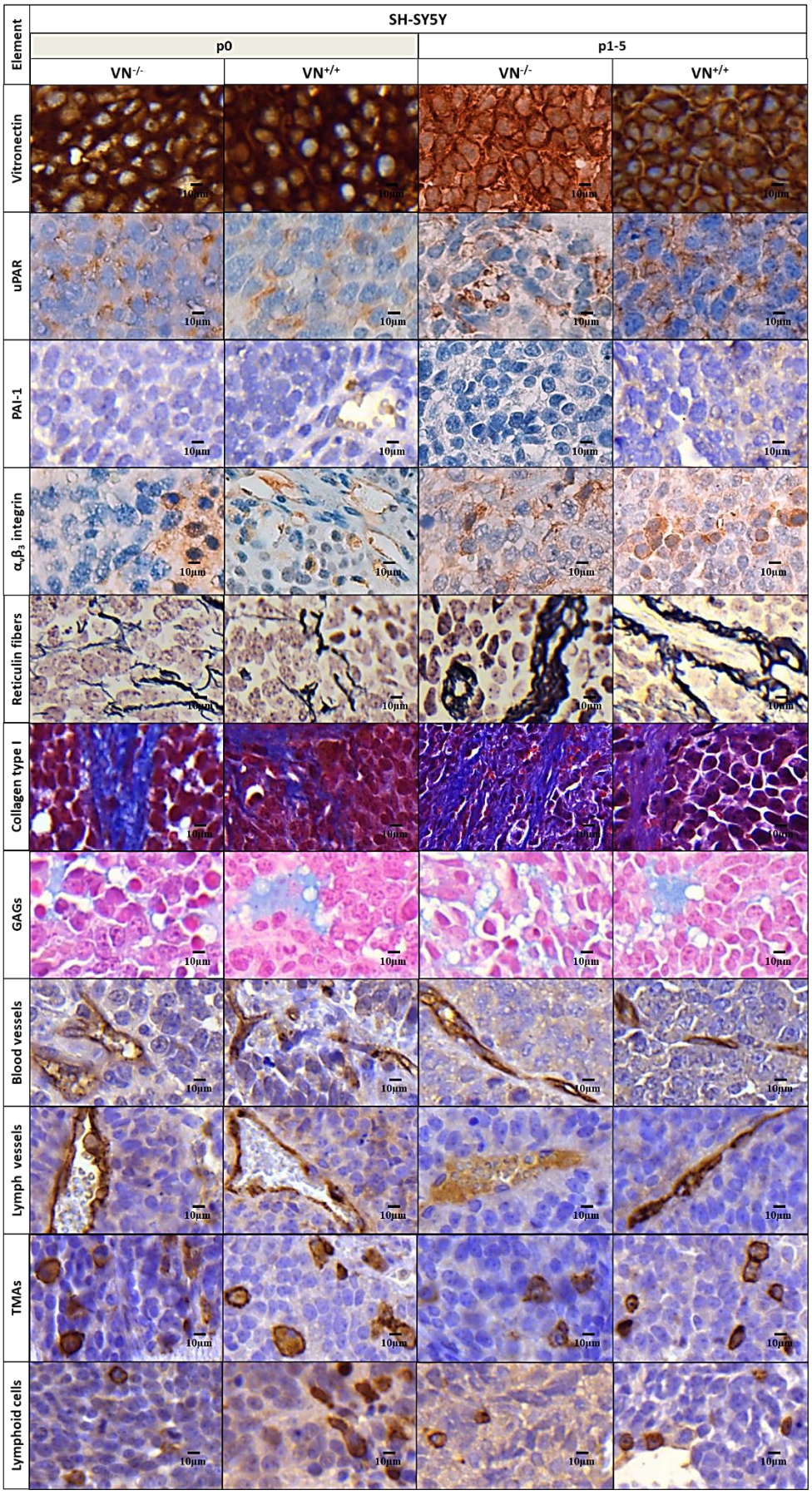

Figure 23. Histological sections of different stains of TME elements in MNNA-derived xenografts. Images at 63x.

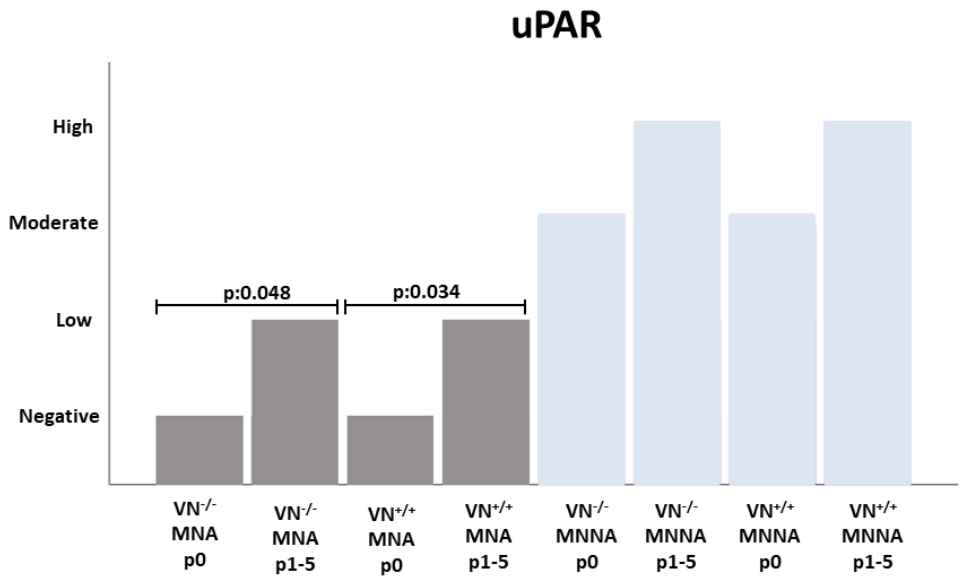

Figure 24.uPAR expression in MNA and MNNA-derived xenografts according to their aggrupation in passages. Statistical significant relationships are shown.

These findings are related to the greater amount of this molecule secreted by SH-SY5Y under *in vitro* conditions. The *in vivo* expression of uPAR by these tumors in both models of VN mice together with the high expression of VN could explain that no differences in tumor growth were found. It would also reinforce the central idea of the research developed by Pirazzoli *et al*., where they observed that an interaction between the two molecules is required for the development of tumors [268]. In addition, NB researches have shown that inhibition of uPAR using CRISPR / Cas9 technology evidenced a decrease in cell proliferation as well as the enabling role in the EMT process (derived from the interaction of uPAR/uPA reduces cell adhesion) [359, 360]. Our results, in combination with these recent observations, would allow uPAR to be considered as a possible NB therapeutic target.

As for PAI-1, no important distinction was found, characterized by a very low or negative presence as our *in vitro* results have already shown (**figures 22 and 23**).

Regarding α_vB_3 integrin, the samples showed positivity in endothelial cells and monocyte/macrophage lineage as described above in human NB (**figures 22 and 23**), remarking that in MNA-derived xenografts, significant differences were found in p0 $VN^{-/-}$ tumors that showed a higher positive expression of this integrin than in p1-5 (67% (6/9) moderate and 11% (1/9) strong vs 89% (8/9) weak and 11% (1/9) moderate, respectively), while the expression in $VN^{+/+}$ was positive without statistically significant modifications as in the MNNA-derived xenografts (**figure 25**). The fact that xenografts derived from MNA cell lines increase the α_vB_3 integrin expression, in contrast to the *in vitro* situation and essentially in the p0 tumors of the

VN KO model may be due to the need to create "special" anchorage points to establish a suitable environment for tumor proliferation while maintaining a stable positive expression in successive passages to promote cell migration. These results could evidence the cooperation between VN and α_vB_3 integrin in NB, as described in ovarian cancer, where it has been shown that by cleaving the interactions of VN- α_vB_3 integrin and FN- α_5B_1 integrin by MMP-2, tumor cells achieve rapid migration [361]. In fact, for tumor cell migration, continuous attachment and detachment of cells concerning ECM components are required; tumor cells need to break down strong adhesions with ECM, as well as molecules that guide their migration [361]. The modified expression of uPAR and $\alpha_v\beta_3$ integrin with an increase of VN characterizing xenografts derived from the MNA cell line in $VN^{-/-}$ can be considered as key conditions in successful tumor growth; it has been shown that the interplay between these molecules can affect intracellular pathways related to cell adhesion and migration [362, 363].

For xenografts derived from MNNA, we found no significant discrepancies in any expression of this molecule to the 2D condition, being able to be explained by their already high levels of *in vitro* expression. Therefore, it seems that this cell line does not need to modify them to proliferate in the *in vivo* condition.

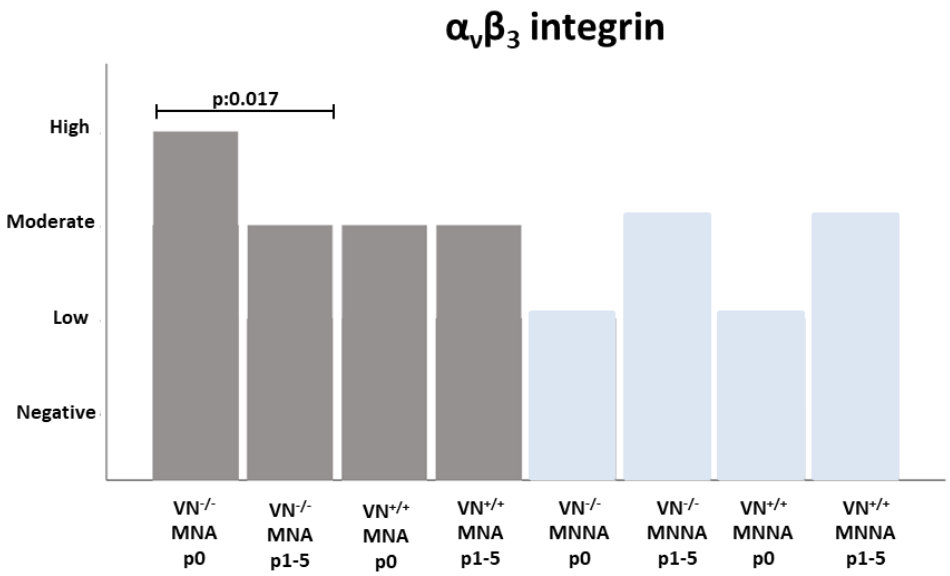

Figure 25. $\alpha_v\beta_3$ integrin expression in MNA and MNNA-derived xenografts according to their aggrupation in passages. Statistical significant relationships are shown.

Aggressive human NB ECM contains numerous reticulin fibers and few collagen type I fibers and GAGs [147, 250, 251]. Similarly, reticulin fibers were found surrounding blood vessels as well as forming bundles or networks in the *in vivo* models used. Collagen type I fibers distribution was limited to large trabecules and around large blood vessels. GAGs were scarce, appearing in

fibrous areas of the stroma. Previous investigations have observed that orthotopic NB models retain stromal traits of aggressive lesions, finding that the murine stroma exhibits important clinical features of aggressive and metastatic NB [211, 214]. We found a statistically significant increase in the number of reticulin fibers in advanced passages in MNA-derived xenografts in both mouse models: in $VN^{-/-}$ p0 66% were positive (6/9 cases, with weak amount) and in p1-5 100% were positive (9/9 cases, presenting 83% moderate amount and 17% high amount); in $VN^{+/+}$ p0 70% were positive (7/10 cases with a weak amount) and in p1-5 100% were positive (10/10, characterized 20%, 60% and 20% with few, moderate and high amount (**figure 26**)). In the MNNA-derived xenografts, the findings showed a notable difference between passages in the $VN^{+/+}$ background, being low in advanced passages: in p0, 100% were positive (7/7 cases, 71% with a slight and 29% a moderate quantity) and in p1-5, 67% not presented reticulin fibers and 33% have a small amount (**figure 26**). As for collagen type I fibers, in the MNA-derived xenografts, the amount decreases in both mice models, being only statistically significant in $VN^{-/-}$ where in p0, 100% of the cases were positive (9/9) in comparison to p1-5 with 83% of the cases negative (5/6 cases). No differences in the amount of collagen type I were found in MNNA-derived xenografts (**figure 27**). Regarding GAGs, the MNA-derived xenografts in $VN^{-/-}$ were lacked this ECM element, whereas a low amount was observed in the $VN^{+/+}$: in p0 50% presented some positivity (5/10 cases) and in p1-5 20% had positivity (2/10); no difference was observed in the MNNA-derived xenografts (**figure 28**).

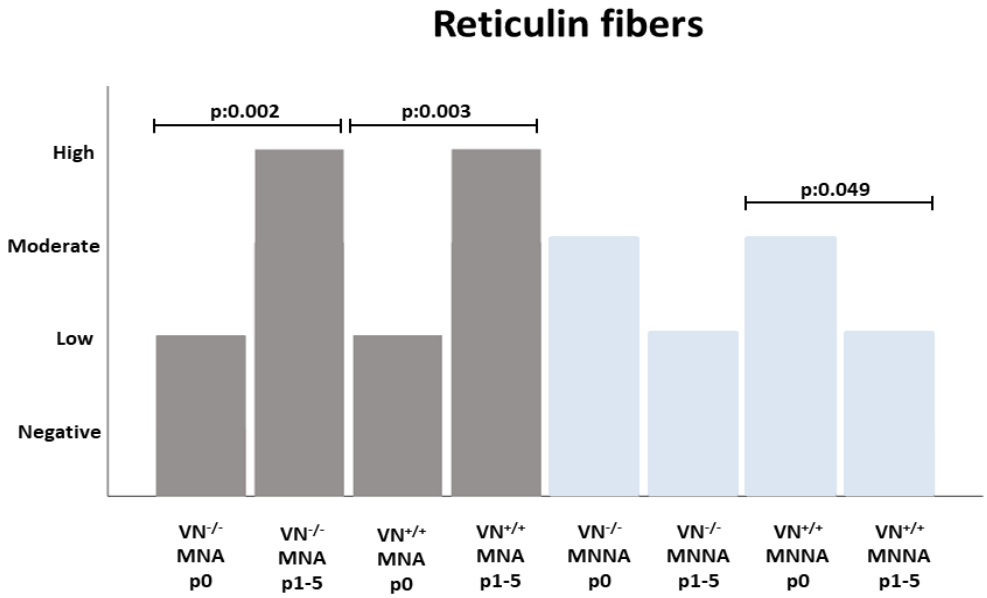

Figure 26. Reticulin fibers amount in MNA and MNNA-derived xenografts according to their aggrupation in passages. Statistical significant relationships are shown.

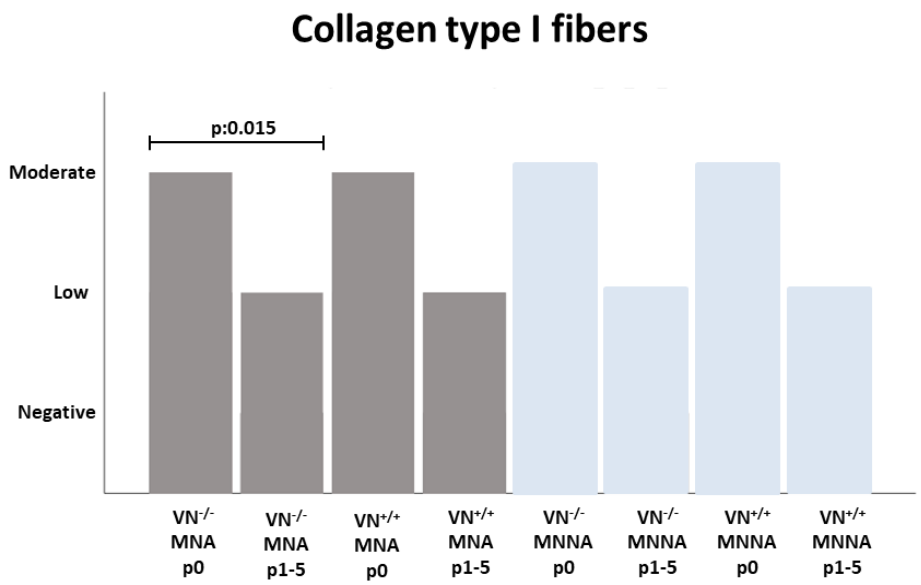

Figure 27. Collagen type I fibers distribution in MNA and MNNA-derived xenografts according to their aggrupation in passages. Statistical significant relationships are shown.

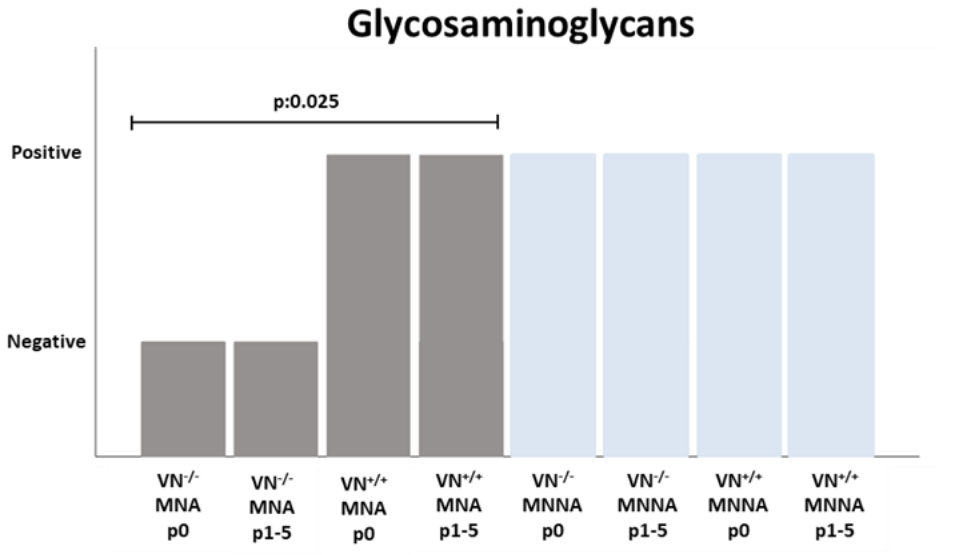

Figure 28. GAGs distribution in MNA and MNNA-derived xenografts according to their aggrupation in passages. Statistical significant relationships are shown.

All these ECM elements imply that the MNA-derived xenografts, mainly in the $VN^{-/-}$ background acquire matrix features related to aggressiveness which facilitate proliferation and invasion of tumor cells, as described in section 3.1 in human NB. Indeed, several investigations have observed an association between a great rigidity of the ECM, which is represented by disorganization and/or increase in the quantity of some elements, with high tumor aggressiveness [364, 365].

The orthotopic models are vascularized tumors characterized by presenting tortuous vessels (blood and lymphatic) as it has been described previously [211, 356] (**figures 22 and 23**). To describe the vascular component, we used the mouse CD34 antibody to detect murine endothelial cells. We did not find relevant differences between MNA and MNNA-derived xenografts. With regard lymph vessels results, we used the mouse-specific LYVE-1 antibody and found significant statistical associations: MNA-derived xenografts were characterized by a decrease in the amount between passages in $VN^{-/-}$ mice [in p0, 33% (3/9 cases) had a low amount and 66% (6/9 cases) a moderate amount, compared to 100% of samples with a low amount (6/6) in p1-5]; whereas a stable and moderate amount of lymph vessels was found in all passages from $VN^{+/+}$. Regarding MNNA-derived xenografts, the amount of lymph vessels also decreases in more advanced passages: in $VN^{-/-}$ mice, p0 44% presented a scant amount (4/9 cases) and 56% a moderate amount (5/9 cases) compared to 100% of samples (6/6) in p1-5 with a low amount; in $VN^{+/+}$ mice, 43% (3/7 cases) of p0 was characterized by a low amount and 57% (4/7 cases) by a moderate amount compared to 33% with a weak in p1-5 (**figure 29**). These results indicate that the tumor xenografts contained numerous blood and lymphatic vessels related to angiogenesis and lymphangiogenesis processes in aggressive NB [255, 366] remarking the MNNA-derived xenografts from $VN^{+/+}$ was the group with minor lymphatic vessel density.

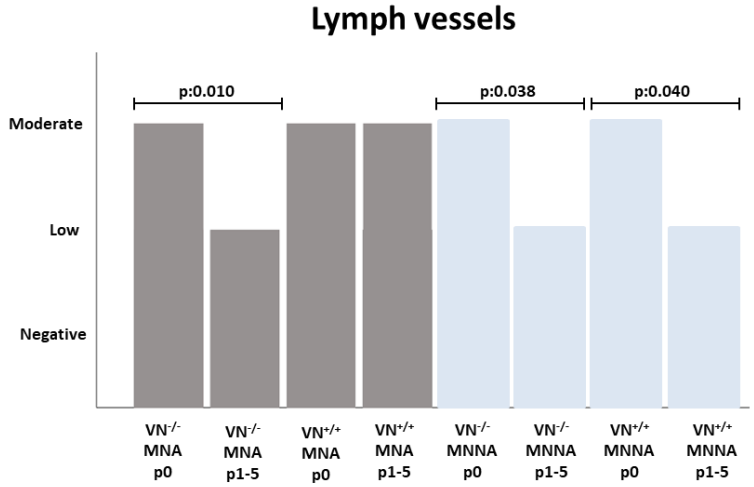

Figure 29. Lymph vessels distribution in MNA and MNNA-derived xenografts according to their aggrupation in passages. Statistical significant relationships are shown.

Concerning the immune cell infiltration compartment, we used the F4/80 and CD45 antibodies to detect murine TAMs and lymphoid cells in the NB orthotopic xenografts. We observed, as clusters in stromal or single cells in perivascular areas, a moderate and low amount of intratumoral **F4/80** and **CD45** positive cells, respectively (**figures 22 and 23**) without any relevant difference between the xenografts. Our results were confirmed by previous studies that

showed a relation between TAMs infiltration with metastatic NB and a high population of TILs (predominantly T cells) correlated with better survival [367, 368].

3.3.4. VN cooperation in genomic instability

To investigate whether the MNA and MNNA-derived xenografts that grown in $VN^{-/-}$ host mice recapitulate the genetic features of the original cell lines or acquire genomic alterations that might confer growth advantage, we performed aSNP and new generation sequencing using a customized NB mechanosequencing panel (NB-mechanopanel (**figure 30, appendix**) from frozen and paraffin-embedded tumor tissues. In addition, as tumor heterogeneity is a hallmark in cancer [148], we also performed aSNP from liquid biopsy (circulating tumor DNA, ctDNA) of some mice. As for tumor xenografts, we have performed the genetic characterization in representative samples, choosing the longest and entire phylum. The genomic profiles from SK-N-BE (2) and SH-SY5Y cultured in 2D, showing the existence of previously described SCAs and gene mutations [335, 337, 369].

Regarding MNA-derived xenografts, from p0 to p3 and p5 were analyzed in $VN^{-/-}$ and $VN^{+}/^{+}$, respectively. We have found: 1) SCAs that were retained in $VN^{-/-}$ and $VN^{+/+}$: 3p- and 17pq-. 2) Other SCAs that were turned into the smallest region of overlap (SRO) in $VN^{-/-}$: 1p-(21.3-12, 2 2Mb) that contains genes related to ECM proteins (*COL11A1*) and for the nervous system development (*NTNG1* and *NGF*); +2p (pter-21, 43 Mb) in p0 and p1, being shorter in p2 and p3, and the fragment of the chromothripsis-like 21q-(22.13-22.2). 3). New chromosomal aberrations in $VN^{-/-}$: +1q (21.1-1-qter, 105 Mb) (where are genes related to cytoskeleton (*ARPC5* and *ACTN2*)), laminins (*LAMB3*, *LAMC1* or *LAMC2*) and α10 integrin (*ITGA10*), 4 focal chromosomal aberrations (FSCA): 9p-(24.3), +9p (24.3-24.2), 9q- (21.13) and 9q- (21.13-21.2) and a SCA of 8 Mb (+9q (21.2-21.33)) on chromosome 9. A fact to remark is that 9p-(24.3) contains two genes associated with migration (*KANK1* and *DOCK8*). On the other hand, some SCAs that appeared on SK-N-BE (2) cell line in chromosomes 7,11,19 and 20 were not present or only in a scant cell proportion in $VN^{-/-}$. The SCAs in $VN^{+/+}$ showed an unsteady behavior between tumor passages compared to $VN^{-/-}$, they experimented a change of 1p-(21.3, 96 Mb) by a copy number/neutral loss of heterogeneity (CNLOH); and from p3 to p5 some new SCAs were added, missing others that appeared in the cell line as +7q (32.3-qter, 28.5 Mb) and the chromothripsis-like on chromosome 21. This situation can be explained by investigations that described this cell line as genetically heterogeneous and also by the observation of SCA fluctuations throughout the passages in various xenografts of different tumor types [369, 370] (**figure 31**).

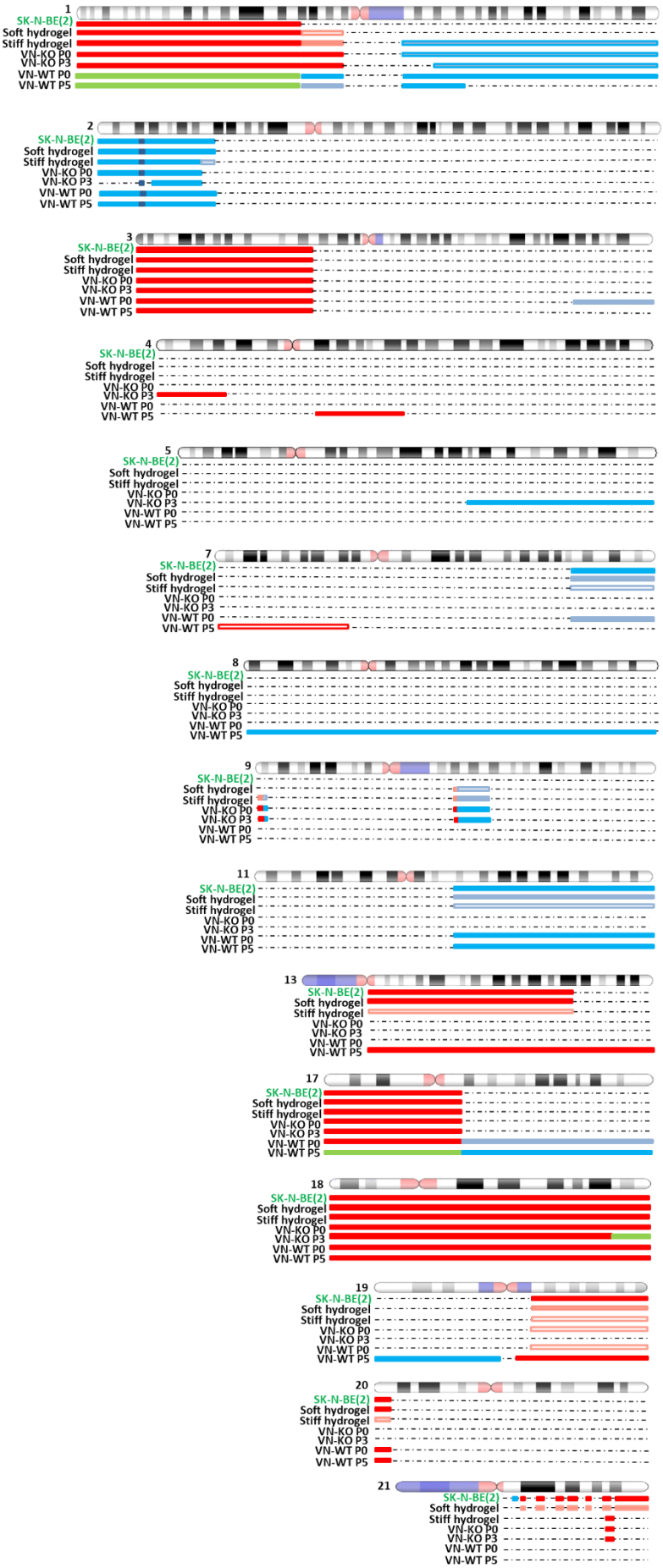
1
SK-N-BE(2)
Soft hydrogel
Stiff hydrogel
VN-KO P0
VN-KO P3
VN-WT P0
VN-WT P5
2
SK-N-BE(2)
Soft hydrogel
Stiff hydrogel
VN-KO P0
VN-KO P3
VN-WT P0
VN-WT P5
3
SK-N-BE(2)
Soft hydrogel
Stiff hydrogel
VN-KO P0
VN-KO P3
VN-WT P0
VN-WT P5
4
SK-N-BE(2)
Soft hydrogel
Stiff hydrogel
VN-KO P0
VN-KO P3
VN-WT P0
VN-WT P5
5
SK-N-BE(2)
Soft hydrogel
Stiff hydrogel
VN-KO P0
VN-KO P3
VN-WT P0
VN-WT P5
7
SK-N-BE(2)
Soft hydrogel
Stiff hydrogel
VN-KO P0
VN-KO P3
VN-WT P0
VN-WT P5
8
SK-N-BE(2)
Soft hydrogel
Stiff hydrogel
VN-KO P0
VN-KO P3
VN-WT P0
VN-WT P5
9
SK-N-BE(2)
Soft hydrogel
Stiff hydrogel
VN-KO P0
VN-KO P3
VN-WT P0
VN-WT P5
11
SK-N-BE(2)
Soft hydrogel
Stiff hydrogel
VN-KO P0
VN-KO P3
VN-WT P0
VN-WT P5
13
SK-N-BE(2)
Soft hydrogel
Stiff hydrogel
VN-KO P0
VN-KO P3
VN-WT P0
VN-WT P5
17
SK-N-BE(2)
Soft hydrogel
Stiff hydrogel
VN-KO P0
VN-KO P3
VN-WT P0
VN-WT P5
18
SK-N-BE(2)
Soft hydrogel
Stiff hydrogel
VN-KO P0
VN-KO P3
VN-WT P0
VN-WT P5
19
SK-N-BE(2)
Soft hydrogel
Stiff hydrogel
VN-KO P0
VN-KO P3
VN-WT P0
VN-WT P5
20
SK-N-BE(2)
Soft hydrogel
Stiff hydrogel
VN-KO P0
VN-KO P3
VN-WT P0
VN-WT P5
21
SK-N-BE(2)
Soft hydrogel
Stiff hydrogel
VN-KO P0
VN-KO P3
VN-WT P0
VN-WT P5

Figure 31. Schematic representation of the chromosomal aberrations detected by aSNP in some of the samples derived from the SK-N-BE (2) cell line. SK-N-BE (2) refers to the genomic analysis of the cell line acquired from the ATCC and cultured in 2D. Soft and stiff hydrogels refer to cells cultured in gelatine scaffolds with 0.5% and 2% of methacrylated alginate respectively. Tumor samples from the experimental $VN^{-/-}$ mice (VN-KO) and control $VN^{+/+}$ mice (VN-WT) are followed by the initial and the last analyzed passage (P0-P5). For each altered chromosome, gains of genomic material are represented in blue, deletions in red, and CNLOH in green boxes. MNA is highlighted with a small purple box. As the percentage of cells affected by the chromosomal aberrations decreases the background color of the box representing them becomes lighter.

As for MNNA-derived xenografts, we did not observe SCA variations compared with the cell line in culture, only in $VN^{+/+}$ p1 remark a loss (+2p (ter-16.3, 49 Mb)) that could be related to the unsuccessful engraftment in this mice background (**figure 32**).

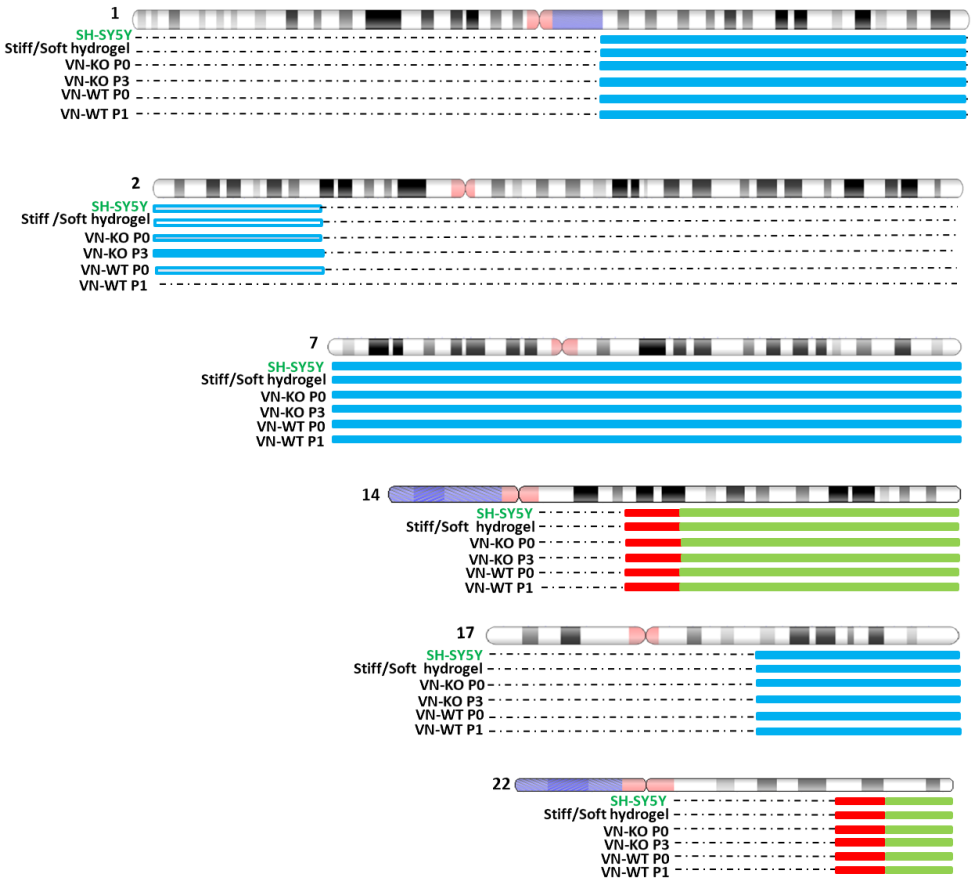

Figure 32. Schematic representation of the chromosomal aberrations detected by aSNP in some of the samples derived from the SH-SY5Y cell line. SH-SY5Y refers to the genomic analysis of the cell line acquired from the ATCC and cultured in 2D. Soft and stiff hydrogels refer to cells cultured in gelatine scaffolds with 0.5% and 2% of methacrylated alginate respectively. Tumor samples from the experimental $VN^{-/-}$ mice (VN-KO) and control $VN^{+/+}$ mice (VN-WT) are followed by the initial and the last analyzed passage (P0-P5). For each altered chromosome, gains of genomic material are represented in blue, deletions in red, and CNLOH in green boxes. As the percentage of cells affected by the chromosomal aberrations decreases the background color of the box representing them becomes lighter.

With regard, the intratumor genetic heterogeneity in MNA and MNNA-derived xenografts an elevated consistency was observed when the aSNP of ctDNA were done, except from the

single detection in ctDNA of 2 SCAs in MNA-derived xenografts in $VN^{+/+}$, one in p1 and other in p2 but a lower proportion of clones

Besides, the use of a customized NB sequencing panel (**figure 30, appendix**) confirmed the previous aSNP results showing that both SK-N-BE (2) cell line and its derived xenografts, presented the two mutations described in *TP53* and *ATRX* genes, as well as the SH-SY5Y cell lines and derived tumors presented the *ALK* mutation. Moreover, the COL11A1 variants (p.I1590= and p.P1323L) and two polymorphisms of DOCK8 (intronic variants of c.1680-9045C>G and c.54-20738C>T) were not detected in MNA-derived xenografts of $VN^{-/-}$, finding them in the rest of samples and even in the cell line (0.4 of allelic frequency).

These modifications evidenced a clonal selection of cells that responds to experimental biotensegral signals acquiring a competitive cell phenotype as described in other studies [365, 371]. A remarkable fact that we have observed was that the genomic aberrations mentioned above in $VN^{-/-}$ tumors appeared when SK-N-BE (2) cell line was cultured in stiffer scaffolds for long times in an independent 3D study using hydrogels as a scaffold [191]. These results together with recent researches where it has been observed that SK-N-BE (2) presents great proliferation rate in rigid 3D scaffolds [191], and with the fact that 3D growing cells capture phenotypic heterogeneity [372], suggest a cancer clonal evolution by selective pressures also in the *in vivo* VN host deficient used. No effect of the environment into the genomic compartment was evidenced in the 3D culture of SH-SY5Y [373].

CHAPTER 4. Conclusions/Conclusiones

Our research approach shifts focus away from tumor cells alone, towards considering tumors as complex and dynamic microenvironments with interactions between cells, fibers, vascular structures, and various molecules, whose physical properties emerge in response to mechanical stimuli, with aim of using them as therapeutic targets. In children suffering from high-risk neuroblastoma, a comprehensive view of their disease is needed, taking into account the tumor macroenvironment (various circumstances of patients and their environment) and applying the previously outlined microenvironmental approach, to elucidate factors that improve pre-treatment risk stratification and/or that could be validated as possible therapeutic targets.

The research carried out in this doctoral thesis, showing the necessity and benefits of microscopic study of neuroblastoma elements, has led to the following conclusions:

1. Vitronectin is a significant component in the extracellular matrix of neuroblastic tumors, produced mainly by undifferentiated neuroblastic cells and some stromal cells, and increased expression by tumor cells is associated with unfavorable independent variables in the INRG classification system.

2. The novel and precise morphometric tools that we developed allow the characterization of the recently synthesized, territorial vitronectin pattern, with an intracellular and pericellular location, and the interterritorial vitronectin pattern, earlier incorporated into the extracellular matrix, located away from the tumor cell. With these tools, we can confirm an elevated presence of territorial vitronectin in neuroblastic tumors with aggressive behavior. Future validation studies are necessary to prove that territorial vitronectin helps generate the biomechanical properties of tumor cell attachment-detachment with the surrounding elements, promoting cell migration.

3. Mathematical methodology based on graph theory has been automatized for analysis of histopathological neuroblastoma images, and can objectively capture the predominant pattern of the arrangement of vitronectin in the tumor. This methodology has detected two important topological characteristics of territorial vitronectin, the Euler number and the branching, which as independent biological factors in our tumor cohort, improve neuroblastoma patient classification by pre-treatment risk stratification system, and tumor genomic instability, respectively. This described organizational pattern of territorial vitronectin, modifying the architecture of the tumor extracellular matrix and creating preferential migration tracks and therefore aggressive tumor behavior, needs validation in international collaborative studies.

4. Vitronectin is an extracellular matrix protein that interacts with several receptors, building interaction points between cell-cell and cell-extracellular matrix. Expression of vitronectin, uPAR, $\alpha_v\beta_3$ integrin, and PAI-1 by tumor and/or stromal cells in human tumor samples infers that these molecules could play a multifunctional role in conjunction with other molecules. This reinforces the need to continue investigating other vitronectin interactions, given their key importance in the tumor stroma of neuroblastoma.

5. 2D neuroblastoma cultures show that both *MYCN*-amplified and non-amplified cell lines express vitronectin. Some variations in uPAR and α_vB_3 integrin expression patterns can be observed, both to a lesser extent in *MYCN*-amplified cells, and the particularly low PAI-1 expression in all the cell lines studied underlines that it is the least abundant vitronectin receptor. In synthesis, the heterogeneity of neuroblastoma cell lines is also evident in the expression of these biomarkers.

6. Tumors derived from *in vivo* orthotopic models retain the histopathological characteristics of patient tumors. Adequate growth of the neuroblastoma cell lines studied in the vitronectin-deficient host, VN-KO mice, has been evidenced. Emphasizing slow tumor growth in the SH-SY5Y cell line with *ALK* gene mutation. Tumor results in terms of percentage of neuroblastic cells, necrosis, and hemorrhage show that SK-N-BE (2), *MYCN*-amplified cells, adapt more aggressively to the vitronectin-defective *in vivo* macroenvironment. We confirm that mutation and amplification of *ALK* and *MYCN* genes, respectively, in our model generates differences in aggressiveness, in parallel to what is observed in patients.

7. Neuroblastic cells from both studied cell lines show increased vitronectin expression in xenotransplanted tumors compared to *in vitro* culture. Modulation of vitronectin secretion appears to be a strategy by which malignant neuroblasts respond to local microenvironmental *in vivo* changes. The host vitronectin-deficient macroenvironment does not seem to influence *in vivo* vitronectin synthesis, although high levels of territorial vitronectin and *MYCN* amplification, together with modified $\alpha_v\beta_3$ integrin expression and increased uPAR expression in SK- N-BE (2) xenografts are key conditions for more pronounced tumor progression.

8. Integrating the constant remodeling processes of the multiple extracellular matrix elements occurring within the macro-microenvironment tumor, related to stromal changes, has clinical and therapeutic importance in our tumor cohort. The proposed stromal grade classification provides predictive patterns of reticular fibers, vitronectin, and immune cells that have to be considered as important targets in the tumor stroma of neuroblastoma patients.

9. Morphometric and topological analysis, applied in combination to study the intricate network of elements that build the neuroblastoma microenvironment, such as vitronectin, fibrous scaffolding, and the vascular system, demonstrates that adding morphometric characteristics of blood vessels (sinusoids shape and metarterioles deformity) to the previous topological model of vitronectin improves pre-treatment risk stratification and the criteria of tumor genetic instability.

10. The characteristics associated with stiffness of the extracellular matrix described in aggressive neuroblastoma are maintained in the tumor passages of orthotopic models. SK-N-BE(2) derived xenografts show a decrease in glycosaminoglycans along with an increase in reticular fibers in the vitronectin-deficient model, whereas non-remarkable differences were observed in SH-SY5Y-derived xenografts.

11. The influence of tumor macro-microenvironments on the cellular adaptation process in the vitronectin-deficient *in vivo* model is confirmed by the pattern of intratumoral genetic heterogeneity of segmental chromosomal alterations of *MYCN*-amplified cells, SK-N-BE (2), and the stable genomic pattern of the *ALK*-mutated cells, SH-SY5Y.

Evaluating the combined application of morphometric, topological and genetic strategies in human tumors and *in vitro* and *in vivo* systems to determine the contact points of the tumor cell with its extracellular matrix in neuroblastoma, our general conclusion is that there is a need to establish immediate preclinical models to shine light on the future use of vitronectin as a new therapeutic target in high-risk neuroblastoma.

Nuestro abordaje de investigación aleja el enfoque de las células tumorales solo hacia los tumores considerados como microambientes complejos y dinámicos, con interacciones entre células, fibras, estructuras vasculares y diversas moléculas, cuyas propiedades físicas emergen en respuesta a estímulos mecánicos, con el objetivo de usarlos como dianas terapéuticas. En los niños que padecen neuroblastoma de alto riesgo, se necesita una visión integral de su enfermedad, teniendo en cuenta el macroambiente tumoral (diversas circunstancias de los pacientes y su entorno) y aplicando el enfoque microambiental descrito anteriormente, para dilucidar los factores que mejoren la estratificación del riesgo previo al tratamiento y/o que podrían validarse como posibles dianas terapéuticas.

La investigación realizada en esta tesis doctoral, muestra la necesidad y los beneficios del estudio microscópico de los elementos del neuroblastoma, ha llevado a las siguientes conclusiones:

1. La vitronectina es un componente importante en la matriz extracelular de los tumores neuroblásticos, producida principalmente por células neuroblásticas indiferenciadas y algunas células del estroma, un aumento de la expresión por parte de las células tumorales se asocia con variables independientes desfavorables del sistema de clasificación de la INRG.

2. Las herramientas morfométricas novedosas y precisas que desarrollamos, permiten la caracterización del patrón de vitronectina territorial, sintetizado recientemente, con una ubicación intracelular y pericelular, y el patrón de vitronectina interterritorial, incorporado anteriormente en la matriz extracelular, ubicada lejos de la célula tumoral. Con estas herramientas, podemos confirmar una presencia elevada de vitronectina territorial en tumores neuroblásticos con comportamiento agresivo. Futuros estudios de validación son necesarios para demostrar que la vitronectina territorial ayuda a generar las propiedades biomecánicas de unión-desunión de las células tumorales con los elementos circundantes, promoviendo la migración celular.

3. La metodología matemática basada en la teoría de grafos ha sido automatizada para el análisis de imágenes histopatológicas de neuroblastoma, y puede capturar objetivamente el patrón predominante de la disposición de la vitronectina en el tumor. Esta metodología ha detectado dos características topológicas importantes de la vitronectina territorial, el número de Euler y la ramificación, que, como factores biológicos independientes en nuestra cohorte tumoral, mejoran la clasificación de pacientes con neuroblastoma de acuerdo con el sistema de estratificación de riesgo pretratamiento y la inestabilidad genómica del tumor, respectivamente. Este patrón organizativo descrito de vitronectina territorial, que modifica la arquitectura de la

matriz extracelular del tumor y crea vías de migración preferenciales y, por lo tanto, un comportamiento tumoral agresivo, necesita validación en estudios de colaboración internacional.

4. La vitronectina como proteína de la matriz extracelular interactúa con varios receptores, construyendo puntos de interacción entre célula-célula y célula-matriz extracelular. La expresión de vitronectina, uPAR, integrina $\alpha_v\beta_3$ y PAI-1 por las células tumorales y/o estromales en las muestras tumorales humanas, implica que estas moléculas podrían desarrollar un papel multifuncional, junto con otras moléculas. Esto refuerza la necesidad de continuar investigando otras interacciones de vitronectina, dada su importancia clave en el estroma tumoral del neuroblastoma.

5. Los cultivos de neuroblastoma 2D, muestran que tanto las líneas celulares amplificadas como las no amplificadas del gen *MYCN* expresan vitronectina. Se pueden observar algunas variaciones en el patrón de expresión de uPAR e integrina α_vB_3, siendo menor ambas en células con *MYCN* amplificado, así como la expresión particularmente baja de PAI-1 en todas las líneas celulares estudiadas, subraya que es el receptor de vitronectina menos abundante. En definitiva, la heterogeneidad de las líneas celulares de neuroblastoma también es evidente en la expresión de estos biomarcadores.

6. Los tumores derivados de los modelos ortotópicos *in vivo* conservan las características histopatológicas de los tumores de los pacientes. Se ha evidenciado un crecimiento adecuado de las líneas celulares de neuroblastoma estudiadas en el huésped deficiente en vitronectina, ratones VN-KO, destacando un crecimiento tumoral lento de la línea celular SH-SY5Y que presenta mutación del gen *ALK*. Los resultados tumorales en términos de porcentaje de células neuroblásticas, necrosis y hemorragia evidencian que células con *MYCN* amplificado, SK-N-BE (2), se adaptan de forma más agresiva al macroambiente *in vivo* defectuoso en vitronectina. Confirmamos que la mutación *y* amplificación de los genes *ALK* de *MYCN,* respectivamente, en nuestro modelo generan diferencias en la agresividad, en paralelo a lo que se observa en los pacientes.

7. Las células neuroblásticas de ambas líneas celulares estudiadas muestran una mayor expresión de vitronectina en tumores xenotrasplantados en comparación con el cultivo *in vitro*. La modulación de la secreción de vitronectina parece ser una estrategia mediante la cual los neuroblastos malignos responden a los cambios microambientales locales *in vivo*. El macroambiente deficiente en vitronectina del huésped no parece influir en la síntesis de vitronectina *in vivo*, aunque la elevada cantidad de vitronectina territorial y la amplificación de

MYCN, junto con la expresión modificada de integrina $\alpha_v\beta_3$ y el aumento de uPAR en los xenoinjertos derivados de SK-N-BE (2), son condiciones clave para una progresión tumoral más acusada.

8. La integración de los procesos constantes de remodelación de los múltiples elementos de la matriz extracelular que ocurren dentro del macro-microambiente tumoral, relacionados con los cambios del estroma, tiene importancia clínica y terapéutica en nuestra cohorte tumoral. La clasificación propuesta de grados estromales proporciona patrones predictivos de fibras de reticulina, vitronectina y células inmunes que deben considerarse como dianas importantes en el estroma tumoral de pacientes con neuroblastoma.

9. El análisis morfométrico y topológico, aplicado en combinación para estudiar la intrincada red de elementos que construyen el microambiente del neuroblastoma, como la vitronectina, el andamiaje fibroso y el sistema vascular, demuestra que añadir características morfométricas de los vasos sanguíneos (forma de los sinusoides y deformidad de las metarteriolas) al modelo topológico anterior de vitronectina, mejora la estratificación del riesgo previo al tratamiento y los criterios de inestabilidad genética del tumor.

10. Las características asociadas con la rigidez de la matriz extracelular descrita en el neuroblastoma agresivo, se mantienen en los pases tumorales de los modelos ortotópicos. Los xenoinjertos derivados de SK-N-BE (2) muestran una disminución de los glucosaminoglucanos junto con un aumento de las fibras reticulares en el modelo deficiente en vitronectina, mientras que no se observaron diferencias notables en los xenoinjertos derivados de SH-SY5Y.

11. Se confirma la influencia de los macro-microambientes tumorales en el proceso de adaptación celular, en el modelo *in vivo* deficiente de vitronectina, por el patrón de heterogeneidad genética intratumoral de alteraciones cromosómicas segmentarias de las células *MYCN* amplificadas*,* SK-N-BE (2), y el patrón genómico estable de las células *ALK* mutadas*,* SH-SY5Y.

Al evaluar la aplicación combinada de estrategias morfométricas, topológicas y genéticas en tumores humanos y sistemas *in vitro* e *in vivo* para determinar los puntos de contacto de la célula tumoral con su matriz extracelular en neuroblastoma, nuestra conclusión general es que es necesario establecer modelos preclínicos inmediatos para revelar el uso futuro de la vitronectina como nueva diana terapéutica en neuroblastoma de alto riesgo.

References

1. Maris, J.M., et al., *Neuroblastoma.* Lancet, 2007. **369**(9579): p. 2106-20.
2. Kaatsch, P., *Epidemiology of childhood cancer.* Cancer Treat Rev, 2010. **36**(4): p. 277-85.
3. Gatta, G., et al., *Embryonal cancers in Europe.* Eur J Cancer, 2012. **48**(10): p. 1425-33.
4. Howlader, N., et al., *SEER Cancer Statistics Review (CSR) 1975-2017.* National Cancer Institute, 2019.
5. Peris-Bonet, R., et al., *Cáncer infantil en españa. Estadísticas 1980-2016. Registro Nacional de TumoresInfantiles (RNTI-SEHOP). .* Edición preliminar presentada en el X Congreso de la SEHOP Madrid., 2017.
6. Castel, V., et al., *Neuroblastoma in adolescents: genetic and clinical characterisation.* Clinical & Translational Oncology, 2010. **12**(1): p. 49-54.
7. Suzuki, M., et al., *Treatment and outcome of adult-onset neuroblastoma.* Int J Cancer, 2018. **143**(5): p. 1249-1258.
8. Stark, D.P. and G. Vassal, *Tumors in Adolescents and Young Adults.* Progress in Tumor Research, 2016. **43**.
9. Siegel , R.L., M. K.D., and A. Jemal, *Cancer Statistics, 2019.* CA Cancer J Clin, 2019. **69**(1): p. 7-34.
10. Esiashvili, N., et al., *Neuroblastoma in adults: Incidence and survival analysis based on SEER data. .* Pediatric blood & cancer. , 2007. **49**(1): p. 41-46.
11. Kholodenko, I.V., et al., *Neuroblastoma Origin and Therapeutic Targets for Immunotherapy.* J Immunol Res, 2018. **2018**: p. 7394268.
12. Johnsen, J.I., C. Dyberg, and M. Wickstrom, *Neuroblastoma-A Neural Crest Derived Embryonal Malignancy.* Front Mol Neurosci, 2019. **12**: p. 9.
13. De Preter, K., et al., *Human fetal neuroblast and neuroblastoma transcriptome analysis confirms neuroblast origin and highlights neuroblastoma candidate genes.* Genome Biol, 2006. **7**(9): p. R84.
14. Russel, H.V., et al., *Solid tumours of childhood. ,* in *DeVita, Hellman, and Rosenberg's Cancer: Principles & Practice of Oncology*, V.T. DeVita, T.S. Lawrence, and S.A. Rosenberg, Editors. 2008, Lippincott Williams and Wilkins. p. 2043-2084.
15. Brodeur, G.M., *Neuroblastoma: biological insights into a clinical enigma.* Nat Rev Cancer, 2003. **3**(3): p. 203-216.
16. Pizzo, P.A., *Neuroblastoma. In: Principles and Practice of Pediatric Oncology. .* 2016: Lippincott Williams & Wilkins.
17. DuBois, S.G., et al., *Metastatic sites in stage IV and IVS neuroblastoma correlate with age, tumor biology, and survival.* J Pediatr Hematol Oncol, 1999. **21**(3): p. 181-9.
18. Mueller, S. and K.K. Matthay, *Neuroblastoma: biology and staging.* Curr Oncol Rep, 2009. **11**(6): p. 431-8.
19. Joyner, B.D., *Neuroblastoma.* Medscape, 2017.
20. Alvi, S., et al., *Clinical manifestations of neuroblastoma with head and neck involvement in children.* Int J Pediatr Otorhinolaryngol, 2017. **97**: p. 157-162.
21. Brodeur, G.M., et al., *Revisions of the international criteria for neuroblastoma diagnosis, staging, and response to treatment.* J Clin Oncol, 1993. **11**(8): p. 1466-77.
22. Kembhavi, S.A., et al., *Imaging in neuroblastoma: An update.* Indian J Radiol Imaging, 2015. **25**(2): p. 129-36.
23. Verly, I.R.N., et al., *Catecholamines profiles at diagnosis: Increased diagnostic sensitivity and correlation with biological and clinical features in neuroblastoma patients.* European Journal of Cancer, 2017. **72**: p. 235-243.

24. Newman, E.A., et al., *Update on neuroblastoma.* J Pediatr Surg, 2019. **54**(3): p. 383-389.
25. Ladenstein, R., et al., *Validation of the mIBG skeletal SIOPEN scoring method in two independent high-risk neuroblastoma populations: the SIOPEN/HR-NBL1 and COG-A3973 trials.* Eur J Nucl Med Mol Imaging, 2018. **45**(2): p. 292-305.
26. Maris, J.M., *Recent advances in neuroblastoma.* N Engl J Med, 2010. **362**(23): p. 2202-11.
27. Shackleton, M., et al., *Heterogeneity in cancer: cancer stem cells versus clonal evolution.* Cell, 2009. **138**(5): p. 822-9.
28. Ngan, E.S., *Heterogeneity of neuroblastoma.* Oncoscience, 2015. **2**(10): p. 837-8.
29. Hiyama, E. and H. Hiyama, *Molecular and Biological Heterogeneity in Neuroblastoma.* Current Genomics 2005. **6**(5): p. 319-332.
30. Mosse, Y.P., et al., *Germline PHOX2B mutation in hereditary neuroblastoma.* Am J Hum Genet, 2004. **75**(4): p. 727-30.
31. Mossé, Y.P., et al., *Identification of ALK as a Major Familial Neuroblastoma Predisposition Gene.* Nature, 2008. **455**(7215): p. 930-935.
32. Cohn, S.L., et al., *The International Neuroblastoma Risk Group (INRG) classification system: an INRG Task Force report.* J Clin Oncol, 2009. **27**(2): p. 289-97.
33. Monclair, T., et al., *The International Neuroblastoma Risk Group (INRG) staging system: an INRG Task Force report.* J Clin Oncol, 2009. **27**(2): p. 298-303.
34. Moroz, V., et al., *Changes over three decades in outcome and the prognostic influence of age-atdiagnosisin young patients with neuroblastoma: A report from the International Neuroblastoma Risk Group Project. .* European journal of cancer 2011. **47**(4): p. 561-571.
35. Brisse, H.J., et al., *Guidelines for imaging and staging of neuroblastic tumors: consensus report from the International Neuroblastoma Risk Group Project.* Radiology, 2011. **261**(1): p. 243-57.
36. Shimada, H., et al., *International neuroblastoma pathology classification for prognostic evaluation of patients with peripheral neuroblastic tumors: a report from the Children's Cancer Group.* Cancer, 2001. **92**(9): p. 2451-61.
37. Shimada, H., et al., *Terminology and morphologic criteria of neuroblastic tumors: recommendations by the International Neuroblastoma Pathology Committee.* Cancer, 1999. **86**(2): p. 349-63.
38. Ruiz-Perez, M.V., A.B. Henley, and M. Arsenian-Henriksson, *The MYCN Protein in Health and Disease.* Genes (Basel), 2017. **8**(4).
39. Campbell, K., et al., *Association of MYCN Copy Number With Clinical Features, Tumor Biology, and Outcomes in Neuroblastoma: A Report From the Children's Oncology Group.* Cancer, 2017. **123**(21): p. 4224-4235.
40. Berbegall, A.P., et al., *Heterogeneous MYCN amplification in neuroblastoma: a SIOP Europe Neuroblastoma Study.* Br J Cancer, 2018. **118**(11): p. 1502-1512.
41. Bogen, D., et al., *The genetic tumor background is an important determinant for heterogeneous MYCN -amplified neuroblastoma.* International Journal of Cancer, 2016. **139**(1): p. 153-163.
42. Cohn, S.L., et al., *Analysis of DNA ploidy and proliferative activity in relation to histology and N-myc amplification in neuroblastoma.* Am J Pathol, 1990. **136**(5): p. 1043-52.
43. George, R.E., W.B. London, and S.L. Cohn, *Hyperdiploidy Plus Nonamplified MYCN Confers a Favorable Prognosis in Children 12 to 18 Months Old With Disseminated Neuroblastoma: A Pediatric Oncology Group Study.* J Clin Oncol 2005. **23**(27): p. 6466-6473.
44. Mlakar, V., et al., *11q deletion in neuroblastoma: a review of biological and clinical implications.* Mol Cancer, 2017. **16**(1): p. 114.

45. Villamon, E., et al., *Genetic instability and intratumoral heterogeneity in neuroblastoma with MYCN amplification plus 11q deletion.* PLoS One, 2013. **8**(1): p. e53740.
46. Schleiermacher, G., et al., *Segmental chromosomal alterations lead to a higher risk of relapse in infants with MYCN-non-amplified localised unresectable/disseminated neuroblastoma (a SIOPEN collaborative study).* Br J Cancer, 2011. **105**(12): p. 1940-8.
47. Schleiermacher, G., et al., *Chromosomal CGH identifies patients with a higher risk of relapse in neuroblastoma without MYCN amplification.* British Journal of Cancer, 2007. **97**(2): p. 238-246.
48. Fusco, P., M.R. Esposito, and G.P. Tonini, *Chromosome instability in neuroblastoma.* Oncol Lett, 2018. **16**(6): p. 6887-6894.
49. Tonini, G.P. and M. Capasso, *Genetic predisposition and chromosome instability in neuroblastoma.* Cancer Metastasis Rev, 2020. **39**(1): p. 275-285.
50. Defferrari, R., K. Mazzocco, and I.M. Ambros, *Influence of segmental chromosome abnormalities on survival in children over the age of 12 months with unresectable localised peripheral neuroblastic tumours without MYCN amplification.* Br J Cancer. , 2015. **112**(2): p. 290-295.
51. Caren, H., et al., *High-risk neuroblastoma tumors with 11q-deletion display a poor prognostic, chromosome instability phenotype with later onset.* Proc Natl Acad Sci U S A, 2010. **107**(9): p. 4323-8.
52. Attiyeh, E.F., W.B. London, and Y.P. Mossé, *Chromosome 1p and 11q deletions and outcome in neuroblastoma.* 2005. **353**(21): p. 2243-2253.
53. Liu, Z. and C.J. Thiele, *Molecular Genetics of Neuroblastoma.*, in *Diagnostic and Therapeutic Nuclear Medicine for Neuroendocrine Tumors. Contemporary Endocrinology.* , K. Pacak and D. Taïeb, Editors. 2017, Humana Press, Cham.
54. Nakagawara, A., et al., *Neuroblastoma.* Jpn J Clin Oncol, 2018. **48**(3): p. 214-241.
55. Pugh, T.J., et al., *The genetic landscape of high-risk neuroblastoma.* Nat Genet, 2013. **45**(3): p. 279-84.
56. Peifer, M., et al., *Telomerase activation by genomic rearrangements in high-risk neuroblastoma.* Nature, 2015. **526**(7575): p. 700-4.
57. Trigg, R.M. and S.D. Turner, *ALK in Neuroblastoma: Biological and Therapeutic Implications.* Cancers (Basel), 2018. **10**(4).
58. Schramm, A., et al., *Mutational dynamics between primary and relapse neuroblastomas.* . Nat Genet., 2015. **47**(8): p. 872-877.
59. Johnsen, J.I., et al., *Molecular mechanisms and therapeutic targets in neuroblastoma.* Pharmacol Res, 2018. **131**: p. 164-176.
60. Ladenstein, R., U. Pötschger, and A.D.J. Pearson, *Busulfan and melphalan versus carboplatin, etoposide, and melphalan as high-dose chemotherapy for high-risk neuroblastoma (HR-NBL1/SIOPEN): an international, randomised, multi-arm, open-label, phase 3 trial.* Lancet Oncol., 2017. **18**(4): p. 500-514.
61. Smith, V. and J. Foster, *High-Risk Neuroblastoma Treatment Review.* Children (Basel), 2018. **5**(9).
62. Matthay, K.K., et al., *Neuroblastoma.* Nat Rev Dis Primers, 2016. **2**: p. 16078.
63. Mody, R., et al., *Irinotecan, Temozolomide, and Dinutuximab With GM-CSF in Children With Refractory or Relapsed Neuroblastoma: A Report From the Children's Oncology Group.* J Clin Oncol, 2020: p. JCO2000203.
64. Mody, R., et al., *Irinotecan-temozolomide with temsirolimus or dinutuximab in children with refractory or relapsed neuroblastoma (COG ANBL1221): an open-label, randomised, phase 2 trial.* Lancet Oncol, 2017. **18**(7): p. 946-957.
65. Richards, R.M., E. Sotillo, and R.G. Majzner, *CAR T Cell Therapy for Neuroblastoma.* Front Immunol, 2018. **9**: p. 2380.

66. Ou, S.H., et al., *Crizotinib for the treatment of ALK-rearranged non-small cell lung cancer: a success story to usher in the second decade of molecular targeted therapy in oncology.* Oncologist, 2012. **17**(11): p. 1351-75.
67. Durand, S., et al., *ALK mutation dynamics and clonal evolution in a neuroblastoma model exhibiting two ALK mutations.* Oncotarget, 2019. **10**(48): p. 4937-4950.
68. Gustafson, W.C., J.G. Meyerowitz, and E.A. Nekritz, *Drugging MYCN through an allosteric transition in Aurora kinase A.* Cancer Cell, 2014. **26**(3): p. 414-424.
69. Dolman, M.E., E. Poon, and M.E. Ebus, *Cyclin-Dependent Kinase Inhibitor AT7519 as a Potential Drug for MYCN-Dependent Neuroblastoma.* Clin Cancer Res, 2015. **21**(22): p. 5100-5109.
70. Greengard, E.G., *Molecularly Targeted Therapy for Neuroblastoma.* Children (Basel), 2018. **5**(10).
71. Rodríguez-Nogales, C., R. Noguera, and P. Couvreur, *Therapeutic Opportunities in Neuroblastoma Using Nanotechnology.* J Pharmacol Exp Ther, 2019. **370**(3): p. 625-635.
72. Zhen, X., et al., *Cellular uptake, antitumor response and tumor penetration of cisplatin-loaded milk protein nanoparticles.* Biomaterials, 2013. **34**(4): p. 1372-82.
73. Monterrubio, C., S. Paco, and N. Olaciregui, *Targeted drug distribution in tumor extracellular fluid of GD2-expressing neuroblastoma patient-derived xenografts using SN-38-loaded nanoparticles conjugated to the monoclonal antibody 3F8.* J Control Release. , 2017. **255**: p. 108-119.
74. Stack, M.S., et al., *The Tumor Microenvironment of High Grade Serous Ovarian Cancer.* Cancers (Basel), 2018. **11**(1).
75. Soysal, S.D., A. Tzankov, and S.E. Muenst, *Role of the Tumor Microenvironment in Breast Cancer.* Pathobiology, 2015. **82**(3-4): p. 142-52.
76. Lin , C.N., C.Y. Chien, and H.C. Chuang, *Are friends or foes? New strategy for head and neck squamous cell carcinoma treatment via immune regulation.* Int J Head Neck Sci. , 2017. **1**: p. 105-113.
77. Wang, M., et al., *Role of tumor microenvironment in tumorigenesis.* J Cancer, 2017. **8**(5): p. 761-773.
78. Pelizzo, G., et al., *Microenvironment in neuroblastoma: isolation and characterization of tumor-derived mesenchymal stromal cells.* BMC Cancer, 2018. **18**(1): p. 1176.
79. Ingber, D.E., *The architecture of life.* Sci Am, 1998. **278**(1): p. 48-57.
80. Ingber, D.E., *Tensegrity-based mechanosensing from macro to micro.* Prog Biophys Mol Biol, 2008. **97**(2-3): p. 163-79.
81. Noguera, R., et al., *Extracellular matrix, biotensegrity and tumor microenvironment. An update and overview.* Histol Histopathol, 2012. **27**(6): p. 693-705.
82. Emon, B., et al., *Biophysics of Tumor Microenvironment and Cancer Metastasis - A Mini Review.* Comput Struct Biotechnol J, 2018. **16**: p. 279-287.
83. Handorf, A.M., et al., *Tissue stiffness dictates development, homeostasis, and disease progression.* Organogenesis, 2015. **11**(1): p. 1-15.
84. Cacho-Díaz, B., D.R. García-Botello, and T. Wegman-Ostrosky, *Tumor microenvironment differences between primary tumor and brain metastases.* J Transl Med. , 2020. **18**(1): p. 1.
85. Balkwill, F.R., M. Capasso, and T. Hagemann, *The tumor microenvironment at a glance.* . J Cell Sci., 2012. **125**: p. 5591-5596.
86. Dunn, G.P., et al., *Cancer immunoediting: from immunosurveillance to tumor escape.* Nat Immunol, 2002. **3**(11): p. 991-8.
87. Bassani, B., et al., *Natural Killer Cells as Key Players of Tumor Progression and Angiogenesis: Old and Novel Tools to Divert Their Pro-Tumor Activities into Potent Anti-Tumor Effects.* Cancers (Basel), 2019. **11**(4): p. 461.

88. Cantoni, C., et al., *NK Cells, Tumor Cell Transition, and Tumor Progression in Solid Malignancies: New Hints for NK-Based Immunotherapy?* J Immunol Res, 2016. **2016**: p. 4684268.
89. Sica, A., et al., *Tumour-associated macrophages are a distinct M2 polarised population promoting tumour progression: potential targets of anti-cancer therapy.* Eur J Cancer, 2006. **42**(6): p. 717-27.
90. Ribeiro Franco, P.I., et al., *Tumor microenvironment components: Allies of cancer progression.* Pathol Res Pract, 2020. **216**(1): p. 152729.
91. Lin, Y., J. Xu, and H. Lan, *Tumor-associated macrophages in tumor metastasis: biological roles and clinical therapeutic applications.* J Hematol Oncol, 2019. **12**(1): p. 76.
92. Veglia, F. and D.I. Gabrilovich, *Dendritic cells in cancer: the role revisited.* Curr Opin Immunol, 2017. **45**: p. 43-51.
93. Wylie, B., et al., *Dendritic Cells and Cancer: From Biology to Therapeutic Intervention.* Cancers (Basel), 2019. **11**(4).
94. Schneider, T., et al., *Non-small cell lung cancer induces an immunosuppressive phenotype of dendritic cells in tumor microenvironment by upregulating B7-H3.* J Thorac Oncol, 2011. **6**(7): p. 1162-8.
95. Squire, R., et al., *The relationship of class I MHC antigen expression to stage IV-S disease and survival in neuroblastoma.* J Pediatr Surg, 1990. **25**(4): p. 381-6.
96. Coughlin, C.M., et al., *Immunosurveillance and survivin-specific T-cell immunity in children with high-risk neuroblastoma.* J Clin Oncol, 2006. **24**(36): p. 5725-34.
97. Raffaghello, L., et al., *Multiple defects of the antigen-processing machinery components in human neuroblastoma: immunotherapeutic implications.* Oncogene, 2005. **24**(29): p. 4634-44.
98. Pistoia, V., et al., *Immunosuppressive microenvironment in neuroblastoma.* Front Oncol, 2013. **3**: p. 167.
99. Liu, T., et al., *Cancer-associated fibroblasts: an emerging target of anti-cancer immunotherapy.* J Hematol Oncol, 2019. **12**(1): p. 86.
100. Fiori, M.E., S. Di Franco, and L. Villanova, *Cancer-associated Fibroblasts as Abettors of Tumor Progression at the Crossroads of EMT and Therapy Resistance.* Mol Cancer, 2019. **18**(1): p. 70.
101. Lee, E., N.B. Pandey, and A.S. Popel, *Crosstalk between cancer cells and blood endothelial and lymphatic endothelial cells in tumour and organ microenvironment.* Expert Rev Mol Med. , 2015. **17**: p. e3.
102. Paduch, R., *The role of lymphangiogenesis and angiogenesis in tumor metastasis.* Cell Oncol (Dordr), 2016. **39**(5): p. 397-410.
103. Sinha, D., et al., *Pericytes Promote Malignant Ovarian Cancer Progression in Mice and Predict Poor Prognosis in Serous Ovarian Cancer Patients.* Clin Cancer Res, 2016. **22**(7): p. 1813-24.
104. Guerra, D.A.P., et al., *Targeting glioblastoma-derived pericytes improves chemotherapeutic outcome.* Angiogenesis, 2018. **21**(4): p. 667-675.
105. Cozzo, A.J., A.M. Fuller, and L. Makowski, *Contribution of Adipose Tissue to Development of Cancer.* Compr Physiol, 2017. **8**(1): p. 237-282.
106. Yu, Z., et al., *Cancer stem cells.* Int J Biochem Cell Biol, 2012. **44**(12): p. 2144-51.
107. Xiao, J., et al., *Dig the root of cancer: targeting cancer stem cells therapy.* Journal of Medical Discovery, 2017. **2**(2): p. JMD17003.
108. Zhong, X., et al., *Cellular components in tumor microenvironment of neuroblastoma and the prognostic value.* PeerJ, 2019. **7**: p. e8017.
109. Borriello, L., R.C. Seeger, and S. Asgharzadeh, *More than the genes, the tumor microenvironment in neuroblastoma.* Cancer Lett, 2016. **380**(1): p. 304-314.

110. Pickup, M.W., J.K. Mouw, and V.M. Weaver, *The extracellular matrix modulates the hallmarks of cancer.* EMBO Rep, 2014. **15**(12): p. 1243-53.
111. Mecham, R.P., *Overview of extracellular matrix.* Curr Protoc Cell Biol, 2012. **Chapter 10**: p. Unit 10 1.
112. Heino, J., *The collagen family members as cell adhesion proteins.* Bioessays, 2007. **29**(10): p. 1001-10.
113. Kular, J.K., S. Basu, and R.I. Sharma, *The extracellular matrix: Structure, composition, age-related differences, tools for analysis and applications for tissue engineering.* J Tissue Eng, 2014. **5**: p. 2041731414557112.
114. Egeblad, M., M.G. Rasch, and V.M. Weaver, *Dynamic interplay between the collagen scaffold and tumor evolution.* Curr Opin Cell Biol, 2010. **22**(5): p. 697-706.
115. Sun, Y. and P.S. Nelson, *Molecular pathways: involving microenvironment damage responses in cancer therapy resistance.* Clin Cancer Res, 2012. **18**(15): p. 4019-25.
116. Vilamaior, P.S.L., S. Suzigan, and H.F. Carvalho, *Structural characterization and distribution of elastic system fibers in the human prostate and some prostatic lesions.* Braz. J. morphol. Sci, 2003. **20**(2): p. 101-107.
117. Mouw, J.K., G. Ou, and V.M. Weaver, *Extracellular matrix assembly: a multiscale deconstruction.* Nat Rev Mol Cell Biol, 2014. **15**(12): p. 771-85.
118. Nikitovic, D., et al., *Proteoglycans-Biomarkers and Targets in Cancer Therapy.* Front Endocrinol (Lausanne), 2018. **9**: p. 69.
119. Iozzo, R.V. and R.D. Sanderson, *Proteoglycans in cancer biology, tumour microenvironment and angiogenesis.* J Cell Mol Med, 2011. **15**(5): p. 1013-31.
120. Xu, J. and D. Mosher, *Fibronectin and Other Adhesive Glycoproteins*, in *The Extracellular Matrix: an Overview. Biology of Extracellular Matrix.* , R. Mecham Editor. 2011, Springer, Berlin, Heidelberg. p. 41-75.
121. Yue, B., *Biology of the extracellular matrix: an overview.* J Glaucoma, 2014. **23**(8 Suppl 1): p. S20-3.
122. Nam, J.M., et al., *Breast cancer cells in three-dimensional culture display an enhanced radioresponse after coordinate targeting of integrin alpha5beta1 and fibronectin.* Cancer Res, 2010. **70**(13): p. 5238-48.
123. Mitra, A.K., et al., *Ligand-independent activation of c-Met by fibronectin and alpha(5)beta(1)-integrin regulates ovarian cancer invasion and metastasis.* Oncogene, 2011. **30**(13): p. 1566-76.
124. Pan, S., T.A. Brentnall, and R. Chen, *Glycoproteins and glycoproteomics in pancreatic cancer.* World J Gastroenterol, 2016. **22**(42): p. 9288-9299.
125. Schneider, G., E. Bryndza, and A. Poniewierska-Baran, *Evidence that vitronectin is a potent migration-enhancing factor for cancer cells chaperoned by fibrinogen: a novel view of the metastasis of cancer cells to low-fibrinogen lymphatics and body cavities.* Oncotarget. , 2016. **7**(43): p. 69829-69843.
126. Preissner, K.T., *Structure and biological role of vitronectin.* Annu Rev Cell Biol, 1991. **7**: p. 275-310.
127. Schvartz, I., D. Seger, and S. Shaltiel, *Vitronectin.* Int J Biochem Cell Biol, 1999. **31**(5): p. 539-44.
128. Tabatabai, G., *The Role of Integrins in Angiogenesis*, in *Biochemical Basis and Therapeutic Implications of Angiogenesis. Advances in Biochemistry in Health and Disease*, J. Mehta, P. Mathur, and N. Dhalla, Editors. 2017, Springer. p. 1-13.
129. Leavesley, D.I., A.S. Kashyap, and T. Croll, *Vitronectin—Master Controller or Micromanager?* IUBMB Life 2013. **65**(10): p. 807-818.
130. Ortega-Marínez, I., *Vitronectin and dermicidin serum levels predict the metastatic progressiob of AJCC I-II early-stage melanoma.* Int. J. Cancer 2016. **139**(7): p. 1598-1607.

131. Aaboe, M., et al., *Vitronectin in human breast carcinomas.* Biochim Biophys Acta, 2003. **1638**(1): p. 72-82.
132. Zhu, W., et al., *Vitronectin silencing inhibits hepatocellular carcinoma in vitro and in vivo.* Future Oncol, 2015. **11**(2): p. 251-8.
133. Yuan, Y., et al., *Role of the tumor microenvironment in tumor progression and the clinical applications (Review).* Oncol Rep, 2016. **35**(5): p. 2499-515.
134. Sasaki, T., K. Hiroki, and Y. Yamashita, *The role of epidermal growth factor receptor in cancer metastasis and microenvironment.* Biomed Res Int, 2013. **2013**: p. 546318.
135. Seoane, J. and R.R. Gomis, *TGF-beta Family Signaling in Tumor Suppression and Cancer Progression.* Cold Spring Harb Perspect Biol, 2017. **9**(12).
136. da Cunha Santos, G., F.A. Shepherd, and M.S. Tsao, *EGFR mutations and lung cancer.* Annu Rev Pathol, 2011. **6**: p. 49-69.
137. Oliveira-Cunha, M., W.G. Newman, and A.K. Siriwardena, *Epidermal growth factor receptor in pancreatic cancer.* Cancers (Basel), 2011. **3**(2): p. 1513-26.
138. Grivennikov, S.I. and M. Karin, *Inflammatory cytokines in cancer: tumour necrosis factor and interleukin 6 take the stage.* Ann Rheum Dis, 2011. **70 Suppl 1**: p. i104-8.
139. Nagarsheth, N., M.S. Wicha, and W. Zou, *Chemokines in the cancer microenvironment and their relevance in cancer immunotherapy.* Nat Rev Immunol. , 2017. **17**(9): p. 559-572.
140. Bikfalvi, A. and C. Billottet, *The CC and CXC chemokines: major regulators of tumor progression and the tumor microenvironment.* Am J Physiol Cell Physiol, 2020. **318**(3): p. C542-C554.
141. Jabłońska-Trypuć, A., M. Matejczyk, and S. Rosochacki, *Matrix metalloproteinases (MMPs), the main extracellular matrix (ECM) enzymes in collagen degradation, as a target for anticancer drugs. .* J Enzyme Inhib Med Chem, 2016. **31**: p. 177-183.
142. Walker, C., E. Mojares, and A. Del Rio Hernandez, *Role of Extracellular Matrix in Development and Cancer Progression.* Int J Mol Sci, 2018. **19**(10).
143. Takahashi, M., et al., *In vivo glioma growth requires host-derived matrix metalloproteinase 2 for maintenance of angioarchitecture.* Pharmacol Res, 2002. **46**(2): p. 155-63.
144. Poola, I., R.L. DeWitty, and J.J. Marshalleck, *Identification of MMP-1 as a putative breast cancer predictive marker by global gene expression analysis.* Nat Med, 2005. **11**(5): p. 481-483.
145. Kumari, S., T.K. Panda, and T. Pradhan, *Lysyl Oxidase: Its Diversity in Health and Diseases.* Indian J Clin Biochem, 2017. **32**(2): p. 134-141.
146. Dong, Y., Q. Zheng, and Z. Wang, *Higher matrix stiffness as an independent initiator triggers epithelial-mesenchymal transition and facilitates HCC metastasis. .* J Hematol Oncol. , 2019. **12**(1): p. 112.
147. Tadeo, I., et al., *A stiff extracellular matrix is associated with malignancy in peripheral neuroblastic tumors.* Pediatr Blood Cancer, 2017. **64**(9).
148. Hanahan, D. and R.A. Weinberg, *Hallmarks of cancer: the next generation.* Cell, 2011. **144**(5): p. 646-74.
149. Diop-Frimpong, B., et al., *Losartan inhibits collagen I synthesis and improves the distribution and efficacy of nanotherapeutics in tumors.* Proc Natl Acad Sci U S A, 2011. **108**(7): p. 2909-14.
150. Xu, S., et al., *The role of collagen in cancer: from bench to bedside.* J Transl Med, 2019. **17**(1): p. 309.
151. Morla, S., *Glycosaminoglycans and Glycosaminoglycan Mimetics in Cancer and Inflammation.* Int J Mol Sci, 2019. **20**(8).
152. Ahmad, K., et al., *Targeting integrins for cancer management using nanotherapeutic approaches: Recent advances and challenges.* Semin Cancer Biol, 2019.

153. Raab-Westphal, S., J.F. Marshall, and S.L. Goodman, *Integrins as Therapeutic Targets: Successes and Cancers.* Cancers (Basel), 2017. **9**(9): p. 110.
154. Alday-Parejo, B., R. Stupp, and C. Ruegg, *Are Integrins Still Practicable Targets for Anti-Cancer Therapy?* Cancers (Basel), 2019. **11**(7).
155. Zhao, Y.Z., Q. Lin, and H. Wong, L,, *Glioma-targeted therapy using Cilengitide nanoparticles combined with UTMD enhanced delivery. .* J Control Release., 2016. **224**: p. 112-125.
156. Kang, W., et al., *Cyclic-RGDyC functionalized liposomes for dual-targeting of tumor vasculature and cancer cells in glioblastoma: An in vitro boron neutron capture therapy study.* Oncotarget, 2017. **8**(22): p. 36614-36627.
157. Eble, J.A. and S. Niland, *The extracellular matrix in tumor progression and metastasis.* Clin Exp Metastasis, 2019. **36**(3): p. 171-198.
158. Roma-Rodrigues, C., et al., *Targeting Tumor Microenvironment for Cancer Therapy.* Int J Mol Sci, 2019. **20**(4).
159. Farkona, S., E.P. Diamandis, and I.M. Blasutig, *Cancer immunotherapy: the beginning of the end of cancer?* BMC Med, 2016. **14**: p. 73.
160. Gun, S.Y., et al., *Targeting immune cells for cancer therapy.* Redox Biol, 2019. **25**: p. 101174.
161. Yu, A.L., et al., *Anti-GD2 antibody with GM-CSF, interleukin-2, and isotretinoin for neuroblastoma.* N Engl J Med, 2010. **363**(14): p. 1324-34.
162. Scarfo, I. and M.V. Maus, *Current approaches to increase CAR T cell potency in solid tumors: targeting the tumor microenvironment.* J Immunother Cancer, 2017. **5**: p. 28.
163. Viallard, C. and B. Larrivee, *Tumor angiogenesis and vascular normalization: alternative therapeutic targets.* Angiogenesis, 2017. **20**(4): p. 409-426.
164. Zirlik, K. and J. Duyster, *Anti-Angiogenics: Current Situation and Future Perspectives.* Oncol Res Treat, 2018. **41**(4): p. 166-171.
165. Kong, D.H., et al., *A Review of Anti-Angiogenic Targets for Monoclonal Antibody Cancer Therapy.* Int J Mol Sci, 2017. **18**(8).
166. Achen, M.G., G.B. Mann, and S.A. Stacker, *Targeting lymphangiogenesis to prevent tumour metastasis.* Br J Cancer, 2006. **94**(10): p. 1355-60.
167. Hsu, M.C., M.R. Pan, and W.C. Hung, *Two Birds, One Stone: Double Hits on Tumor Growth and Lymphangiogenesis by Targeting Vascular Endothelial Growth Factor Receptor 3.* Cells, 2019. **8**(3).
168. Nishida-Aoki, N. and T.S. Gujral, *Emerging approaches to study cell-cell interactions in tumor microenvironment.* Oncotarget, 2019. **10**(7): p. 785-797.
169. Klinghammer, K., W. Walther, and J. Hoffmann, *Choosing wisely - Preclinical test models in the era of precision medicine.* Cancer Treat Rev, 2017. **55**: p. 36-45.
170. Ben-David, U., et al., *Genetic and transcriptional evolution alters cancer cell line drug response.* Nature, 2018. **560**(7718): p. 325-330.
171. Kasai, F., et al., *Changes of heterogeneous cell populations in the Ishikawa cell line during long-term culture: Proposal for an in vitro clonal evolution model of tumor cells.* Genomics, 2016. **107**(6): p. 259-66.
172. Medico, E., et al., *The molecular landscape of colorectal cancer cell lines unveils clinically actionable kinase targets.* Nat Commun, 2015. **6**: p. 7002.
173. Gillet, J.P., S. Varma, and M.M. Gottesman, *The clinical relevance of cancer cell lines.* J Natl Cancer Inst, 2013. **105**(7): p. 452-8.
174. Horbach, S.P.J.M. and W. Halffman, *The ghosts of HeLa: How cell line misidentification contaminates the scientific literature. .* PLoS One, 2017. **12**(10): p. e0186281.
175. Persson, C.U., et al., *Neuroblastoma patient-derived xenograft cells cultured in stem-cell promoting medium retain tumorigenic and metastatic capacities but differentiate in serum.* Sci Rep, 2017. **7**(1): p. 10274.

176. Bate-Eya, L.T., et al., *Newly-derived neuroblastoma cell lines propagated in serum-free media recapitulate the genotype and phenotype of primary neuroblastoma tumours.* Eur J Cancer, 2014. **50**(3): p. 628-37.
177. Petrie, R.J. and K.M. Yamada, *At the leading edge of three-dimensional cell migration.* J Cell Sci, 2012. **125**(Pt 24): p. 5917-26.
178. Edmondson, R., et al., *Three-dimensional cell culture systems and their applications in drug discovery and cell-based biosensors.* Assay Drug Dev Technol, 2014. **12**(4): p. 207-218.
179. Longati, P., et al., *3D pancreatic carcinoma spheroids induce a matrix-rich, chemoresistant phenotype offering a better model for drug testing.* BMC Cancer, 2013. **13**: p. 95.
180. Yılmaz, Ö. and S. Sakarya, *Is 'Hanging Drop' a Useful Method to Form Spheroids of Jimt, Mcf-7, T-47d, Bt-474 That are Breast Cancer Cell Lines.* Single Cell Biol 2018. **7**(1): p. 170.
181. Kuo, C.T., J.Y. Wang, and Y.F. Lin, *Three-dimensional spheroid culture targeting versatile tissue bioassays using a PDMS-based hanging drop array.* Sci Rep, 2017. **7**(1): p. 4363.
182. Hickman, J.A., R. Graeser, and R. de Hoogt, *Three-dimensional models of cancer for pharmacology and cancer cell biology: capturing tumor complexity in vitro/ex vivo.* Biotechnol J. , 2014. **9**(9): p. 1115-1128.
183. Kienast, Y., et al., *Real-time imaging reveals the single steps of brain metastasis formation.* Nat Med, 2010. **16**(1): p. 116-22.
184. Fang, D.D., et al., *Expansion of CD133(+) colon cancer cultures retaining stem cell properties to enable cancer stem cell target discovery.* Br J Cancer, 2010. **102**(8): p. 1265-75.
185. Knight, E. and S. Przyborski, *Advances in 3D cell culture technologies enabling tissue-like structures to be created in vitro.* J Anat. , 2015. **227**(6): p. 746-756.
186. Naahidi, S., et al., *Biocompatibility of hydrogel-based scaffolds for tissue engineering applications.* Biotechnol Adv, 2017. **35**(5): p. 530-544.
187. Chan, B.P. and K.W. Leong, *Scaffolding in tissue engineering: general approaches and tissue-specific considerations.* Eur Spine J, 2008. **17 Suppl 4**: p. 467-79.
188. Kucinska, M., M. Murias, and P. Nowak-Sliwinska, *Beyond mouse cancer models: Three-dimensional human-relevant in vitro and non-mammalian in vivo models for photodynamic therapy.* Mutat Res, 2017. **773**: p. 242-262.
189. Duarte Campos, D.F., et al., *Exploring Cancer Cell Behavior In Vitro in Three-Dimensional Multicellular Bioprintable Collagen-Based Hydrogels.* Cancers (Basel), 2019. **11**(2).
190. Curtin, C., et al., *A physiologically relevant 3D collagen-based scaffold-neuroblastoma cell system exhibits chemosensitivity similar to orthotopic xenograft models.* Acta Biomater, 2018. **70**: p. 84-97.
191. Monferrer, E., et al., *A three-dimensional bioprinted model to evaluate the effect of stiffness on neuroblastoma cell cluster dynamics and behavior.* Sci Rep, 2020. **10**(1): p. 6370.
192. Holen, I., et al., *In vivo models in breast cancer research: progress, challenges and future directions.* Dis Model Mech, 2017. **10**(4): p. 359-371.
193. Landgraf, M., et al., *Rational Design of Mouse Models for Cancer Research.* Trends Biotechnol, 2018. **36**(3): p. 242-251.
194. Zhao, S., J. Huang, and J. Ye, *A fresh look at zebrafish from the perspective of cancer research.* J Exp Clin Cancer Res, 2015. **34**: p. 80.
195. Zhou, Q., J. Facciponte, and M. Jin, . *Humanized NOD-SCID IL2rg–/– mice as a preclinical model for cancer research and its potential use for individualized cancer therapies.* Cancer Lett, 2014. **314**(1): p. 13-19.

196. Day, C.P., G. Merlino, and T. Van Dyke, *Preclinical mouse cancer models: a maze of opportunities and challenges.* Cell, 2015. **163**(1): p. 39-53.
197. Lai, Y., X. Wei, and S. Lin, *Current status and perspectives of patient-derived xenograft models in cancer research.* J Hematol Oncol, 2017. **10**(1): p. 106.
198. Okada, S., K. Vaeteewoottacharn, and R. Kariya, *Application of Highly Immunocompromised Mice for the Establishment of Patient-Derived Xenograft (PDX) Models.* Cells, 2019. **8**(8).
199. Collins, A.T. and S.H. Lang, *A systematic review of the validity of patient derived xenograft (PDX) models: the implications for translational research and personalised medicine.* PeerJ, 2018. **6**: p. e5981.
200. Siolas, D. and G.J. Hannon, *Patient-derived tumor xenografts: transforming clinical samples into mouse models. .* Cancer Res. , 2013. **73**(17): p. 5315-5319.
201. Zhan, B., S. Wen, and J. Lu, *Identification and causes of metabonomic difference between orthotopic and subcutaneous xenograft of pancreatic cancer.* Oncotarget, 2017. **8**(37): p. 61264-61281.
202. Jung, J., *Human tumor xenograft models for preclinical assessment of anticancer drug development.* Toxicol Res, 2014. **30**(1): p. 1-5.
203. Zhang, Z., L. Song, and J. Guo, *The Application of Pre-clinical Animal Models to Optimise Nanoparticulate Drug Delivery for Hepatocellular Carcinoma.* Pharm Nanotechnol, 2018. **6**(4): p. 221-231.
204. Khanna, C., et al., *Biologically relevant orthotopic neuroblastoma xenograft models: primary adrenal tumor growth and spontaneous distant metastasis.* In Vivo, 2002. **16**(2): p. 77-85.
205. Daudigeos-Dubus, E., et al., *Establishment and characterization of new orthotopic and metastatic neuroblastoma models.* In Vivo, 2014. **28**(4): p. 425-34.
206. Hidalgo, M., et al., *Patient-derived xenograft models: an emerging platform for translational cancer research.* Cancer Discov, 2014. **4**(9): p. 998-1013.
207. Gao, H., J.M. Korn, and S. Ferretti, *High-throughput screening using patient-derived tumor xenografts to predict clinical trial drug response.* Nat Med, 2015. **21**(11): p. 1318-1325.
208. Huang, K.L., S. Li, and P. Mertins, *Proteogenomic integration reveals therapeutic targets in breast cancer xenografts [published correction appears in Nat Commun. 2017 Apr 25;8:15479].* Nat Commun. , 2017. **8**: p. 14864.
209. Braekeveldt, N., et al., *Neuroblastoma patient-derived orthotopic xenografts retain metastatic patterns and geno- and phenotypes of patient tumours.* Int J Cancer, 2015. **136**(5): p. E252-61.
210. Rubio-Viqueira, B., et al., *An in vivo platform for translational drug development in pancreatic cancer.* Clin Cancer Res, 2006. **12**(15): p. 4652-61.
211. Braekeveldt, N. and D. Bexell, *Patient-derived xenografts as preclinical neuroblastoma models.* Cell Tissue Res, 2018. **372**(2): p. 233-243.
212. Allen, T.M., et al., *Humanized immune system mouse models: progress, challenges and opportunities.* Nat Immunol, 2019. **20**(7): p. 770-774.
213. Ornell, K.J. and J.M. Coburn, *Developing preclinical models of neuroblastoma: driving therapeutic testing.* BMC Biomedical Engineering, 2019. **1**: p. 33.
214. Braekeveldt, N., et al., *Neuroblastoma patient-derived orthotopic xenografts reflect the microenvironmental hallmarks of aggressive patient tumours.* Cancer Lett, 2016. **375**(2): p. 384-389.
215. Chao, C., et al., *Patient-derived Xenografts from Colorectal Carcinoma: A Temporal and Hierarchical Study of Murine Stromal Cell Replacement.* Anticancer Res, 2017. **37**(7): p. 3405-3412.
216. Yoshida, G.J., *Applications of patient-derived tumor xenograft models and tumor organoids.* J Hematol Oncol, 2020. **13**(1): p. 4.

217. Braekeveldt, N., et al., *Patient-Derived Xenograft Models Reveal Intratumor Heterogeneity and Temporal Stability in Neuroblastoma.* Cancer Res, 2018. **78**(20): p. 5958-5969.
218. Morton, C.L. and P.J. Houghton, *Establishment of human tumor xenografts in immunodeficient mice.* Nat Protoc, 2007. **2**(2): p. 247-50.
219. Pergolini, I., V. Morales-Oyarvide, and M. Mino-Kenudson, *Tumor engraftment in patient-derived xenografts of pancreatic ductal adenocarcinoma is associated with adverse clinicopathological features and poor survival. .* PLoS One, 2017. **12**(8): p. e0182855.
220. Fusco, P., et al., *Patient-derived organoids (PDOs) as a novel in vitro model for neuroblastoma tumours.* BMC Cancer, 2019. **19**(1): p. 970.
221. Kersten, K., et al., *Genetically engineered mouse models in oncology research and cancer medicine.* EMBO Mol Med, 2017. **9**(2): p. 137-153.
222. Mizejewski, G.J., *Breast cancer, metastasis, and the microenvironment: disabling the tumor cell-tostroma communication network.* Journal of Cancer Metastasis and Treatment, 2019. **5**: p. 35.
223. Ren, B., et al., *Tumor microenvironment participates in metastasis of pancreatic cancer.* Mol Cancer, 2018. **17**(1): p. 108.
224. Dagogo-Jack, I. and A.T. Shaw, *Tumour heterogeneity and resistance to cancer therapies.* Nat Rev Clin Oncol, 2018. **15**(2): p. 81-94.
225. Weis, S.M. and D.A. Cheresh, *Tumor angiogenesis: molecular pathways and therapeutic targets.* Nat Med, 2011. **17**(11): p. 1359-70.
226. Orcid, L.J.B. and C. Werner, *Evaluation of Three-Dimensional in Vitro Models to Study Tumor Angiogenesis.* ACS Biomaterials Science and Engineering 2017. **4**(2).
227. Tovar, E., C. Essenburg, and C.R. Graveel, *In vivo Efficacy Studies in Cell Line and Patient-derived Xenograft Mouse Models.* bio-protocol, 2017. **7**(1).
228. Zhao, P., et al., *Application of a Three-Dimensional Reconstruction System in Breast Cancer with Ipsilateral Supraclavicular Lymph Node Metastasis: A Case Series.* Breast Care (Basel), 2019. **14**(3): p. 176-179.
229. Finley, S.D., L.H. Chu, and A.S. Popel, *Computational systems biology approaches to anti-angiogenic cancer therapeutics.* Drug Discov Today, 2015. **20**(2): p. 187-97.
230. Gerisch, A. and M.A. Chaplain, *Mathematical modelling of cancer cell invasion of tissue: local and non-local models and the effect of adhesion.* J Theor Biol, 2008. **250**(4): p. 684-704.
231. Kolev, M. and B. Zubik-Kowal, *Numerical solutions for a model of tissue invasion and migration of tumour cells. .* Comput Math Methods Med, 2011. **2011**: p. 452320.
232. Kubitschke, H., et al., *Roadmap to Local Tumour Growth: Insights from Cervical Cancer.* Sci Rep, 2019. **9**(1): p. 12768.
233. Bilous, M., C. Serdjebi, and A. Boyer, *Quantitative mathematical modeling of clinical brain metastasis dynamics in non-small cell lung cancer. .* Sci Rep. , 2019. **9**(1): p. 13018.
234. Baptista, L.P.R., V.V. Sinatti, and J.H. Da Silva, *Computational evaluation of natural compounds as potential inhibitors of human PEPCK.* Adv Appl Bioinform Chem, 2019. **12**: p. 15-32.
235. Cornelis, F., et al., *In vivo mathematical modeling of tumor growth from imaging data: soon to come in the future?* Diagn Interv Imaging, 2013. **94**(6): p. 593-600.
236. Gavrielides, M.A., et al., *Observer variability in the interpretation of HER2/neu immunohistochemical expression with unaided and computer-aided digital microscopy.* Arch Pathol Lab Med, 2011. **135**(2): p. 233-42.
237. Feuchtinger, A., et al., *Image analysis of immunohistochemistry is superior to visual scoring as shown for patient outcome of esophageal adenocarcinoma.* Histochem Cell Biol, 2015. **143**(1): p. 1-9.

238. Stalhammar, G., et al., *Digital image analysis outperforms manual biomarker assessment in breast cancer.* Mod Pathol, 2016. **29**(4): p. 318-29.
239. Abdalla, F., et al., *Correlation of nuclear morphometry of breast cancer in histological sections with clinicopathological features and prognosis.* Anticancer Res, 2009. **29**(5): p. 1771-6.
240. Mudaliar, K. and K. Hutchens, *Morphometric Image Analysis as a Tool in the Diagnosis of Transected Squamous Neoplasms.* Journal of Clinical and Anatomic Pathology, 2013. **1**: p. 102.
241. Chen, L., et al., *Disease Risk Assessment Using a Voronoi-Based Network Analysis of Genes and Variants Scores.* Front Genet, 2017. **8**: p. 29.
242. Sudbo, J., R. Marcelpoil, and A. Reith, *New algorithms based on the Voronoi Diagram applied in a pilot study on normal mucosa and carcinomas.* Anal Cell Pathol, 2000. **21**(2): p. 71-86.
243. Ramadan, E., S. Alinsaif, and M.R. Hassan, *Network topology measures for identifying disease-gene association in breast cancer.* BMC Bioinformatics, 2016. **17 Suppl 7**: p. 274.
244. Kourou, K., T.P. Exarchos, and K.P. Exarchos, *Machine learning applications in cancer prognosis and prediction.* Comput Struct Biotechnol J, 2014. **13**: p. 8-17.
245. Dhahri, H., et al., *Automated Breast Cancer Diagnosis Based on Machine Learning Algorithms.* J Healthc Eng, 2019. **2019**: p. 4253641.
246. Kim, S., S. Jung, and Y. Park, *Effective liver cancer diagnosis method based on machine learning algorithm*, in *7th International Conference on Biomedical Engineering and Informatics*. 2014, IEEE: Dalian, China.
247. Heindl, A., S. Nawaz, and Y. Yuan, *Mapping spatial heterogeneity in the tumor microenvironment: a new era for digital pathology.* Lab Invest, 2015. **95**(4): p. 377-84.
248. Kong, J., et al., *Computer-aided evaluation of neuroblastoma on whole-slide histology images: Classifying grade of neuroblastic differentiation.* Pattern Recognit, 2009. **42**(6): p. 1080-1092.
249. D'Cruze, L., M. Susruthan, and G. Barathi, *Morphometrical analysis of the spectrum of small round cell tumors in a tertiary care centre* Indian Journal of Pathology and Oncology, 2018. **5**(2): p. 314-317.
250. Tadeo, I., E. Gamero-Sandemetrio, and A.P. Berbegall, *1p36 deletion results in a decrease in glycosaminoglycans which is associated with aggressiveness in neuroblastic tumors.* Histol Histopathol. , 2018. **33**(5): p. 487-495.
251. Tadeo, I., A.P. Berbegall, and V. Castel, *Extracellular Matrix Composition Defines an Ultra-High-Risk Group of Neuroblastoma Within the High-Risk Patient Cohort.* Br J Cancer, 2016. **115**(4): p. 480-489.
252. Tadeo, I., E. Gamero-Sandemetrio, and A. Berbegall, *Lymph microvascularization as a prognostic indicator in neuroblastom.* Oncotarget, 2018. **9**(40): p. 26157-26170.
253. Tadeo, I., et al., *Vascular patterns provide therapeutic targets in aggressive neuroblastic tumors.* Oncotarget, 2016. **7**(15): p. 19935-47.
254. Aravindan, N., et al., *Cancer stem cells in neuroblastoma therapy resistance.* Cancer Drug Resist, 2019. **2**: p. 948-967.
255. Roy Choudhury, S., et al., *Targeting angiogenesis for controlling neuroblastoma.* J Oncol, 2012. **2012**: p. 782020.
256. Yoon, K.J. and M.K. Danks, *Cell adhesion molecules as targets for therapy of neuroblastoma.* Cancer Biol Ther, 2009. **8**(4): p. 306-311.
257. Felding-Habermann, B. and D.A. Cheresh, *Vitronectin and its receptors.* Curr Opin Cell Biol, 1993. **5**(5): p. 864-8.
258. Czekay, R.P., et al., *Plasminogen activator inhibitor-1 detaches cells from extracellular matrices by inactivating integrins.* J Cell Biol, 2003. **160**(5): p. 781-91.

259. Madsen, C.D., et al., *uPAR-induced cell adhesion and migration: vitronectin provides the key.* J Cell Biol, 2007. **177**(5): p. 927-39.
260. Annis, M.G., et al., *Integrin-uPAR signaling leads to FRA-1 phosphorylation and enhanced breast cancer invasion.* Breast Cancer Res, 2018. **20**(1): p. 9.
261. Schneider, G., et al., *Vitronectin in the ascites of human ovarian carcinoma acts as a potent chemoattractant for ovarian carcinoma: Implication for metastasis by cancer stem cells.* J Cancer Stem Cell Res, 2016. **4**.
262. Shimada, H., et al., *Histopathologic prognostic factors in neuroblastic tumors: definition of subtypes of ganglioneuroblastoma and an age-linked classification of neuroblastomas.* J Natl Cancer Inst, 1984. **73**(2): p. 405-16.
263. Pikor, L., et al., *The detection and implication of genome instability in cancer.* Cancer Metastasis Rev, 2013. **32**(3-4): p. 341-52.
264. Negrini, S., V.G. Gorgoulis, and T.D. Halazonetis, *Genomic instability--an evolving hallmark of cancer.* Nat Rev Mol Cell Biol, 2010. **11**(3): p. 220-8.
265. Ambros, I.M., et al., *Ultra-High Density SNParray in Neuroblastoma Molecular Diagnostics.* Front Oncol, 2014. **4**: p. 202.
266. Sokol, E., et al., *Age, Diagnostic Category, Tumor Grade, and Mitosis-Karyorrhexis Index Are Independently Prognostic in Neuroblastoma: An INRG Project.* J Clin Oncol, 2020. **38**(17): p. 1906-1918.
267. Hurt, E.M., K. Chan, and M.A. Serrat, *Identification of vitronectin as an extrinsic inducer of cancer stem cell differentiation and tumor formation.* Stem Cells, 2010. **28**(3): p. 390-398.
268. Pirazzoli, V., G.M. Ferraris, and N. Sidenius, *Direct evidence of the importance of vitronectin and its interaction with the urokinase receptor in tumor growth.* Blood, 2013. **121**(12): p. 2316-23.
269. Placencio, V.R. and Y.A. DeClerck, *Plasminogen Activator Inhibitor-1 in Cancer: Rationale and Insight for Future Therapeutic Testing.* Cancer Res, 2015. **75**(15): p. 2969-74.
270. Smith, H.W. and C.J. Marshall, *Regulation of cell signalling by uPAR.* Nat Rev Mol Cell Biol, 2010. **11**(1): p. 23-36.
271. Li, P., et al., *Role of urokinase plasminogen activator and its receptor in metastasis and invasion of neuroblastoma.* J Pediatr Surg, 2004. **39**(10): p. 1512-9.
272. Sugiura, Y., et al., *The plasminogen-plasminogen activator (PA) system in neuroblastoma: role of PA inhibitor-1 in metastasis.* Cancer Res, 1999. **59**(6): p. 1327-36.
273. Isogai, C., et al., *Plasminogen activator inhibitor-1 promotes angiogenesis by stimulating endothelial cell migration toward fibronectin.* Cancer Res, 2001. **61**(14): p. 5587-94.
274. Brooks, P.C., et al., *Antiintegrin alpha v beta 3 blocks human breast cancer growth and angiogenesis in human skin.* J Clin Invest, 1995. **96**(4): p. 1815-22.
275. Burke, P.A., S.J. DeNardo, and L.A. Miers, *Cilengitide targeting of alphavbeta3 integrin receptor synergizes with radioimmunotherapy to increase efficacy and apoptosis in breast cancer xenografts.* Cancer Res, 2002. **62**: p. 4263–4272.
276. Gladson, C.L., *Expression of integrin alpha v beta 3 in small blood vessels of glioblastoma tumors.* J Neuropathol Exp Neurol, 1996. **55**(11): p. 1143-9.
277. Erdreich-Epstein, A., H. Shimada, and S. Groshen, *Integrins alpha(v)beta3 and alpha(v)beta5 are expressed by endothelium of high-risk neuroblastoma and their inhibition is associated with increased endogenous ceramide.* Cancer Res, 2000. **60**(3): p. 712-721.
278. Gladson, C.L., S. Hancock, and M.M. Arnold, *Stage-specific expression of integrin alphaVbeta3 in neuroblastic tumors.* Am J Pathol. , 1996. **148**(5): p. 1423-1434.

279. Erdreich-Epstein, A., A.R. Singh, and S. Joshi, *Association of high microvessel αvβ3 and low PTEN with poor outcome in stage 3 neuroblastoma: rationale for using first in class dual PI3K/BRD4 inhibitor, SF1126.* Oncotarget, 2016. **8**(32): p. 52193-52210.
280. Dohn, L.H., H. Pappot, and B.R. Iversen, *uPAR Expression Pattern in Patients with Urothelial Carcinoma of the Bladder--Possible Clinical Implications.* PLoS One, 2015. **10**(8): p. e0135824.
281. Boonstra, M.C., F.P. Verbeek, and A.P. Mazar, *Expression of uPAR in tumor-associated stromal cells is associated with colorectal cancer patient prognosis: a TMA study.* BMC Cancer., 2014. **14**: p. 269.
282. Lindberg, P., A. Larsson, and B.S. Nielsen, *Expression of plasminogen activator inhibitor-1, urokinase receptor and laminin gamma-2 chain is an early coordinated event in incipient oral squamous cell carcinoma.* Int J Cancer, 2006. **118**(12): p. 2948-56.
283. Lijnen, H.R., *Pleiotropic functions of plasminogen activator inhibitor-1.* J Thromb Haemost, 2005. **3**(1): p. 35-45.
284. van der Burg, M.E., S.C. Henzen-Logmans, and E.M. Berns, *Expression of urokinasetype plasminogen activator (uPA) and its inhibitor PAI-1 in benign, borderline, malignant primary and metastaticovarian tumors. .* Int J Cancer, 1996. **69**: p. 475-479.
285. Stefansson, S. and D.A. Lawrence, *The serpin PAI-1 inhibits cell migration by blocking integrin alpha V beta 3 binding to vitronectin.* Nature, 1996. **383**(6599): p. 441-443.
286. Waltz, D.A., et al., *Plasmin and plasminogen activator inhibitor type 1 promote cellular motility by regulating the interaction between the urokinase receptor and vitronectin.* J Clin Invest, 1997. **100**(1): p. 58-67.
287. De Lorenzi, V., et al., *Urokinase links plasminogen activation and cell adhesion by cleavage of the RGD motif in vitronectin.* EMBO Rep, 2016. **17**(7): p. 982-98.
288. Nakatsuka, E., K. Sawada, and K. Nakamura, *Plasminogen activator inhibitor-1 is an independent prognostic factor of ovarian cancer and IMD-4482, a novel plasminogen activator inhibitor-1 inhibitor, inhibits ovarian cancer peritoneal dissemination.* Oncotarget, 2017. **8**(52): p. 89887-89902.
289. Offersen, B.V., et al., *The myofibroblast is the predominant plasminogen activator inhibitor-1-expressing cell type in human breast carcinomas.* Am J Pathol, 2003. **163**(5): p. 1887-99.
290. Yasuda, T., et al., *Localization of plasminogen activators and their inhibitor in squamous cell carcinomas of the head and neck.* Head Neck, 1997. **19**(7): p. 611-6.
291. Heß, K., C. Böger, and H.M. Behrens, *Correlation between the expression of integrins in prostate cancer and clinical outcome in 1284 patients.* Ann Diagn Pathol. , 2014. **18**(6): p. 343-350.
292. Schnell, O., B. Krebs, and E. Wagner, *Expression of integrin alphavbeta3 in gliomas correlates with tumor grade and is not restricted to tumor vasculature.* Brain Pathol, 2008. **18**(3): p. 378-386.
293. Beer, A.J., et al., *Patterns of alphavbeta3 expression in primary and metastatic human breast cancer as shown by 18F-Galacto-RGD PET.* J Nucl Med, 2008. **49**(2): p. 255-9.
294. Bello, L., J. Zhang, and D.C. Nikas, *Alpha(v)beta3 and alpha(v)beta5 integrin expression in meningiomas.* Neurosurgery, 2000. **47**(5): p. 1185-1195.
295. Singer, C.F., et al., *Stromal coexpression of uPA/PAI-1 protein predicts poor disease outcome in endocrine-treated postmenopausal patients with receptor-positive early breast cancer.* Breast, 2019. **46**: p. 101-107.
296. Theek, B., et al., *Semi-Automated Segmentation of the Tumor Vasculature in Contrast-Enhanced Ultrasound Data.* Ultrasound Med Biol, 2018. **44**(8): p. 1910-1917.
297. Webster, J.D., E.R. Simpson, and A.M. Michalowski, *Quantifying histological features of cancer biospecimens for biobanking quality assurance using automated morphometric pattern recognition image analysis algorithms.* J Biomol Tech, 2011. **22**(3): p. 108-118.

298. Despotović , S.Z., N.M. Milićević , and D.P. Milošević, *Remodeling of extracellular matrix of the lamina propria in the uninvolved human rectal mucosa 10 and 20 cm away from the malignant tumor.* Tumour Biol, 2017. **39**(7): p. 1010428317711654.
299. Iizuka, Y., T. Utsunomiy, and S. Fushimi, *Morphometric analysis of tumor stromal lymphatic vessels and lymphangiogenesis in oral squamous cell carcinoma.* Journal of Oral and Maxillofacial Surgery, Medicine, and Pathology, 2019. **31**(1): p. 47-51.
300. Peck, A.R., et al., *Validation of tumor protein marker quantification by two independent automated immunofluorescence image analysis platforms.* Mod Pathol, 2016. **29**(10): p. 1143-54.
301. Aeffner, F., et al., *Introduction to Digital Image Analysis in Whole-slide Imaging: A White Paper from the Digital Pathology Association.* J Pathol Inform, 2019. **10**: p. 9.
302. Gladson, C.L., et al., *Vitronectin expression in differentiating neuroblastic tumors: integrin alpha v beta 5 mediates vitronectin-dependent adhesion of retinoic-acid-differentiated neuroblastoma cells.* Am J Pathol, 1997. **150**(5): p. 1631-46.
303. Pons, S., et al., *Vitronectin regulates Sonic hedgehog activity during cerebellum development through CREB phosphorylation.* Development, 2001. **128**(9): p. 1481-92.
304. Abe, A., et al., *alphavbeta5 integrin mediates the effect of vitronectin on the initial stage of differentiation in mouse cerebellar granule cell precursors.* Brain Res, 2018. **1691**: p. 94-104.
305. Shimizu, S., et al., *Foxa (HNF3) up-regulates vitronectin expression during retinoic acid-induced differentiation in mouse neuroblastoma Neuro2a cells.* Cell Struct Funct, 2002. **27**(4): p. 181-8.
306. Sugahara, M., Y. Nakaoki, and A. Yamaguchi, *Vitronectin is Involved in the Morphological Transition of Neurites in Retinoic Acid-Induced Neurogenesis of Neuroblastoma Cell Line Neuro2a.* Neurochem Res, 2019. **44**(7): p. 1621-1635.
307. Munn, L.L., *Dynamics of tissue topology during cancer invasion and metastasis.* Phys Biol, 2013. **10**(6): p. 065003.
308. Marinaro, G., et al., *Networks of neuroblastoma cells on porous silicon substrates reveal a small world topology.* Integr Biol (Camb), 2015. **7**(2): p. 184-97.
309. Solovei, I., et al., *Topology of double minutes (dmins) and homogeneously staining regions (HSRs) in nuclei of human neuroblastoma cell lines.* Genes Chromosomes Cancer, 2000. **29**(4): p. 297-308.
310. Pogue, B.W., M.A. Mycek, and D. Harper, *Image analysis for discrimination of cervical neoplasia.* J Biomed Opt, 2000. **5**(1): p. 72-82.
311. Varberg, K.M., et al., *Kinetic Analysis of Vasculogenesis Quantifies Dynamics of Vasculogenesis and Angiogenesis In Vitro.* J Vis Exp, 2018(131).
312. Hannezo, E. and B.D. Simons, *Statistical theory of branching morphogenesis.* Dev Growth Differ, 2018. **60**(9): p. 512-521.
313. Monferrer, E., et al., *High Oct4 expression: implications in the pathogenesis of neuroblastic tumours.* BMC Cancer, 2019. **19**(1): p. 1.
314. Tadeo, I., *Estudio del armazón arquitectónico y del sistema vascular de los tumores neuroblásticos.* , in *Departament de Patologia*. 2014, Universitat de Valencia.
315. Zuñiga, V., *Análisis microscópico digital del infiltrado inmune en neuroblastoma. impacto pronóstico*, in *Departament de Patologia*. 2018, Universitat de Valencia.
316. Kumar, S. and V.M. Weaver, *Mechanics, malignancy, and metastasis: the force journey of a tumor cell.* Cancer Metastasis Rev, 2009. **28**(1-2): p. 113-27.
317. Jain, R.K., J.D. Martin, and T. Stylianopoulos, *The role of mechanical forces in tumor growth and therapy.* Annu Rev Biomed Eng, 2014. **16**: p. 321-46.
318. Zhu, Z., et al., *Yin-yang effect of tumour cells in breast cancer: from mechanism of crosstalk between tumour-associated macrophages and cancer-associated adipocytes.* Am J Cancer Res, 2020. **10**(2): p. 383-392.

319. Zheng, S., et al., *Development and validation of a stromal immune phenotype classifier for predicting immune activity and prognosis in triple-negative breast cancer.* Int J Cancer, 2020. **147**(2): p. 542-553.
320. Li, W., et al., *Integrated tumor stromal features of hepatocellular carcinoma reveals two distinct subtypes with prognostic/predictive significance.* Aging (Albany NY), 2019. **11**(13): p. 4478-4509.
321. Zhang, Q., et al., *Integrated multiomic analysis reveals comprehensive tumour heterogeneity and novel immunophenotypic classification in hepatocellular carcinomas.* Gut, 2019. **68**(11): p. 2019-2031.
322. Wartenberg, M., et al., *Integrated Genomic and Immunophenotypic Classification of Pancreatic Cancer Reveals Three Distinct Subtypes with Prognostic/Predictive Significance.* Clin Cancer Res, 2018. **24**(18): p. 4444-4454.
323. Preissner, K.T. and U. Reuning, *Vitronectin in vascular context: facets of a multitalented matricellular protein.* Semin Thromb Hemost, 2011. **37**(4): p. 408-24.
324. Shi, K., et al., *Vitronectin significantly influences prognosis in osteosarcoma.* Int J Clin Exp Pathol, 2015. **8**(9): p. 11364-11371.
325. Heyman, L., et al., *Vitronectin and its receptors partly mediate adhesion of ovarian cancer cells to peritoneal mesothelium in vitro.* Tumour Biol, 2008. **29**(4): p. 231-44.
326. Pietras, K. and A. Ostman, *Hallmarks of cancer: interactions with the tumor stroma.* Exp Cell Res, 2010. **316**(8): p. 1324-31.
327. Bussard, K.M., L. Mutkus, and K. Stumpf, *Tumor-associated stromal cells as key contributors to the tumor microenvironment.* Breast Cancer Res, 2016. **18**(1): p. 84.
328. Tranchevent, L.C., et al., *Predicting clinical outcome of neuroblastoma patients using an integrative network-based approach.* Biol Direct, 2018. **13**(1): p. 12.
329. Radhakrishnan, A., et al., *Machine Learning for Nuclear Mechano-Morphometric Biomarkers in Cancer Diagnosis.* Sci Rep, 2017. **7**(1): p. 17946.
330. Nyirenda, N., D.L. Farkas, and V.K. Ramanujan, *Preclinical evaluation of nuclear morphometry and tissue topology for breast carcinoma detection and margin assessment.* Breast Cancer Res Treat, 2011. **126**(2): p. 345-54.
331. Cheng, J., et al., *Identification of topological features in renal tumor microenvironment associated with patient survival.* Bioinformatics, 2018. **34**(6): p. 1024-1030.
332. Bulin, A.L., M. Broekgaarden, and T. Hasan, *Comprehensive high-throughput image analysis for therapeutic efficacy of architecturally complex heterotypic organoids.* Sci Rep, 2017. **7**(1): p. 16645.
333. Lee, S.L., et al., *Computer-assisted image analysis of the tumor microenvironment on an oral tongue squamous cell carcinoma tissue microarray.* Clin Transl Radiat Oncol, 2019. **17**: p. 32-39.
334. Ehteshami Bejnordi, B., M. Mullooly, and R.M. Pfeiffer, *Using deep convolutional neural networks to identify and classify tumor-associated stroma in diagnostic breast biopsies.* Mod Pathol. , 2018. **31**(10): p. 1502-1512.
335. Thiele, C.J., *Neuroblastoma Cell Lines*, in *Human Cell Culture*, J. Masters, Editor. 1998, Lancaster, UK: Kluwer Academic Publishers. p. 21-53.
336. Brodeur, G.M., G. Sekhon, and M.N. Goldstein, *Chromosomal aberrations in human neuroblastomas.* Cancer, 1977. **40**(5): p. 2256-63.
337. Kryh, H., H. Carén, and J. Erichsen, *Comprehensive SNP array study of frequently used neuroblastoma cell lines; copy neutral loss of heterozygosity is common in the cell lines but uncommon in primary tumors.* BMC Genomics, 2011. **12**: p. 443.
338. Harenza, J.L., et al., *Corrigendum: Transcriptomic profiling of 39 commonly-used neuroblastoma cell lines.* Sci Data, 2017. **4**: p. 170183.
339. Carpenter, E.L., et al., *Dielectrophoretic capture and genetic analysis of single neuroblastoma tumor cells.* Front Oncol, 2014. **4**: p. 201.

340. Stock, C., et al., *Genes proximal and distal to MYCN are highly expressed in human neuroblastoma as visualized by comparative expressed sequence hybridization.* Am J Pathol, 2008. **172**(1): p. 203-14.
341. Meyer, A., et al., *Integrin expression regulates neuroblastoma attachment and migration.* Neoplasia, 2004. **6**(4): p. 332-42.
342. Horwacik, I. and H. Rokita, *Modulation of interactions of neuroblastoma cell lines with extracellular matrix proteins affects their sensitivity to treatment with the anti-GD2 ganglioside antibody 14G2a.* Int J Oncol, 2017. **50**(5): p. 1899-1914.
343. Ciccarone, V., et al., *Phenotypic diversification in human neuroblastoma cells: expression of distinct neural crest lineages.* Cancer Res, 1989. **49**(1): p. 219-25.
344. Tomayko, M.M. and C.P. Reynolds, *Determination of subcutaneous tumor size in athymic (nude) mice.* Cancer Chemother Pharmacol, 1989. **24**(3): p. 148-54.
345. Murayama, T. and N. Gotoh, *Patient-Derived Xenograft Models of Breast Cancer and Their Application.* Cells, 2019. **8**(6).
346. Cornillie, J., et al., *Establishment and Characterization of Histologically and Molecularly Stable Soft-tissue Sarcoma Xenograft Models for Biological Studies and Preclinical Drug Testing.* Mol Cancer Ther, 2019. **18**(6): p. 1168-1178.
347. Tentler, J.J., et al., *Patient-derived tumour xenografts as models for oncology drug development.* Nat Rev Clin Oncol, 2012. **9**(6): p. 338-50.
348. Pettan-Brewer, C., J. Morton, and S. Cullen, *Tumor growth is suppressed in mice expressing a truncated XRCC1 protein.* Am J Cancer Res, 2012. **2**(2): p. 168-177.
349. Linnebacher, M., et al., *Cryopreservation of human colorectal carcinomas prior to xenografting.* BMC Cancer, 2010. **10**: p. 362.
350. Sorio, C., et al., *Successful xenografting of cryopreserved primary pancreatic cancers.* Virchows Arch, 2001. **438**(2): p. 154-8.
351. Bajou, K., et al., *Plasminogen activator inhibitor-1 protects endothelial cells from FasL-mediated apoptosis.* Cancer Cell, 2008. **14**(4): p. 324-34.
352. Morscher, R.J., et al., *Inhibition of Neuroblastoma Tumor Growth by Ketogenic Diet and/or Calorie Restriction in a CD1-Nu Mouse Model.* PLoS One, 2015. **10**(6): p. e0129802.
353. Lakoma, A., et al., *The MDM2 small-molecule inhibitor RG7388 leads to potent tumor inhibition in p53 wild-type neuroblastoma.* Cell Death Discov, 2015. **1**.
354. Teitz, T., et al., *Preclinical models for neuroblastoma: establishing a baseline for treatment.* PLoS One, 2011. **6**(4): p. e19133.
355. Martin, T.A., L. Ye, and A.J. Sanders, *Cancer Invasion and Metastasis: Molecular and Cellular Perspective*, in *Metastatic Cancer Clinical and Biological Perspectives*, J. Rahul, Editor. 1970, Landes Bioscience. p. 135-168.
356. Patterson, D.M., J.M. Shohet, and E.S. Kim, *Preclinical models of pediatric solid tumors (neuroblastoma) and their use in drug discovery.* Curr Protoc Pharmacol, 2011. **Chapter 14**: p. Unit 14 17.
357. Bomken, S., et al., *Percentage tumor necrosis following chemotherapy in neuroblastoma correlates with MYCN status but not survival.* Pediatr Hematol Oncol, 2011. **28**(2): p. 106-14.
358. Zormpas-Petridis, K., et al., *MRI Imaging of the Hemodynamic Vasculature of Neuroblastoma Predicts Response to Antiangiogenic Treatment.* Cancer Res, 2019. **79**(11): p. 2978-2991.
359. Rysenkova, K.D., et al., *CRISPR/Cas9 nickase mediated targeting of urokinase receptor gene inhibits neuroblastoma cell proliferation.* Oncotarget, 2018. **9**(50): p. 29414-29430.
360. Semina, E.V., et al., *Downregulation of uPAR promotes urokinase translocation into the nucleus and epithelial to mesenchymal transition in neuroblastoma.* J Cell Physiol, 2020. **235**(9): p. 6268-6286.

361. Kenny, H.A., et al., *The initial steps of ovarian cancer cell metastasis are mediated by MMP-2 cleavage of vitronectin and fibronectin.* J Clin Invest, 2008. **118**(4): p. 1367-79.
362. Mahmood, N., C. Mihalcioiu, and S.A. Rabbani, *Multifaceted Role of the Urokinase-Type Plasminogen Activator (uPA) and Its Receptor (uPAR): Diagnostic, Prognostic, and Therapeutic Applications.* Front Oncol, 2018. **8**: p. 24.
363. Chandrasekar, N., et al., *Downregulation of uPA inhibits migration and PI3k/Akt signaling in glioblastoma cells.* Oncogene, 2003. **22**(3): p. 392-400.
364. Lu, P., V.M. Weaver, and Z. Werb, *The extracellular matrix: a dynamic niche in cancer progression.* J Cell Biol, 2012. **196**(4): p. 395-406.
365. Craig, A.J., et al., *Tumour evolution in hepatocellular carcinoma.* Nat Rev Gastroenterol Hepatol, 2020. **17**(3): p. 139-152.
366. Ribatti, D., et al., *Podoplanin and LYVE-1 expression in lymphatic vessels of human neuroblastoma.* J Neurooncol, 2010. **100**(1): p. 151-2.
367. Asgharzadeh, S., et al., *Clinical significance of tumor-associated inflammatory cells in metastatic neuroblastoma.* J Clin Oncol, 2012. **30**(28): p. 3525-32.
368. Mina, M., et al., *Tumor-infiltrating T lymphocytes improve clinical outcome of therapy-resistant neuroblastoma.* Oncoimmunology, 2015. **4**(9): p. e1019981.
369. Cariati, F., et al., *Dissecting Intra-Tumor Heterogeneity by the Analysis of Copy Number Variations in Single Cells: The Neuroblastoma Case Study.* Int J Mol Sci, 2019. **20**(4).
370. Ben-David, U., et al., *Patient-derived xenografts undergo mouse-specific tumor evolution.* Nat Genet, 2017. **49**(11): p. 1567-1575.
371. Greaves, M. and C.C. Maley, *Clonal evolution in cancer.* Nature, 2012. **481**(7381): p. 306-13.
372. Calandrini, C., et al., *An organoid biobank for childhood kidney cancers that captures disease and tissue heterogeneity.* Nat Commun, 2020. **11**(1): p. 1310.
373. López-Carrasco, A., *Impact of extracelular matrix properties on neuroblastoma heterogenity*. 2020. p. Article in preparation.

Appendix

-Clinical and biological section

Tables 2 and 3. Descriptors of the clinical and genetic data regarding OS and EFS, respectively.

Factor		N(%)	tOS mean	95% IC		5 year (%)
Age	<18months	70 (55)	132	123	142	89.7±4.6
	≥18months	57 (45)	93	73	114	45.7±7.9
Stage	L1/L2/MS	90 (71)	143	132	155	84.8±4.6
	M	34 (27)	79	55	102	40.2±9.3
Histopathologic category	GN/GNB	15 (13)	137	113	161	87.5±11
	nGNB/NB	101 (87)	123	108	137	69±5.4
Histopathologic differentiation	dNB	12 (10)	126.6	103	150	90.9±8.7
	pd	79 (62)	126.7	112	142	77.8±5.3
	uNB	15 (12)	61.30	25	98	21.8±13.4
MYCN status	MNNA	97 (76)	126	115	137	82.3±4.8
	MNA	24 (19)	59	30	88	26.3±10.1
11q	ND	94 (74)	134	119	149	78.8±5
	D	24 (19)	62	43	81	32±11.9
1p	ND	78 (61)	130.10	119	142	81.3±5.6
	D	48 (38)	97.60	74	121	51.9±8.6
17q	NG	68 (54)	151.50	138	165	90±4.2
	G	54 (43)	96.10	76	117	51±8.1
Ploidy	Hiperploid	62 (49)	104	90	119	71.5±6.6
	Diploid	16 (13)	106	68	144	56.3±13.1
Genetic profile	NCA	47 (37)	135	122	149	91.3±4.9
	SCA	72 (57)	107	88	126	56.9±7
Risk group	Non-High risk	88 (70)	135	125	146	93±3.4
	High risk	36 (29)	73	49	96	33±8.6

Factor		N	(%)	tEFS mean	95% IC		5 year (%)
Age	<18months	70	(55)	127	117	138	87.7±4.7
	≥18months	57	(45)	77	56	98	46.5±7.7
Stage	L1/L2/MS	90	(71)	137	125	150	82.5±4.4
	M	34	(27)	57	38	75	37.2±9.1
Histopathologic category	GN/GNB	15	(13)	136	109	162	88.5±10.5
	nGNB/NB	101	(87)	112	96	127	66±5.3
Histopathologic differentiation	dNB	12	(10)	124	109	139	80.8±12.2
	pd	79	(62)	73	55	92	72.4±5.6
	uNB	15	(12)	32	13	51	9.1±8.7
MYCN status	MNNA	97	(76)	118	103	133	79.6±4.6
	MNA	24	(19)	52	23	82	26±10.1
11q	ND	94	(74)	120	104	137	72.5±6.1
	D	24	(19)	51	31	72	31.1±11.3
1p	ND	78	(61)	123	110	136	79.4±5.1
	D	48	(38)	89	65	112	51.1±8.4
17q	NG	68	(54)	120	106	134	85.6±4.8
	G	54	(43)	89	68	111	48.6±7.8
Ploidy	Hiperploid	62	(49)	93	79	106	66±6.7
	Diploid	16	(13)	87	48	126	44.4±14.8
Genetic profile	NCA	47	(37)	127	110	144	87.2±5.4
	SCA	72	(57)	96	76	115	55.4±6.8
Risk group	Non-High risk	88	(70)	127	112	141	87.2±4
	High risk	36	(29)	58	35	81	30±8.4

L1 and L2: localized and MS: special metastatic; M: metastatic; GN: ganglioneurona nGNB: ganglioneuroblastoma nodular; NB: neuroblastoma; dNB: differentiating neuroblastoma; pdNB: poorly differentiated neuroblastoma; uNB: undifferentiated neuroblastoma; MNNA: *MYCN* non-amplified; MNA: *MYCN* amplified; ND: non deletion; D: deletion; NCA: numerical chromosomal aberration; SCA: segmental chromosomal aberration; Hiperp.: Hiperploid; Dip.: diploid; EFS: event-free survival; OS: overall survival.

Table 4.p-values resulting of the Kaplan Meier test comparing INRG variables with EFS and OS.

Factor		EFS p-value	OS p-value
Age	<18months ≥18months	0.000	0.000
Stage	L1/L2/MS M	0.000	0.000
Histopathologic category	GN/GNB nGNB/NB	0.100	0.180
Histopathologic differentiation	dNB pd uNB	0.000	0.000
MYCN status	MNNA MNA	0.000	0.000
11q	ND D	0.000	0.000
1p	ND D	0.001	0.000
17q	NG G	0.000	0.000
Ploidy	Hiperp. Dip.	0.200	0.400
Gen. profile	NCA SCA	0.002	0.001
Risk group	Non-HR HR	0.000	0.000

L1 and L2: localized and MS: special metastatic; M: metastatic; GN: ganglioneuroma; nGNB: ganglioneuroblastoma nodular; NB: neuroblastoma; dNB: differentiating neuroblastoma; pdNB: poorly differentiated neuroblastoma; uNB: undifferentiated neuroblastoma; MNNA: *MYCN* non-amplified; MNA: *MYCN* amplified; ND: non deletion; D: deletion; NCA: numerical chromosomal aberration; SCA: segmental chromosomal aberration; Hiperp.: Hiperploid; Dip.: diploid; EFS: event-free survival; OS: overall survival.

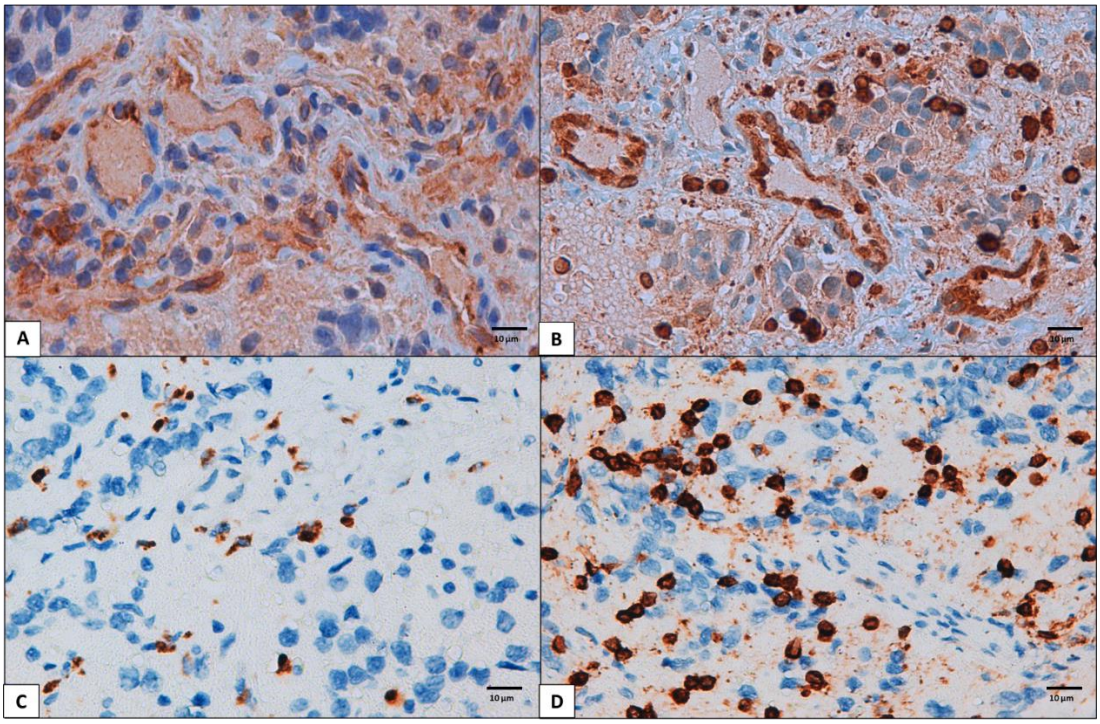

Figure 9. Histopathological NB image of A) $\alpha_v\beta_3$ integrin, B) VN, C) CD68 marker for macrophages and D) CD45 marker to detect lymphoid cells. Images at 40x.

-Morphometric measurements section

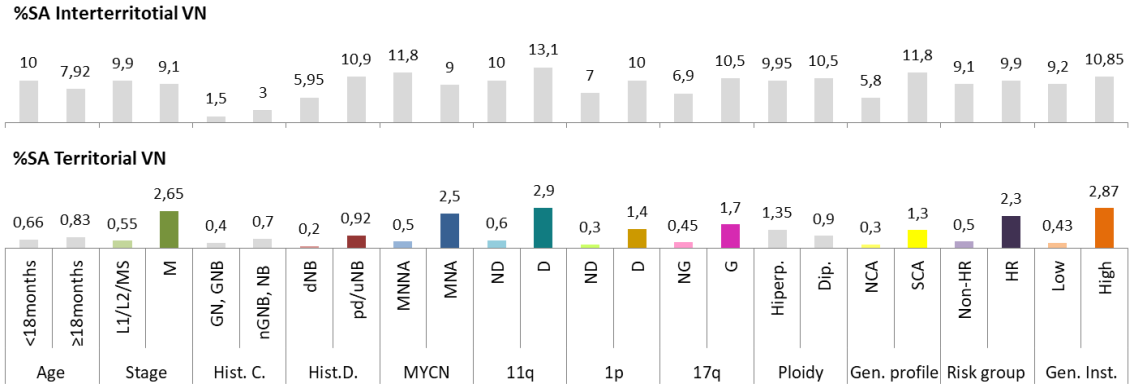

Figure 12. Distribution of the amount of VN using IPP software depending on the INRG clinical and biological variables. The median value is shown. Variables in grey means that median is not statistically significant; colored variables show significant statistical relationship; dark colour of the INRG category is the group that presents the high median value. L1 and L2: localized and MS: special metastatic; M: metastatic; Hist. C.: histopathologic category; GN:ganglioneuroma; nGNB: ganglioneuroblastoma nodular; NB: neuroblastoma; Hist. D: histopathologic differentiation; dNB: differentiating neuroblastoma; pdNB: poorly differentiated neuroblastoma; uNB: undifferentiated neuroblastoma; NOS was excluded from statistical analysis; MNNA: *MYCN* non-amplified; MNA: *MYCN* amplified; ND: non deletion; D: deletion; NG: no gain;G: gain; Gen. Profile: genetic profile; NCA: numerical chromosomal aberration; SCA:

segmental chromosomal aberration; Hiperp.: Hiperploid; Dip.: diploid; Tetrap.:tetraploid; HR: High-risk; Gen. Instab.:genetic instability.

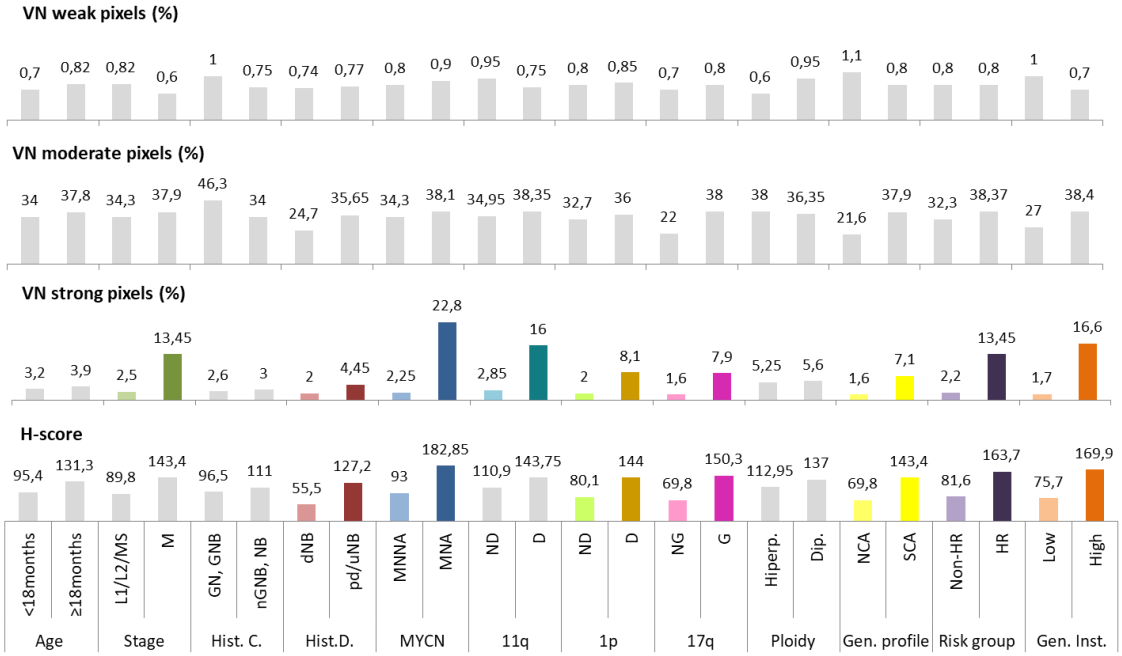

Figure 13. Distribution of the amount of VN using DensitoQ. software depending on the INRG clinical and biological variables. Data obtained through DensitoQuant module from Pannoramic MIDI software. The median value is shown. Variables in grey means that median is not statistically significant; colored variables show significant statistical relationship; dark colour of the INRG category is the group that presents the high median value; %SA: percentage of stained area. L1 and L2: localized and MS: special metastatic; M: metastatic; Hist. C.: histopathologic category; GN:ganglioneuroma; nGNB: ganglioneuroblastoma nodular; NB: neuroblastoma; Hist. D: histopathologic differentiation; dNB: differentiating neuroblastoma; pdNB: poorly differentiated neuroblastoma; uNB: undifferentiated neuroblastoma; NOS was excluded from statistical analysis; MNNA: *MYCN* non-amplified; MNA: *MYCN* amplified; ND: non deletion; D: deletion; NG: no gain; G: gain; Gen. Profile: genetic profile; NCA: numerical chromosomal aberration; SCA: segmental chromosomal aberration; Hiperp.: Hiperploid; Dip.: diploid; Tetrap.:tetraploid; HR: High-risk; Gen. Instab.:genetic instability.

Table 5. Results of the correlation between the morphometric data obtained after two algorithm customization in different softwares**.**

Parameter	Spearman´s correlation	p-value
%SA Interterritorial VN and weak pixels	0.260	0.031
%SA Interterritorial VN and moderate pixels	0.785	0.000
%SA Territorial VN and strong pixels	0.896	0.000
%SA Interterritorial and H-score	0.757	0.000
%SA Territorial VN and H-score	0.814	0.000

SA: stained area; VN: vitronectin.

Table 6. Correlation between the subjective scoring and the morphometric data. The mean % of stained area is shown.

Subjective score	%SA Interterritorial VN	%SA Territorial VN	Weak	Moderate	Strong	H-score
Negative (0)	0.25±0.23	0.06±0.04	0.16±0.10	1.30±1.30	0.40±0.40	6.3±3.5
Weak-Moderate(1+-2+)	8.8±7.25	1.40±2.40	1.90±2.70	32.55±22.35	7±10.70	85.90±63.40
Strong (3+)	24±10.80	7.40±5.70	1.10±0.90	53.90±20.20	30.25±22.20	199.10±38.25

SA: stained area; VN: vitronectin.

-Morphometric and topologycal features to obtained and ECM patterns section

Obtention of morphometric categories variables

Regarding our findings, the % SA of GAGs, as a low amount of this element was found in NB patients with poor prognosis, we differentiated the following categories: good: > % SA of GAGs over the median value, intermediate: ≤median and ≥1 (first quartile), and bad: values below 1% of SA. For reticulin and blood/lymph vessels as you can find in publications and in the table 7, we had 3 parameters, and for lymph vessels only 2, in case of reticulin: when length/dendrites were below and in case of width over the median values, were related to poor prognosis. In blood/lymph vessels when the 3 or 2 parameters, respectively were over the median were associated with poor outcome, then we distinguished: good: when the parameters have a value related to good prognosis (in reticulin: length and dendrites over the median, and width under the median or in blood/lymph vessels when all parameters below the median), intermediate: only 1 parameter is related to poor prognosis as long as it was not that presented the highest Exp (B) value, for the 3 elements, and bad: when the respective element (in lymph vessels is only possible 2), presented 2 or more parameters related to poor prognosis.

As for VN, as you know a high %SA of territorial VN is associated with poor prognosis, we discriminated: good: when the %SA is under the median value, intermediate: %SA is below the third quartile, bad: %SA over the third quartile.

With regard, the immune system, our studies showed that a high infiltraction of CD68 and CD163 (over the median) together with a low infiltration of CD11c (under the median) were related to poor prognosis, so: good: when the infiltration of macrophages were low and high infiltration of DCs, intermediate: when only one variable was related to poor outcome and bad: when two o more variables are associated to poor prognosis. And finally, with regard to stem cells, we have observed that a high amount of positive cells of the previously named markers are correlated with poor outcome (all the markers over the median, except for CD105 that we

have used the third quartile). Then, we discriminate among: good: when all the variables are connected to grate prognosis, intermediate: when one variable was related to poor outcome, and bad: two or more variables were related to unsuccessful outcome.

-In vivo experiments section

Genotyping protocol

The genotype of each animal (total 122 animals) was determined by PCR of the genomic DNA extracted from ear tissue fragments at 21 days of age. By using the Maxwell® 16 FFPE Plus LEV DNA Purification Kit (Promega). To perform the PCR, we followed the cycling steps by The Jackson Laboratory protocol since we purchased the animals from this repository (B6.129S7-*Rag1*^{tm1Mom}/J and B6.129S2 (D2)-*Vtn*^{tm1Dgi}/J) and the primers that were used:

- VN $^{-/-}$ strain:

PRIMER	5' LABEL	SEQUENCE 5' → 3'	3' LABEL	PRIMER TYPE	REACTION	NOTE
21140		TTT TGC CGC TGA GAC TAC TG		Common	A	
21141		CAG TTA TGA GCT GCC GTG TG		Wild type Reverse	A	
oIMR2088		AGA CTG CCT TGG GAA AAG CG		Mutant Reverse	A	

-RAG1$^{-/-}$ strain:

PRIMER	5' LABEL	SEQUENCE 5' → 3'	3' LABEL	PRIMER TYPE	REACTION	NOTE
23267		TCT GGA CTT GCC TCC TCT GT		Wild type Forward	A	
23268		CAT TCC ATC GCA AGA CTC CT		Common	A	
oIMR8162		TGG ATG TGG AAT GTG TGC GAG		Mutant Forward	A	PGK R

There is a common forward primer for both alleles, and two reverse primers, one for the wild-type allele and one for the mutant allele. After a 38 cycle reaction, the amplification product for the VN strain is for the wild-type 393 bp allele and for the 250 bp mutant allele. While for the RAG1 strain after 38 cycles, the amplification product for the wild-type allele is 192 bp and for the mutant allele 197 bp.

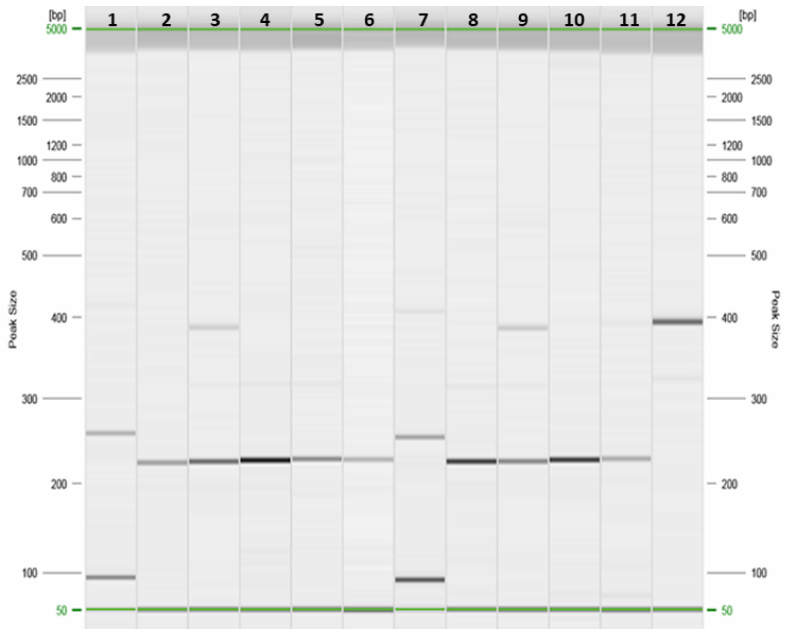

Electrophoresis results of VN in different mice: samples lanes 2-6 and 8-11 were mutant and lane 12 was wild type.

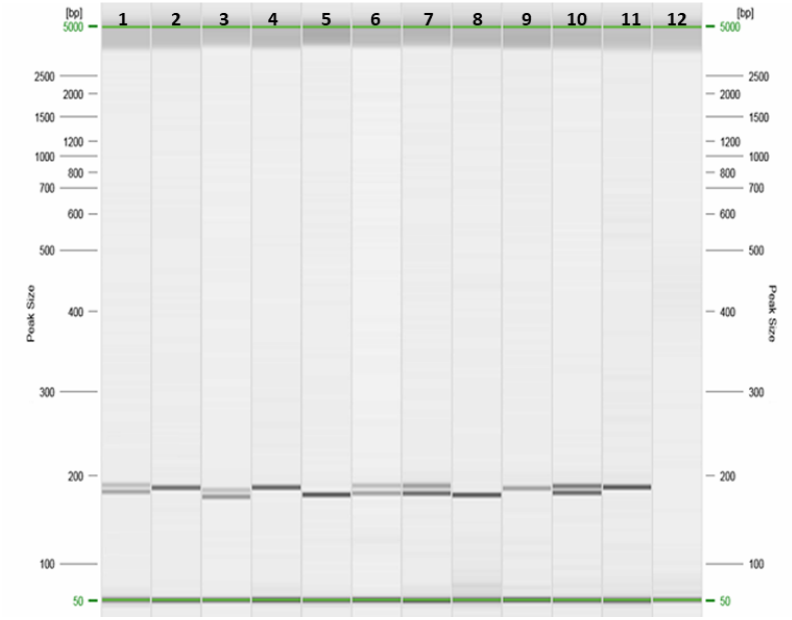

Electrophoresis results of RAG1 in different mice: samples lanes 1,3,6,7 and 10 were heterozygous. Lanes 2,4,9 and 12 were mutant and lanes 5 and 8 were wild type.

Table 13. Description of data and p-valuues related to metasatasis and adjacent implant presence in MNA and MNNA-derived xenografts.

	Cell line	Background	Parameter	Passages		
				P0	P1-5	p-value
Metastasis	SK-N-BE (2)	$VN^{-/-}$	Number	0 (0%)	1 (11%)	0.303
			Volume (mm^3)	0	130	
			Time (weeks)	8	13	
		$VN^{+/+}$	Number	2 (20%)	3 (30%)	0.932
			Volume (mm^3)	20	170	
			Time (weeks)	8	12	
		p-value		0.596	0.524	
	SH-SY5Y	$VN^{-/-}$	Number	3 (33%)	0 (0%)	0.014*
			Volume (mm^3)	220	0	
			Time (weeks)	8	14	
		$VN^{+/+}$	Number	0 (0%)	2 (65%)	0.016*
			Volume (mm^3)	0	48	
			Time (weeks)	8	12	
		p-value		0.09	0.001*	
Adjacent implants	SK-N-BE (2)	$VN^{-/-}$	Number	4 (45%)	0 (0%)	0.023*
			Volume (mm^3)	145	0	
			Time (weeks)	8	13	
		$VN^{+/+}$	Number	4 (40%)	3 (21%)	0.324
			Volume (mm^3)	192	45	
			Time (weeks)	8	12	
		p-value		0.845	0.136	
	SH-SY5Y	$VN^{-/-}$	Number	3 (33%)	3 (18%)	0.412
			Volume (mm^3)	333	430	
			Time (weeks)	8	14	
		$VN^{+/+}$	Number	3 (43%)	0(0%)	0.175
			Volume (mm^3)	106	0	
			Time (weeks)	8	12	
		p-value		0.696	0.414	

In white the MNA-derived xenografts are marked, and in light grey the MNNA-derived xenograft. Chi-square test used to compare the number of positive implants and metastasis. P-values in the columns refer to the comparison within the same mouse background but different passage, while p-values in the rows compare different background within the same passage. *(p-values<0.05).

Table 14. Description of data and p-values related to % of neuroblastic cells in MNA and MNNA-derived xenografts.

	Cell line	Background	Parameter	Passages		p-value
				P0	P1-5	
%Neuroblastic cells	SK-N-BE (2)	$VN^{-/-}$	Mean	65.60	72.80	
			SD	15	17.30	
			Median	60	75	
			Q1-Q3	50-70	60-87.50	0.387
		$VN^{+/+}$	Mean	77	74.30	
			SD	14.95	11.40	
			Median	80	75	
			Q1-Q3	60-90	68.75-81.25	
		p-value		0.113	0.877	0.472
	SH-SY5Y	$VN^{-/-}$	Mean	73.30	75	
			SD	10	20	
			Median	70	80	
			Q1-Q3	65-80	72.50-87.50	0.251
		$VN^{+/+}$	Mean	77.10	65	
			SD	9	5	
			Median	80	65	
			Q1-Q3	65-80	60-70	
		p-value		0.472	0.064	0.117

In white the MNA-derived xenografts are marked, and in light grey the MNNA-derived xenografts. Chi-square test was used to compare the number of neuroblastic cells. P-values in the columns refer to the comparison within the same mouse background but different passage, while p-values in the rows compare different background within the same passage.

Table 15. Description of data and p-values related to % of necrosis in MNA and MNNA-derived xenografts.

	Cell line	Background	Parameter	Passages		p-value
				P0	P1-5	
%Necrosis	SK-N-BE (2)	$VN^{-/-}$	Mean	18.90	13.45	0.489
			SD	14.50	11.30	
			Median	30	10	
			Q1-Q3	5-30	3-25	
		$VN^{+/+}$	Mean	9.20	12	0.285
			SD	12	8.9	
			Median	3.50	13	
			Q1-Q3	0-18.75	4.25-20	
		p-value		0.113	0.926	
	SH-SY5Y	$VN^{-/-}$	Mean	7.80	8.60	0.9
			SD	7.10	9.30	
			Median	10	7.50	
			Q1-Q3	0-12.50	0.25-10	
		$VN^{+/+}$	Mean	8.60	16.70	0.383
			SD	7.50	15.30	
			Median	10	20	
			Q1-Q3	0-15	0-30	
		p-value		0.830	0.487	

In white the MNA-derived xenografts are marked, and in light grey the MNNA-derived xenografts. Chi-square test was used to compare the amount of necrosis. P-values in the columns refer to the comparison within the same mouse background but different passage, while p-values in the rows compare different background within the same passage.

Table 16. Description of data and p-values related to % of hemorrhagic areas in MNA and MNNA-derived xenografts.

	Cell line	Background	Parameter	Passages		p-value
				P0	P1-5	
%Hemorrhage	SK-N-BE (2)	$VN^{-/-}$	Mean	6.30	9.20	0.340
			SD	8.40	9.90	
			Median	2	5	
			Q1-Q3	0-15	1.50-15	
		$VN^{+/+}$	Mean	4	6.60	0.108
			SD	7	6.40	
			Median	0	5	
			Q1-Q3	0-10	2-10	
		p-value		0.447	0.688	
	SH-SY5Y	$VN^{-/-}$	Mean	3.45	6.30	0.452
			SD	5.40	6.30	
			Median	2	7.50	
			Q1-Q3	0-6	0-10	
		$VN^{+/+}$	Mean	3.30	5	0.667
			SD	3.60	5	
			Median	2	5	
			Q1-Q3	0-5	0-10	
		p-value		0.758	0.793	

In white the MNA-derived xenografts are marked, and in light grey the MNNA-derived xenografts. Chi-square test was used to compare the amount of hemorrhagic areas. P-values in the columns refer to the comparison within the same mouse background but different passage, while p-values in the rows compare different background within the same passage

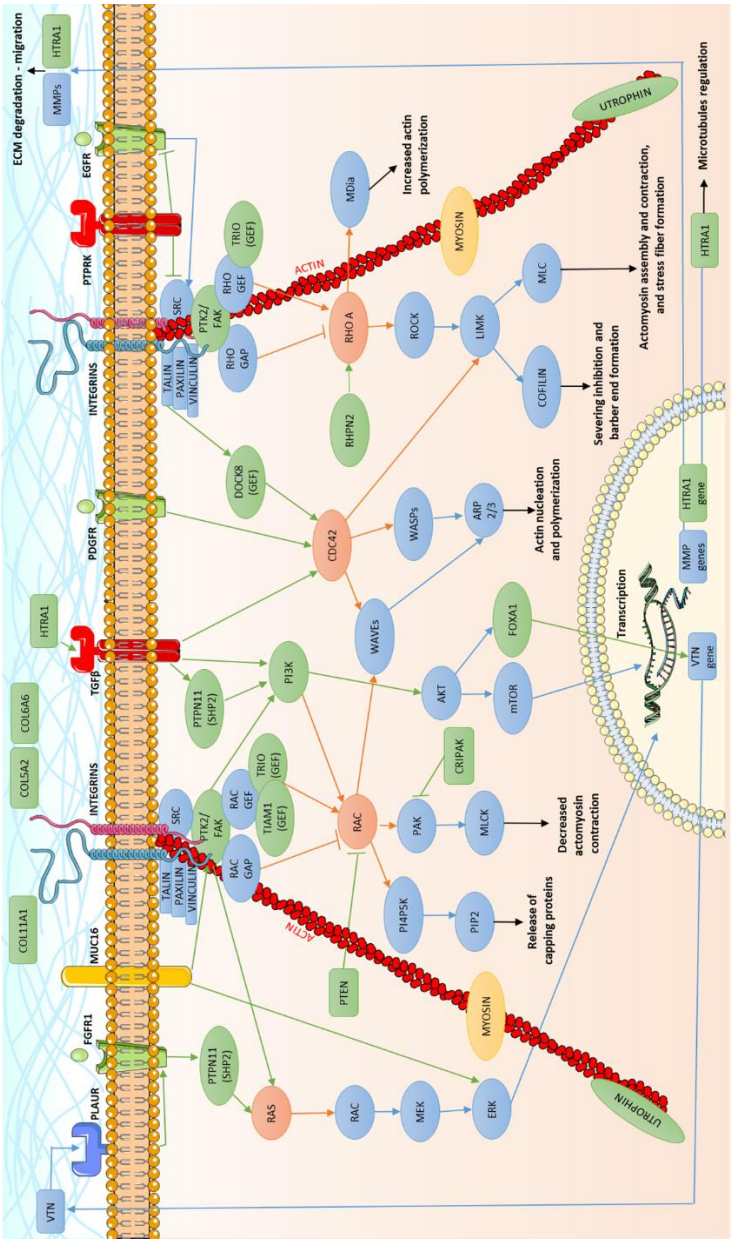

Figure 30. New generation sequencing NB-mechanopanel. This panel has been confected after an exhaustive bibliographic search. Including genes, which pathogenic mutations in cancer have previously been described, that intervene in the main cytoskeleton remodeling pathways (*RhoA, Rac1* and *Cdc42*). Some genes whose protein products are part of the ECM or are involved in its degradation and destruction (*COL11A1, COL6A6, COL5A2, HTRA1*, etc.) and genes encoding cell membrane receptors involved in transduction have also been. from ECM signals to the cell and the cytoskeleton (*PLAUR, MUC16, FGFR1*, etc). Finally, in addition to the genes related to the cytoskeleton, some specific genes of interest in cancer have been included, such as *ALK, TERT, ATRX, TP53, PTEN, BRAF, KRAS, NRAS*, etc.